

**Polyphenylene Dendrimers -
Design and Synthesis of Monodisperse
Functional Nanoparticles**

Dissertation zur Erlangung des Grades
"Doktor der Wissenschaften"
am Fachbereich Chemie und Pharmazie
der Johannes Gutenberg-Universität in Mainz

vorgelegt von

Stefan Bernhardt
geb. in Hofheim a. Ts.

Mainz 2005

Dekan: Herr Prof. Dr. P. Langguth

1. Berichterstatter:

2. Berichterstatter:

Tag der mündlichen Prüfung: 26.06.2006

Die vorliegende Arbeit wurde in der Zeit von März 2002 bis März 2005 am Max-Planck-Institut für Polymerforschung in Mainz unter Anleitung von Herrn Prof. Dr. K. Müllen durchgeführt.

Dedicated to my wife

If we knew what we were doing it wouldn't be research.

Einstein, Albert

Index of Abbreviations:

AFM	atomic force microscopy
Anal.	analysis
calcd.	calculated
TBAF	tetrabutylammoniumfluoride-hexahydrate
CD ₂ Cl ₂	deuterated methylenechloride
δ	chemical shift / ppm
d	doublet
d ⁸ THF	deuterated tetrahydrofuran
DEE	diethylether
DMF	dimethylformamide
DMSO	dimethylsulfoxide
eq.	equivalent
EtOH	ethanol
FD	field desorption
G1, G2, G3,	first-, second-, and third-dendrimer generation
GS	ground state
h	hours
J	coupling constant / Hz
LE	locally-excited state
m	multiplett
m / g	weight in gram
MALDI-TOF	matrix-assisted laser desorption/ionization-time of flight
MCH	methylcyclohexane
MeOH	methanol
MS	mass spectrometry
n	refractive index
NMR	nuclear magnetic resonance
PE	petroleum ether, low boiling
PMI	perylene monoimide
PPh ₃	triphenylphosphine
ppm	parts per million (chemical shift in NMR spectroscopy)
RT	room temperature
s	singulet
SM	single molecule
T	temperature / °K or °C
t	triplet
TCSPC	time-correlated single photon counting
TEA	triethylamine
THF	tetrahydrofuran
TIPS	tri- <i>iso</i> -propylsilyl
TPA	triphenylamine
UV	ultraviolet
Φ_{flu}	fluorescence quantum yield
τ_{flu}	decay time of fluorescence
k_{fwd} and k_{rev}	forward and reverse electron transfer rate constants
CS	charge-separated state

Table of contents

1	INTRODUCTION	1
1.1	Dendrimer Chemistry, a Short Overview	1
1.1.1	Linear Building Blocks	3
1.1.2	Branched Building Blocks	4
1.2	Polyphenylene Dendrimers	5
1.3	Synthesis of Polyphenylene Dendrimers	6
1.3.1	Palladium Catalysed Aryl-Aryl Coupling Reactions	6
1.3.2	Diels-Alder Cycloaddition	7
1.3.2.1	Divergent Synthesis	8
1.3.2.2	Convergent Synthesis	9
1.4	Diversification of Shape	10
1.4.1	Core	10
1.4.2	Branching Units	11
1.5	Shape Persistence	12
1.5.1	Solid-State NMR	12
1.5.2	PFM-AFM Measurements	13
1.5.3	SANS Experiments	13
1.6	Functionalization	13
1.6.1	Postsynthetic	14
1.6.2	Presynthetic	15
1.7	Nomenclature	15
1.8	Motivation	16
1.9	References	16
2	PYRENE AS CHROMOPHORE AND ELECTROPHORE - ENCAPSULATION IN A RIGID POLYPHENYLENE SHELL	18
2.1	Introduction	18
2.2	Synthesis of Dendronized Pyrenes	24
2.2.1	Synthesis of the Pyrene Core 1,3,6,8-Tetraethynyl-pyrene	24
2.2.2	Synthesis of First- to Fourth-Generation Dendronized Pyrenes	24
2.2.3	Improving the Film Forming Ability	27
2.2.4	Dendronized Pyrenes with a Higher Symmetry	28
2.2.5	Modification of the Pyrene Core – Toward New Dendrimer Shapes	29
2.3	Characterization of the Cores and the According Dendrimers	32
2.3.1	Characterization of the Cores	32
2.3.2	Characterization of the Dendrimers	33
2.4	Visualization and Simulation	35
2.4.1	Crystal Structure of a First-Generation Dendrimer	35
2.4.2	Molecular Modeling	36
2.5	Pyrene as Chromophore	39
2.5.1	Absorption and Emission in Solution	39
2.5.2	Absorption and Emission in Solid-State	43
2.5.3	Fluorescence Quenching Experiments	45

2.5.4	Temperature Dependent Fluorescence Spectroscopy.....	47
2.6	Pyrene as Electrophore	49
2.6.1	Reduction of Dendronized Pyrenes on a Potassium Mirror	49
2.6.2	Electrochemical Studies	52
2.7	Organic Light-Emitting Diodes	54
2.8	Conclusion	56
2.9	References.....	58
3	BENZOPHENONE FUNCTIONALIZED POLY-PHENYLENE DENDRIMERS – FROM INSIDE TO OUTSIDE	62
3.1	Introduction	62
3.2	Multiple Benzophenones in the Dendrimer Backbone	67
3.2.1	Synthesis of the Branching Reagent	67
3.2.2	Synthesis of the Dendrimers	71
3.2.3	Visualization and Simulation	75
3.2.4	Postsynthetic Functionalizations of the Dendrimer Backbone.....	76
3.2.4.1	Pyrenyl Functionalized Dendrimer Backbone.....	82
3.2.5	Characterization of Charge/Spin Carrying Dendrimers	84
3.2.5.1	Trityl Cations.....	84
3.2.5.2	Trityl Radicals	88
3.2.5.3	Benzophenone Radical Anions.....	91
3.2.6	Further Postsynthetic Reactions.....	94
3.3	Benzophenone as Core.....	97
3.3.1	Synthesis of a Benzophenone Core.....	98
3.3.2	Synthesis of the Dendrimers	99
3.3.3	Visualisation and Simulation	101
3.3.4	Postsynthetic Functionalizations in the Core	101
3.3.5	Reduction of the Dendronized Benzophenone Core	103
3.4	Multiple Benzophenones on the Dendrimer Surface.....	106
3.4.1	Synthesis of the Endcapping Reagent	106
3.4.2	Synthesis of the Dendrimers	107
3.4.3	Visualisation and Simulation	108
3.4.4	Postsynthetic Functionalizations on the Dendrimer Surface.....	109
3.5	Conclusion	110
3.6	References.....	111
4	TRIPHENYLAMINE (TPA) PERYLENEMONOIMIDE (PMI) DONOR- ACCEPTOR SYSTEMS	116
4.1	Introduction	116
4.2	Synthesis	118
4.2.1	Synthesis of the TPA Cores	118
4.2.2	Synthesis of the Dendrimers	120
4.3	Visualization and Simulation.....	124
4.4	Photophysical Investigations.....	126
4.4.1	Ensemble Measurements.....	126

4.4.2	Single Molecule Spectroscopy.....	132
4.5	Cyclovoltametry.....	134
4.6	Conclusion.....	135
4.7	References.....	136
5	CONCLUSION AND OUTLOOK.....	116
6	EXPERIMENTAL PART.....	140
6.1	General Procedures.....	140
6.2	Synthetic Procedures.....	140
6.2.1	General Synthetic Procedures.....	140
6.2.1.1	Diels-Alder-Cycloaddition of Ethynyl- and Tetraphenylcyclopentadiene Derivatives.....	140
6.2.1.2	Desilylation of Tri-iso-propylsilylethynyl Derivatives.....	140
6.2.2	Special Synthetic Procedures.....	141
6.2.3	Crystal Structure Data of 2-31.....	174

1. INTRODUCTION

From the second half of the twentieth century till now, polymers have become one of the most used materials all over the world. Endless possibilities of varying the structure and the functionalization resulted in a wide range of new materials. Furthermore, the variation of the monomers allows engineering a material for a specific application. The wide field of polymers can classically be divided into three classes: linear, cross-linked, and branched polymers. Recently, a fourth class of polymer topologies has been dedicated to dendritic macromolecules.¹⁻⁸ On the following pages, the chemistry of dendrimers is shortly overviewed, before a more detailed introduction is given about the dendrimers used in this work.

1.1 Dendrimer Chemistry, a Short Overview

The term dendrimer (greek; dendron = tree, meros = part) graphically describes the architecture of this new class of molecules (Figure 1). Although the earlier name “cascade molecules” is more suitable to design their own nomenclature, the expression dendrimers has been established in the meantime.

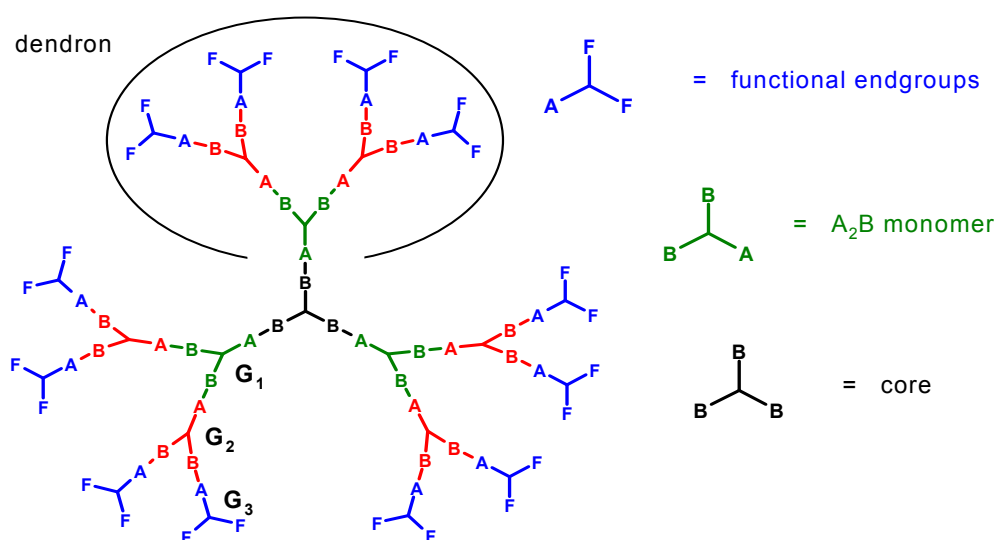
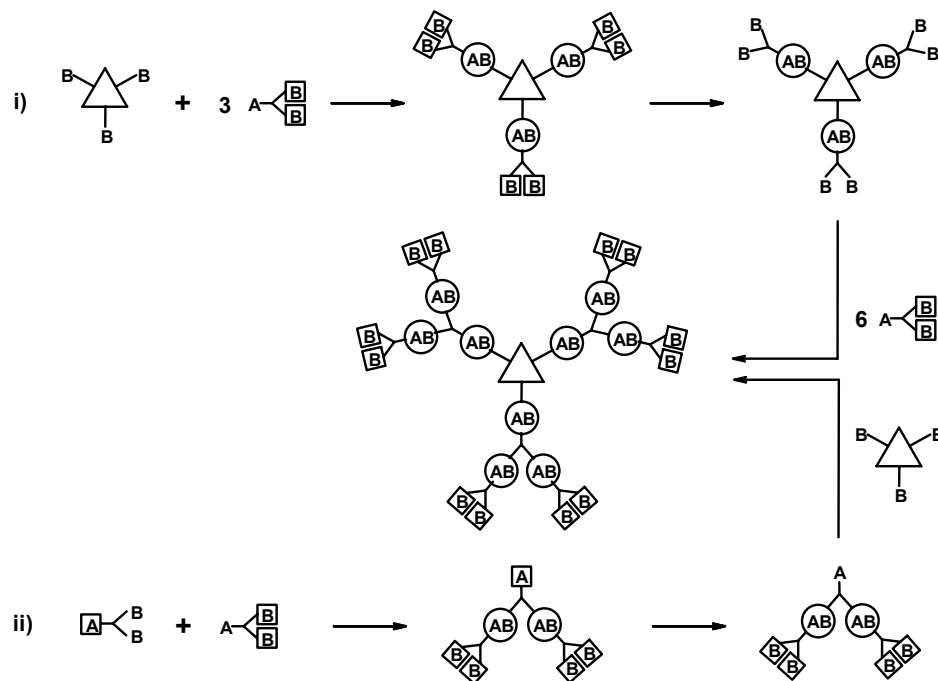


Figure 1. Schematic structure of a third-generation dendrimer: B_3 core and AB_2 monomer.

Generally, these molecules emanate from a core and like a tree they more and more ramify with each subsequent branching unit (generation). Dendrimers consist of two parts: the core and the branches that are sometimes called dendrons. These fractal-like constructs generally possess excellent solubility's, when compared to classical "polymers", which therefore facilitates their purification and characterization. It should be noted that the unique three-dimensional branched structure and the nature of the peripheral functional groups are important factors that determine the chemical physical properties of these cascade molecules. Additionally, dendritic polymers in general possess low intrinsic viscosities when compared to their linear counterparts.

These highly branched macromolecules are synthesized by a step-wise approach with either linear or branched building blocks. The iterative approach of synthesizing dendrimers

provides an opportunity to control the architecture and the molecular weight of resulting generations of macromolecules. Typically, an n-directional core molecule with n-number of surface functional groups is treated with a linear or a branched monomer to yield what is called a first tier or first-generation dendrimer.



Scheme 1. Synthesis of dendritic macromolecules. i) divergent method: the synthesis starts on the polyfunctional core and follows a step by step growth. ii) convergent method: construction of dendrons and final reaction with the core molecule.

Deprotection of the surface terminal groups of the first tier molecules followed by treatment with an adequate amount of monomer provides the next generation. Two conceptually different synthetic approaches for the construction of high-generation dendrimers exist: the divergent approach and the convergent approach. (Scheme 1)

i) The divergent method in which one branching unit after another is successively attached to the core molecules; hence, the multiplication of the number of peripheral groups is dependent on the branching multiplicity (usually 2 or 3). This way, the dendrimers can be build up step by step until steric effects prevent further reactions of the end groups.

ii) The convergent method, which takes the opposite course. The skeleton is constructed stepwise starting from the end groups towards the inside and is finally treated with a core molecule to yield the dendrimer.

Both assembly approaches have their advantages and disadvantages; for example problems occur in the divergent synthesis from an incomplete reaction of the end groups, since these structural defects accumulate with the build-up of further generations.⁹ Because the by-products reveal similar physical properties, chromatographic separation is not always possible. In the convergent course, however, a segment growing with each reaction step is coupled with only one branching unit. Thus, this approach facilitates the removal of undesired by-products. However, higher generation dendrimers are difficult to obtain by the convergent

approach since the focal point of the larger dendrons (due to steric reasons) cannot get close enough to the core's reactive site. Despite of some architectural defects, very low monodispersity can be achieved and have been reported for dendrimer constructed following both approaches. The effects of using a linear or a branched monomer in the construction procedure are critical to the installed architectural features of the dendrimer (Figure 2).

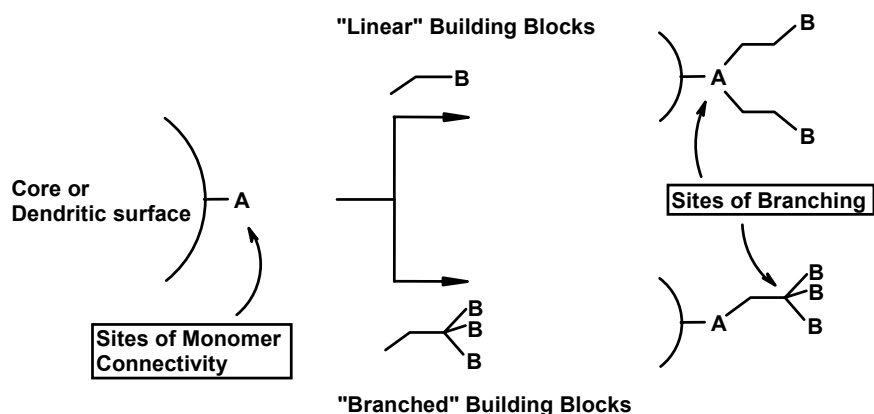
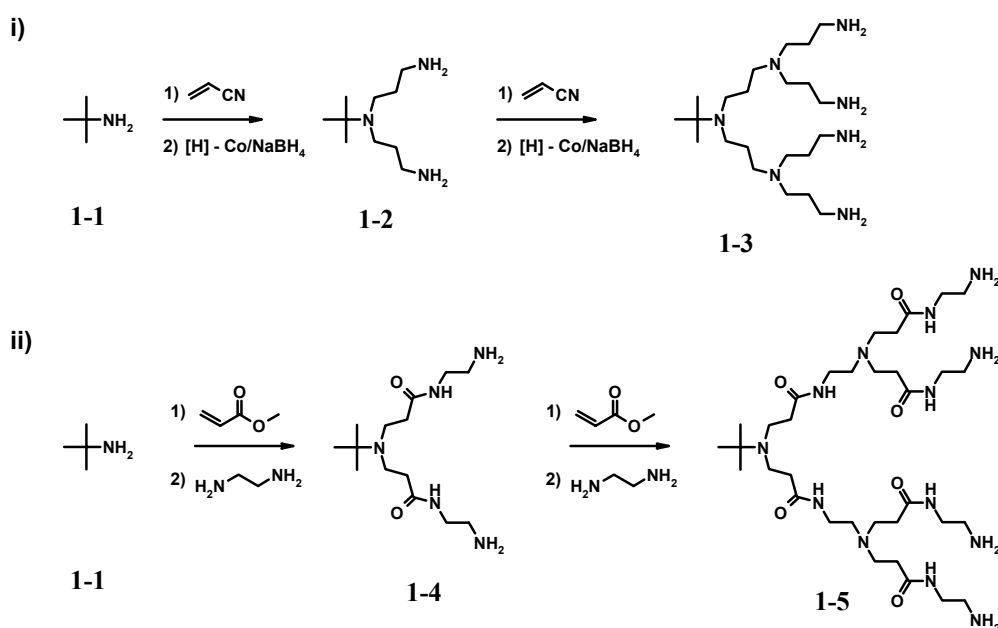


Figure 2. Linear vs. branched building blocks.

1.1.1 Linear Building Blocks

More than two decades after FLORY's initial groundwork (1978)¹⁰ concerning macromolecular networks and branched polymers, VÖGTLE et al. reported the synthesis and characterization of the first example of a cascade molecule.⁴ MICHAEL-type addition of a primary amine **1-1** to acrylonitrile (the linear monomer) afforded a tertiary amine with two arms (Scheme 2; i).



Scheme 2. Dendrimer synthesis using linear building blocks: i) VÖGTLE's original procedure¹¹, ii) TOMALIA's synthesis of PAMAM dendrimers **1-5**.^{3,12}

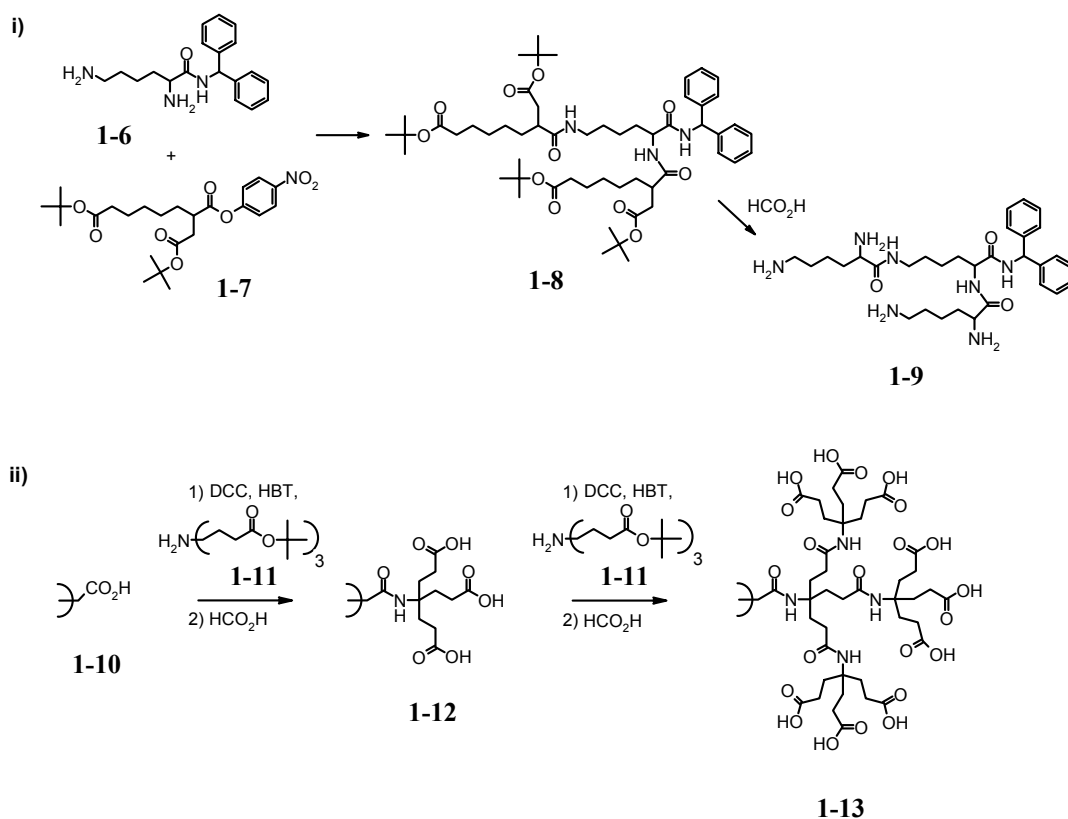
Subsequent reduction of the nitriles afforded a new diamine **1-2**, which upon repetition of the simple synthetic sequence provided the desired tetraamine **1-3**. Further growth of VÖGTLE's original dendrimer¹¹ was impeded due to difficulties associated with nitrile reduction, which was later circumvented.^{13,14}

The addition of a primary amine to excess of methylacrylate (the linear monomer) followed by amidation with excess ethylenediamine afforded the meanwhile commercially available poly(amidoamine) (PAMAM) starburst series of dendrimers introduced by TOMALIA et al. (**1-4** and **1-5**, Scheme 2; ii).^{3,12}

Typically, linear building blocks afford branching only by the direct attachment of two or more units at a particular site on the substrate (Figure 2). Hence, only divergent strategies have been used with these monomers. Advantages include ready availability and decreased costs of monomer owing to their simple structure. On the other hand, branched building blocks possess inherent branching points remote from the site of connection.

1.1.2 Branched Building Blocks

The second approach to dendrimer construction, as first suggested in a patent by DENKEWALTER et al.¹⁵ employed a protected amino acid, *N,N'*-bis(*t*-butoxycarbonyl)*L*-lysine **1-7**, as the monomer (Scheme 3; i).



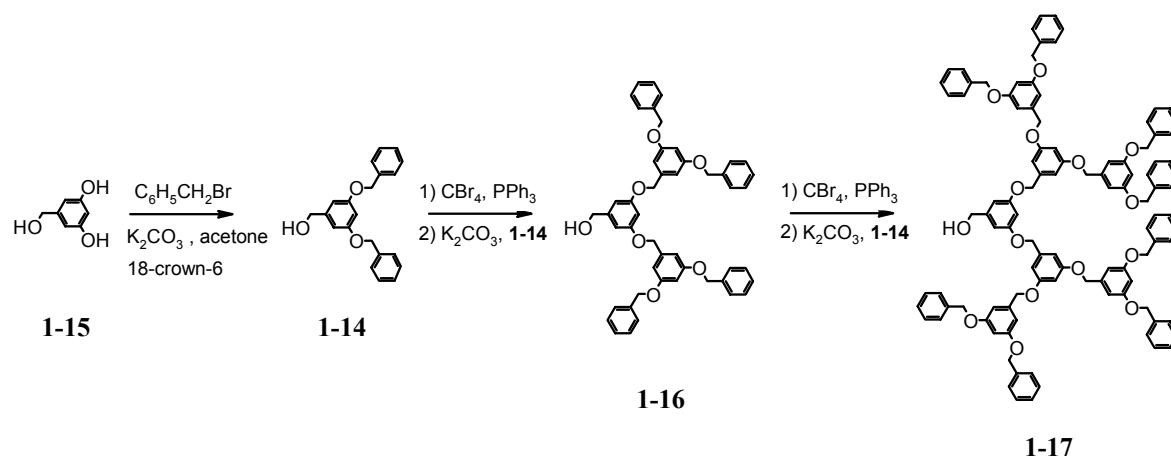
Scheme 3. Dendrimer synthesis using branched building blocks: i) DENKEWALTER's polylysine dendrimers **1-9**;¹⁵ ii) NEWKOME's polyamide dendrimers **1-13**.¹⁶

The two directional asymmetric core **1-6** was constructed from *L*-lysine and benzhydrylamine. Coupling of the building blocks was accomplished by the use of an activated *p*-nitrophenyl ester followed by removal of the *t*-butoxycarbonyl (*t*-BOC)

protecting groups. The new free polyamine moieties **1-9** were now available for the construction of the next generation.

In 1985, NEWKOME et al.¹⁶ devised a workable 1 → 3 building block procedure, which generated the so called "arborols" **1-13** (Scheme 3; ii). Their synthesis is also divergent in that they were constructed from the inside out. Use of the related 1 → 3 building block (BEHERA' s amine **1-11**)¹⁷ under DCC coupling conditions with a carboxylic acid terminated core **1-10** followed by treatment with formic acid (to hydrolyze terminal *t*-butyl ester moieties) and repetition of this sequence has afforded a variety of polyamide dendrimers **1-13**.

The beauty of the branched monomer approaches is that convergent procedures are also possible as demonstrated by FRÉCHET et al.,¹⁸ where large branched monomers, called "dendrons" **1-16** were synthesized from the periphery to the core using 3,5-dihydroxybenzyl alcohol **1-14** as the key monomer (Scheme 4).



Scheme 4. FRÉCHET's aryl ether dendrimers **1-17**.¹⁸

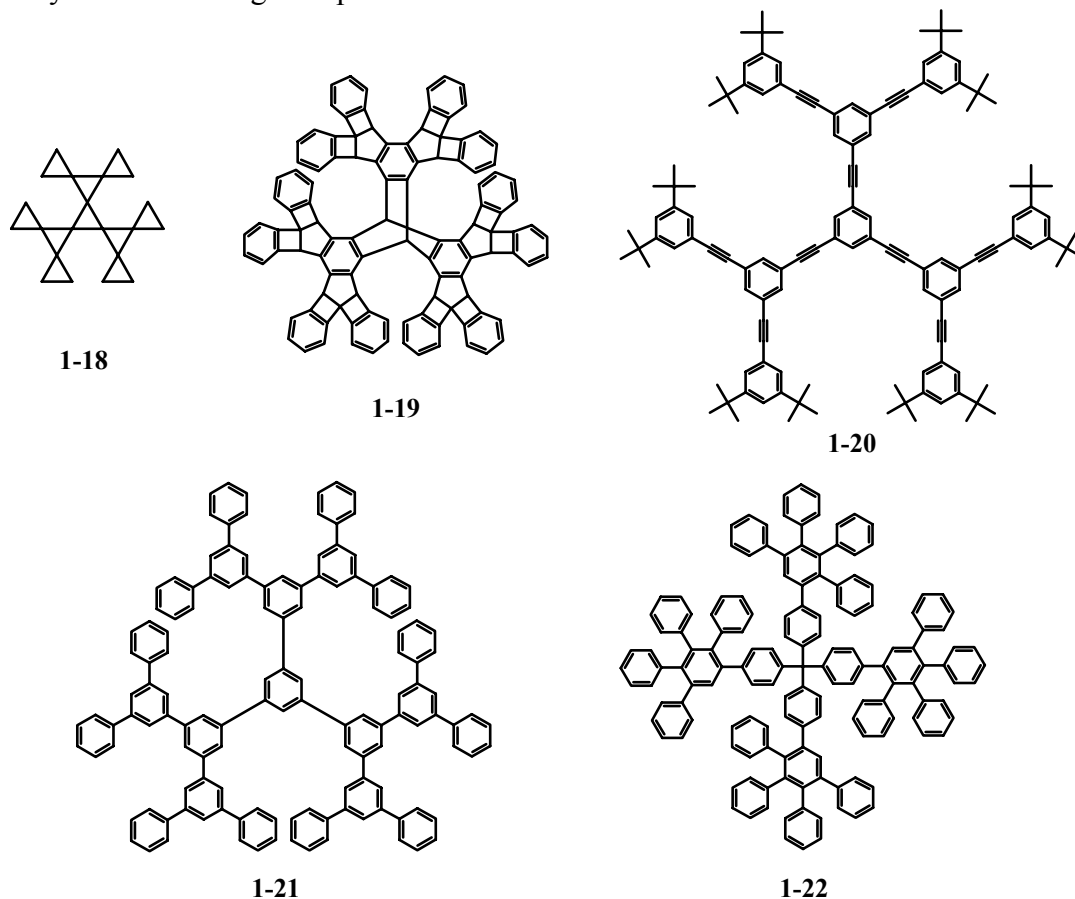
Two main synthetic transformations, the selective alkylation of phenolic hydroxyl groups to **1-15**, and conversion of a benzylic alcohol to a benzylic bromide thus affording a reactive focal moiety, were responsible for the construction of the dendron **1-16**. These monomers can be simple or complex in design and have been used in both divergent and convergent synthetic strategies. In addition, branched monomers can also be used to install utilitarian functionality within cascade molecules. Alternatively, the one-step polymerization of branched monomers results in what is called a hyperbranched polymer,¹⁹⁻²¹ possessing a higher degree of polydispersity and lower degree of branching as compared to the analogous dendrimer.

Physical properties of the dendrimers e.g. absorption on a surface or fluorescence indicated that the nature of the backbone has a big influence on the properties of the dendrimers. Thus a distinction has to be made between the before mentioned flexible, mostly aliphatic backbones and such backbones being more stiff.

1.2 Polyphenylene Dendrimers

Only few examples of shape persistent dendrimers are known in the literature (compare also chapter 1.5). HART introduced nanometer sized dendrimers in which benzene units are bound to each other via two σ bonds (**1-18**, Scheme 5).²² These dendrimers, based on extended iptycenes, turned out to be very stiff and shape persistent as they did not allow

any rotational movement. Branched triangulenes **1-19** were used by DEMEIJERE et al.²³ for the synthesis of shape persistent dendrimers. MOORE et al. presented dendrimers like **1-20** constructed from phenylacetylene units (Scheme 5).²⁴ The branching takes place in the 3- and 5-positions of the benzene rings. The *t*-butyl endgroups were necessary to ensure the solubility of the resulting nanoparticles.



Scheme 5. Shape persistent polyphenylene dendrimers: **1-18** Iptycenes by HART et al.,²² **1-19** branched triangulenes by DEMEIJERE et al.,²³ **1-20** poly(phenylenevinylene)dendrimers by MOORE et al.,²⁴ **1-21** polyphenylene dendrimers by MILLER and NEENAN^{25,26} and **1-22** polyphenylene dendrimers by MÜLLEN et al.²⁷

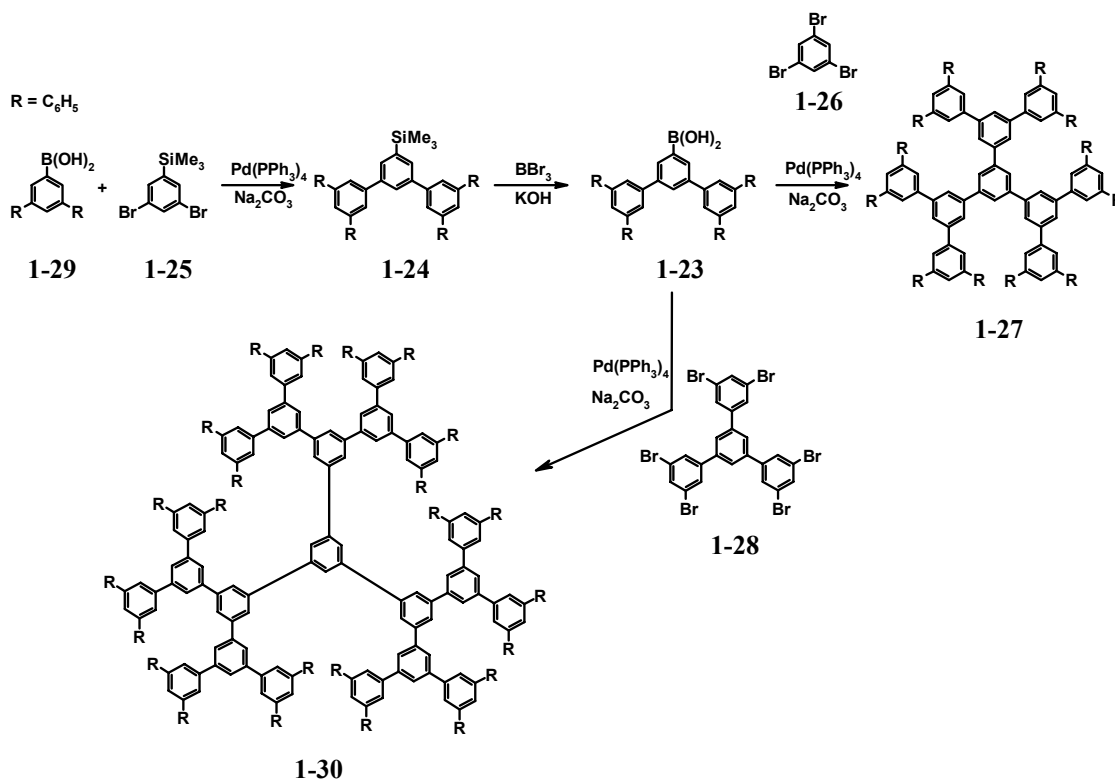
MILLER and NEENAN introduced dendrimer like **1-21** consisting only of benzene.^{25,26} Similarly to **1-20**, these dendrimers are branched in the 3- and 5-positions of the phenyl rings. In our group, polyphenylene dendrimers **1-22** were introduced, possessing branching points in the 3- and 4-positions, contrary to **1-21**.²⁷ Since the synthesis and functionalization of this type of shape persistent dendrimers was the topic of this work, their chemistry is introduced in more detail on the following pages.

1.3 Synthesis of Polyphenylene Dendrimers

1.3.1 Palladium Catalysed Aryl-Aryl Coupling Reactions

The first synthesis of polyphenylene dendrimers was reported by MILLER and NEENAN in 1990.²⁵ They used a convergent approach based on repeated palladium catalyzed aryl-aryl couplings (Scheme 6). The coupling of 3,5-dibromo-1-(trimethylsilyl)benzene (**1-24**) with the

phenylboronic acid **1-23** gave the first-generation polyphenylene dendron **1-25**. Subsequent treatment with BBr_3 generated the activated dendrons **1-26** carrying a boronic acid function. The second-generation polyphenylene dendrimer **1-28** was obtained from the SUZUKI cross-coupling reaction of **1-26** with 1,3,5-tribromo-benzene (**1-27**) in 31% yield.



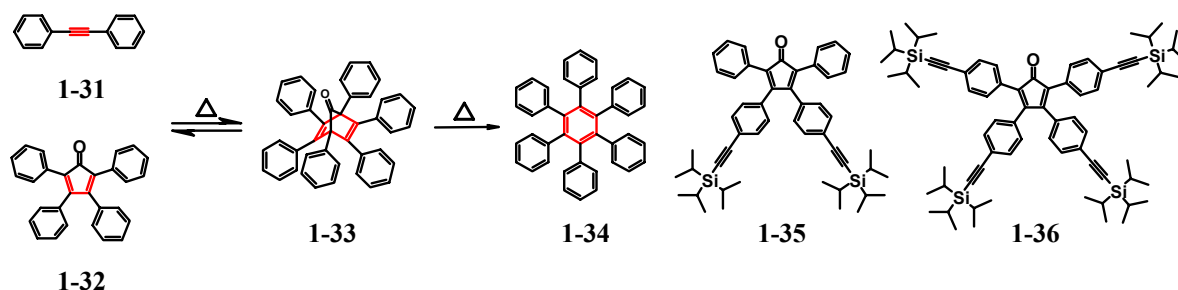
Scheme 6. Palladium catalyzed synthesis of polyphenylene dendrimers as reported by MILLER and NEENAN.²⁵

The third-generation dendrimer **1-30** was realized through the SUZUKI cross-coupling reaction of **1-26** with the enlarged core **1-29**.

1.3.2 Diels-Alder Cycloaddition

In our group, synthetic concepts have been developed that allow the synthesis of polyphenylene dendrimers which exhibit a branching in the 3- and 4-positions. Since this type of polyphenylene dendrimers was used during the course of this work, the synthesis, the three-dimensional structure, and the functionalization of these polyphenylene dendrimers is described in the next chapters.^{27,28} For the construction of this meanwhile established class of polyphenylene dendrimers the [4+2] DIELS-ALDER cycloaddition turned out to be the reaction of choice as it combined high yield conversion with a wide variety of possible functional groups. A tetraphenylcyclopentadienone derivative reacts with a phenylacetylene to give three-dimensional, purely aromatic precursors for polyaromatic hydrocarbons (PAH's).^{29,30} The reaction was described by DILTHEY in 1933 and takes place in two steps: firstly, the aromatic ethynyl compound **1-31** reacts as the dienophil in a reversible DIELS-ALDER cycloaddition with tetraphenylcyclopentadienone (**1-32**), the diene, to give a norbonadiene-7-on **1-33** (Scheme 7). This intermediate can be isolated in the most cases due to its stability. With higher temperatures carbon monoxide is extruded irreversibly whereupon hexaphenylbenzene (**1-34**) is formed. One prerequisite for the synthesis of monodisperse

dendrimers is that the growth and activation reactions can be carried out quantitatively as otherwise structural defects appear. To use the DIELS-ALDER cycloaddition for the synthesis of polyphenylene dendrimers, a new branching unit based on tetraphenylcyclopentadienone was developed, 3,4-Bis[4-(tri-*isopropylsilyl*ethynyl)-phenyl]-2,5-diphenylcyclopentadienone (**1-35**, Scheme 7), carrying the diene function as well as protected ethynyl groups.^{27,28}



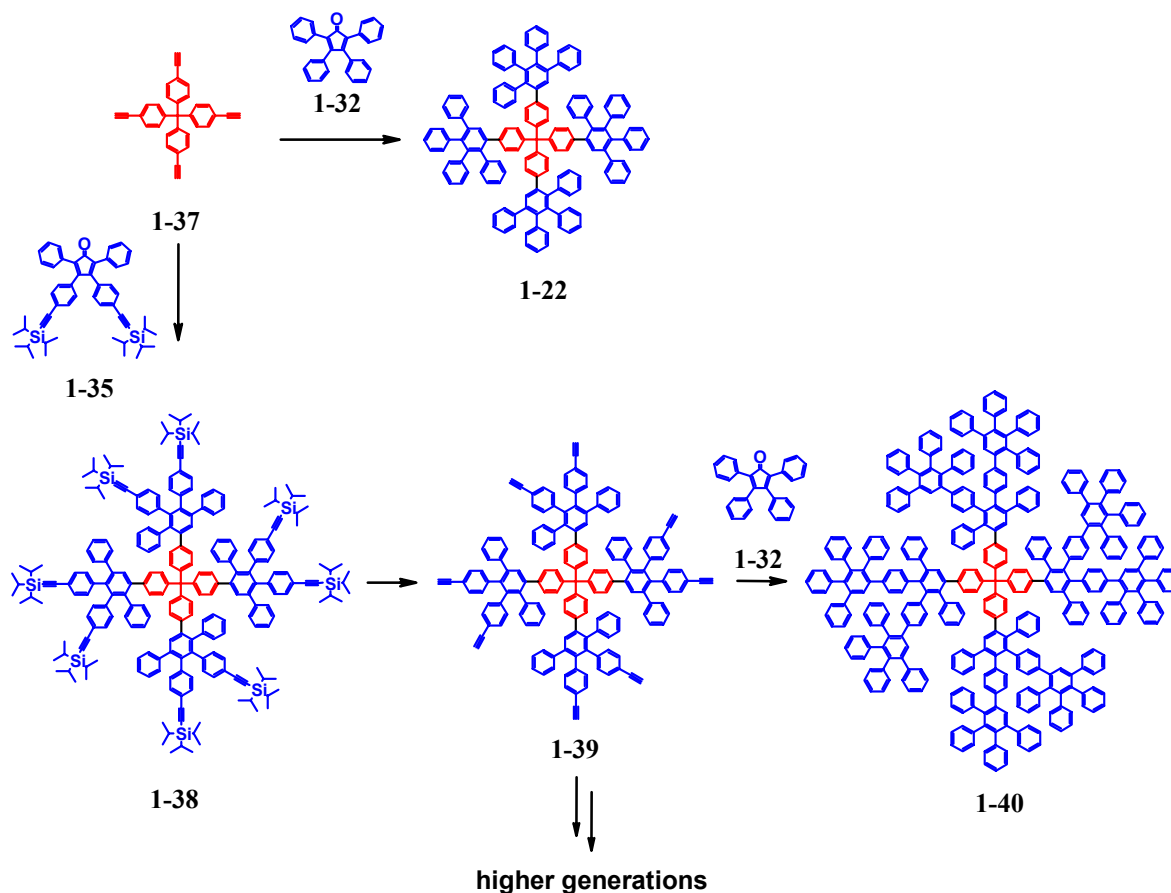
Scheme 7. DIELS-ALDER cycloaddition of tetraphenylcyclopentadienone (**1-32**) with diphenylacetylene (**1-31**) to hexaphenylbenzene (**1-34**).^{29,30} AB₂ and AB₄ branching units **1-35** and **1-36**, respectively.^{27,28}

The sterically demanding triisopropylsilyl (TIPS) groups prevent the tetraphenylcyclopentadienone from reacting with itself during the course of the cycloaddition. On the other side, they can be removed quantitatively using fluoride ions. So the synthesis of polyphenylene dendrimers consists of two main steps: DIELS-ALDER cycloaddition of the tetraphenylcyclopentadienone **1-35** with free ethynyl groups (growth step) and subsequent deprotection of the TIPS protected ethynyl functions (activation step). The advantages of the described synthetic protocol are the absence of side reactions and almost quantitative yields since the reaction can be carried out to completion due to the irreversible carbon monoxide extrusion. This is contrary to other types of dendrimers, where structural defects cannot be avoided during the synthesis, mainly due to incomplete growth or activation steps. The new branching unit **1-35** possesses the multiplicity of two. Furthermore, a branching agent **1-36** was developed carrying four protected ethynyl functions (Scheme 7). This high multiplicity had only been achieved previously by moieties based on heteroatoms. The divergent as well as the convergent approach have been applied for the synthesis of MÜLLEN-type polyphenylene dendrimers.

1.3.2.1 Divergent Synthesis

Scheme 8 shows the divergent synthesis of dendrimers starting from the tetra-(4-ethynylphenyl)-methane core **1-37**. DIELS-ALDER cycloaddition of **1-37** with the branching agent **1-35** gives the first-generation dendrimer **1-38** carrying eight TIPS protected ethynyl functions on its surface. Subsequent deprotection with fluoride ions takes place quantitatively and furnishes the first-generation dendrimer **1-39** with eight free ethynyl protons. They can be reacted in the next step with the branching unit **1-35** to give the second-generation dendrimer carrying 16 TIPS protected ethynyl functions on the surface. When unsubstituted tetraphenylcyclopentadienone **1-32** is used as the termination agent the unfunctionalized first- and second-generation dendrimers **1-22** and **1-40** are obtained, respectively. Using this synthetic protocol monodisperse polyphenylene dendrimers can be

obtained up to the third-generation in an overall yield of 80 %. The DIELS-ALDER reaction of the AB₂ branching unit **1-35** and the deprotected third-generation dendrimer does not go to completion mainly due to steric hindrance.³¹ Thus, the fourth-generation is only available when the sterically less demanding termination unit **1-32** is used.

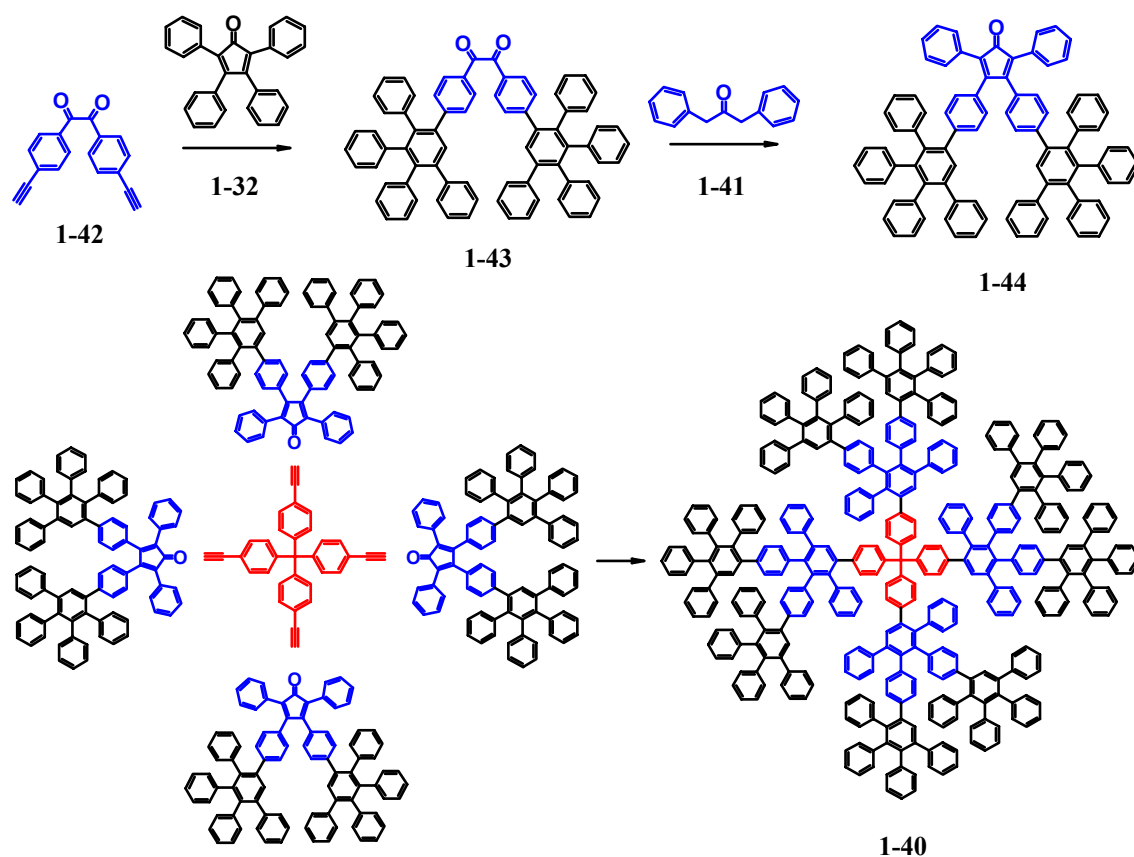


Scheme 8. Divergent synthesis of polyphenylene dendrimers starting from the tetra-(4-ethynylphenyl)-methane core **1-37**.

1.3.2.2 Convergent Synthesis

MILLER and NEENAN used dendrons (= dendritic branches) for the convergent synthesis of their dendrimers.²⁵ The convergent synthesis of polyphenylene dendrimers of the MÜLLEN-type was developed by WIESLER³² and is shown in Scheme 9. The synthesis of the required polyphenylene dendrons consists of two steps. Firstly, the DIELS-ALDER cycloaddition of tetraphenylcyclopentadienone (**1-32**) with 4,4'-diethynylbenzil (**1-41**) to the phenyl substituted benzil **1-42** and secondly, the KNOEVENAGEL-condensation of the benzil with 1,3-diphenylacetone (**1-43**) to give the first-generation dendron **1-44**. The synthesis of a second-generation dendron has not been realized up to now, since with larger tails the benzil derivate exists exclusively in the trans conformation, making the two times KNOEVENAGEL-condensation with **1-43** impossible. Scheme 9 shows the four times cycloaddition of the dendron **1-44** with tetra-(4-ethynylphenyl)-methane (**1-37**) which yields

the clean second-generation dendrimer **1-40**. The divergent as well as the convergent approach yield the same products.



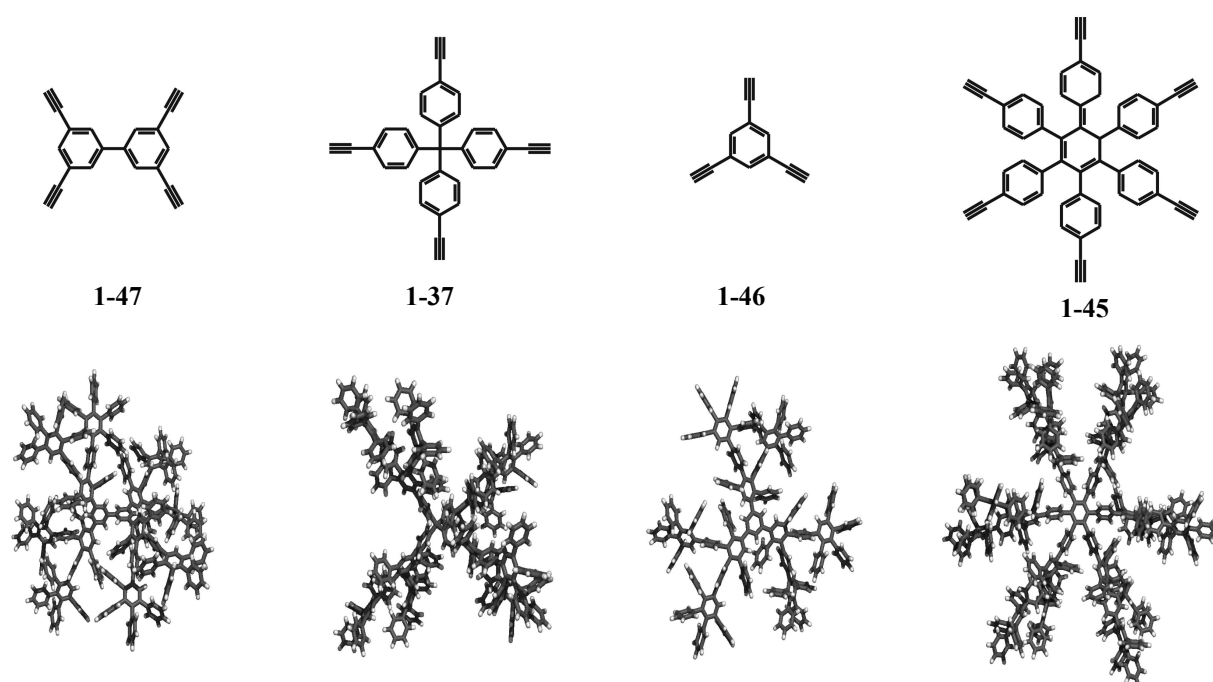
Scheme 9. Synthesis of a polyphenylene dendron **1-44** and convergent synthesis of the second-generation dendrimer **1-40**.

The convergent approach provides a fast access to second-generation dendrimers but can not be used to synthesize higher generation dendrimers. However, in combination with a desymetrized core, a functionalized second-generation dendron is an extremely powerful tool as it allows the introduction of a single function on the surface of a second-generation dendrimer.³³

1.4 Diversification of Shape

1.4.1 Core

Due to the shape persistence of the dendritic polyphenylene scaffold the number of ethynyl groups as well as the geometry of the core have a strong influence upon the structure of the resulting dendrimers. Different core units have been realized up to now and allow the synthesis of varying but well defined dendrimer geometries.³⁴ Scheme 9 shows the three-dimensional structures of the according second-generation dendrimers, obtained from molecular modeling. The 3,3',5,5'-tetraethynylbiphenyl core (**1-45**) leads to a growth that results in a kind of dumb-shell shape of the dendrimer. The tetraphenylmethane core **1-37** induces a globular shape, whereas 1,3,5-triethynylbenzene (**1-46**) and hexa-(4-ethynylphenyl)benzene (**1-47**) induce a dendrimer growth along the plain of the central phenyl core.

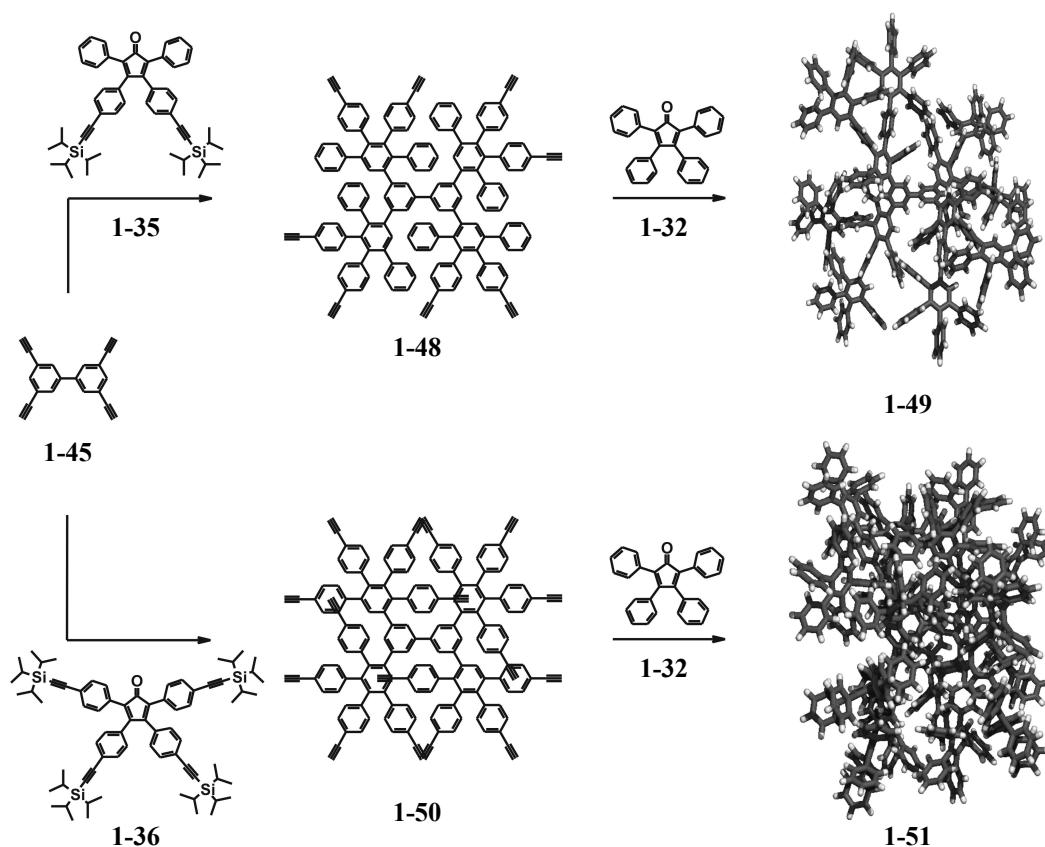


Scheme 10. Variation of the core and the three-dimensional structures of the corresponding second-generation dendrimers, derived from molecular mechanics calculations.¹

1.4.2 Branching Units

The structure of polyphenylene dendrimers can also be influenced by applying branching units with a different number of branching points (different multiplicity). Scheme 11 shows the structural difference between a second-generation dendrimer synthesized with an AB_2 building block and one synthesized using an AB_4 building block. The AB_4 building block **1-36** with the multiplicity four possesses the double amount of branching points compared to the AB_2 building block **1-35**. Thus, the size of the dendrimer shell as well as the density of the phenyl rings can be influenced. The cycloaddition of the biphenylene core **1-45** with the AB_4 branching unit **1-36** gives the first-generation dendrimer carrying 16 TIPS protected ethynyl functions on its surface (Scheme 11). Deprotection of the ethynyl groups furnishes the activated first-generation dendrimer **1-50**, which is subsequently reacted with tetraphenylcyclopentadienone (**1-32**) to yield the second-generation dendrimer **1-51**. The structure of the dendrimer is more compact and possesses pronounced cavities whereas dendrimer **1-49**, synthesized with the AB_2 branching unit, possesses more small and open structures.

¹ Three dimensional structures of the dendrimers were derived from calculations using the MMFF method.



Scheme 11. Variation of the branching unit (upper part AB_2 branching unit, down part: AB_4 branching unit) considering the biphenyl core **1-45** as example.

1.5 Shape Persistence

Two-dimensional drawings of dendrimers show the layer-by-layer arrangement of the generations with the functional groups located on the surface. Thus, the viewer gains the impression that dendrimers exist as spherical nanoparticles with all tiers pointing outward and the end groups invariably located at the surface. As the architecture of a dendrimer strongly influences its physical properties, one of the main interests in dendrimer research is to learn about the real structure of these molecules. In this respect, the main concerns are the dynamic of the dendritic backbone as well as the position of the functional groups at the end of the dendritic branches. Several studies have been performed on polyphenylene dendrimers, which allowed an insight into their dynamic and shape persistence. In the following, the results of three meaningful methods are shortly presented.

1.5.1 Solid-State NMR

Solid-state NMR allows the observation of intramolecular dynamics over a broad timescale. The dynamics of the polyphenylene dendrimer backbone has been investigated using special solid-state NMR methods (REPT-HDOR (HMQC), static 2D ^{13}C exchange spectroscopy and magic angle spinning (MAS) exchange techniques).^{35,36} Slow angular motions were only found for the terminal phenyl rings on the penta-phenyl repeating units. The slowed dynamics (millisecond to second timescale) can be attributed to intramolecular restrictions due to a dense packing of phenyl rings. In contrast to earlier calculations,²⁷ the

motion of whole polyphenylene dendrons is excluded even at higher temperature. Additionally, the measurements showed that the radial segment density in polyphenylene dendrimers is caused by truly extended arms. Due to the increasing sterical hindrance, the dense-shell packing limit is reached for generation four making further monodisperse dendrimer growth impossible.

1.5.2 PFM-AFM Measurements

PFM-AFM (pulsed force mode-AFM) experiments can give information about the stiffness (change of architecture upon deformation) and adhesion properties of molecules. For polyphenylene dendrimers adsorbed on mica, theoretical and experimental height values of the investigated polyphenylene dendrimers were identical, which can be attributed to the rigidity of this kind of dendrimers.³⁷ The dendrimers turned out to be even stiffer than the mica surface, further proving for the shape persistence of the MÜLLEN-type polyphenylene dendrimers.

1.5.3 SANS Experiments

SANS (small-angle neutron scattering) techniques can be used to determine the structure of dendrimers in solution. For polyphenylene dendrimers the segments of different generations were found to be in a well defined distance to the center of the dendrimer proving the stiff and shape persistent nature of the backbone.³⁸ Polyphenylene dendrimers can thus be considered to be "dense-shell" dendrimers in which the highest segment density is observed in the periphery of the molecules. This is contrary to other investigated dendrimers, constructed from flexible branching units. There the maximum segment density can be found in the center of the molecules ("dense-core" model) and terminal functional groups can easily undergo backfolding.

1.6 Functionalization

Since the first reports on dendrimers by TOMALIA and NEWKOME,^{3,16} research on these branched molecules has mainly focused on the preparation and molecular characterization of a wide variety of dendritic macromolecules. Gradually, the interest in this field of chemistry has shifted towards the introduction of specific functions to tailor dendrimers for several applications. The combination of discrete numbers of functionalities in one molecule and a high local density of active groups are typical characteristics of dendritic molecules.

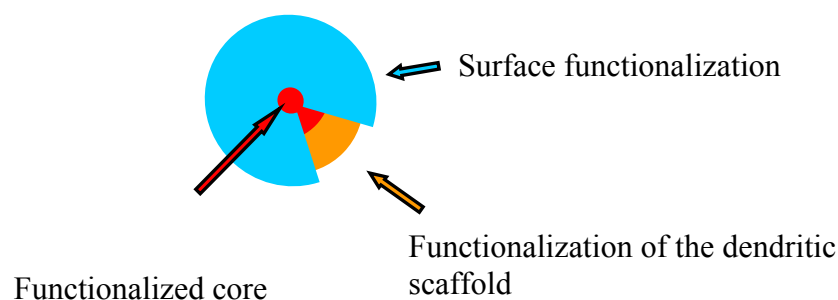


Figure 3. Functionalization of polyphenylene dendrimers.

Polyphenylene dendrimers build up from the tetragonal tetraphenylmethane core **1-37** have a globular, ball like shape. So functionalization of the dendrimers can happen at three topologically different places: (a) in the core, (b) in the scaffold, and (c) on the surface (Figure 3).

(a) Significant progress has been made using dendritic frameworks to surround functionalized cores. Dendritic shielding actually amounts to an encapsulation that can create a distinct microenvironment around the core moiety and hence affect its properties. Examples are a changed aggregation behavior of the encapsulated function or differences in the lifetime and redoxpotential compared with the nondendronized analogs.³⁹⁻⁴¹ To enable the growth of polyphenylene dendrimers an ethynyl substituted derivative of the desired core moiety needs to be available.

(b) The specific functionalization of the dendritic scaffold is only possible if the branching unit carries both, the desired function and additional groups that allow further dendrimer growth.⁴² Besides of the site isolation concept the multiplication of functions can be realized by this. The density and structure of the dendritic shell strongly influences the properties of the embedded functions which makes these molecules highly interesting e.g. for host-guest chemistry.

(c) The functionalization of the dendrimer surface can be realized by adding the functionalized monomer in the last step of the dendrimer synthesis. By this, the properties of the dendrimer can be influenced in a defined way e.g. increasing the solubility of the dendrimer by attaching alkyl chains. With polyphenylene dendrimers the well-defined functionalization of the surface originates from the stiff and shape persistent dendritic scaffold which induces a globular shape and prevents the external functional groups from back folding. Many examples of a defined surface functionalization of polyphenylene dendrimers are reported, e.g. with perylene monoimide (PMI) dyes. There, the high number of the dyes together with their prevented self-aggregation led to highly fluorescent nanomaterials.³³

In principle, dendrimers can be functionalized either by a polymeranalogous reaction of already existing functional groups (postsynthetic) or by applying the appropriate cyclopentadienone building block (presynthetic).

1.6.1 Postsynthetic

To apply a polymer analogous chemical transformation generally functional groups are required that exhibit a high reactivity as well as a high selectivity.

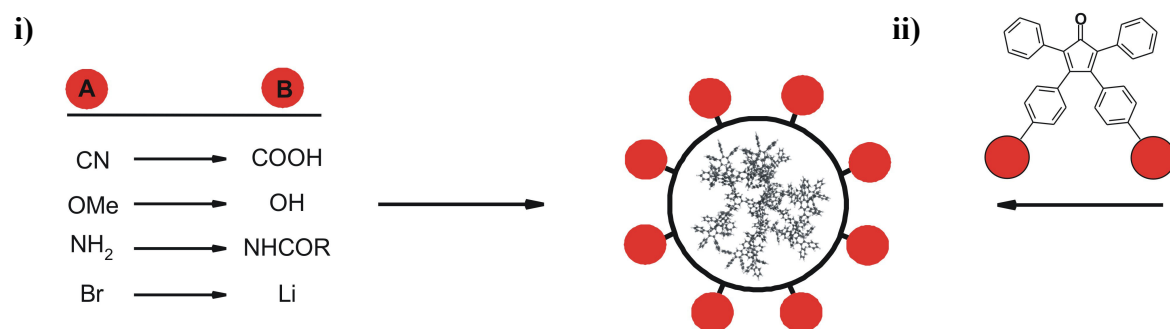


Figure 4. i) Postsynthetic and ii) presynthetic functionalization of the polyphenylene dendrimer surface.

Due to the high number of performed reactions, species, which still possess unreacted functions can normally not be separated from the desired product. Unreacted groups might lead to problems in following reaction steps or even lead to structural defects. The postsynthetic functionalization of polyphenylene dendrimers with carboxy and hydroxy groups has been realized by the conversion of pre-functionalized dendrimers yielding monodisperse higher generation dendrimers (Figure 4i).

1.6.2 Presynthetic

The functionalization of polyphenylene dendrimers using functionalized branching units is the more elegant way to obtain well defined monodisperse products. In this case the number of functions as well as their geometrical arrangement is well known (Figure 4ii). Unfortunately, this often comes together with a high synthetic effort as for every desired function the corresponding cyclopentadienone has to be synthesized. Another disadvantage of this approach is that the desired function has to be thermally stable under the conditions of the DIELS-ALDER cycloaddition step, often requiring protecting group chemistry. With this approach, e.g. methoxy-, cyano-, and halogen substituents or even alkyl chains could be introduced on the dendrimer surface.

1.7 Nomenclature

The nomenclature of dendrimers using the IUPAC nomenclature rules is very difficult due to complex long names. This complicates the explicit assignment not only for the one who has synthesized the molecule but also for the potential reader. Thus, in most cases scientists prefer their own nomenclature, which is not universally valid for all kinds of dendrimers. In this work, a nomenclature will be used that has been established during previous work on the MÜLLEN-type polyphenylene dendrimers (Figure 5).

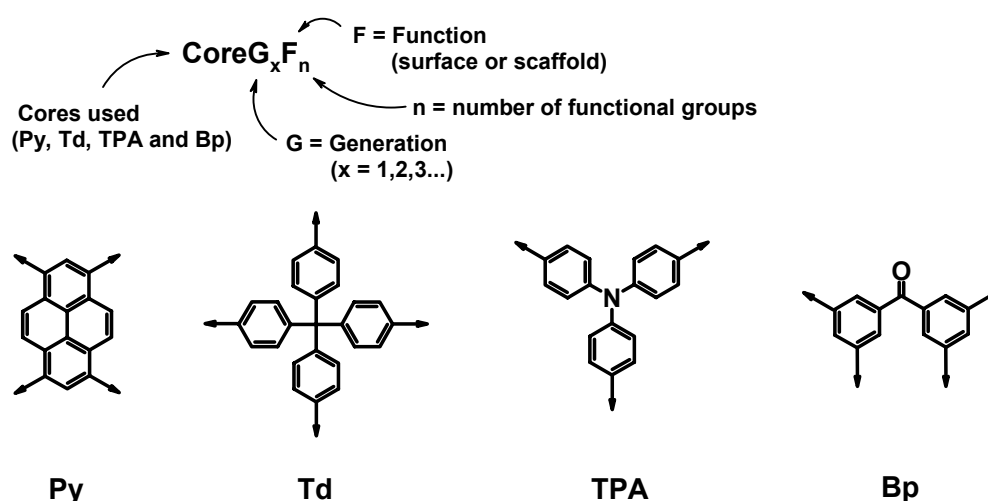


Figure 5. Nomenclature of polyphenylene dendrimers. Py = pyrene, Td = tetraeder core **1-37**, TPA = triphenylamine, BP = benzophenone.

The first syllable stands for the used core, the second for the generation and the third one for the fashion and number of the functional groups embedded in the dendritic scaffold or attached on the surface. For example, TdG₁TIPS₈ names the first-generation dendrimer **1-38**,

constructed from the tetraphenylmethane core **1-37** and possessing eight TIPS protected ethynyl groups on the surface.

1.8 Motivation

From the begin of dendrimer research, several applications were proposed for dendritic structures, such as in medicine, host-guest chemistry as well as in catalysis. This originated mainly from two properties specific for dendrimers. Firstly, the attachment of a large number of active functions on a dendrimer surface, and secondly, the encapsulation and shielding of functions in the inner (core, scaffold) of a dendrimer. On the last pages, the outstanding properties of polyphenylene dendrimers, such as high chemical stability, monodispersity and shape persistent dendritic structure have been introduced. Furthermore, the possibilities of functionalization of the core, scaffold and surface of polyphenylene dendrimers were shown.

This work focuses mainly on the synthesis and characterization of newly functionalized polyphenylene dendrimers. Classical concepts were applied as well as new ones developed. The three main topics of this work will be briefly introduced in the following. A detailed introduction is given in the begin of each corresponding chapter.

In chapter 2, the synthesis and characterization of polyphenylene dendrimers with a pyrene core is presented. The optical and electronic properties of the pyrene core will be used to quantify the amount of shielding provided by the surrounding polyphenylene shell. Furthermore, these new nanoparticles will be tested for their potential application in organic light emitting diodes.

In chapter 3, the synthesis of benzophenone functionalized dendrimers is shown. A benzophenone core as well as benzophenone carrying branching units will be used to place keto groups in defined positions throughout the dendrimer structure (core, scaffold and surface). Benzophenone is known to be highly reactive towards many reagents, thus further postsynthetic functionalizations of the benzophenone bearing dendrimers are described. In this regard, especially charge/spin carrying centers, generated from the embedded keto groups, represent a main goal of this approach.

The combination of a functional core and a functionalized dendrimer surface is presented in chapter 4. A dendritic donor acceptor system with Triphenylamine (TPA) as donating core and perylene monoimide (PMI) as acceptor chromophore will be synthesized. Further functionalization of the dendrimers will be done in order to enhance surface binding properties. The goal of this approach is a dendritic donor-acceptor system, which can be studied by single molecule spectroscopy without the usually applied polymer matrix.

1.9 References

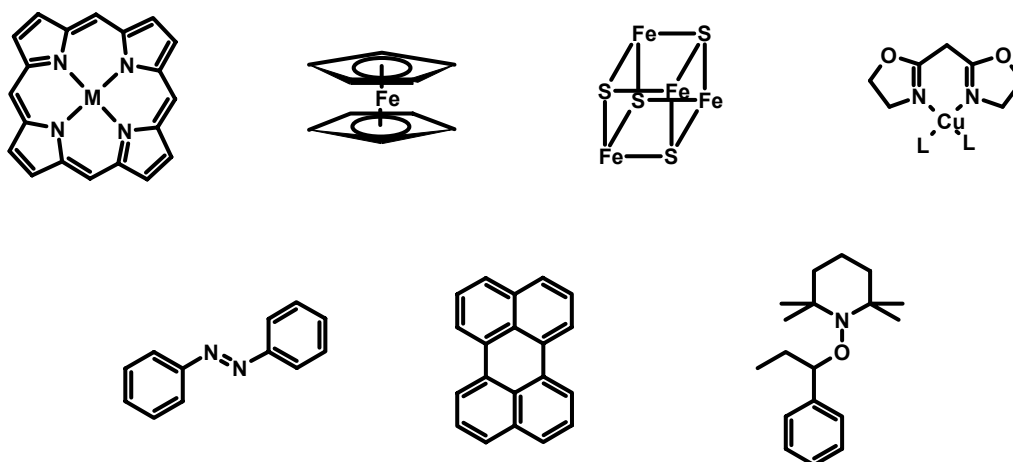
- (1) Newkome, G. R.; Moorefield, C. N.; Vögtle, F. *Dendrimers and Dendrons: Concepts, Syntheses, Application*; Wiley-VCH: Weinheim, 2001.
- (2) Fréchet, J. M. J.; Tomalia, D. *Dendrimers and Other Dendritic Polymers*; Wiley.: Chichester, England, 2001.
- (3) Tomalia, D. A.; Baker, H.; Dewald, J.; Hall, M.; Kallos, G.; Martin, S.; Roeck, J.; Ryder, J.; Smith, P. *Polymer Journal* **1985**, *17*, 117.
- (4) Vögtle, F.; Gestermann, S.; Hesse, R.; Schwierz, H.; Windisch, B. *Progress in Polymer Science* **2000**, *25*, 987.

- (5) Fréchet, J. M. J. *Journal of Polymer Science Part A-Polymer Chemistry* **2003**, *41*, 3713.
- (6) Tomalia, D. A. *Aldrichimica Acta* **2004**, *37*, 39.
- (7) Gitsov, I.; Lin, C. *Current Organic Chemistry* **2005**, *9*, 1025.
- (8) Tomalia, D. A. *Progress in Polymer Science* **2005**, *30*, 294.
- (9) Bosman, A. W.; Janssen, H. M.; Meijer, E. W. *Chemical Reviews* **1999**, *99*, 1665.
- (10) Flory, P. J. *Macromolecules* **1978**, *11*, 1122.
- (11) Buhleier, E.; Wehner, W.; Vögtle, F. *Synthesis* **1978**, 155.
- (12) Tomalia, D. A.; Baker, H.; Dewald, J.; Hall, M.; Kallos, G.; Martin, S.; Roeck, J.; Ryder, J.; Smith, P. *Macromolecules* **1986**, *19*, 2466.
- (13) Wörner, C.; Mülhaupt, R. *Angewandte Chemie-International Edition* **1993**, *32*, 1306.
- (14) Debrabandervandenberg, E. M. M.; Meijer, E. W. *Angewandte Chemie-International Edition* **1993**, *32*, 1308.
- (15) Denkewalter, R. G.; Kolc, J.; Lukasavage, W. J.; a) U.S. Pat. 4,-289,872, Sept. 15, 1981. b) U.S. Pat. 4,-360,646, Nov. 23, 1982. c) U.S. Pat. 4,-410,688, Oct. 18, 1983.
- (16) Newkome, G. R.; Yao, Z. Q.; Baker, G. R.; Gupta, V. K. *Journal of Organic Chemistry* **1985**, *50*, 2003.
- (17) Newkome, G. R.; Moorefield, C. N.; Baker, G. R.; Johnson, A. L.; Behera, R. K. *Angewandte Chemie-International Edition* **1991**, *30*, 1176.
- (18) Hawker, C. J.; Fréchet, J. M. J. *Journal of the American Chemical Society* **1990**, *112*, 7638.
- (19) Fréchet, J. M. J.; Hawker, C. J.; Gitsov, I.; Leon, J. W. *Journal of Macromolecular Science-Pure and Applied Chemistry* **1996**, *A33*, 1399.
- (20) Hult, A.; Johansson, M.; Malmström, E. in *Branched Polymers II*, **1999**; Vol. 143, pp 1.
- (21) Jikei, M.; Kakimoto, M. *Progress in Polymer Science* **2001**, *26*, 1233.
- (22) Hart, H. *Pure and Applied Chemistry* **1993**, *65*, 27.
- (23) Kozhushkov, S. I.; Haumann, T.; Boese, R.; DeMeijere, A. *Angewandte Chemie-International Edition* **1993**, *32*, 401.
- (24) Xu, Z. F.; Kahr, M.; Walker, K. L.; Wilkins, C. L.; Moore, J. S. *Journal of the American Chemical Society* **1994**, *116*, 4537.
- (25) Miller, T. M.; Neenan, T. X. *Chemistry of Materials* **1990**, *2*, 346.
- (26) Miller, T. M.; Neenan, T. X.; Zayas, R.; Bair, H. E. *Journal of the American Chemical Society* **1992**, *114*, 1018.
- (27) Morgenroth, F.; Kübel, C.; Müllen, K. *Journal of Materials Chemistry* **1997**, *7*, 1207.
- (28) Morgenroth, F.; Müllen, K. *Tetrahedron* **1997**, *53*, 15349.
- (29) W. Dilthey; Hurtig, G. *Chemische Berichte* **1934**, *67*, 2004.
- (30) W. Dilthey; W. Schommer; H. Dierichs; Trösken, O. *Chemische Berichte* **1933**, *66*, 1627.
- (31) Berresheim, A. J.; Dissertation Johannes Gutenberg-Universität (Mainz), 2000.
- (32) Wiesler, U. M.; Müllen, K. *Chemical Communications* **1999**, 2293.
- (33) Weil, T.; Wiesler, U. M.; Herrmann, A.; Bauer, R.; Hofkens, J.; De Schryver, F. C.; Müllen, K. *Journal of the American Chemical Society* **2001**, *123*, 8101.
- (34) Wiesler, U. M.; Berresheim, A. J.; Morgenroth, F.; Lieser, G.; Müllen, K. *Macromolecules* **2001**, *34*, 187.
- (35) Wind, M.; Saalwächter, K.; Wiesler, U. M.; Müllen, K.; Spiess, H. W. *Macromolecules* **2002**, *35*, 10071.
- (36) Wind, M.; Wiesler, U. M.; Saalwächter, K.; Müllen, K.; Spiess, H. W. *Advanced Materials* **2001**, *13*, 752.
- (37) Zhang, H.; Grim, P. C. M.; Foubert, P.; Vosch, T.; Vanoppen, P.; Wiesler, U. M.; Berresheim, A. J.; Müllen, K.; De Schryver, F. C. *Langmuir* **2000**, *16*, 9009.
- (38) Rosenfeldt, S.; Dingenouts, N.; Potschke, D.; Ballauff, M.; Berresheim, A. J.; Müllen, K.; Lindner, P.; Saalwächter, K. *Journal of Luminescence* **2005**, *111*, 225.
- (39) Gorman, C. B.; Smith, J. C. *Accounts of Chemical Research* **2001**, *34*, 60.
- (40) Hecht, S.; Fréchet, J. M. J. *Angewandte Chemie-International Edition* **2001**, *40*, 74.
- (41) Herrmann, A.; Weil, T.; Sinigersky, V.; Wiesler, U. M.; Vosch, T.; Hofkens, J.; De Schryver, F. C.; Müllen, K. *Chemistry-A European Journal* **2001**, *7*, 4844.

2. PYRENE AS CHROMOPHORE AND ELECTROPHORE - ENCAPSULATION IN A RIGID POLYPHENYLENE SHELL

2.1 Introduction

Throughout hundreds of million years nature has created an enormous structural diversity still not fully investigated and far from being understood. Combining different building blocks and using a variety of interactions, e.g. van der Waals forces or hydrogen bonding, results in macroscopic organization and impressing systems such as enzymes and proteins. They usually possess a globular shape mainly because hydrophilic groups are exposed towards the surrounding medium and hydrophobic groups are trapped in the interior. These unique properties together with specific interactions such as hydrogen bonding lead to the formation of the catalytically active center. During the last years, dendrimers have shown to be suitable model compounds for mimicking complex natural systems, enzymes.¹⁻⁵ Especially the encapsulation of active core functionalities within dendritic backbones has been one of the major objectives in recent dendrimer chemistry.



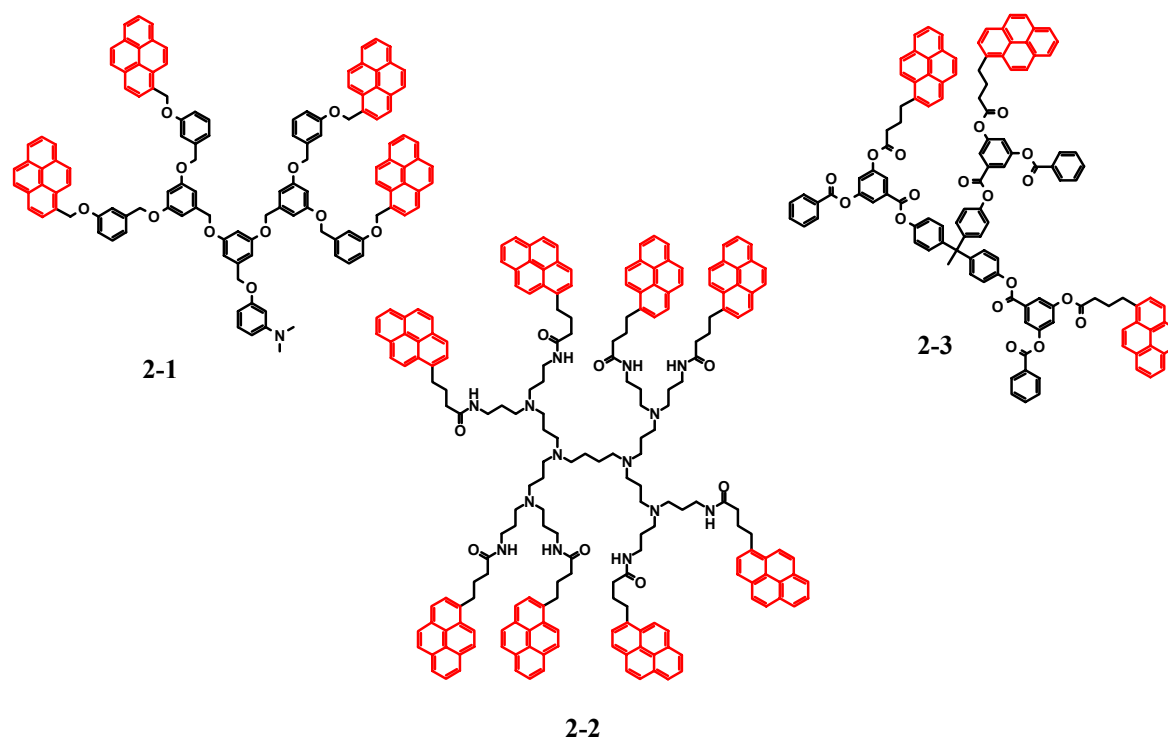
Scheme 12. Examples of dendrimer core functionalities exploited in spherical encapsulation.

Ideally, spherical particles are obtained, where the diameter is a function of the core size and the size and number of the surrounding dendrons. The properties of the dendrimer shell (stiff or flexible, hydrophilic or hydrophobic) are dependent on the building blocks used. Some core functionalities, used over the last few years, are shown in Scheme 12. They vary greatly in size – from compact metal-ion complexes to large porphyrins. Right from the beginning of dendrimer synthesis, researchers were not only interested in synthetic aspects, but also in the question of what shape do these new macromolecules possess in solution. Varieties of experimental tools have been, and still are, used to determine the effect of the dendrimer shell upon the properties of the core.

The environment of a chromophore has a great influence upon its absorption and emission properties by stabilizing or destabilizing the electronic states of the chromophore. In a first simple approach, HAWKER, WOOLEY, and FRÉCHET attached solvatochromic probes to the core or focal point of dendrimers.⁶ They studied the effect of the microenvironment on the properties of an encapsulated dye and found a pronounced bathochromic shift of the

absorption maxima in nonpolar solvents with increasing generation. The most dramatic change occurred between the third- and fourth-generation dendrimers, which was attributed to the transition from an extended to a globular structure more efficiently encapsulating the core. MOORE and co-workers used the emission of phenylacetylene dendrimers modified with an electron donor at the focal point to probe the local environment.^{7,8} An anomalous spectral shift in the fluorescence maximum of the charge transfer state was observed with higher generations. The fluorescence maximum displayed an abrupt change between the fourth- and fifth-generation dendrimers, which suggested the occurrence of dendritic encapsulation and supported the earlier findings of HAWKER and co-workers. AIDA et al.^{9,10} investigated dendrimers with a porphyrin core - porphyrin being of considerable interest due to its application as model compound for photosynthesis.^{11,12} They found that higher generation dendrimers were more efficiently quenched than a first-generation dendrimer when a small quencher was used. The opposite effect was found for larger quenchers. This was attributed to the entrapping of small molecules in the inner of the dendrimer, mainly due to some affinity between quencher and dendrons. Larger quenchers were expectedly hindered in diffusion to the core because of steric reasons.

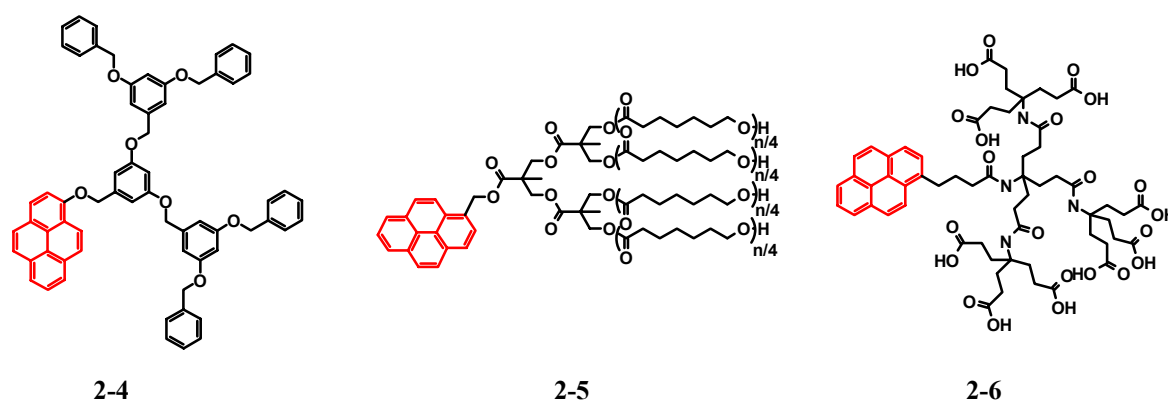
One very famous and extensively used chromophore is pyrene. The fluorescence properties of pyrene are well known and characterized by long lifetimes^{13,14} and sensitive solvatochromic shifts.^{15,16} Due to its characteristic excimer formation, pyrene can be used to study aggregation phenomena. THOMAS, POLARZ and ANTONIETTI for example studied the influence of spatial restriction on the excimer formation of pyrene using mesoporous silica materials.¹⁷ In addition pyrene was extensively used to probe the environment in micelles^{18,19} or to study the surface properties of inorganic oxides when adsorbed to these surfaces.²⁰⁻²² These examples clearly show that pyrene is obviously one matter of choice to exploit the dendrimer shape and structure.



Scheme 13. Dendrimers decorated with pyrenyl moieties on the surface (**2-1** FOX et al.²³, **2-2** BAKER and CROOKS,²⁴ **2-3** ADAM et al.²⁵).

Consequently, pyrene has been introduced in the exterior, interior or throughout the dendritic structure, and the photophysical behavior of these dendrimers has been investigated. ADAM et al. synthesized phenyl ester dendrimers, possessing, irrespective of the generation, one pyrenyl moiety per dendron (**2-3**, Scheme 13).²⁵ They observed rising excimer formation with the higher generation dendrimers indicating an increase of the mobility with larger dendron size. BAKER and CROOKS described the functionalization and spectroscopic properties of poly(propylene)imine dendrimers fully substituted with pyrene (**2-2**, Scheme 13).²⁴ Fluorescence spectroscopy showed an increasing excimer-monomer equilibrium with higher generation, leading to the conclusion that pyrene molecules were aggregated on the dendrimer periphery in such a way that excimer formation is enhanced. Furthermore, excitation spectra indicated an interaction between the pyrenyl moieties prior to excitation (pre-aggregation). FOX et al. introduced FRÉCHET-type dendrimers with a pyrenyl decorated surface (**2-1**, Scheme 13).²³ A photo-induced electron transfer from the electron donor on the focal point (N,N-dimethylaminobenzene) to the chromophores on the dendrimer surface was observed.

Pyrene on the focal point of poly(arylether) monodendrons was introduced by SHAPIRO and HANSON (**2-4**, Scheme 14).²⁶ They measured the fluorescence quenching by molecular oxygen which was found to decrease for monodendrons with increasing generation.

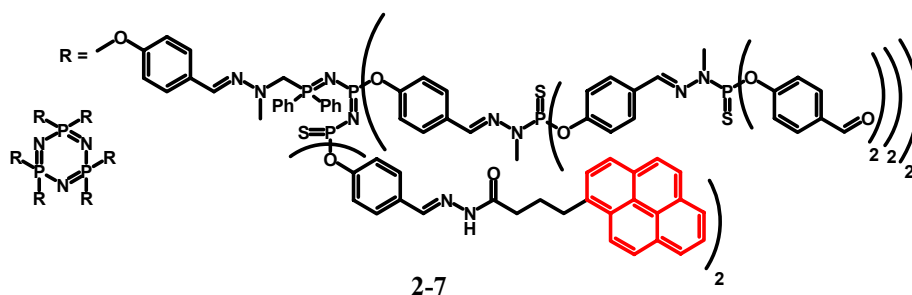


Scheme 14. Dendrimers with pyrene attached to their focal point (**2-4** SHAPIRO and HANSON,²⁶ **2-5** FRÉCHET et al.,²⁷ **2-6** CARDONA et al.²⁸)

The increased density of the larger monodendrons obviously provided a more efficient barrier to diffusing oxygen. Pyrene exhibits a sensitive solvatochromic behavior, with the relative intensity of emission bands dependent on the solvent polarity.^{13,14} FRÉCHET et al. used this effect to determine the influence of chain length and solvent polarity on the encapsulation of a poly(ϵ -caprolactone) dendronized pyrene (**2-5**, Scheme 14).²⁷ They found a solvation-induced encapsulation effect mainly due to an extent and collapse of the dendrimer backbone. CARDONA and coworkers synthesized poly(amido) dendrimers (**2-6**, Scheme 14) and used a wide variety of molecular and ionic quenchers to assess the relative structural permeability's of a single pyrenyl residue attached on the focal point.²⁸ The approach of the quenchers toward the pyrenyl moiety was increasingly hindered with increasing dendrimer generation.

The introduction of chromophores in the dendritic scaffold was presented by MAJORAL and coworkers (**2-7**, Scheme 15).²⁹ They functionalized third-generation phosphorous dendrimers with pyrenyl moieties specifically in the first-generation layer. Contrary to the pyrenyl decorated poly(propylene)imine dendrimers presented by BAKER and CROOKS²⁴ (**2-2**,

Scheme 13), no pre-association of pyrene in the ground state was found. The interaction with the dendrimer backbone did obviously not hamper the mobility of the pyrenyl moieties.



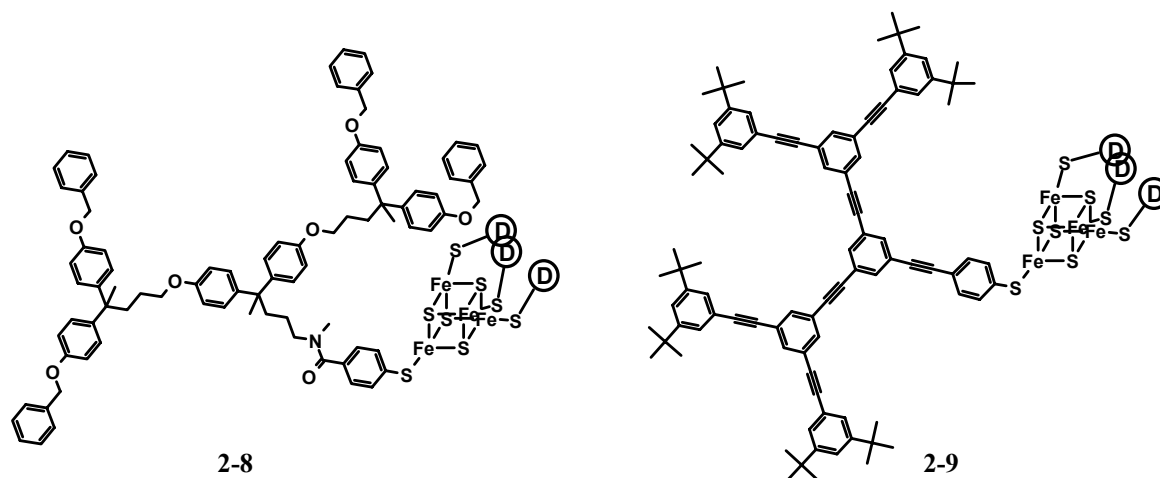
Scheme 15. Phosphorous dendrimers with pyrene attached to its inner dendritic backbone by MAJORAL et al.²⁹

SCHLÜTER and coworkers introduced dendrimers functionalized with pyrene in the core, in the dendritic scaffold as well as on the surface. Their intention was to create light harvesting systems with a long lifetime of the charge-separated photoexcited state to mimic charge-separation processes in biological systems. However, up to now only the synthesis of a first-generation dendrimer is described in the literature.^{30,31}

Also the non-covalent incorporation of chromophores into the cavities present inside dendrimers has received some attention. Recently, PALEOS and coworkers investigated the properties of pyrene non-covalently trapped within poly(propylene)imine and poly(amido)amine dendrimers.^{32,33} The results showed that pyrene can be sequestered in the interior cavities and selectively released by protonation of interior tertiary amines at the branching points. This is the consequence of the hydrophobic nature of pyrene and the enhanced hydrophilicity of the dendrimer backbone upon protonation.

Dendrimer encapsulated redox-active cores such as metalloporphyrins have been extensively studied as they represent simple synthetic models for heme-containing electron transfer proteins such as cytochrome c.^{4,34,35} Electron-transfer proteins are able to control precisely the rate of electron transfer from one redox center to another. GRAY et al. dramatically illustrated that the relative rate of electron transfer from a redox center to various points at the surface of heme-based proteins can vary substantially.³⁶⁻³⁸ Understanding how electron transfer is governed by a topologically regular architecture of a given size would therefore help to explain how the structural features in the specific but topologically complex electron-transfer proteins govern electron-transfer rates. DIEDERICH and coworkers systematically changed the microenvironment of the core by varying the generation number. They wanted to know, how a protein shell is achieving remarkably high oxidation potentials in such enzymes.^{4,39,40} The authors reported that the increasingly electron-rich environment around the core in higher generation NEWKOME-type dendrimers with zinc porphyrin cores led to facilitated oxidation and inhibited reduction processes.^{4,40} A related study by FRÉCHET and coworkers involved poly(benzyl)ether dendrimers with a zinc porphyrin core.⁴¹ A decrease in the peak current and an increase of the peak potential difference in cyclic voltammetry experiments demonstrated increasingly slow electron transfer kinetics as the size of the dendrimer shell increased. A detailed analysis of the observed electrochemical irreversibility was provided by KAIFER and co-workers, who thoroughly studied ferrocene modified with dendritic ligands.^{42,43} The authors showed that the heterogeneous electron-transfer rate constant as well as the diffusion coefficients decreased as the generation number increased. The influence of the dendrimer conformation, especially the conformational

flexibility, upon the properties of redox-active cores was demonstrated by GORMAN and coworkers.^{44,45}



Scheme 16. Dendrimers with a redox-active iron-sulfur core; flexible **2-8**, and rigid **2-9**. One arm is drawn out fully. The three other arms are identical with the one shown but are abbreviated as a circled-D for ease of visualization.

They found that a rigid dendrimer shell (**2-9**, Scheme 16) hampered the electron transfer from the electrode to an iron-sulfur core significantly more than the according dendrimer **2-8** possessing a flexible dendritic shell. Molecular dynamics simulations of these systems indicated that flexible architectures have a more mobile and therefore less sterically shielded redox-active core compared to rigid architectures.

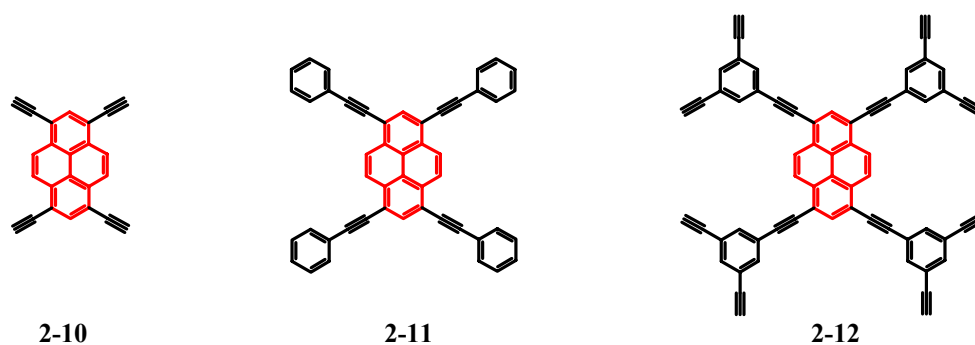
In our own group, C. HAMPEL synthesized polyphenylene dendrimers possessing either a triphenylamine or a naphthalene moiety as redox-active core.⁴⁶ Cyclovoltametry experiments showed, in accordance to the before mentioned work by FRÉCHET and coworkers, a hampered electron transfer to the core with increasing dendrimer generation. Additionally, the attenuation of the electron transfer process was clearly demonstrated since decreasing values for the heterogeneous electron-transfer rate k_0 were found with increasing density of the dendrimer shell.

A vast number of physical methods are available to complete the above-mentioned techniques. For instance, NMR relaxation experiments can be used in connection with paramagnetic cores, with conventional proton relaxation, or even to probe the entire dendritic framework. Other methods dealing with dendrimer conformation and dynamics, such as gel-permeation chromatography (GPC), differential viscosimetry, and computational methods have been reviewed recently by BOSMAN, JANSSEN, and MEIJER.⁴⁷

As pointed out on the last pages, chromophores and electrophores were of great importance for the investigation of structure-property relationships in dendritic systems. However, from a more applied perspective, dendrimers have been used to spatially arrange the different components necessary for the construction of organic light-emitting diodes. MOORE and coworkers have described devices based on phenylacetylene dendrimers having a luminescent anthracene core and peripheral tertiary aromatic amines.⁴⁸ The triaryl amines in their dendrimers served as the hole-transporting element, while the phenylacetylene dendrons acted as electron transporters. More recently, FREEMAN et al. prepared naphthyldiphenylamine terminated poly(benzyl ether) dendrimers having coumarin or pentathiophene cores.⁴⁹ Two-component single-layer devices consisting of the dendrimer, which served as both hole

transporter and emitter, as well as an oxadiazole derivative, which acted as the external electron transporter, were fabricated and good matching of the photoluminescence and electroluminescence was observed. Monolayers and their films bearing pyrene derivatives have shown to exhibit interesting photophysical properties which make them promising candidates for an application in organic light-emitting diodes (OLEDs).⁵⁰⁻⁵³ In addition, encapsulation is anticipated to be of critical importance in isolation of information in yet unprecedented single-molecule information storage schemes. In such a scheme, the presence or absence of single electrons on individual molecules encodes binary information. This scheme would represent the smallest possible switch being able to implement the highest density memory.⁴⁵ One possibility is an array of oxidized and reduced molecules. Placing oxidized molecules in close proximity to create this ordered array would lead to electron transfer between the differently charged species, thereby losing information. Thus, molecular structure-property relationships that govern the rate of electron transfer between redox centers is required to implement a one electron = one bit information storage scheme in a rational way.

In this chapter the synthesis and characterization of polyphenylene dendrimers with a pyrene core are presented. As mentioned in the introduction (chapter 1.5) this type of dendrimers is characterized by its shape persistence and strict monodispersity, therefore allowing an excellent control over the shape and size of the resulting macromolecules. Improved optical and electronic properties, e.g. a hampered aggregation of the pyrene core, were expected from its encapsulation. Contrary to the before described dendrimers with a monofunctional pyrene attached at the focal point (Scheme 14), the tetra substituted pyrene cores **2-10**, **2-11**, and **2-12**, respectively, will be used (Scheme 17).



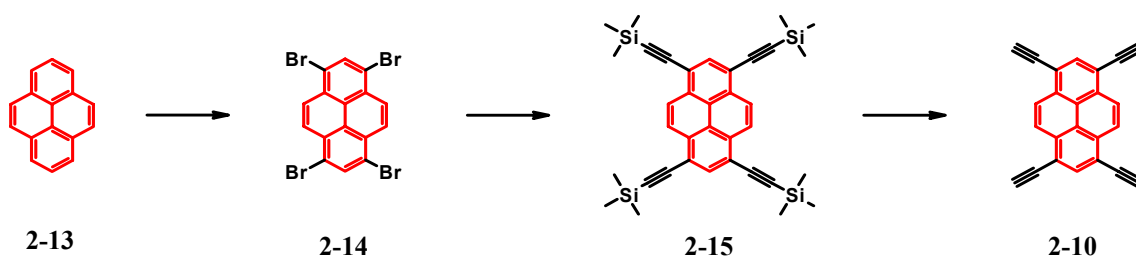
Scheme 17. Pyrene cores for the build-up of polyphenylene dendrimers used in the course of this work.

A significantly enhanced steric shielding is expected from this, resulting in an even more pronounced site-isolation of the core. The influence of the polyphenylene dendrimer shell upon the optical and electronic properties of the pyrene core will be the main topic to investigate herein. Furthermore, using different substitution patterns should lead to altered physical properties of the pyrene core and to a deeper knowledge about the efficiency of encapsulation/shielding of active core functions in this type of dendrimer. In cooperation with DuPont, some of the dendrimers will be applied as emitting layer in organic light-emitting diodes. Tailoring the physical properties of these new dendrimers will therefore be another main issue.

2.2 Synthesis of Dendronized Pyrenes

2.2.1 Synthesis of the Pyrene Core 1,3,6,8-Tetraethynyl-pyrene

The synthesis of the pyrene core 1,3,6,8-tetraethynyl-pyrene (**2-10**) starts with 1,3,6,8-tetrabromopyrene (**2-14**) (Scheme 18), which was readily obtained by bromination of pyrene (**2-13**) according to a literature procedure.^{54,55} Recrystallization from nitrobenzene gave **2-14** as a light brown solid in almost quantitative yield. The introduction of the ethynyl groups, required for the growth of the dendrimer, was accomplished by HAGIHARA-SONOGASHIRA⁵⁶⁻⁵⁸ cross-coupling of **2-14** with trimethylsilylethyne. While **2-14** is almost insoluble in common organic solvents, the trimethylsilyl (TMS) protected ethynyl groups produced a very good solubility of 1,3,6,8-tetrakis-trimethylsilyl-ethynyl-pyrene (**2-15**). After purification by column chromatography **2-15** was obtained as an orange solid in 83% yield.

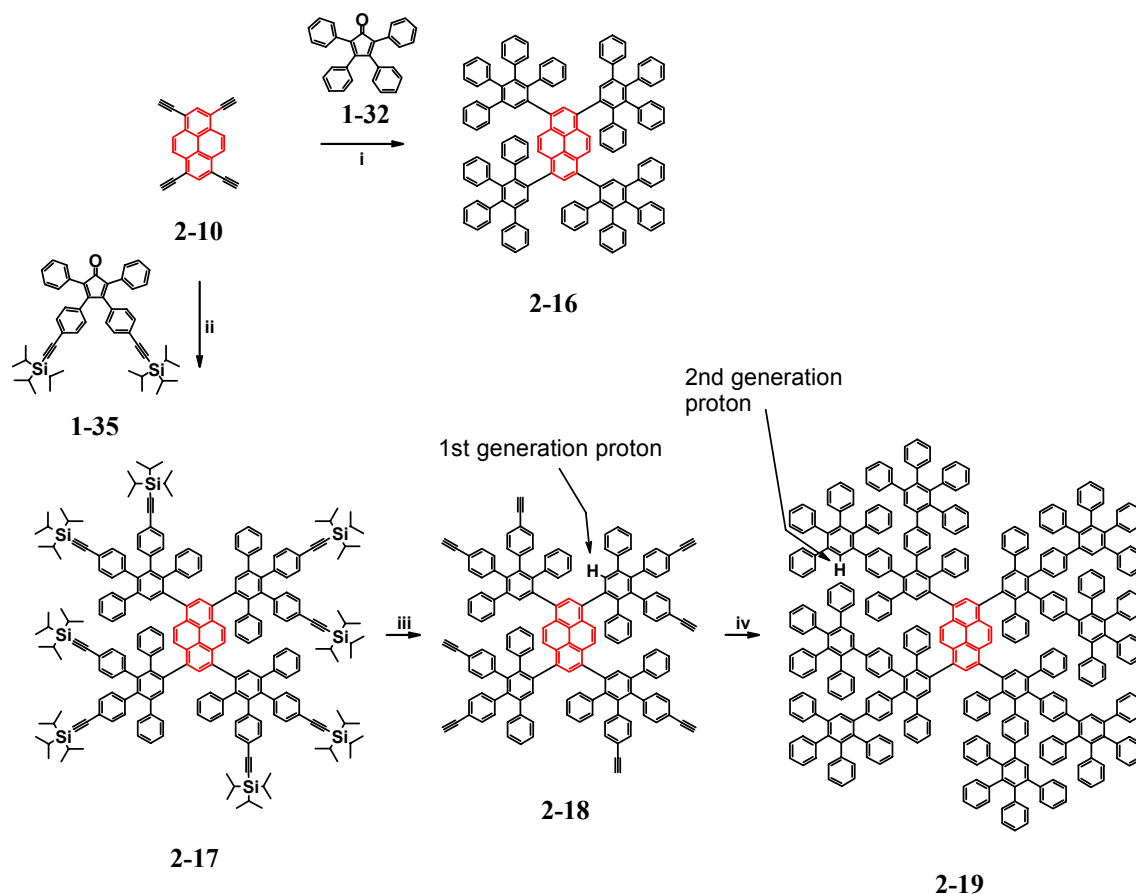


Scheme 18. Synthesis of 1,3,6,8-tetraethynyl-pyrene (**2-10**). i) bromine, nitrobenzene, 165 °C, 90% ii) 6 eq. trimethylsilyl-ethyne, [Pd(PPh₃)₂]Cl₂, PPh₃, CuI, toluene, TEA, 80 °C, 83%; iii) 8 eq. K₂CO₃, MeOH, 95%.

Subsequent cleavage of the TMS protecting groups with K₂CO₃ in MeOH proceeded smoothly and gave the activated pyrene core 1,3,6,8-tetraethynyl-pyrene (**2-10**) in high yield. The solubility of **2-10** in common organic solvents was reduced due to self-aggregation of the pyrene moieties, mainly because of π -interaction. **2-10** was therefore purified by filtration and washing.

2.2.2 Synthesis of First- to Fourth-Generation Dendronized Pyrenes

The preparation of structurally defined monodisperse polyphenylene dendrimers with a pyrene core has been realized by repetitive coupling and activation steps based on the DIELS-ALDER cycloaddition.^{59,60} The synthesis of the first- and second-generation dendrimer is depicted in Scheme 19. In spite of the reduced solubility of 1,3,6,8-tetraethynyl-pyrene (**2-10**), the unfunctionalized first-generation dendrimer **2-16** was obtained from the DIELS-ALDER cycloaddition with tetraphenylcyclopentadienone (**1-32**) in refluxing *o*-xylene in almost quantitative yield.



Scheme 19. Synthesis of the first- and second-generation dendrimers **2-16** and **2-19**, respectively. i) 6 eq. **1-32**, *o*-xylene, 160 °C, 95%; ii) 6 eq. **1-35**, *o*-xylene, 160 °C, 71%; iii) TBAF, THF, 93%; iv) 16 eq. **1-32**, 160 °C, 73%.

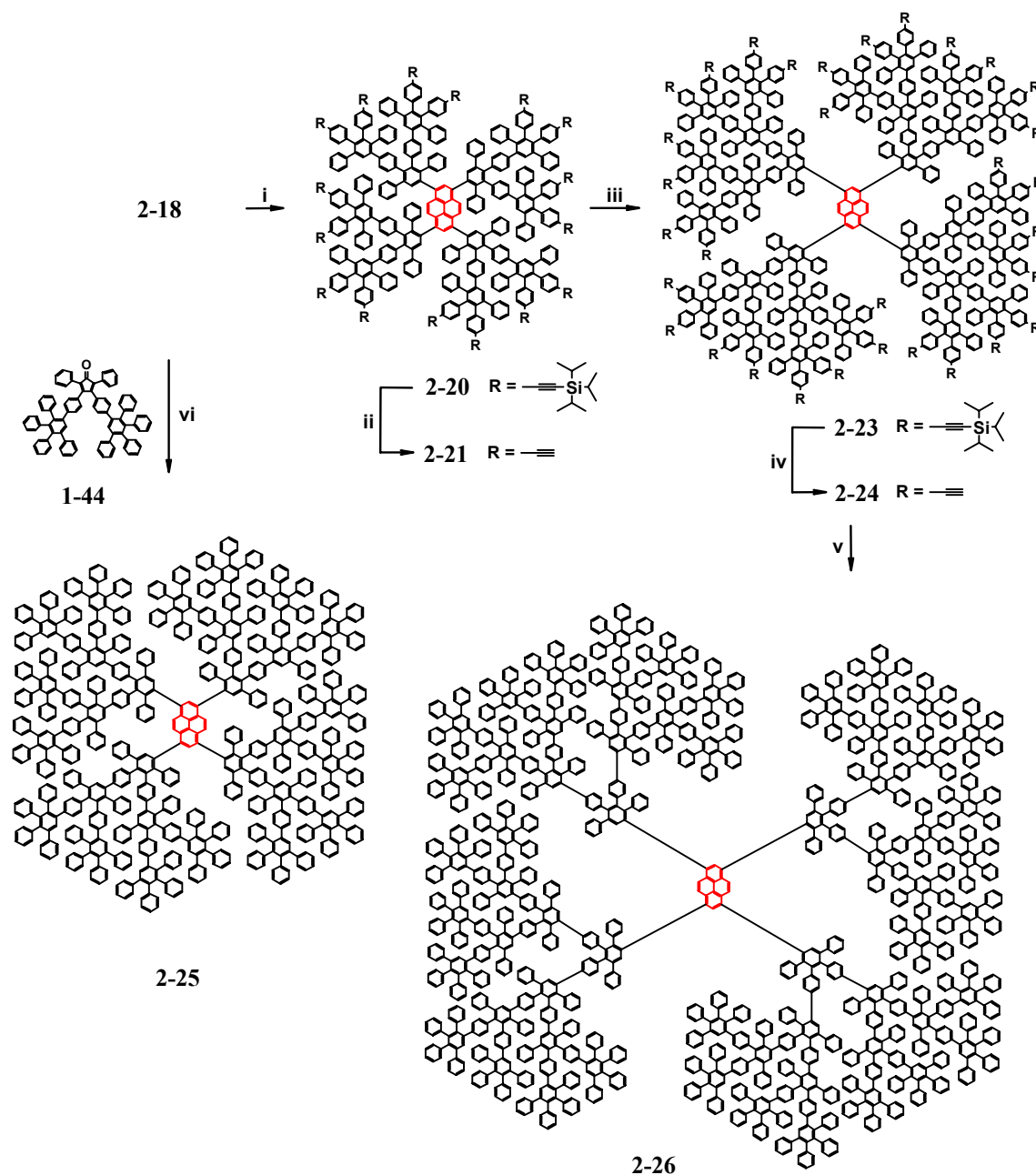
Carried out with conventional heating in an oil bath the reaction took about 12-16 hours to complete. When carried out in a microwave apparatus at higher temperature and under pressure, reaction time was dramatically shortened to 5 minutes.² This new type of performing reactions, not only for the DIELS-ALDER cycloaddition step, has often been applied as a test reaction in small scale and gave always comparable yields and a much shortened reaction time.

Microwave Assisted Organic Synthesis (MAOS)⁶¹⁻⁶⁷

Closed-vessel microwave heating techniques have been the state of the art for sample preparation in the analytical laboratory for over fifteen years. However, the application of microwaves in the organic synthesis community is only now beginning to receive widespread attention. There are two specific mechanisms of interaction between materials and microwaves: (1) dipole interactions and (2) ionic conduction. Both mechanisms require efficient coupling between components of the target material and the rapidly oscillating electrical field of the microwaves. Dipole interactions occur with polar molecules. The polar ends of a molecule tend to align themselves and oscillate in step with the oscillating electrical field of the microwaves. Collisions and friction between the moving molecules result in

² Temperature: 180 °C, pressure: 5 bar, solvent: *o*-xylene, PowerMax modus, CEM Discover (CEM GmbH, Carl-Friedrich-Gauß Str. 9, 47475 Kamp-Lintfort).

heating. Broadly, the more polar a molecule, the more efficiently it will couple with (and be influenced by) the microwave field. Ionic conduction is only minimally different from dipole interactions. Obviously, ions in solution do not have a dipole moment. They are charged species that are distributed and can couple with the oscillating electrical field of the microwaves. The efficiency or rate of microwave heating of an ionic solution is a function of the concentration of ions in solution.



Scheme 20. Synthesis of the third- and fourth-generation dendrimers **2-25** and **2-26**, respectively. i) 12 eq. **1-35**, *o*-xylene, 150 °C, 76%; ii) TBAF, THF, 91%; iii) 32 eq. **1-35**, *o*-xylene, 160 °C, 85%; iv) TBAF, THF, 89%; v) 65 eq. **1-32**, Ph₂O, 190 °C, 85%. vi) 16 eq. **1-44**, *o*-xylene, 170 °C, 55%.

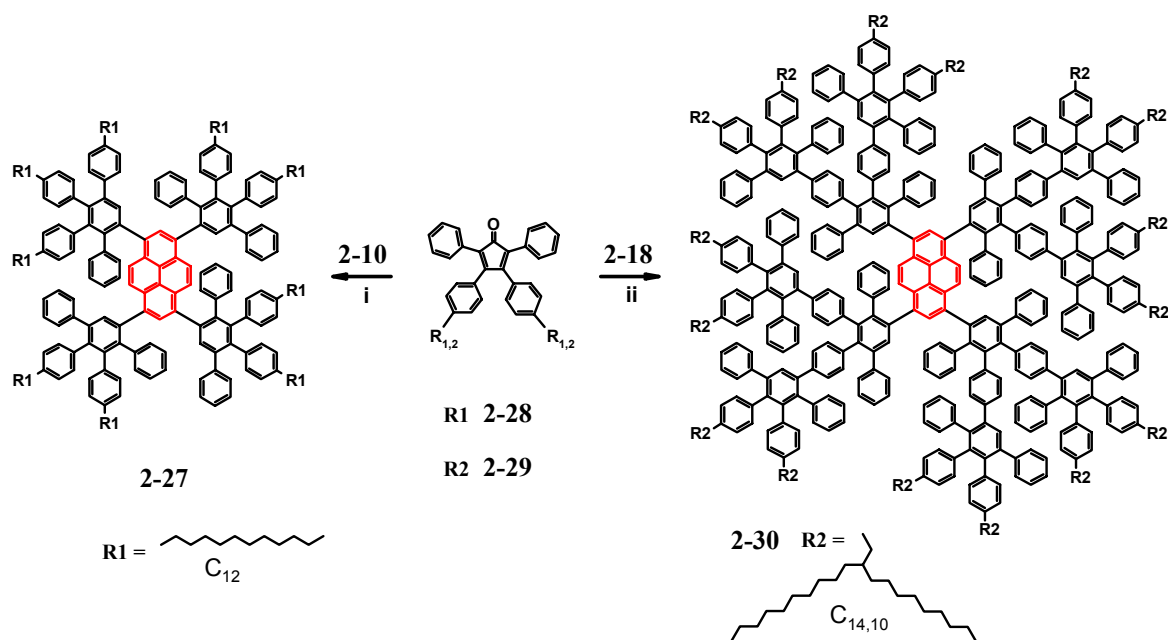
Since the first-generation dendrimer **2-16** is very badly soluble in common organic solvents, purification was achieved by repetitive precipitation from EtOH. The reduced

solubility of unsubstituted first-generation dendrimers has also been found for other cores e.g. **1-22** based on the tetraphenylmethane core **1-37**. The reaction of 1,3,6,8-tetraethynyl-pyrene (**2-10**) with the AB₂ branching unit 3,4-bis(4-triisopropylsilyl ethynylphenyl)-2,5-diphenylcyclopentadienone (**1-35**) gave the first-generation dendrimer **2-20**, decorated with 8 triisopropylsilyl (TIPS) protected ethynyl groups. Quantitative desilylation of the TIPS protecting groups with TBAF yielded the first-generation dendrimer **2-18** activated for further dendrimer growth. Subsequent DIELS-ALDER cycloaddition with the termination agent **1-32** gave the unfunctionalized second-generation dendrimer **2-19** (Scheme 19).

Higher generation dendrimers were accessible by repeating the before mentioned growth and deprotection protocol as shown in Scheme 20. Using this divergent synthetic protocol, monodisperse polyphenylene dendrimers with a pyrene core could be constructed up to the fourth-generation dendrimer **2-26**. The growth of fifth-generation polyphenylene dendrimers of the MÜLLEN-type has by now not been possible mainly due to steric crowding in the outer dendrimer shell leading to polydisperse products from the cycloaddition step.⁶⁸ The third-generation dendrimer **2-25** was obtained using a combination of convergent and divergent synthetic steps, firstly, the synthesis of the second-generation dendron **1-44**⁶⁹ and secondly, the reaction with the ethynyl substituted first-generation dendrimer **2-18**. Due to the higher steric demand of dendron **1-44**, the yield of the DIELS-ALDER cycloaddition step was reduced compared as to the yields normally achieved (> 85%). Nevertheless, once having prepared a large amount of dendron **1-44**, this method allows an accelerated synthesis of second- an higher generation dendrimers. Certainly, **2-25** would also be available by the reaction of **2-21** with tetraphenylcyclopentadienone (**1-32**). Purification of the higher generation dendrimers was achieved by either precipitation after the TIPS deprotection step or by column chromatography after the cycloaddition reaction (to remove branching unit).

2.2.3 Improving the Film Forming Ability

Amorphous glassy films with a low degree of crystallinity are very important for the fabrication of several devices, e.g. organic light-emitting diodes (OLED's). In first experiments, films of unsubstituted dendronized pyrenes, e.g. of **2-19** were prepared from spin coating or drop casting. Aggregate formation was observed, yielding films of low transparency. To investigate the use of polyphenylene dendrimers with pyrene core in OLED's, the film forming ability needed to be improved. Recently, we have shown that alkyl substituted polyphenylene dendrimers are able to self assemble onto graphite to form monolayers.⁷⁰⁻⁷² Thus, to improve the film forming properties of the herein presented dendrimers, derivatives were synthesized, possessing additional alkyl chains on the dendrimer surface. For this, the alkyl chain functionalized tetraphenylcyclopentadienones **2-28** and **2-29** were used in the last step of the divergent synthesis (Scheme 21). Tetraphenylcyclopentadienone **2-28**, carrying a linear alkyl chain is an already well known building block.⁷³ Tetraphenylcyclopentadienone **2-29** possesses branched alkyl chains and was synthesized by M. KASTLER and D. WASSERFALLEN in the group of Prof. MÜLLEN. Branched alkyl chains of that type showed to lower significantly the isotropization temperature of liquid crystalline polyaromatic hydrocarbons, additionally a much higher solubility was observed.⁷⁴ The reaction of the ethynyl substituted first-generation dendrimer **2-18** with **2-29** was carried out in refluxing diphenyl ether and afforded **2-30** as pure product. To simplify the synthesis of applicable materials, the first-generation dendrimer **2-27** was synthesized by reacting the pyrene core **2-10** with the alkyl chain functionalized tetraphenylcyclopentadienone **2-28**.



Scheme 21. Synthesis of alkyl decorated dendrimers with a pyrene core. i) 1,3,6,8-tetraethynyl-pyrene (**2-10**), 6 eq. **2-28**, *o*-xylene, 150 °C, 78%; ii) **2-18**, 14 eq. **2-29**, Ph₂O, 220 °C, 63%.

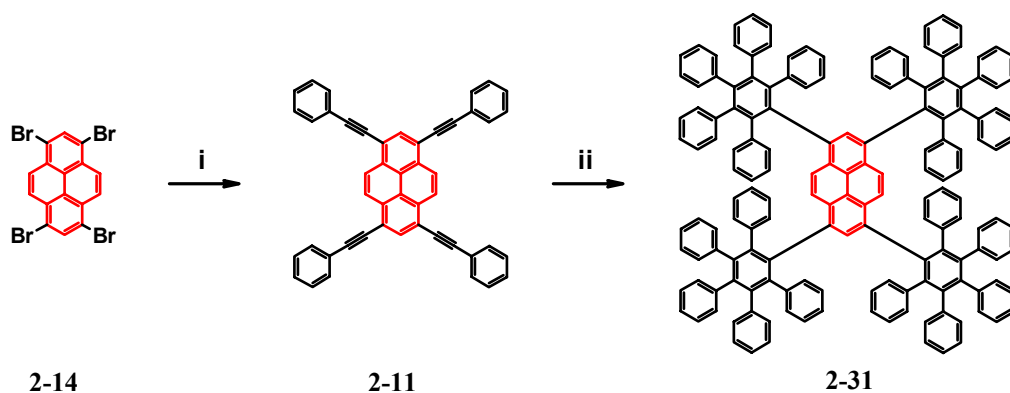
Dendrimer **2-27**, decorated with the linear alkyl chains is a solid at room temperature, whereas **2-30**, substituted with the branched alkyl chains, is a liquid. Branched alkyl chains are more potent solubilizers in contrast to linear alkyl chains. Additionally, in the case of **2-30** the double amount of alkyl chains has been attached compared with **2-27**. Thus the difference in the melting points of **2-27** and **2-30** results probably from both, the nature and the number of introduced chains.

2.2.4 Dendronized Pyrenes with a Higher Symmetry

Investigating the influence of the dendritic encapsulation on the optical and electronic properties of the pyrene core is one main goal of this work. Knowledge about the spatial arrangement of the dendritic arms around the pyrene core is therefore crucial. A particularly convincing and aesthetically appealing way of looking at dendrimer structures rests upon X-ray analysis of single crystals. However, the growth of single crystals of large dendritic molecules of suitable size and perfection has encountered a variety of problems and has so far been restricted to comparatively small molecules. Major problem is the conformational flexibility of most dendrimers.

Recently we have succeeded in growing crystals of first-generation dendrimers, constructed from different cores.⁷⁵ The first-generation dendrimer **2-16** is practically insoluble in organic solvents independent of the temperature thus not allowing the growth of single crystals. Therefore, the first-generation polyphenylene dendrimer **2-31** was synthesized, possessing an additional benzene ring on each dendritic branch (Scheme 22). HAGIHARA-SONOGASHIRA cross-coupling of 1,3,6,8-tetrabromopyrene (**2-14**) with phenylacetylene gave 1,3,6,8-tetrakis-phenylethynyl-pyrene (**2-11**) as an orange solid in 92% yield (Scheme 22). The high reaction temperature of 230 °C was chosen in order to accelerate the reaction. Since **2-11** is almost not soluble in common organic solvents, purification was

readily achieved by washing with CH_2Cl_2 . The FD-mass spectrum of **2-11** is depicted in Figure 6 proving its purity. Subsequent DIELS-ALDER cycloaddition with tetraphenylcyclopentadienone (**1-32**) gave the unsubstituted first-generation dendrimer **2-31** in 90% yield. **2-31** possesses a good solubility in organic solvents such as CH_2Cl_2 or THF.



Scheme 22. Synthesis of **2-31**, suitable for crystal formation. (i) 6 eq. phenylacetylene, $[\text{Pd}(\text{PPh}_3)_2]\text{Cl}_2$, PPh_3 , CuI , toluene, TEA, 80°C , 92%; (ii) 6 eq. **1-32**, diphenyl ether, 230°C , 90%.

Due to the higher molecular symmetry of **2-31**, a higher tendency toward crystallization was expected.

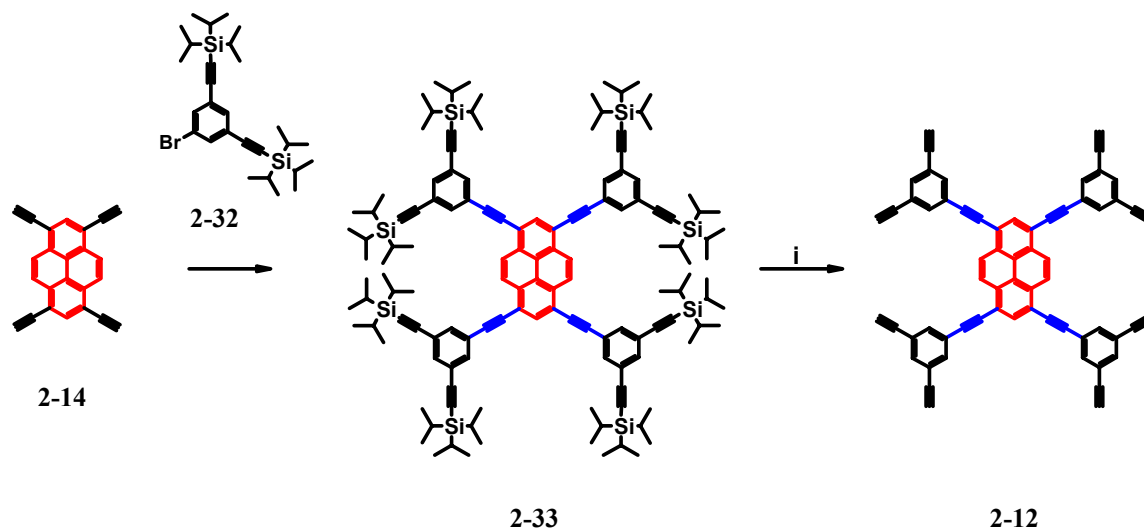
2.2.5 Modification of the Pyrene Core – Toward New Dendrimer Shapes

The shape of polyphenylene dendrimers is governed by the rigidity and shape persistence of the all-phenyl backbone. Regiospecific changes in the structure of the dendrimer backbone can therefore dramatically influence the shape of the whole dendrimer. Pyrene as core in such a dendrimer can thereby be used as a sensitive chromophore probe for the changes applied. In cooperation with Prof. P. DECK,³ the core **2-12** was synthesized. **2-12** possesses eight terminal ethynyl groups for the subsequent dendrimer growth step, which is the double amount as in core **2-10**. Scheme 23 shows the synthetic concept. As a kind of “switchable element”, additional triple bonds (blue) were introduced between the pyrene core (red) and the surrounding phenyl rings (black) from where the dendrimer growth is going to start. In between two phenyl rings, a triple bond leads to a rigid rod-like conformation. This structure motif was for example used by MOORE et al. who synthesized shape persistent dendrimers based on phenylacetylene units.⁷⁶ On the other side, hydrogenation of diphenylacetylene yields phenylethylbenzene where the single bonds in between the phenyl rings produce a lot of flexibility. When such flexibility is introduced between the core of a polyphenylene dendrimer and the surrounding dendrons, it is expected that the whole dendrimer becomes less shape persistent. One can imagine the shape persistent dendrons tumbling around the core.

Recently, E. ANDREITCHENKO investigated the influence of hydrogenation on the structure of dendrimers with triple bonds incorporated into the dendrimer backbone.⁷⁷ She observed a decrease of dendrimer diameter, which was attributed to an increased mobility of the dendritic

³ Present address: Paul A. Deck, Department of Chemistry, Virginia Tech, 107 Davidson Hall, Blacksburg VA 24061.

arms. Such structural changes in dendronized pyrenes should result in a change of the microenvironment around the pyrene core, thus leading to changed photophysical properties.

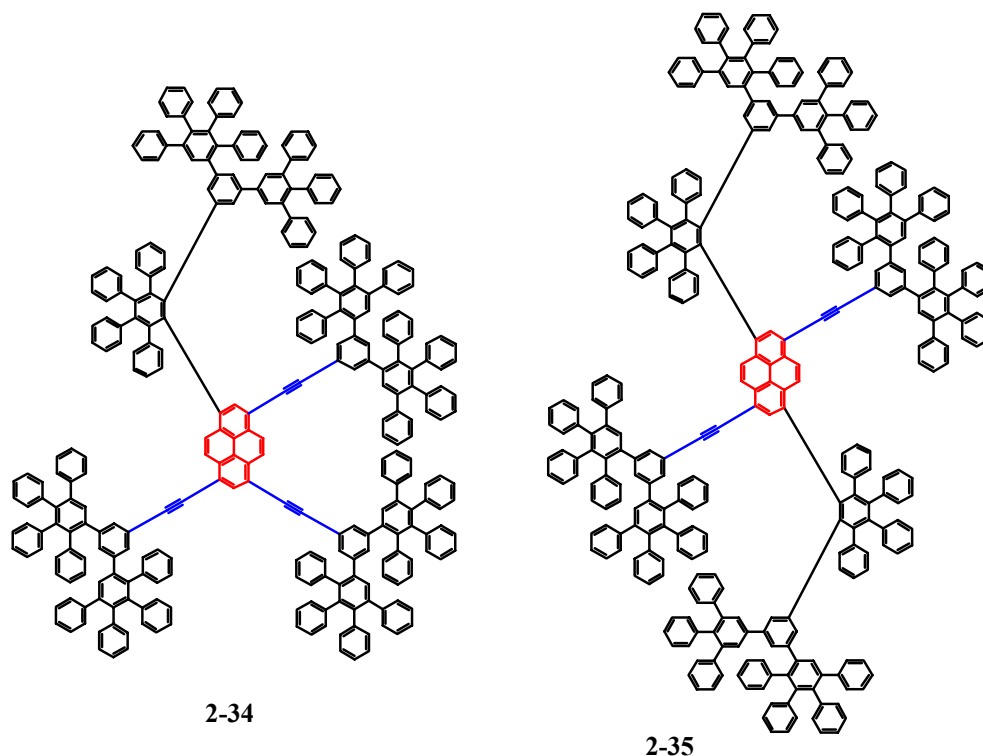


Scheme 23. Synthesis of the pyrene core **2-12**. i) TBAF, THF, 95%.

Generally, the shielding of a core in dendrimers can be enhanced by increasing the number of starting points on the core available for the growth of the dendritic branches. Four is the maximum number of bromine atoms that can be introduced via the bromination reaction of pyrene (Scheme 18). Thus, four was also the maximum number of available ethynyl bonds for the dendrimer growth. The number of starting points can therefore only be increased when further substituents are attached.

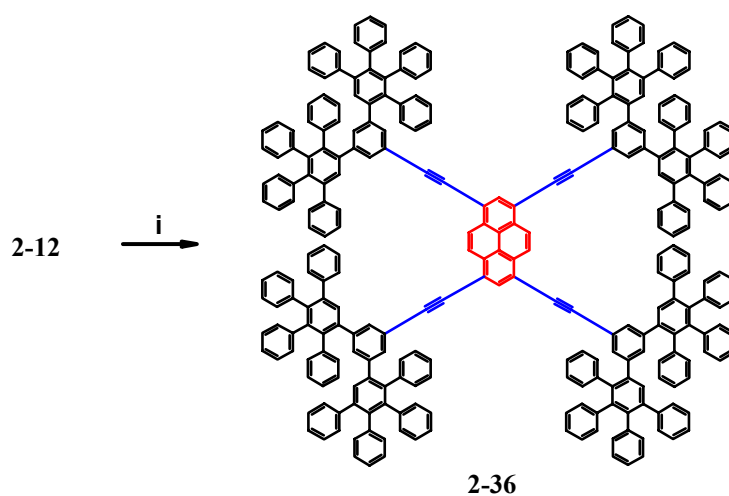
For this purpose, the building block **2-32** was synthesized (Scheme 23). Likewise an AB_2 branching unit it carries two complementary functions: firstly, a bromine, designed for the HAGIHARA-SONOGASHIRA cross-coupling with 1,3,6,8-tetrabromo-pyrene (**2-14**) and secondly, TIPS protected ethynyl groups for the further dendrimer growth. Subsequent cleavage of the TIPS protecting groups with TBAF gave the ethynyl substituted pyrene core **2-12**, activated for the growth of polyphenylene dendrimers via DIELS-ALDER cycloaddition. Likewise the pyrene core **2-10**, **2-12** is almost insoluble in common organic solvents thus allowing its purification by filtration and washing. The characterization of **2-12** is described in the next chapter. When **2-12** was reacted with tetraphenylcyclopentadienone (**1-32**) at 150 °C in refluxing *o*-xylene a mixture of products was obtained. Due to MALDI-TOF mass spectrometry, the mixture contained mostly compound **2-34**, formed by the DIELS-ALDER cycloaddition of **1-32** not only with the terminal ethynyl groups but also with one of the inner triple bonds (Scheme 24). This was in the first moment somewhat surprising since the triple bond in diphenylacetylenes undergoes DIELS-ALDER cycloaddition with tetraphenylcyclopentadienones only at higher temperatures (≈ 220 °C) mainly due to steric hindrance.^{78,79} Further experiments with higher temperature and long reaction time in a microwave apparatus yielded reaction mixtures mainly containing the two-times “overreacted” species **2-35**. Only a small amount of the three-times “overreacted” species could be detected (structure not shown). This indicated that the introduction of two additional tetraphenylcyclopentadienones (**1-32**) resulted in an inherent increase of the steric hindrance, making further cycloaddition reactions almost impossible. The overreacted species **2-34** and **2-35** could not be purified by column chromatography. Irrespective of the impurities, crude ^1H NMR signal pattern of the residual pyrene protons showed that the two additional

tetraphenylcyclopentadienones in **2-35** had reacted opposite to each other, probably because of steric hindrance.



Scheme 24. Structures of side products **2-34** and **2-35** obtained during the synthesis of **2-36**.

When the reaction temperature was decreased to 120 °C, the desired first-generation dendrimer **2-36** was obtained together with only a small amount of **2-34** (Scheme 25). Further lowering the reaction temperature led to an enormous increase of the reaction time needed to have all eight terminal ethynyl groups reacted but still small traces of **2-34** were detected. **2-36** could be separated from **2-34** by time consuming column chromatography.



Scheme 25. Synthesis of the first-generation dendrimer **2-36**. i) **1-32**, toluene, 120 °C.

Due to the inherent problems in the purification of **2-36** only an amount of 50 mg could be obtained as pure substance. Therefore, further planned hydrogenation experiments were not carried out. However, dendrimers like **2-36** might be interesting with the inner triple bonds representing potent active sides. For example, NEWKOME et al. used dendrimer embedded triple bonds for the specific incorporation of *o*-carborane moieties.⁸⁰ Such dendrimers possess a high local concentration of boron clusters and are therefore thought to be useful in disease treatment based on boron neutron capture therapy.

2.3 Characterization of the Cores and the According Dendrimers

2.3.1 Characterization of the Cores

Figure 6 shows the FD-mass spectrum of **2-10** displaying a single signal at a mass of 298.1 g·mol⁻¹, perfectly agreeing with the calculated value of 298.4 g·mol⁻¹. No signals at higher mass were observed, proving the quantitative cleavage of the four TMS groups which is a prerequisite for the subsequent defined dendrimer growth.

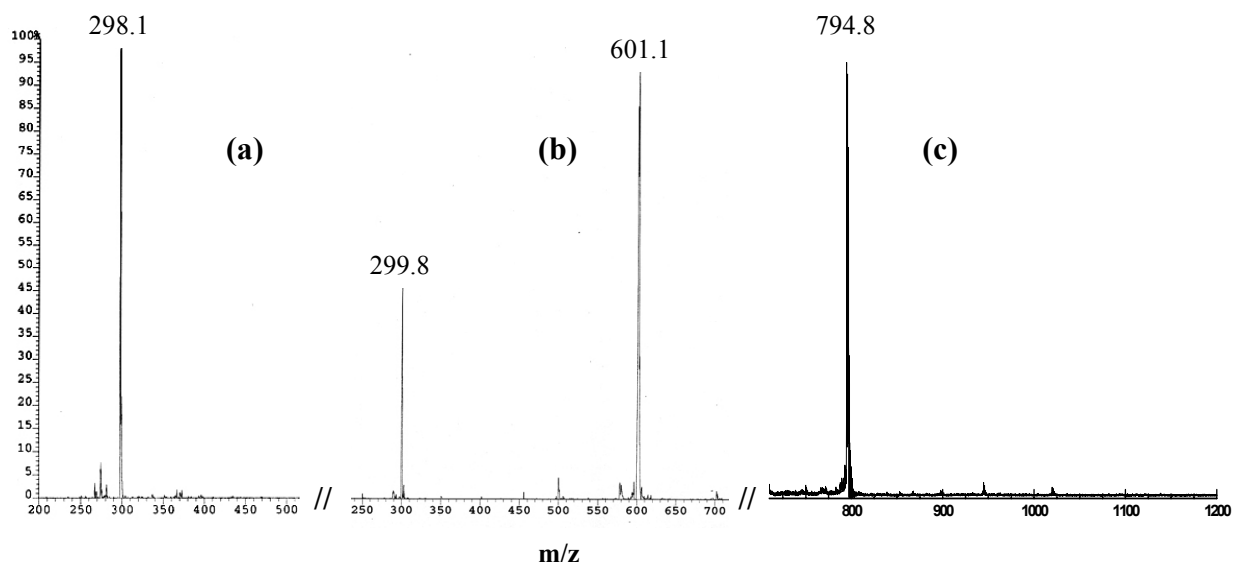


Figure 6. FD-mass spectrum of (a) 1,3,6,8-Tetraethynyl-pyrene (**2-10**), (b) 1,3,6,8-tetrakisphenylethynyl-pyrene (**2-11**), (c) MALDI-TOF mass spectra of **2-12** (calculated mass: a) 298.4 g·mol⁻¹, b) 602.7 g·mol⁻¹, c) 794.9 g·mol⁻¹).

Also for the other cores, **2-11** (Figure 6b) and **2-12** (Figure 6c), single distinctive mass signals were detected in accordance with their calculated molecular weight. In the case of **2-12**, the double-charged species (M)²⁺ could be detected at a molecular mass of 299.8 g·mol⁻¹. The ¹H NMR spectrum of 1,3,6,8-tetraethynyl-pyrene (**2-10**) is shown in Figure 7. The two singlets at $\delta = 8.70$ ppm and $\delta = 8.30$ ppm can be assigned to the six aromatic pyrene protons H_c and H_b, respectively. The ethynyl proton H_a appeared as a singlet at $\delta = 4.27$ ppm.

The full characterization of **2-10**, **2-11**, and **2-12** shows the successful substitution of the pyrene moiety with four and eight ethynyl groups, respectively. The high number of starting points for the DIELS-ALDER cycloaddition is expected to yield a dense polyphenylene shell around the pyrene core thus leading to an efficient shielding. In the next chapter, the characterization of the according dendrimers is presented.

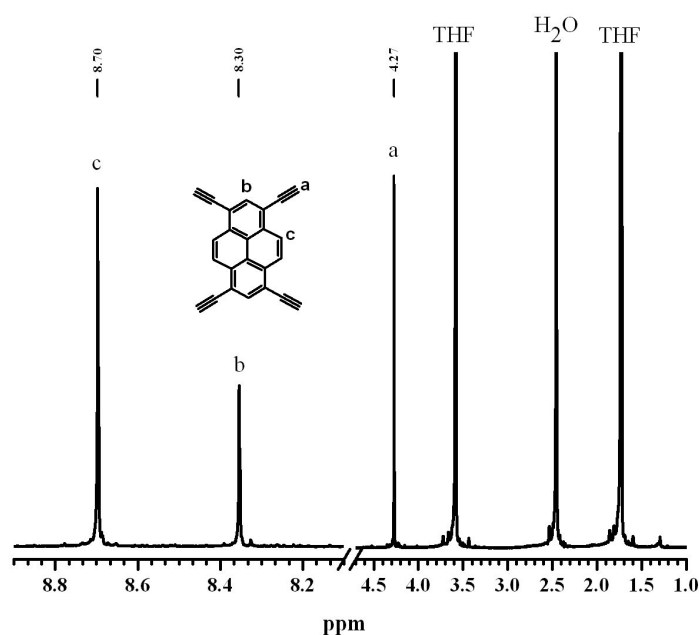


Figure 7. ^1H NMR spectrum of 1,3,6,8-tetraethynyl-pyrene (**2-10**) (500 MHz, THF, 300 K).

2.3.2 Characterization of the Dendrimers

The monodispersity of the described dendrimers could easily be verified by applying MALDI-TOF mass spectrometry. For all the dendrimers, the calculated and experimentally determined m/z ratios are in good agreement. Figure 8 shows the MALDI-TOF mass spectra of the fourth-generation dendrimer **2-26** (a) and that of the alkyl substituted second-generation derivative **2-30** (b) as typical example.

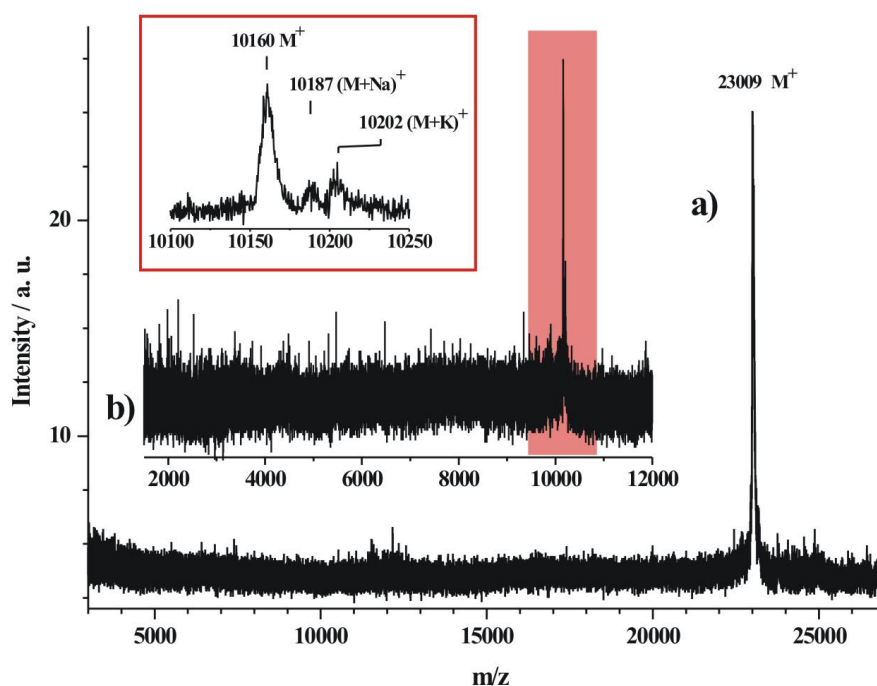


Figure 8. MALDI-TOF mass spectra of a) **2-26** and b) **2-30**. (calculated mass: a) $23031 \text{ g}\cdot\text{mol}^{-1}$, b) $10155 \text{ g}\cdot\text{mol}^{-1}$; matrix: dithranol)

The spectra were measured using 9-nitroanthracene (dithranol) as matrix. For the fourth-generation dendrimer **2-26** a molecular mass of $23009 \text{ g}\cdot\text{mol}^{-1}$ was detected. This is in good agreement with the calculated mass of $23031 \text{ g}\cdot\text{mol}^{-1}$. The addition of tetraphenylcyclopentadienone (**1-32**) and the extrusion of carbon monoxide during the DIELS-ALDER cycloaddition leads to an increase of the mass of $356 \text{ g}\cdot\text{mol}^{-1}$. The spectrum of **2-26** displayed exclusively a single signal of the desired product proving that all 32 ethynyl bonds of **2-24** had reacted. For **2-30** a single signal of the product was detected together with additional molecular mass peaks of clusters like $(M + \text{Na})^+$ and $(M + \text{K})^+$. These examples show that MALDI-TOF mass spectrometry is probably the most versatile and powerful method for proving the structural perfection of polyphenylene dendrimers with a high molecular weight.

All higher generation dendrimers possess a good solubility in common organic solvents (CH_2Cl_2 , toluene or THF, e.g. **2-20** even in hexane) thus allowing purification by column chromatography as well as their full characterization by standard spectroscopic techniques such as NMR spectroscopy. Characterization by ^1H NMR spectroscopy showed well-separated and clearly assignable signals for the aromatic pyrene protons as well as for the ethynyl or TIPS protons. Figure 9 displays the ^1H NMR spectrum of **2-18** as example.

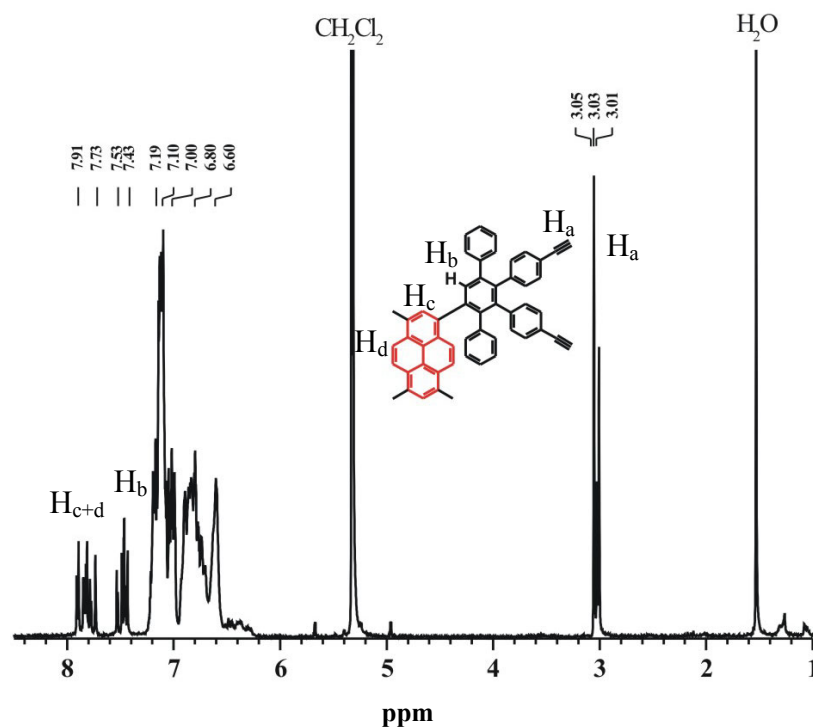


Figure 9. ^1H NMR spectrum of **2-18** (250 MHz, CD_2Cl_2 , 300K).

The ethynyl protons (H_a) appeared as a multiplett with a chemical shift of ≈ 3.0 ppm. During the DIELS-ALDER cycloaddition, two rotational conformers are produced, where the functional groups are located in the para- or in the meta-position in respect to the newly formed bond (compare also chapter 4.3). Due the existence of the different conformers, the ethynyl groups in **2-18** exhibit a different chemical environment leading to unequal chemical shifts. The same has been observed for second-generation dendrimers with a methoxy group functionalized surface.⁸¹ In the aromatic region, only some of the signals could be distinguished due to a strong signal overlap. The protons H_c and H_d of the pyrene core appeared as a multiplett at low field (7.73-7.91 ppm). For proton H_b , located on the

pentaphenyl benzene ring, a multiplett was detected at 7.43-7.53 ppm. The down-field shift of the signal of H_b can be explained by an additional deshielding due to the ring current of the adjacent phenyl rings.⁶⁸ For the higher generation dendrimers, these specific protons displayed further signals thereby reflecting the layer-by-layer build-up of the polyphenylene dendrimers (compare also Scheme 19). In the case of the ethynyl or TIPS substituted dendrimers the intensity ratios between aromatic and aliphatic signals corresponded to the expected values (see Experimental Part).

2.4 Visualization and Simulation

2.4.1 Crystal Structure of a First-Generation Dendrimer

Crystals of **2-31** suitable for structure determination were obtained from CH₂Cl₂ by slow evaporation at room temperature. Pertinent crystallographic data like unit cell parameters, interplanar angles, assignment of the planes as well as measuring conditions is provided in the Appendix. A projection of the crystal structure is shown in Figure 10.

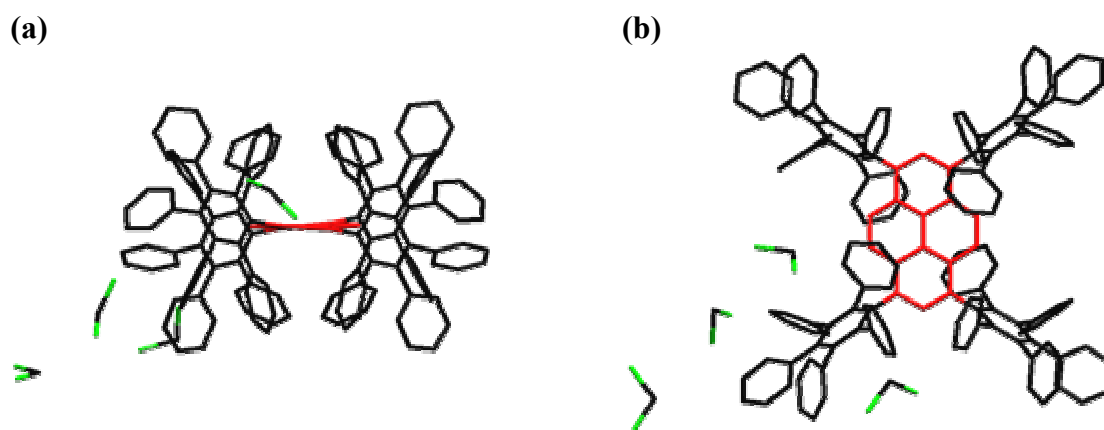


Figure 10. Crystallographic structure of **2-31** crystallized from CH₂Cl₂. (a) side view, (b) top view.

The molecule is located on a center of symmetry in the monoclinic cell (space group C2/c) and the crystal contains 8 well ordered CH₂Cl₂ molecules per dendrimer unit. The four central phenyl rings of the pentaphenylbenzene substituents are oriented approximately perpendicular to the pyrene core. Thus the dendrimer assumes the shape of a cross. The crystal structure of the first-generation dendrimer **2-31** shows that already the first-generation polyphenylene shell produces a high steric shielding in the plane as well as perpendicular to the plane of the pyrene core. Because of the shape persistence of the polyphenylene dendrons, one can expect the shielding to be even more pronounced with higher generations. The packing diagram reveals that these star-shaped molecules are packed in a fashion leaving channels in which the included solvent molecules are trapped (Figure 11).

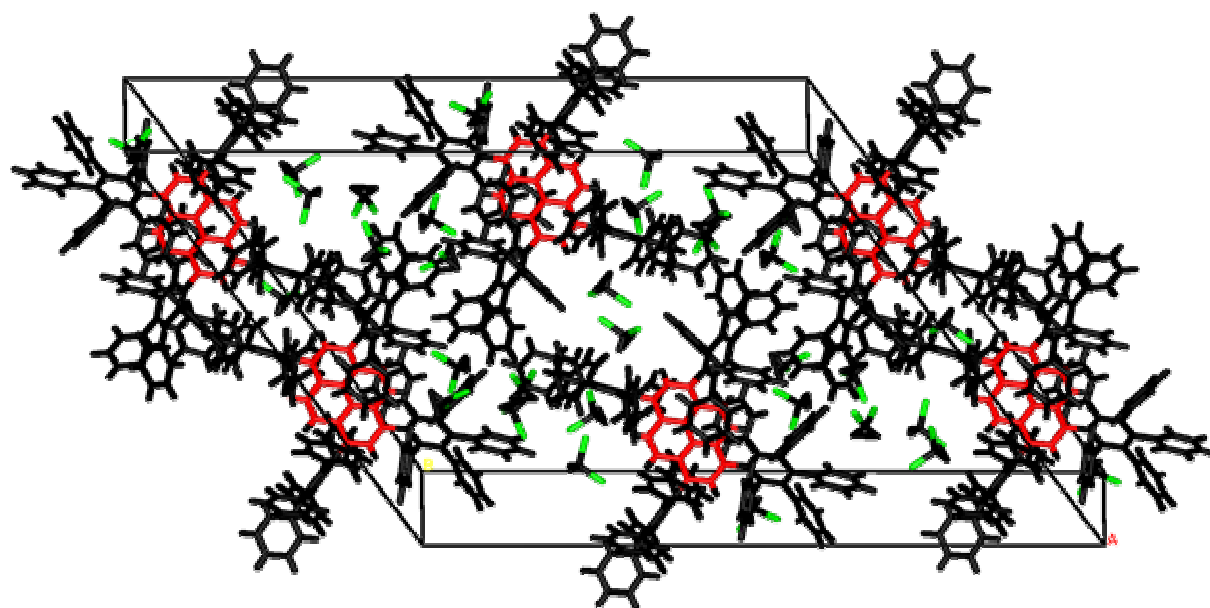


Figure 11. Packing of **2-31** in the crystals, CH_2Cl_2 .

2.4.2 Molecular Modeling

Crystals of higher generation dendronized pyrenes suitable for structure determination could not be obtained, mainly due to the large number of possible conformers. To get an impression of the size and the shape of higher generation dendrimers, molecular modeling was performed. A force field method was chosen due to the large number of atoms in the dendritic molecule. The obtained structure for the first-generation dendrimer **2-16** is depicted in Figure 14a. For the first-generation dendrimer shell, it showed an almost perfect similarity to the crystal structure of the first-generation dendrimer **2-31**, where the only difference to **2-16** is an additional benzene ring on each branch. This suggests that molecular modeling is a relatively reliable method to determine the structure of higher generation polyphenylene dendrimers. Table 1 lists the radii of the unfunctionalized dendrimers **2-16**, **2-19**, **2-25**, and **2-26**, obtained from molecular modeling using the MMFF method.⁸²

Table 1. Number of phenyl rings, molecular weight and radii of dendrimers **2-16**, **2-19**, **2-25**, and **2-26**.

	2-16	2-19	2-25	2-26
no. of phenyl rings	20	60	140	300
molecular weight / g mol^{-1}	1725	4768	10856	23031
radius / nm	1.24	2.10	2.96	3.82

An almost linear increase of the radius is found for increasing dendrimer generation with the size ranging from 1.24 nm for **2-16** to 3.82 nm for **2-26**. Contrary, the number of phenyl rings increases exponentially. When the number of phenyl rings is plotted against the radius of the corresponding dendrimer, a trend results (Figure 12a) that suggests that the dendrimer shell becomes more and more dense with increasing dendrimer generation.

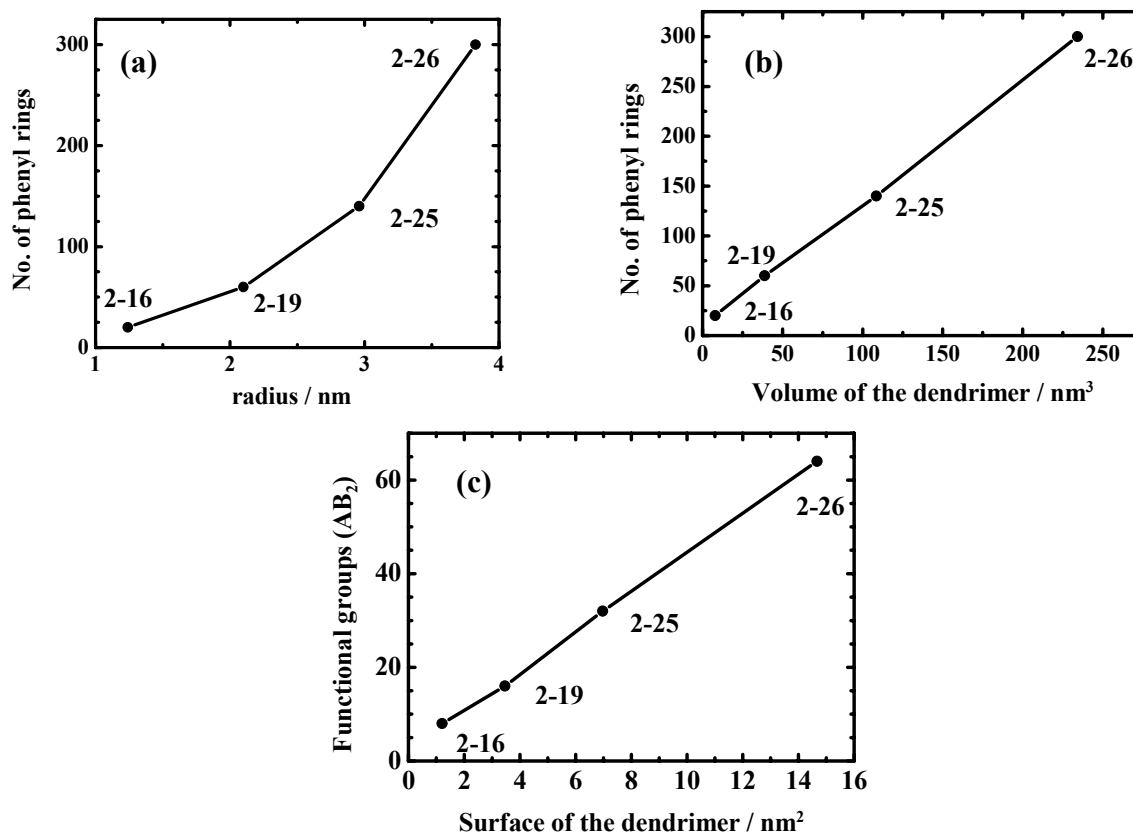


Figure 12. Number of phenyl rings versus the diameter (a), number of phenyl rings versus the dendrimer volume $V = 4/3\pi r^3$ (b), and functional groups (AB_2 branching) versus the dendrimer surface $A = 4\pi r^2$ (c) of 2-16, 2-19, 2-25, and 2-26.

However, when the number of phenyl rings is plotted against the volume of the dendrimer, a linear trend results (Figure 12b), which indicates, that the density of the dendrimer shells is constant irrespective of the generation. Furthermore, when the number of peripheral functional groups⁴ is plotted against the dendrimer surface, a linear trend results as well, indicating that the surface density of functional groups is invariant from the dendrimer generation (Figure 12c). Due to the stiff phenyl-phenyl bonds and the high density of phenyl rings, back folding of dendrons is not possible in the MÜLLEN-type dendrimers, therefore these dendrimers fall into the class of “dense-shell” dendrimers (see also chapter 1.5).

“Dense-shell” opposite “dense-core” model

The first theoretical work about the three-dimensional structures of dendrimers was presented by DE GENNES and HERVET, who developed the concept of dense.⁸³ Their self-consistent field model indicated that dendrimers can freely grow up to a certain limiting generation. Due to the fact that the number of branches increases exponentially with the number of generations, whereas the radius of the dendrimers increases only linearly, the outer shells have progressively higher densities leading to a globular architecture. DE GENNES and HERVET concluded that dendrimers must have lower densities in the center than on the surface and that terminal reactive groups should be on the surface (“dense-shell model”). Recent

⁴ Calculated for an endcapping reagent that has been used in the last step of the dendrimer synthesis, carrying two functional groups.

empirical studies (especially on the position of functional groups within dendrimers) cannot confirm the ideal structure which has been postulated by DE GENNES and HERVET. Viscosimetry,⁸⁴ NMR,⁸⁵ and fluorescence depolarization⁸⁶ measurements have shown for FRÉCHET-type polyaryl-ether dendrimers that, due to the flexible nature of these dendrimers, end groups are found throughout the dendrimer volume. Furthermore, the shape and size of the dendrimers are also solvent dependent. Both of these trends are in qualitative agreement with the model of LESCANEC and MUTHUKUMAR,⁸⁷ implying that the end groups can be found throughout the dendrimer volume. Small-Angle-Neutron-Scattering confirms the flexible character of poly(propylene imine) dendrimers, showing that this type has a homogenous density distribution.⁸⁸ Subsequent theoretical work, however, has demonstrated convincingly that flexible dendrimers exhibit their maximum density in the core of the molecule (“dense-core model”) and that there is a finite probability for the end groups to be located at any position within the molecule.^{89,90}

The three-dimensional structures obtained from molecular modeling showed that all higher-generation dendrimers constructed from the pyrene core **2-10** adopt ball-like structures. This can be attributed to the substitution pattern on the pyrene core, directing the dendrimer growth in all directions. As an example, the three dimensional structure of the fourth-generation dendrimer **2-26** is shown in Figure 13. Fully elongated dendrimer arms are displayed which fits with physical data of polyphenylene dendrimers obtained by different methods,⁹¹⁻⁹³ showing that the rigidity of the polyphenylene backbone and the high density of the outer shell prevent backfolding of dendrimer arms and lead to the shape persistence of the herein described type of dendrimers.

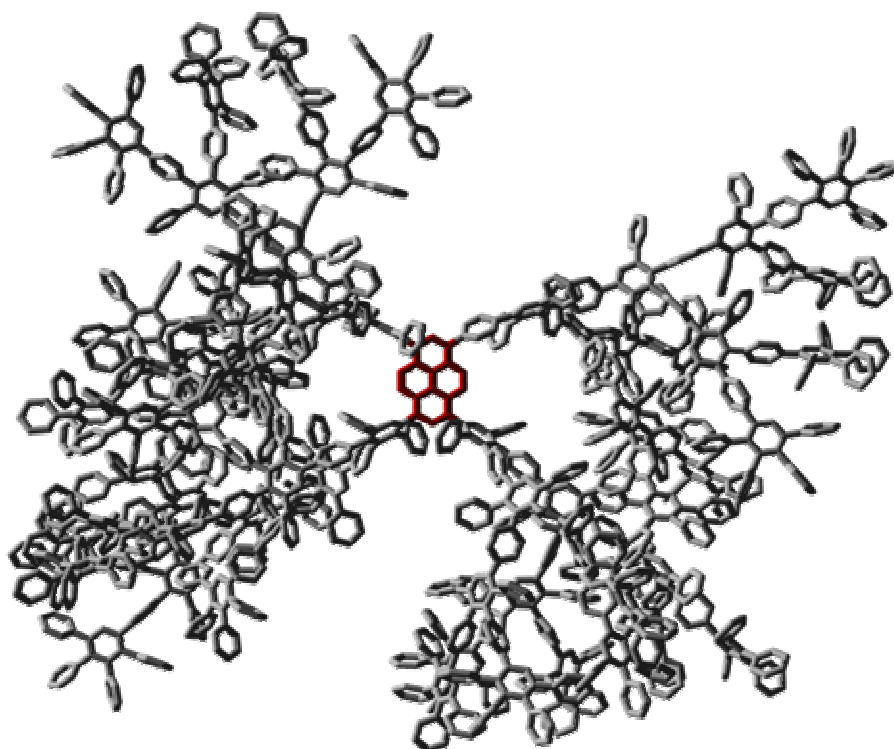


Figure 13. Three-dimensional structure of **2-26**, obtained by molecular modeling using the MMFF method.⁸²

Irrespective of the large dendritic shell, the pyrene core still seems to be accessible for small molecules as larger voids can be seen reaching from the outside to the center.

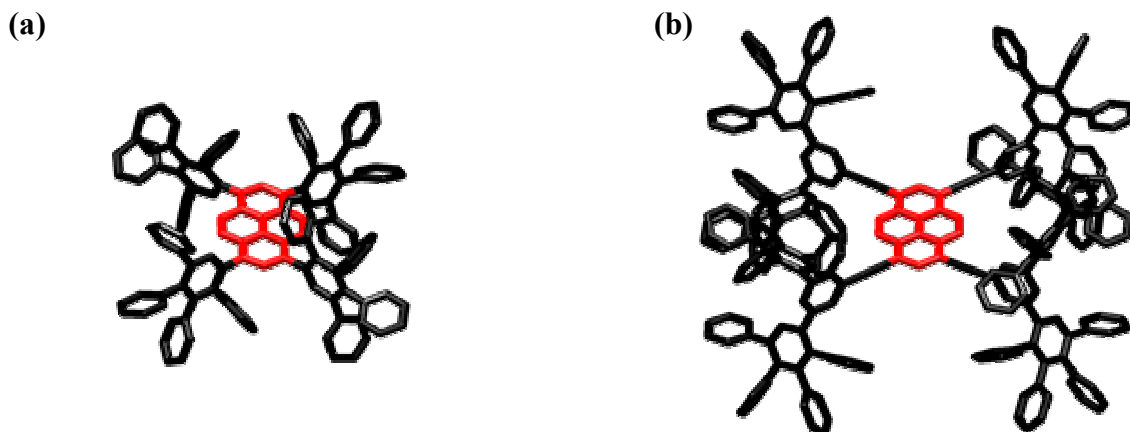


Figure 14. Three dimensional structures of (a) **2-16** and (b) **2-36** obtained by molecular modeling using the MMFF method.⁹⁴

Three-dimensional structures of the first-generation dendrimers **2-16** and **2-36** obtained by molecular modeling showed a significantly enlarged dendritic shell for **2-36** (Figure 14). This can be attributed to two facts. Firstly, the double amount of ethynyl bonds with the core **2-12** leads to a more extended and dense polyphenylene shell around the core. Secondly, the inner triple bonds elongate the dendrimer arms thereby enlarging the dendrimer diameter. However, the implemented triple bonds lead to significantly more free space around the pyrene core when compared with the structure of **2-16**. As described on the last pages X-ray crystallography and molecular modeling can provide a detailed insight into the conformation and shape of polyphenylene dendrimers. The herein investigated dendronized pyrenes exhibit a spherical shape with the pyrene core densely surrounded by the polyphenylene shell.

2.5 Pyrene as Chromophore

In the next chapters, the influence of the surrounding polyphenylene shell upon the photo-physical properties of the pyrene core is investigated using UV/vis spectroscopy in solution as well as in solid-state. Further, fluorescence quenching experiments as well as temperature dependent fluorescence spectroscopy will be applied for the optical characterization of these new materials.

2.5.1 Absorption and Emission in Solution

The absorption and emission spectra of pyrene, the unsubstituted dendrimers **2-16**, **2-19**, **2-25**, and **2-26** are depicted in Figure 15. Corresponding wavelengths of the maxima ($\lambda_{\text{max abs}}$, $\lambda_{\text{max em}}$) and extinction coefficients $\epsilon(\lambda)$ are summarized in Table 2. In the absorption spectra of the first- to fourth-generation dendrimers **2-16**, **2-19**, **2-25**, and **2-26** two distinct bands, one in the visible region (≈ 395 nm) and the other in the UV region (280 nm), were observed. The absorption in the visible is due to the π - π^* -transition of the pyrene core and showed a red-shift of up to 55 nm as compared to unsubstituted pyrene (337 nm), in accordance with other phenyl substituted pyrenes e.g. 1,3,6,8-tetraphenylpyrene (380 nm).⁹⁵ The absorption band in the UV region can be predominantly attributed to the polyphenylene dendrons,^{96,97} which is indicated by a linear increase of the molar extinction coefficients $\epsilon(\lambda)$ with the size of the attached polyphenylene dendrons (Table 2).

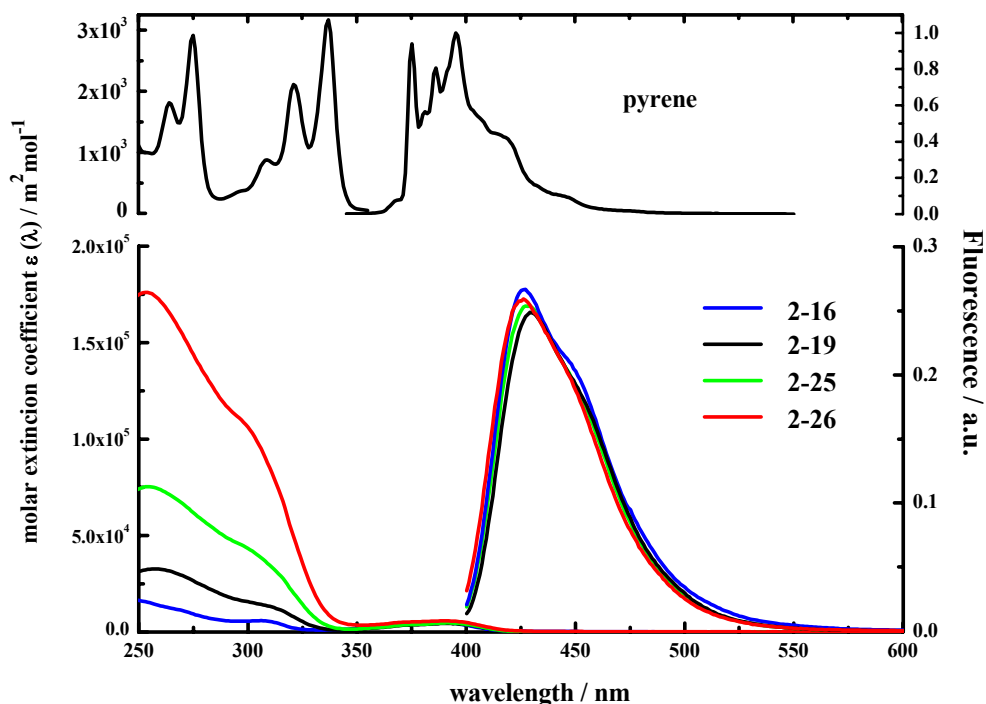


Figure 15. Absorption and emission spectra of dendronized pyrenes **2-16**, **2-19**, **2-25** and **2-26** in CHCl_3 . The emission spectra are excited at 390 nm and normalized to the same optical density at the excitation wavelength.

Going to higher generations has no influence on the absorption maxima and the extinction coefficients of the pyrene core. The molar extinction coefficients are in line with values reported by others, e.g for pyrene-labeled (hydroxypropyl)cellulose.⁹⁸

Table 2. UV/vis absorption and emission data of unsubstituted pyrene and the dendronized pyrenes **2-16**, **2-19**, **2-25**, **2-26**, and **2-30**.

	$\lambda_{\text{max abs}} / \text{nm}$	$\lambda_{\text{max em}} / \text{nm}$	$\epsilon_{310 \text{ nm}} / \text{m}^2 \text{mol}^{-1} \text{ (a)}$	$\epsilon_{390 \text{ nm}} / \text{m}^2 \text{mol}^{-1} \text{ (a)}$
pyrene	337, 321, 309, 275	395, 386, 381, 375		
2-16	391, 306, 248	425	$5.51 \cdot 10^3$	$4.83 \cdot 10^3$
2-19	393, 258	427	$1.29 \cdot 10^4$	$4.35 \cdot 10^3$
2-30	391, 259	427	$1.56 \cdot 10^4$	$4.48 \cdot 10^3$
2-25	394, 255	425	$3.46 \cdot 10^4$	$4.73 \cdot 10^3$
2-26	394, 253	423	$8.51 \cdot 10^4$	$5.84 \cdot 10^3$

(a) extinction coefficient of absorption at 310 and 390 nm.

The emission spectra of **2-16**, **2-19**, **2-25**, and **2-26**, obtained upon excitation of the pyrene core at 390 nm, displayed a red shifted emission (425 nm) compared to the emission of parent pyrene (395 nm). No change of the emission maximum or the fluorescence intensity of the pyrene core was observed upon changing the dendrimer generation.

Recently, polyphenylene dendrimers with a perylene core were synthesized in our group. There, excitation at the absorption wavelength of the polyphenylene dendrons resulted in an emission of the perylene core, indicating an efficient intramolecular energy transfer.⁹⁶

Excitation of the polyphenylene shell of dendronized pyrenes at 310 nm resulted in a strong emission of the pyrene core at 425 nm indicating an efficient energy transfer from the polyphenylene dendrons to the pyrene core (Figure 16). With increasing dendrimer generation, the fluorescence intensity of the dendrimers showed a linear increase up to the third-generation **2-25**. (inset in Figure 16). Remarkably, the fluorescence intensity of **2-25** when excited at 390 nm is significantly lower than if excited at 310 nm, which underlines the efficiency of the energy transfer. However, going from the third- to the fourth-generation dendrimer only a small increase of the fluorescence intensity was found indicating a decrease of the energy transfer efficiency. This is surprising since the fourth-generation dendrimer **2-26** (300 phenyl rings) consists of more than double the amount of phenylenes as in the third-generation dendrimer **2-25** (140 phenyl rings) and should therefore theoretically be able to transfer significantly more energy to the core than **2-25**.

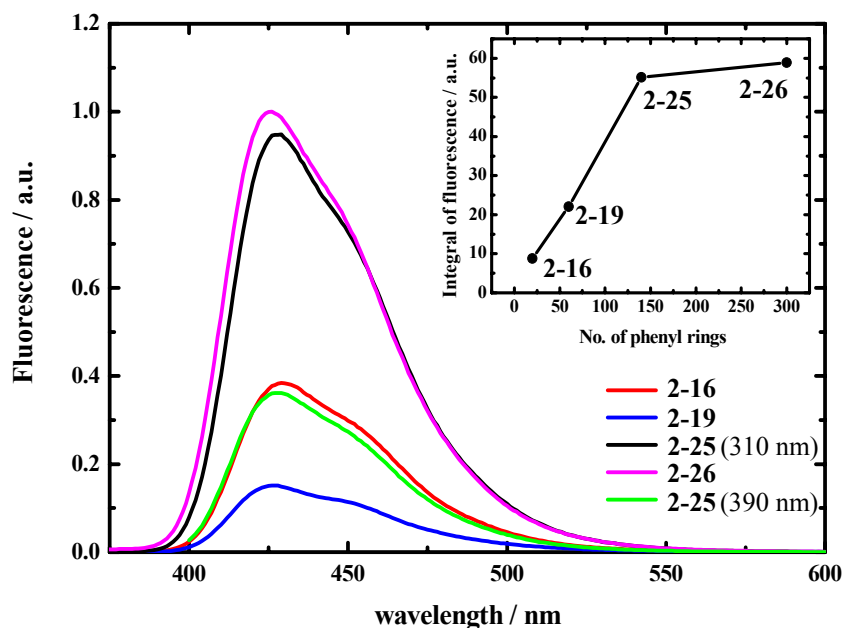


Figure 16. Fluorescence emission spectra of **2-16**, **2-19**, **2-25**, and **2-26** in CHCl_3 excited at 310 nm. The spectra were normalized to the same concentration of pyrene. The emission spectrum of **2-25**, directly excited at the absorption maximum of pyrene (390 nm) at the same concentration, is also shown. Inset: Integral of fluorescence versus number of phenyl rings; excitation at 310 nm.

The inner ring of the pentaphenylbenzene unit of the fourth-generation layer has a calculated distance to the pyrene core of ≈ 3.3 nm. Since an efficient energy transfer was observed only up to third-generation dendrimer shell, it can be suggested that the FÖRSTER radius for dendronized pyrenes has a value of around 3.3 nm.

“FÖRSTER resonance energy transfer” (FRET)⁹⁹

Fluorescence energy transfer describes an energy transfer mechanism between two fluorescent molecules. A fluorescent donor is excited at its specific fluorescence excitation wavelength. By a long-range dipole-dipole coupling mechanism, this excited state is then nonradiatively transferred to a second molecule, the acceptor. The donor returns to the electronic ground state. The described energy transfer mechanism is termed “FÖRSTER resonance energy transfer” (FRET), named after the German scientist THEODOR FÖRSTER. When both molecules are fluorescent, the term “fluorescence resonance energy transfer” is

often used. The FRET efficiency is determined by three parameters: a) the distance between the donor and the acceptor, b) the spectral overlap of the donor emission spectrum and the acceptor absorption spectrum, and c) the relative orientation of the donor emission dipole moment and the acceptor absorption dipole moment. An efficient interaction radius R_0 can be calculated from the steady-state spectra and the fluorescence quantum yield of the donor chromophore (Φ_D) with the equations 1 and 2

$$R_0^6 = 8.875 \cdot 10^{-5} \frac{\kappa^2 \phi_D J}{n^4} \quad \text{Eq. 1}$$

where κ^2 in a first approximation is equal to 2/3 for the usually assumed random orientation of the chromophores, Φ_D is the donor fluorescence quantum yield, n is the refractive index of the solvent, and J is the spectra overlap integral defined by

$$J = \frac{\int F_D(\lambda) [\varepsilon_A(\lambda)] \lambda^4 d\lambda}{\int F_D(\lambda) d\lambda} \quad \text{Eq. 2}$$

where $F_D(\lambda)$ represents the molar extinction coefficient of the acceptor moiety and $\varepsilon(\lambda)$ represents the donor fluorescence spectrum on a wavelength (λ) scale. The donor-to-acceptor distance r influences the FRET efficiency with an inverse 6th order law due to the dipole-dipole mechanism. One major field where FRET is used is biophysics. Since conformational changes of the donor or acceptor chromophore strongly influence the FRET efficiency, it is a powerful tool for the structural investigation of proteins and nucleic acids

Applying equation 2, spectral overlaps J were calculated using the absorption spectra of **2-19**, **2-25** and **2-26** in CHCl_3 and emission spectra and fluorescence quantum yield from the according second- to fourth-generation dendrimers with a tetraphenylmethane core.¹⁰⁰ Values of $J = 5.1 \cdot 10^{-14} \text{ cm}^6 \cdot \text{mmol}^{-1}$ for **2-19**, $5.8 \cdot 10^{-14} \text{ cm}^6 \cdot \text{mmol}^{-1}$ for **2-25**, and $8.0 \cdot 10^{-14} \text{ cm}^6 \cdot \text{mmol}^{-1}$ for **2-26** were obtained. Compared to polyphenylene dendrimers with a perylenediimide core, the overlap was increased by about a factor of seven. Using equation 2 and assuming a κ^2 of 0.67 for random orientation and with the refractive index of chloroform ($n = 1.446$) the Förster radius R_0 was determined. Values of $R_0 = 3.2 \text{ nm}$ (**2-19**), 3.6 nm (**2-25**), and 3.8 nm (**2-26**) resulted. Based on the emission spectra for **2-19**, **2-25**, and **2-26** (Figure 16), and assuming that **2-19** is > 99% efficient in energy transfer, **2-25** is about 95% and **2-26** is about 40%. These values suggest that the average distance from a phenyl donor to the pyrene core increases from about 2.0 nm for **2-27** to 3.0 nm for **2-25** and 4.0 nm for **2-26**. The distances match quite well with the radii of the dendrimers determined from molecular modeling (Table 1) and indicate that the increased donor-acceptor distance leads to the decreased energy transfer efficiency.

The fluorescence quantum yields of **2-16**, **2-19**, **2-25**, and **2-26** were determined using 9,10-diphenylanthracene as the reference chromophore.¹⁰¹ Upon excitation at a wavelength of 350 nm, the quantum yields for **2-16**, **2-19**, **2-25**, and **2-26** were found to be 0.96, 0.97, 0.97, and 0.92 in CHCl_3 , respectively (Table 3). Only a small decrease of the fluorescence quantum yield was observed going from the third- to the fourth-generation dendrimer.

Table 3. Fluorescence quantum yields of dendrimers **2-16**, **2-19**, **2-25**, and **2-26** in CHCl₃.

	2-16	2-19	2-25	2-26
Fluorescence quantum yield (Q _f) ^(a)	0.96 ± 0.03	0.97 ± 0.02	0.97 ± 0.03	0.92 ± 0.02

(a) Errors were estimated using Gauss's law of propagation of error.

This is in contrast to results from similarly polyphenylene dendronized perylene where the fluorescence quantum yield decreased from 0.83 down to 0.73 for a third-generation dendrimer.¹⁰² New non-radiative deactivation pathways were suggested in this case, which do not seem to apply to a pyrene core.

Pyrene exhibits a sensitive solvatochromic behavior, with the relative intensity of emission bands dependent on the solvent polarity.^{15,16} FRÉCHET et al. used this effect to determine the influence of chain length and solvent polarity on the encapsulation of a poly(ϵ -caprolactone) dendronized pyrene.¹⁰³ They found a solvation-induced encapsulation effect mainly due to a structural extent and collapse of the flexible dendrimer backbone. This should also be tested for polyphenylene dendronized pyrenes. Accordingly, the TIPS substituted dendrimers **2-20** and **2-23** were dissolved in cyclohexane and CH₂Cl₂, respectively. The TIPS-groups were necessary to ensure the solubility of the dendrimers in cyclohexane. Emission spectra showed a small bathochromic shift of the pyrene emission when changing from the polar CH₂Cl₂ to the unpolar cyclohexane. (Table 4). One can attribute this to the creation of a stable hydrophobic environment around the pyrene core, due to the large number of surrounding phenyl rings. This result correlates with the structure of the first-generation dendrimer **2-31**, determined by X-ray crystallography, showing the polyphenylene dendrons densely surrounding the pyrene core (Figure 10).

Table 4. Influence of solvent polarity on the emission maximum of the dendronized pyrenes **2-20** and **2-23**.

	$\lambda_{\text{max em}} / \text{nm}$	
	CH ₂ Cl ₂	cyclohexane
2-20	424	429
2-23	425	429

Since the bathochromic shift observed for **2-20** was almost the same as for **2-23**, one can suggest the hydrophobic environment to be present even in the first-generation dendrimer **2-20**. Opposite to dendrimers constructed from flexible building units, the shape and conformation of the stiff polyphenylene dendrons do not change with the polarity of the surrounding medium.

2.5.2 Absorption and Emission in Solid-State

Solid-state absorption and fluorescence spectra of **2-30** have been recorded for films prepared by spin-coating from toluene solutions onto quartz substrates, and are depicted in Figure 17. The spectra of the films showed the absorption maximum of the pyrene core at 393 nm, not shifted within the error of measurement as compared to the solution spectrum. The shoulder in the absorption band in the UV region at 260 nm can be assigned to the polyphenylene dendrons.⁹⁶ The solid-state emission maximum of unsubstituted pyrene

($\lambda_{\text{max em}} = 446 \text{ nm}$) was red shifted by 51 nm compared to that in solution ($\lambda_{\text{max em}} = 395 \text{ nm}$), indicating that emission in solid-state occurred mainly from aggregated species. In contrast, **2-30** exhibited an emission spectrum with a maximum located at $\lambda = 449 \text{ nm}$, which was a bathochromic shift of only 20 nm. Almost no broadening relative to solution spectra was observed. The smaller bathochromic shift of **2-30** in the solid-state can be attributed to a suppressed aggregate formation of the pyrene core due to the shielding by the second-generation dendrons.

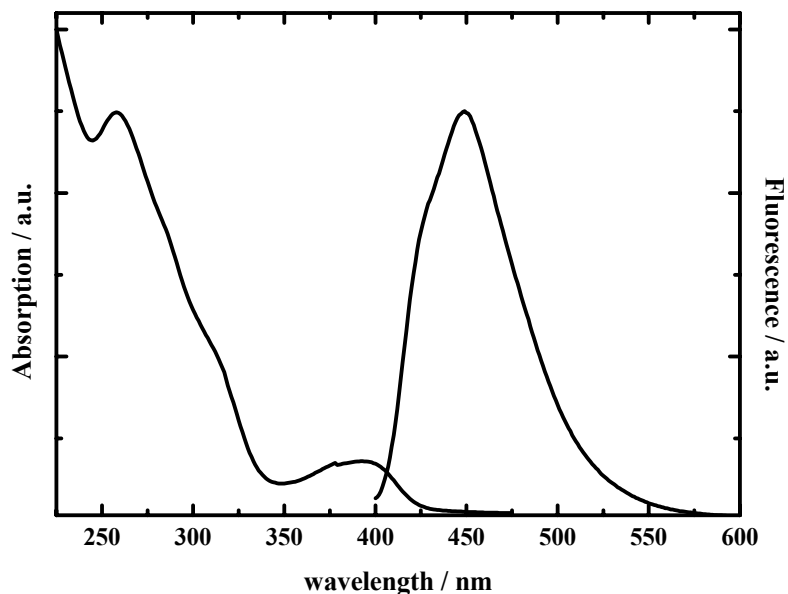


Figure 17. Absorption and emission spectra of **2-30** in a film prepared from toluene solution by spin coating (excitation at 310 nm).

Figure 18 shows a picture of films of unsubstituted pyrene (left side) and dendrimer **2-30** (right side) obtained by simple drop casting from toluene solution on a quartz substrate.

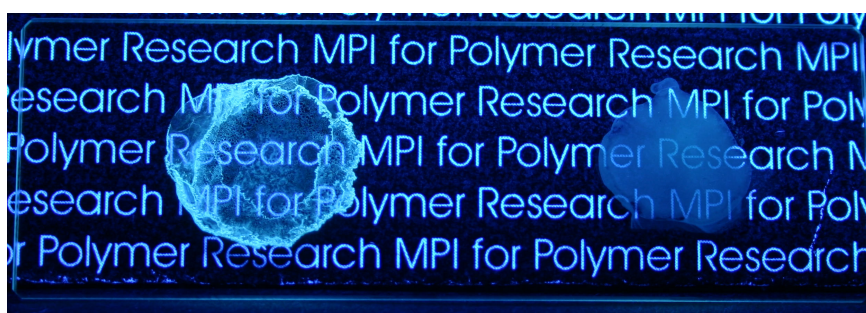


Figure 18. Picture of films of unsubstituted pyrene (left side) and dendrimer **2-30** (right side), obtained by drop casting from toluene solution on a quartz substrate.

It can clearly be seen that the transparency of thin films of the dendritic structure **2-30** is higher as compared to those prepared from unsubstituted pyrene mainly due to crystallization of the nondendronized chromophore. The branched alkyl chains attached on the dendrimer surface of **2-30** obviously prevented the crystallization of the nanospheres.

2.5.3 Fluorescence Quenching Experiments

The fluorescence intensity of a fluorophore depends on the natural lifetime of its first excited singlet state and on the rate that non-radiative processes deactivate the first excited state. Thereby, quenching processes depend significantly on the location and accessibility of the fluorophore within a macromolecular structure. Fluorescent probes, such as dansyl chloride, are therefore used especially in biochemistry to study the various binding sites in large macromolecules.^{104,105}

For pyrenyl moieties on the focal point of poly(amido) dendrimers **2-6** (Scheme 14) decreasing STERN-VOLMER quenching constants were found with increasing dendrimer generation.²⁸ This was attributed to a higher steric congestion with increasing dendron size, making the chromophore less accessible.

STERN-VOLMER fluorescence quenching

The Stern-Volmer expression (eq. 3) provides a link between the experimental measurables and the physical aspects of the quenching process:^{106,107}

$$F_0/F = 1 + K_{SV} [Q] = 1 + \langle k_q \rangle \langle \tau \rangle_0 [Q] \quad \text{Eq. 3}$$

In this expression F_0 , F , K_{SV} , $\langle k_q \rangle$, $\langle \tau \rangle_0$ and $[Q]$ are the fluorescence intensity in the absence and presence of quencher, STERN-VOLMER quenching constant, average bimolecular quenching constant, mean fluorophore lifetime in the absence of quencher, and the analytical concentration of quencher, respectively.

We used nitromethane and N,N-dimethylaniline, respectively, both well-known molecular charge transfer quenchers.¹⁰⁸ During charge-transfer quenching, transfer of an electron (charge) takes place from the pyrene excited singlet state to the quencher with the formation of a transient charge-transfer complex thereby decreasing pyrene fluorescence.

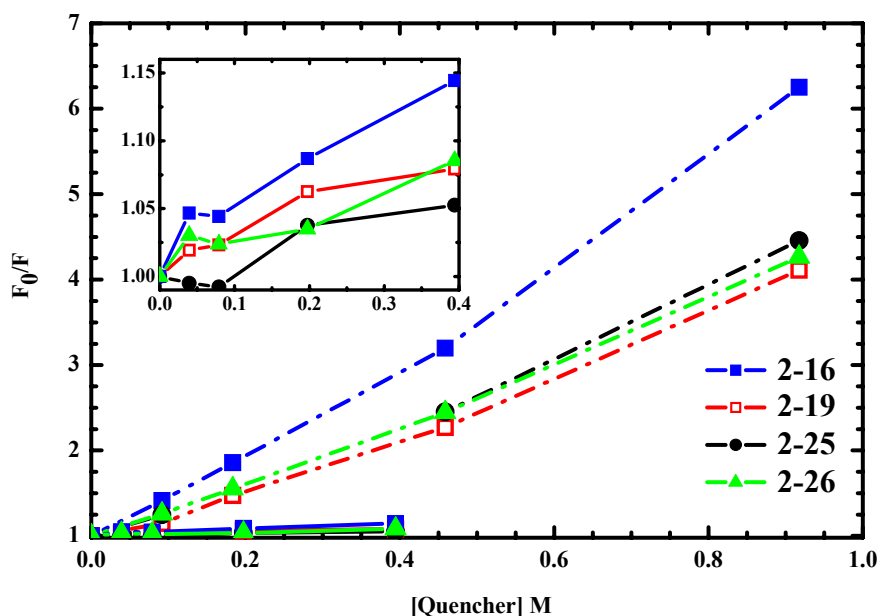


Figure 19. STERN-VOLMER quenching plots for nitromethane (dash-dot) and N,N-dimethylaniline (solid) in CHCl_3 , measured for the first- to the fourth-generation dendrimers **2-16**, **2-19**, **2-25**, and **2-26**, respectively.

The fluorescence quenching of polyphenylene dendronized pyrenes was well described by the STERN-VOLMER expression (nitromethane: $r^2 > 0.996$; N,N-dimethylaniline: $r^2 > 0.97$) (Figure 19). For nitromethane, the STERN-VOLMER quenching constant K_{SV} decreased clearly when going from the first-generation dendrimer **2-16** to the second-generation dendrimer **2-19** (Table 5). In particular, no further decrease of K_{SV} was observed for the third- and fourth-generation dendrimers **2-25** and **2-26**, respectively. For N,N-dimethylaniline, K_{SV} values were about 15 times lower than for nitromethane. Similar to nitromethane, K_{SV} decreased significantly only between the first- and the second-generation dendrimer **2-16** and **2-19**, respectively.

Table 5. STERN-VOLMER quenching constant K_{SV} for **2-16**, **2-19**, **2-25**, and **2-26**, respectively, obtained by different quenching agents.

Quencher	K_{SV} / M^{-1} (a)			
	2-16	2-19	2-25	2-26
CH ₃ NO ₂	5.72 ± 0.28	3.43 ± 0.19	3.77 ± 0.22	3.57 ± 0.12
C ₆ H ₅ N(CH ₃) ₂	0.33 ± 0.04	0.19 ± 0.03	0.16 ± 0.04	0.19 ± 0.04

(a) Errors were estimated using Gauss's law of propagation of error.

The values obtained for K_{SV} were much smaller (factor 100) than those reported for poly(amido) dendrimers **2-6** with pyrene attached at the focal point.²⁸ One can attribute this to two reasons: Firstly, polyphenylene dendrimers possess a less polar interior than poly(amido) dendrimers thus the diffusion of polar quenchers like nitromethane to the pyrene core is not favoured for the former ones. Secondly, in our case the dendrimers were constructed from a fourfold substituted pyrene core, thus a much higher steric hindrance was produced than for the single substituted pyrene in the poly(amido) dendrimers. The herein obtained K_{SV} values significantly decreased when going from the first-generation dendrimer **2-16** to the second-generation dendrimer **2-19**. Remarkably enough, K_{SV} did not further decrease for the third- and fourth-generation dendrimers. Thus, one can suggest that the second-generation dendrons already produced the maximum steric shielding that one can achieve in this case. The much larger K_{SV} values found for nitromethane compared to N,N-dimethylaniline can be attributed to a size exclusion effect provided by the polyphenylene shell, thus hampering the diffusion of the larger quencher N,N-dimethylaniline.

Another important class of molecular quenching agents exhibits external heavy-atom-quenching efficiencies that are roughly proportional to Z^4 where Z is the atomic number. Quenchers of this type, as shown by WILKINSON and co-workers,¹⁰⁹ quench fluorescence by enhancing intersystem crossing by spin-orbit coupling which is accompanied by a correspondingly enhanced triplet-state population. When methyl iodide was used, no fluorescence quenching was observed. The efficiency of heavy-atom-quenchers depends more on the distance between quencher and chromophore compared as for the before described charge-transfer-quenchers, thus one can suggest that the shielding of the pyrene core was that efficient, that methyl iodide was not able to come in a distance where quenching is possible.

2.5.4 Temperature Dependent Fluorescence Spectroscopy

In concentrated solutions pyrene shows strong characteristic excimer fluorescence at 475 nm which arises from the close proximity of two pyrene molecules.^{110,111}

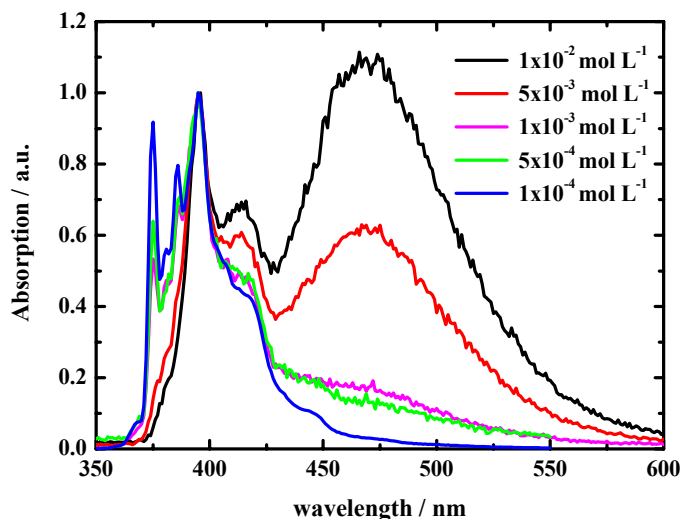


Figure 20. Characteristic excimer fluorescence of pyrene in solutions with different concentration (Excitation: 337 nm, solvent: CHCl_3). Spectra are normalized to the emission maximum of the nonaggregated species at 395 nm.

The formation of pyrene excimer can be observed in solutions with a pyrene concentration of $5 \cdot 10^{-4} \text{ mol l}^{-1}$ and higher (Figure 20). Investigating the temperature dependence of the monomer excimer equilibrium of pyrene makes it possible to determine thermodynamic functions,^{17,112} such as the enthalpy and entropy for the excimer formation from the temperature dependence of the fluorescence spectra. Using the approach by STEVENS and BAN,¹¹³ conclusions can be derived regarding the steric or electronic environment of the pyrene moiety. We wanted to use this technique to gain quantitative information about the shielding of the pyrene core for different dendrimer generations. Thus, the first- and second-generation dendrimers **2-18** and **2-19** as well as for comparison unsubstituted pyrene were dissolved in tetrachloroethane and temperature dependent fluorescence spectra were recorded. The obtained spectra are shown in Figure 21. Preliminary measured absorption spectra showed that the molar extinction coefficient as well as the absorption wavelength of the investigated compounds did not vary for the temperatures applied during the fluorescence measurements. Due to the bad solubility of the unfunctionalized first-generation dendrimer **2-16**, the ethynyl-substituted derivative **2-18** was used instead. The ethynyl groups were not expected to significantly enlarge the dendrimer size thus not influencing the shielding properties of the polyphenylene shell.

At room temperature, excimer formation of the dendronized pyrene core was observed for 10^{-2} molar solutions of **2-18**, whereas the second-generation dendrimer **2-19** at the same concentration displayed only emission from non-aggregated species. This concentration was therefore used for the next following experiments. When the 10^{-3} M solution of unsubstituted pyrene was excited at a wavelength of 340 nm and a temperature of 300 K the fluorescence spectrum showed a maximum at 397 nm with a shoulder at 417 nm due to non-aggregated pyrene molecules. Some excimer fluorescence was observed at 475 nm. When the temperature was increased to 400 K, the fluorescence band at 409 nm increased, while the

excimer fluorescence disappeared probably due to accelerated motion of the pyrene molecules inhibiting the aggregate formation.

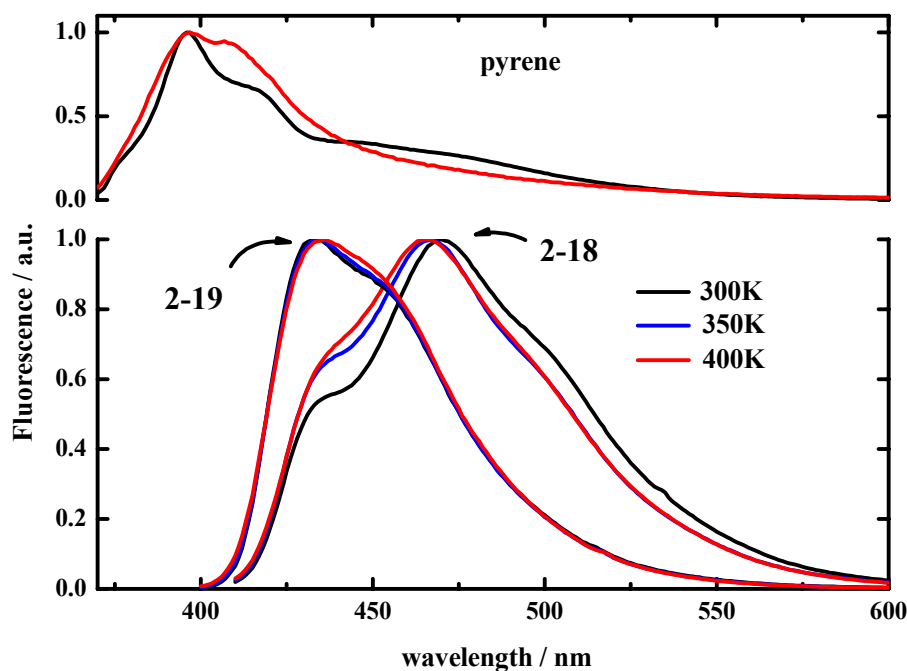


Figure 21. Temperature dependent fluorescence spectra of unsubstituted pyrene ($c = 10^{-3}$ M, upper part) and dendronized pyrenes **2-18** and **2-19** ($c = 10^{-2}$ M, lower part) in tetrachloroethane, normalized to their absorption maximum.

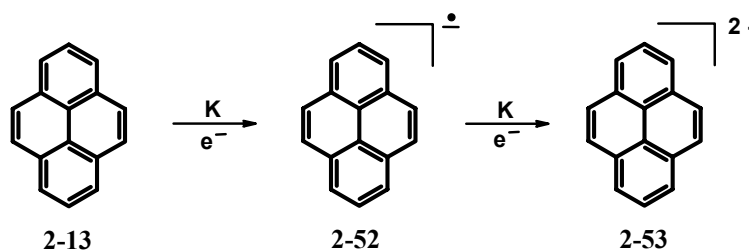
When excited at 390 nm and a temperature of 300 K, the 10^{-2} M solution of the first-generation dendrimer **2-18** showed strong excimer fluorescence at 470 nm. A shoulder at $\lambda = 440$ nm indicated non-aggregated species. At 400 K a small increase of the intensity of this band was noticed while strong excimer fluorescence at 470 nm was still detectable. This suggests that the polyphenylene shell of the first-generation dendrimer is too small to efficiently inhibit excimer formation. Surprisingly even at higher temperatures, which are normally expected to hamper the formation of self-association due to an increased rotational motion of the dendrons within the molecules. However, the small increase of the intensity of the absorption band at 440 nm indicated that at a certain lower concentration ($c < 10^{-2}$ M) **2-18** exists exclusively in the non-associated form at high temperature. The emission maximum of **2-18** is hypsochromically shifting with increasing temperature (300 K: 470 nm, 400 K: 466 nm). This further shows that aggregate formation of dendronized pyrene **2-18** is diminished at higher temperatures. A solution of the second-generation dendrimer **2-19** with the same concentration at 300 K showed only fluorescence at $\lambda = 436$ nm coming from non-aggregated species. When the temperature was increased to 400 K no change of the spectral shape and the wavelength of the emission maximum was observed, which rules out underlying excimer fluorescence at lower temperature.

The obtained results can be attributed to the larger diameter of the dendritic polyphenylene shell in the case of the second-generation dendrimer **2-19** (**2-18**: $d = 3.00$ nm, **2-19**: $d = 4.20$ nm). This obviously avoids the excimer formation due to an efficient steric shielding of the core moiety and reconfirms the results derived from the quenching experiments. The quantitative determination of thermodynamic values for the excimer

formation was not possible as only a small influence of the temperature on the excimer equilibrium of the dendrimers **2-18** and **2-19** was observed. Nevertheless, we can conclude that the excimer formation of pyrene in highly concentrated solutions is efficiently avoided by attaching second-generation polyphenylene dendrons. Moreover, the small influence of temperature on the monomer-excimer equilibrium of dendronized pyrenes suggests a stiff, non-temperature dependent arrangement of the dendritic shell. This conclusion is confirmed by earlier investigation of polyphenylene dendrimers using small-angle neutron scattering and solid-state NMR spectroscopy.^{91,92} In the latter case the slowed motion of the terminal phenyl groups was proven directly and furthermore, it was demonstrated that the dendrons can not reorient even at high temperatures.

2.6 Pyrene as Electrophore

The reduction of polyaromatic hydrocarbons (PAH)¹¹⁴ with alkali metals yields negatively charged – conjugated molecules that may undergo structural changes from distortions,¹¹⁵ rearrangements,¹¹⁶ and aggregations^{117,118} up to the formation of new chemical bonds,¹¹⁹ as is the case in reductive dimerization processes.¹²⁰⁻¹²² The reduction of pyrene can yield different products, depending on solvent, counter ion, and temperature.¹²³



Scheme 26. Reduction of pyrene with potassium.

The first species which is formed upon reduction of pyrene is the radical monoanion **2-52** (Scheme 26). Further reduction leads to the diamagnetic dianion **2-53**. When encapsulated in a polyphenylene shell, the charge/spin carrying pyrene species are thought to be stabilized either by conjugation with the neighboring phenyl rings of the dendrimer backbone or by steric shielding. The latter effect might in this case prevent side reactions either with the solvent or with traces of impurities. Furthermore, it might hamper structural changes that can happen during the reduction as mentioned above, thereby allowing a more controlled reduction process. To test the accessibility of an increasingly shielded pyrene core toward charging, their alkali metal reduction was performed.

2.6.1 Reduction of Dendronized Pyrenes on a Potassium Mirror

The reduction of the dendronized pyrenes **2-19** and **2-26** has been carried out on a potassium mirror under high vacuum in absolute THF using a technique previously described.¹²² **2-19** and **2-26** were chosen for this experiment, as they both possess a good solubility in THF and significantly different diameters. The formation of the charged species was followed using EPR- and UV/vis spectroscopy. Due to the large amount of data obtained, firstly, the results are presented and later discussed overall.

Upon contact with the potassium mirror the color of the solution of the second-generation dendrimer **2-19** turned from light yellow to green and two absorption bands at $\lambda = 456$ and

640 nm occurred in the UV/vis spectrum. This can be ascribed to the formation of the radical anion of the substituted pyrene (Figure 22a).

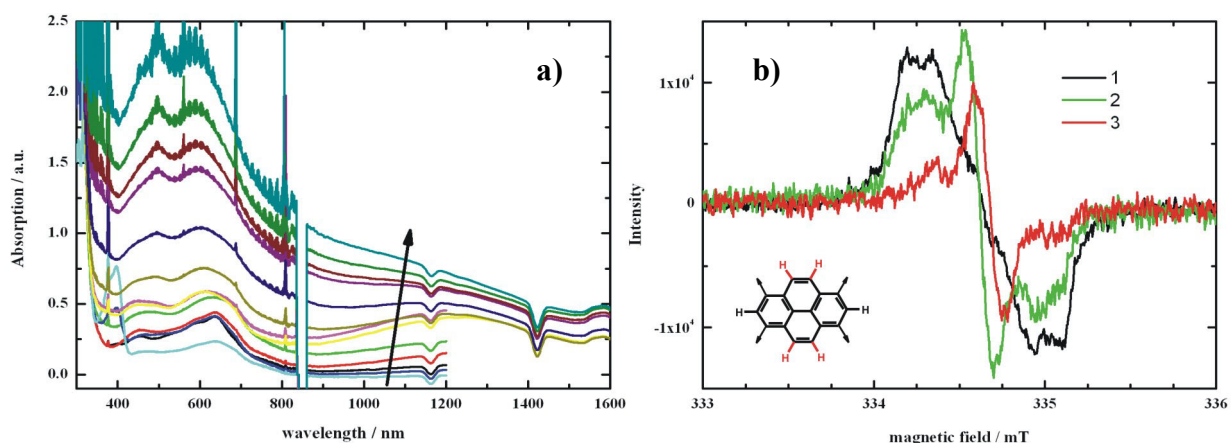


Figure 22. a) UV/vis spectra of **2-19** in the order of further reduction (rt, K, THF). b) EPR spectra (1 - 3) in the order of further reduction (rt, K, THF).

In literature, absorption maxima were found at 540 nm for 1-phenylpyrene.¹²⁴ The absorption band of the neutral starting material at $\lambda = 394$ nm disappeared upon prolonged contact suggesting a quantitative conversion. The UV/vis spectra of **2-19**, **1-40**, and **2-26** were taken, when EPR spectroscopy of the according sample indicated a significant charged state. Since no dilution could be performed prior to the UV/vis measurement, some of the spectra shown in Figure 22, Figure 23, and Figure 24, respectively, exhibit a very high absorption resulting in less accurate spectra. The EPR spectroscopic control of the pyrene reduction of **2-19** showed first a broad signal with five shoulders, which might be attributed to the four protons at position 4,5,9, and 10 of the pyrene core ($a_H \approx 0.22$ mT) (Figure 22b, black line). Upon further reduction the intensity of this signal was diminished, but instead of reaching a diamagnetic dianionic state, a new sharp signal appeared in the center of the spectrum and increased in intensity ($\Delta_{H_{pp}} \approx 0.2$ mT, red line). This new signal could not be explained by reduction of the pyrene core.

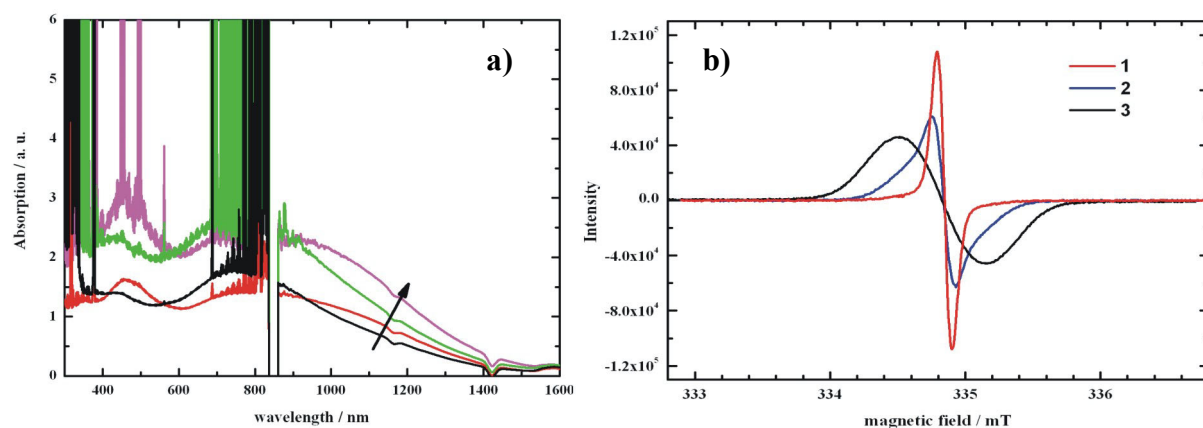


Figure 23. a) UV/vis spectra of the control sample **1-40** in the order of further reduction (rt, K, THF). b) EPR spectra (1 - 3) in the order of further reduction (rt, K, THF).

Therefore, in a control experiment the unfunctionalized second-generation dendrimer **1-40** with the tetragonal tetraphenylmethane core was considered for charging. After some reduction time on the potassium mirror, the colorless solution turned dark green and broad absorption bands at $\lambda = 450$ and 750 nm could be observed in the UV/vis spectra (Figure 23a). The EPR measurements of this solution exhibited a sharp signal ($\Delta_{\text{Hpp}} \approx 0.1$ mT) very similar to the one found for the dendronized pyrene **2-19** after prolonged reduction (Figure 23b, red line). Upon reduction of the pyrene bearing fourth-generation dendrimer **2-26** immediately a strong sharp signal showed up in the EPR spectra ($\Delta_{\text{Hpp}} \approx 0.1$ mT, Figure 24a, black line) as also found for **1-40** characteristic for the charging of the polyphenylene shell.

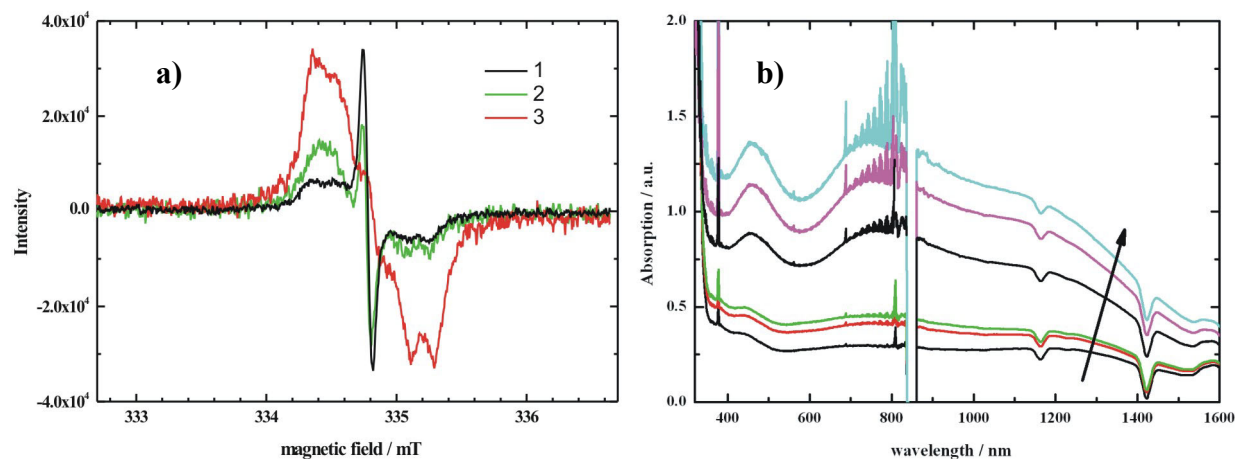


Figure 24. a).EPR spectra of **2-26** (1 – 3) in the order of further reduction (rt, K, THF). b) UV/vis spectra in the order of further reduction (rt, K, THF)

However after equilibrating with neutral compound (comproportionation) a broad signal with 4 shoulders ($a_{\text{H}} \approx 0.19$ mT, red line) was found. It showed good similarity to the EPR spectra of **2-19** (Figure 22b) therefore strongly supporting the assignment of this signal to the radical monoanion of pyrene. The pyrene radical monoanion of **2-26** could not be observed in the absorption spectra recorded during the reduction, mainly due to unresolved spectra of very high absorption (Figure 24b). Here the absorption maxima occurred around 450 and 800 nm, comparable to those of the control sample. Upon further reduction the sharp line in the EPR spectrum reappeared and revealed close similarity to the control sample **1-40**. In all three samples the sharp line broadened upon elongated contact with the potassium mirror but no defined number of transferred electrons can be ascribed ($\Delta_{\text{Hpp}} \approx 0.6$ mT).

The alkali metal reduction of the second- and fourth-generation dendrimers **2-19** and **2-26** showed that the radical anion of the pyrene core could be received in both cases. However, slight differences were observed during the reduction of the two dendrimers. With the second-generation dendrimer **2-19** the radical anion of pyrene was formed immediately as indicated by UV/vis and EPR spectroscopy. Contrary, in the case of the fourth-generation dendrimer **2-26** an intense sharp signal in the EPR occurred in the beginning. The same sharp signal was observed for the reduction of the polyphenylene dendrimer **1-40** without a pyrene core under the same conditions. This leads to the conclusion that charging of the polyphenylene shell of **1-40** and **2-26** initially happened upon contact with the potassium mirror. The sharp EPR signal indicated a highly mobile electron spin, which might be due to hopping between different oligomeric phenylene sides. Thus, no specific charged bi- or triphenyl units¹²⁵⁻¹²⁹

could be identified. The observed differences in the reduction between **2-19** and **2-26** can be attributed to the larger diameter of the fourth-generation dendrimer **2-26** (**2-26**: $d = 6.8$ nm, **2-19**: $d = 3.9$ nm)⁸². This hampered the diffusion of electrons to the pyrene core to such an extent that in the beginning only the charged polyphenylene shell of **2-26** was detected by EPR. Contrary, for **2-19** the diffusion of electrons to the core is easier due to the smaller distance between core and outer dendritic shell thus the pyrene radical anion could immediately be observed.

To show the nondestructive nature of the reduction, a reoxidation experiment was performed. When the sealed glass tubes of both reduced **2-19** and the unfunctionalized second-generation dendrimer **1-40** were opened the color of the solutions immediately faded away due to the reaction with oxygen. After evaporation of the solvent MALDI-TOF mass spectra of the obtained yellowish solids were recorded and showed signals that can be assigned to the mass of the starting materials. In both cases, no degradation of the polyphenylene dendrons could be observed.

In the next chapter, the influence of the polyphenylene shell upon the electronic properties of the pyrene core is further investigated using cyclic voltammetry.

2.6.2 Electrochemical Studies

Cyclic voltammetry (CV) is perhaps the most versatile electroanalytical technique for the study of electroactive species. Its versatility combined with ease of measurement has resulted in extensive use of CV in the fields of electrochemistry, inorganic chemistry, organic chemistry, and biochemistry.

Cyclic Voltammetry

In cyclic voltammetry (CV), the current response of a stationary electrode in an unstirred solution is excited by a triangular potential waveform. Figure 25 shows the current response when a solution that is 6 mM in $K_3(Fe(CN)_6)$ and 1 M in KNO_3 is subjected to the cyclic excitation signal. Important parameters in a cyclic voltammogram are the cathodic peak potential E_{pc} , the anodic peak potential E_{pa} , the cathodic peak current i_{pc} , and the anodic peak current i_{pa} . How these parameters are established is illustrated Figure 25. For a reversible electrode reaction, anodic and cathodic peak currents are approximately equal in absolute value, but opposite in sign, and the difference in peak potential is $0.059/n$, where n is the number of electrons involved in the half-reaction.

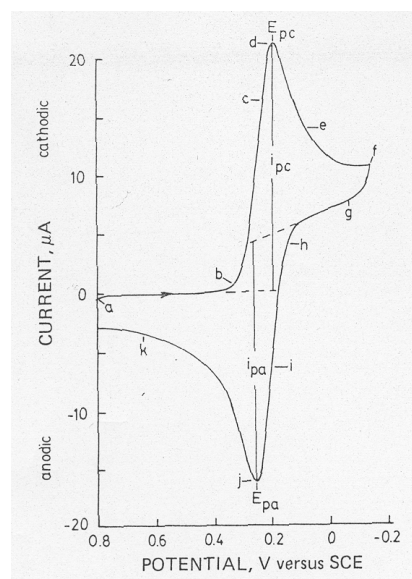


Figure 25. Cyclic voltammogram of 0.6 mM $K_3Fe(CN)_6$ in 1 M KNO_3 . Scan initiated at 0.8 V versus SCE in negative direction at 0.05 V·s⁻¹.

This chapter shows how cyclic voltammetry can be used to verify the extent of shielding in a polyphenylene dendronized pyrene core. As already mentioned in the introduction, redox active molecules e.g. porphyrin, have been used as core in a large variety of dendrimers.^{34,35,39,130} Cyclic voltammetry of these dendrimers showed a decrease in the peak current and an increase of the peak potential difference which was attributed to slowed

electron transfer kinetics due to steric shielding of the core.⁴⁰ Polyphenylene dendrimers of the MÜLLEN type with a redoxactive triphenylamine core have been synthesized by C. HAMPEL. Also in this case, a decreased electron transfer rate to the core was found for an increasing dendrimer generation.⁴⁶

In the case of dendronized pyrene, already the reduction on a potassium mirror indicated a hampered electron transfer to the core (chapter 2.6.1). To investigate also the oxidation behavior, cyclic voltametry has been performed in cooperation with J. W. F. ROBERTSON. For that, solutions of the first- to fourth-generation dendrimers **2-16**, **2-19**, **2-25**, and **2-26** in CH_2Cl_2 were prepared. In the linear mode (the potential is increased in a continuous way) it was not possible to distinguish some peak maxima for the higher generation dendrimers **2-25** and **2-26**, respectively. In order to increase speed and sensitivity, a potential modulation (Differential Pulse Voltametry) was used. The potential is scanned with a series of pulses in that technique. Each potential pulse is fixed, of small amplitude (10 – 100 mV), and is superimposed on a slowly changing base potential. The current is measured at two points for each pulse, the first point just before the application of the pulse and the second at the end of the pulse. The difference between the current measurements at these points for each pulse is determined and plotted against the base potential. The obtained spectra are depicted in Figure 26.

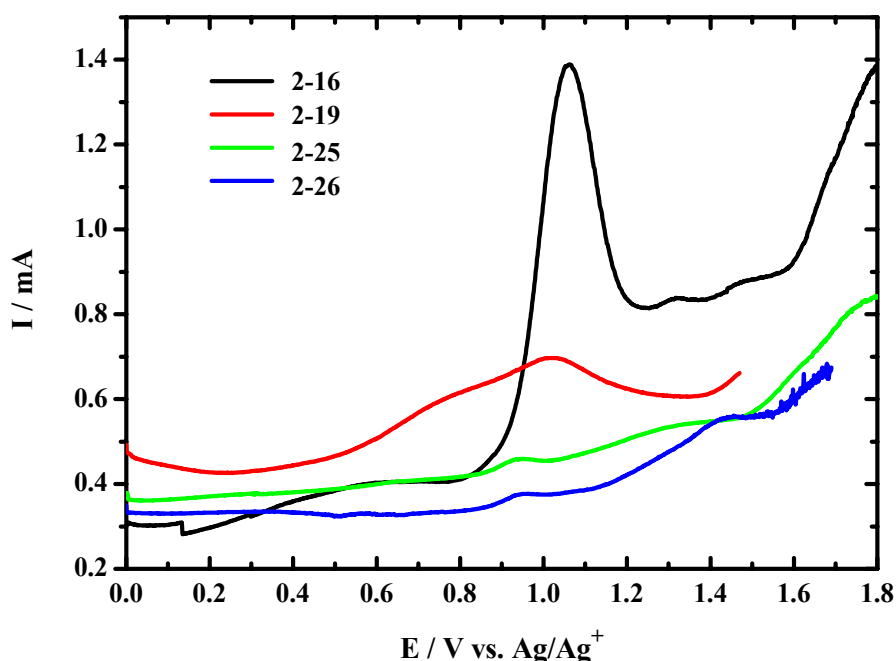


Figure 26. Differential pulse voltametry (oxidation) of dendrimers **2-16**, **2-19**, **2-25**, and **2-26** in CH_2Cl_2 .

For the first-generation dendrimer **2-16**, a maximum was observed at a potential of 1060 mV and can be assigned to the radical cation of the pyrene core. A second and a third maximum displayed at 1320 and 1480 mV, indicating further oxidation to the pyrenyl dication and higher. Also for the third- and fourth-generation dendrimers **2-25** and **2-26**, further oxidation peaks were observed at 1360 and 1460 mV, respectively. With increasing dendrimer generation, the cathodic peak current i_{pc} dramatically decreases, similar as to the results found by C. HAMPEL.⁴⁶ Table 6 summarizes the data obtained from the differential pulse voltametry experiments. The strongest decrease was found for going from the first-

the second-generation dendrimer shell. Further enlarged dendrimer shells have a smaller influence on the maximum peak current i_{pc} , especially only a minor decrease was observed when going from the third- to the fourth-generation dendrimer. This can be attributed to slowed electron transfer kinetics with increasing dendrimer generation and fits almost perfect with the trend obtained from the STERN-VOLLMER quenching experiments as described in chapter 2.5.3.

Table 6. Data of differential pulse voltametry of the oxidation of dendronized pyrenes **2-16**, **2-19**, **2-25**, and **2-26**.

	E_{pc} / mV	i_{pc} / μ A
2-16	1060	1.38
2-19	1020	0.70
2-25	940	0.46
2-26	950	0.38

However, the strongest difference in peak potential maxima E_{pc} occurred between the second- and the third-generation dendrimers **2-19** and **2-25**, respectively. Furthermore, the shape of the oxidation curves became broader and less defined with increasing generation thereby indicating a slowed electron transfer.

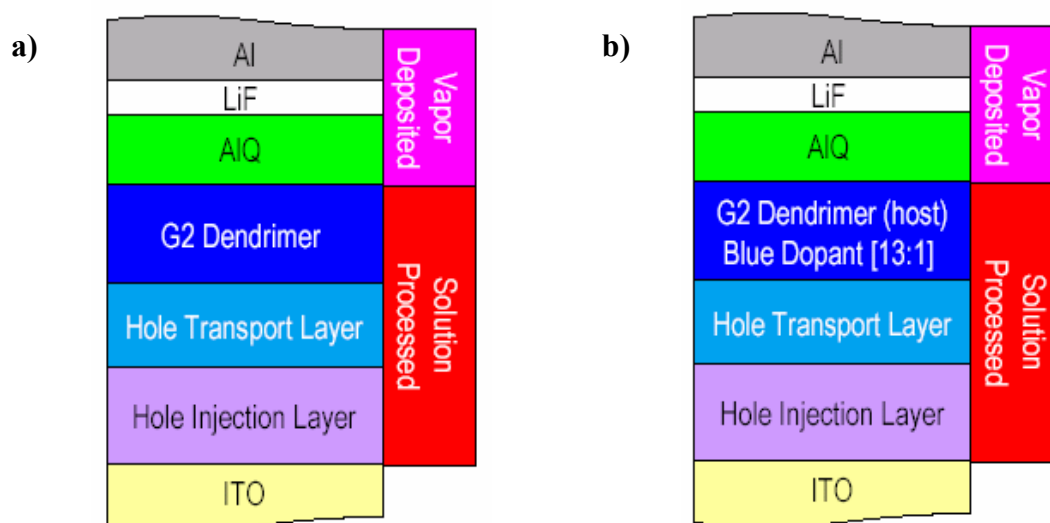
From the obtained electrochemical data, it became obvious, that surrounding the pyrene core with higher-generation polyphenylene dendrons leads to an efficient shielding from the electrode and a hampered electron transfer to the core.

2.7 Organic Light-Emitting Diodes

An organic light-emitting diode (OLED)¹³¹ is a thin-film light-emitting diode (LED), in which the emissive layer is an organic compound. One of the great benefits of an OLED display over the traditional LCD displays found in computer displays, is that OLED displays do not require a backlight to function. This means that they draw far less power and can therefore be used with small portable devices which have mostly been using monochrome low-resolution displays to conserve power. OLEDs work on the principle of electroluminescence. The key to the operation of an OLED is an organic fluorophore. Excitons, which consist of a bound, excited electron and hole pairs (empty state) are generated inside the emissive layer. When the exciton's electron and hole combine, a photon can be emitted. A major challenge in OLEDs is tuning the devices such that holes and electrons meet in the emissive layer in equal quantities, which is difficult, since the mobility of holes is typically much higher than that of electrons. Light emission can only occur, when singlet excitons form in the emissive layer, because the materials currently employed are fluorophors and cannot emit light from a triplet state. This is a problem, since only one in four excitons is a singlet. To create the excitons, a thin film of the fluorophore is sandwiched between electrodes of differing work functions. Electrons are injected into one side from a metal cathode (usually aluminium), while holes are injected in the other from an anode (usually ITO = indium tin oxide). These electrons and holes move in the electric field into the emissive layer where they combine to form excitons.

In cooperation with DuPont in the United States, namely Dr. F. UCKERT, the first-generation dendrimer **2-27**, decorated with alkyl chains, as well as the second-generation dendrimer **2-19** were tested for their possible application in organic light-emitting diodes (OLEDs). First results are presented on the following pages, however, further experiments are performed at the moment.

OLEDs were fabricated using the typical layer arrangement shown in Scheme 27. Starting from ITO (Indium tin oxide) as transparent support a hole injection layer (“DuPont Buffer”) and a hole-transport layer have been deposited using a spin-coating technique. Subsequently, a film of approximately 40 nm thickness was grown from **2-19** being the emitting layer. On top of the dendrimer film AIQ (Aluminium quinoline, commonly used electron transport material), lithium fluoride and finally an aluminium film as electrode were vapor deposited (Scheme 27a). In an alternative approach (Scheme 27b), a mixture of **2-19** and a blue dopant was used as the emitting layer. All devices were fabricated in a glove box atmosphere.



Scheme 27. Device architecture of the OLEDs with incorporated second-generation dendrimer **2-19**. a) only **2-19** as emitting layer and b) **2-19** together with a blue dopant. ITO (Indium tin oxide), AIQ (Aluminium quinoline), LiF (Lithium fluoride), Al (Aluminium)

Electroluminescence (EL) spectra were measured and showed surprising and yet not fully understood results. Figure 27 displays the EL spectra of both OLEDs, with only **2-19** as the emitting layer and with **2-19** and a blue dopant as the emitting layer. With **2-19** as the emitting layer, only minor emission of the dendrimer could be observed at ≈ 440 nm. Major emission came from AIQ at ≈ 500 nm. This indicates that the hole transport ability of **2-19** is much better than that of AIQ. However, when the emitting layer was a mixture of **2-19** and a blue dopant, uncharacteristic dopant emission occurred at ≈ 470 nm. Reason for this might be an incomplete energy transfer from the host **2-19** to the dopant. From the alkyl chain functionalized first-generation dendrimer **2-27**, OLEDs were fabricated in the same way as described before for **2-19** (Scheme 27a). For comparison, a device with BAlQ (bis(2-methyl-8-quinolinolato)(*para*-phenylphenolato)aluminium(III)) as electron transport layer instead of AIQ was built. A control sample was prepared with the same device architecture but with other blue emitting material (developed by DuPont) as the emitting layer.

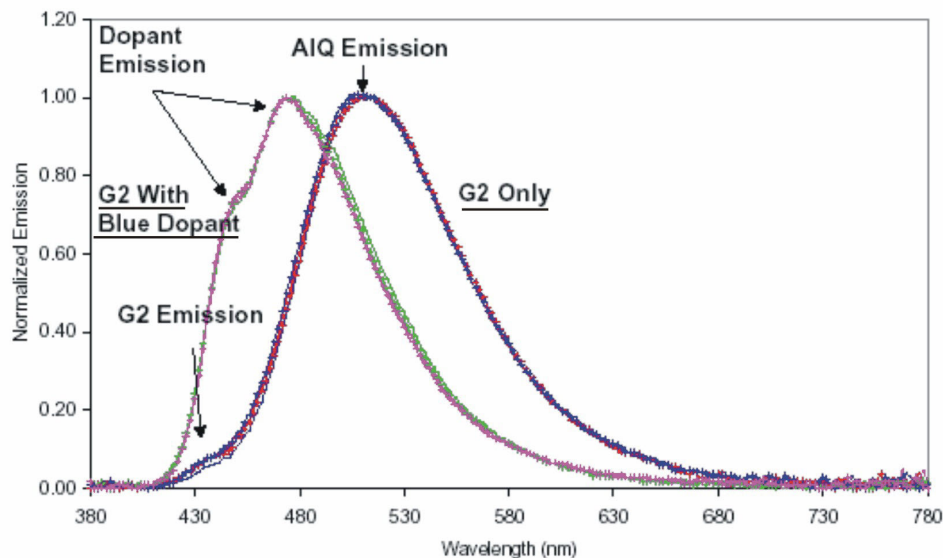


Figure 27. Electroluminescence spectra obtained for OLEDs build from **2-19**. OLEDs with pure **2-19** as emitting layer: red and blue curve, OLEDs with **2-19** and blue dopant: purple and green curve.

Typical current-voltage, light-voltage, and current-light curves were measured in order to investigate the optical properties of the devices. Two main results from these experiments were as follows:

- Current efficiencies were poor, below 1 Cd/Amp, the control sample had the normal efficiency of 3-4 Cd/Amp.
- Color was poor compared to controls.

From these first results, it must be concluded that the applied dendrimers **2-19** and **2-27** can obviously not compete with the already known blue emitting materials supplied by DuPont. However, the surprisingly good hole transport ability of the polyphenylene dendrimers might lead to alternative applications, which is currently explored at DuPont laboratories.

2.8 Conclusion

Starting from the fourfold ethynyl substituted chromophore 1,3,6,8-tetraethynyl-pyrene (**2-10**) as core, a series of polyphenylene dendrimers has been prepared in high yield by a divergent growth method. Monodisperse spherical particles of maximum 7.65 nm and a molecular weight of 23030 g·mol⁻¹ could be obtained (fourth-generation dendrimer **2-26**). All dendrimers showed a good solubility in organic solvents thus allowing easy processibility. The crystal structure of a first-generation dendrimer as well as molecular modeling indicates that these dendrimers possess a dendrimer shell of very high density thereby efficiently encapsulating the pyrene core.

Steady state UV/vis spectroscopy as well as electrochemical methods has been applied to determine the influence of the surrounding polyphenylene dendrimer shell on the optical and electronic properties of the encapsulated pyrene core. An efficient intramolecular energy transfer from the polyphenylene dendrons to the pyrene core was observed. The FÖRSTER radius R_0 was determined to be significantly bigger as compared to similarly dendronized

perylene, mainly due to the increased overlap of donor emission spectrum (polyphenylene dendrons) and acceptor absorption spectrum (pyrene core) in the case of the pyrenyl dendrimers. The fluorescence quantum yields were almost identical high ($Q_f \geq 0.92$) for all dendrimer generations due to suppressed aggregation of the fluorophore. A minor shift of the pyrene emission maximum was detected upon changing the polarity of the surrounding medium which indicates that the conformation and shape of the polyphenylene dendrimer backbone is almost invariant toward polarity changes, significantly contrary to dendrimers constructed from flexible building blocks.

Fluorescence quenching studies have been performed to investigate the amount of shielding applied to the core. Quenching showed to be more efficient with smaller quenchers suggesting some size exclusion provided by the dendrimer shell. Interestingly, the second-, third- and fourth-generation dendrimer layers suppressed the diffusion of the quencher to the core in an equal amount. From the synthetic point of view, this is a big advantage as the above-mentioned improvements of the optical properties can be achieved by simply applying a second-generation dendrimer shell, allowing the fast synthesis of suitable materials on the gram scale.

Temperature dependent fluorescence spectroscopy displayed pyrene excimer formation for high-concentrated solutions of the first-generation dendrimer **2-18** even at higher temperatures. Quite contrary, no excimers were found in solutions of the second-generation dendrimer **2-19**, mainly due to the higher sterical congestion. Since the temperature displayed only a little influence on the excimer monomer equilibrium the polyphenylene dendrimer shell has to be regarded as stiff and shape persistent even at high temperatures.

To improve the film formation of dendronized pyrenes, a large number of linear and branched alkyl chains have been introduced on the periphery of the spherical particles. Amorphous transparent films were obtained from these derivatives by simple drop casting method showing blue emission mainly from the non-aggregated species. This further proves the distinguished site isolation caused by the polyphenylene shell.

The conducted alkali metal reduction of the encapsulated pyrene core was carried out to give the corresponding pyrene radical anions. A slower electron transfer to the core was observed for the fourth-generation dendrimer **2-26** as compared to the second-generation dendrimer **2-19**. This suggests a diffusion controlled reduction process, strongly influenced by the density and diameter of the surrounding dendrimer shell. These findings are supported by results from differential pulse voltametry experiments. They showed a decreasing cathodic peak current i_{pc} with increasing dendrimer generation, which can be attributed to slowed electron transfer kinetics with increasing dendrimer shell diameter.

The optical properties of the dendronized pyrenes suggested an application in organic light-emitting diodes (OLEDs) which was tested in cooperation with DuPont. First results were obtained, however, OLEDs with dendronized pyrenes as the emissive layer showed comparable bad performance.

In conclusion, the combination of a pyrene core and a polyphenylene dendrimer shell resulted in materials possessing a high fluorescence quantum yield and a good solubility. Irrespective of the temperature and the polarity of the surrounding medium an efficient shielding of the core could be achieved. Further, the encapsulation of the pyrene against charging (reduction and oxidation) was shown to be dependent on the dendrimer generation.

2.9 References

- (1) Liang, C.; Fréchet, J. M. J. *Progress in Polymer Science* **2005**, *30*, 385-402.
- (2) Felber, B.; Diederich, F. *Helvetica Chimica Acta* **2005**, *88*, 120-153.
- (3) Smith, D. K.; Diederich, F. *Chemistry-A European Journal* **1998**, *4*, 1353-1361.
- (4) Dandliker, P. J.; Diederich, F.; Zingg, A.; Gisselbrecht, J. P.; Gross, M.; Louati, A.; Sanford, E. *Helvetica Chimica Acta* **1997**, *80*, 1773-1801.
- (5) Ardoin, N.; Astruc, D. *Bulletin de la Societe Chimique de France* **1995**, *132*, 875-909.
- (6) Hawker, C. J.; Wooley, K. L.; Fréchet, J. M. J. *Journal of the American Chemical Society* **1993**, *115*, 4375-4376.
- (7) Devadoss, C.; Bharathi, P.; Moore, J. S. *Angewandte Chemie-International Edition* **1997**, *36*, 1633-1635.
- (8) Devadoss, C.; Bharathi, P.; Moore, J. S. *Journal of the American Chemical Society* **1996**, *118*, 9635-9644.
- (9) Jiang, D. L.; Aida, T. *Journal of the American Chemical Society* **1998**, *120*, 10895-10901.
- (10) Jin, R. H.; Aida, T.; Inoue, S. *Chemical Communications* **1993**, 1260-1262.
- (11) Guldi, D. M. *Chemical Society Reviews* **2002**, *31*, 22-36.
- (12) Harriman, A.; Sauvage, J. P. *Chemical Society Reviews* **1996**, *25*, 41.
- (13) Birks, J. B. *Photophysics of Aromatic Molecules*; Wiley Interscience: London, **1970**.
- (14) Carmichael, I.; Hug, G. L. *Handbook of Photochemistry*; 2 ed., Marcel Dekker, New York, **1993**.
- (15) Castanheira, E. M. S.; Martinho, J. M. G. *Chemical Physics Letters* **1991**, *185*, 319-323.
- (16) Dong, D. C.; Winnik, M. A. *Canadian Journal of Chemistry/Revue Canadienne de Chimie* **1984**, *62*, 2560-2565.
- (17) Thomas, A.; Polarz, S.; Antonietti, M. *Journal of Physical Chemistry B* **2003**, *107*, 5081-5087.
- (18) Kwon, G.; Naito, M.; Yokoyama, M.; Okano, T.; Sakurai, Y.; Kataoka, K. *Langmuir* **1993**, *9*, 945-949.
- (19) Lianos, P.; Zana, R. *Journal of Physical Chemistry* **1980**, *84*, 3339-3341.
- (20) Rutan, S. C.; Harris, J. M. *Journal of Chromatography A* **1993**, *656*, 197-215.
- (21) Zilberstein, J.; Bromberg, A.; Berkovic, G. *Journal of Photochemistry and Photobiology A-Chemistry* **1994**, *77*, 69-81.
- (22) Mao, Y.; Thomas, J. K. *Langmuir* **1992**, *8*, 2501-2508.
- (23) Stewart, G. M.; Fox, M. A. *Journal of the American Chemical Society* **1996**, *118*, 4354-4360.
- (24) Baker, L. A.; Crooks, R. M. *Macromolecules* **2000**, *33*, 9034-9039.
- (25) Wilken, R.; Adams, J. *Macromolecular Rapid Communications* **1997**, *18*, 659-665.
- (26) Riley, J. M.; Alkan, S.; Chen, A. D.; Shapiro, M.; Khan, W. A.; Murphy, W. R.; Hanson, J. E. *Macromolecules* **2001**, *34*, 1797-1809.
- (27) Hecht, S.; Vladimirov, N.; Fréchet, J. M. J. *Journal of the American Chemical Society* **2001**, *123*, 18-25.
- (28) Cardona, C. M.; Wilkes, T.; Ong, W.; Kaifer, A. E.; McCarley, T. D.; Pandey, S.; Baker, G. A.; Kane, M. N.; Baker, S. N.; Bright, F. V. *Journal of Physical Chemistry B* **2002**, *106*, 8649-8656.
- (29) Brauge, L.; Caminade, A. M.; Majoral, J. P.; Slomkowski, S.; Wolszczak, M. *Macromolecules* **2001**, *34*, 5599-5606.
- (30) Modrakowski, C.; Flores, S. C.; Beinhoff, M.; Schlüter, A. D. *Synthesis* **2001**, 2143-2155.
- (31) Beinhoff, M.; Weigel, W.; Jurczok, M.; Rettig, W.; Modrakowski, C.; Brüdgam, I.; Hartl, H.; Schlüter, A. D. *European Journal of Organic Chemistry* **2001**, *20*, 3819-3829.
- (32) Pistolis, G.; Malliaris, A.; Tsiourvas, D.; Paleos, C. M. *Chemistry-A European Journal* **1999**, *5*, 1440-1444.
- (33) Pistolis, G.; Malliaris, A.; Paleos, C. M.; Tsiourvas, D. *Langmuir* **1997**, *13*, 5870-5875.
- (34) Dandliker, P. J.; Diederich, F.; Gisselbrecht, J. P.; Louati, A.; Gross, M. *Angewandte Chemie-International Edition* **1996**, *34*, 2725-2728.
- (35) Weyermann, P.; Diederich, F. *Helvetica Chimica Acta* **2002**, *85*, 599-617.
- (36) Langen, R.; Chang, I. J.; Germanas, J. P.; Richards, J. H.; Winkler, J. R.; Gray, H. B. *Science* **1995**, *268*, 1733-1735.

- (37) Winkler, J. R.; Gray, H. B. *Chemical Reviews* **1992**, *92*, 369-379.
- (38) Wuttke, D. S.; Bjerrum, M. J.; Winkler, J. R.; Gray, H. B. *Science* **1992**, *256*, 1007-1009.
- (39) Weyermann, P.; Gisselbrecht, J. P.; Boudon, C.; Diederich, F.; Gross, M. *Angewandte Chemie-International Edition* **1999**, *38*, 3215-3219.
- (40) Dandliker, P. J.; Diederich, F.; Gross, M.; Knobler, C. B.; Louati, A.; Sanford, E. M. *Angewandte Chemie-International Edition* **1994**, *33*, 1739-1742.
- (41) Pollak, K. W.; Leon, J. W.; Fréchet, J. M. J.; Maskus, M.; Abruna, H. D. *Chemistry of Materials* **1998**, *10*, 30-38.
- (42) Wang, Y.; Cardona, C. M.; Kaifer, A. E. *Journal of the American Chemical Society* **1999**, *121*, 9756-9757.
- (43) Cardona, C. M.; Kaifer, A. E. *Journal of the American Chemical Society* **1998**, *120*, 4023-4024.
- (44) Gorman, C. B.; Smith, J. C. *Accounts of Chemical Research* **2001**, *34*, 60-71.
- (45) Gorman, C. B. *Advanced Materials* **1997**, *9*, 1117-1119.
- (46) Christina Hampel, Dissertation. Johannes Gutenberg Universität (Mainz), 2001.
- (47) Bosman, A. W.; Janssen, H. M.; Meijer, E. W. *Chemical Reviews* **1999**, *99*, 1665-1688.
- (48) Wang, P. W.; Liu, Y. J.; Devadoss, C.; Bharathi, P.; Moore, J. S. *Advanced Materials* **1996**, *8*, 237.
- (49) Freeman, A. W.; Koene, S. C.; Malenfant, P. R. L.; Thompson, M. E.; Frechet, J. M. J. *Journal of the American Chemical Society* **2000**, *122*, 12385-12386.
- (50) Otsubo, T.; Aso, Y.; Takimiya, K. *Journal of Materials Chemistry* **2002**, *12*, 2565-2575.
- (51) Cimrova, V.; Vyprachticky, D. *Applied Physics Letters* **2003**, *82*, 642-644.
- (52) Aso, Y.; Okai, T.; Kawaguchi, Y.; Otsubo, T. *Chemistry Letters* **2001**, 420-421.
- (53) Jia, W. L.; McCormick, T.; Liu, Q. D.; Fukutani, H.; Motala, M.; Wang, R. Y.; Tao, Y.; Wang, S. N. *Journal of Materials Chemistry* **2004**, *14*, 3344-3350.
- (54) Ogino, K.; Iwashima, S.; Inokuchi, H.; Harada, Y. *Bulletin of the Chemical Society of Japan* **1965**, *38*, 473-477.
- (55) Vollmann *Justus Liebigs Annalen der Chemie* **1937**, *531*, 1.
- (56) Wang, Y. F.; Deng, W.; Liu, L.; Guo, Q. X. *Chinese Journal of Organic Chemistry* **2005**, *25*, 8-24.
- (57) Sonogashira, K.; Takahashi, S. *Journal of Synthetic Organic Chemistry Japan* **1993**, *51*, 1053-1063.
- (58) Dieck, H. A.; Heck, F. R. *Journal of Organometallic Chemistry* **1975**, *93*, 259-263.
- (59) Wiesler, U. M.; Weil, T.; Müllen, K. in *Dendrimers III: Design, Dimension, Function, Topics in Current Chemistry*, Springer Verlag, Heidelberg, **2001**, *212*, 1-40.
- (60) Morgenroth, F.; Reuther, E.; Müllen, K. *Angewandte Chemie-International Edition* **1997**, *36*, 631-634.
- (61) Bierbaum, R.; Nuchter, M.; Ondruschka, B. *Chemical Engineering & Technology* **2005**, *28*, 427-431.
- (62) Desai, B.; Kappe, C. O. in *Immobilized Catalysts, Solid Phases, Immobilization and Applications, Topics in Current Chemistry*, Springer-Verlag, Heidelberg **2004**, *242*, 177-208.
- (63) de la Hoz, A.; Diaz-Ortiz, A.; Moreno, A. *Chemical Society Reviews* **2005**, *34*, 164-178.
- (64) Kappe, C. O. *Angewandte Chemie-International Edition* **2004**, *43*, 6250-6284.
- (65) Hayes, B. L. *Aldrichimica Acta* **2004**, *37*, 66-77.
- (66) Perreux, L.; Loupy, A. *Tetrahedron* **2001**, *57*, 9199-9223.
- (67) Lidstrom, P.; Tierney, J.; Wathey, B.; Westman, J. *Tetrahedron* **2001**, *57*, 9225-9283.
- (68) Wiesler, U. M. Dissertation, Johannes Gutenberg Universität (Mainz), 2001.
- (69) Wiesler, U. M.; Müllen, K. *Chemical Communications* **1999**, 2293-2294.
- (70) Loi, S.; Butt, H. J.; Hampel, C.; Bauer, R.; Wiesler, U. M.; Müllen, K. *Langmuir* **2002**, *18*, 2398-2405.
- (71) Loi, S.; Wiesler, U. M.; Butt, H. J.; Müllen, K. *Chemical Communications* **2000**, 1169-1170.
- (72) Loi, S.; Wiesler, U. M.; Butt, H. J.; Müllen, K. *Macromolecules* **2001**, *34*, 3661-3671.
- (73) Iyer, V. S.; Yoshimura, K.; Enkelmann, V.; Epsch, R.; Rabe, J. P.; Müllen, K. *Angewandte Chemie-International Edition* **1998**, *37*, 2696-2699.
- (74) Pisula, W.; Kastler, M.; Wasserfallen, D.; Pakula, T.; Müllen, K. *Journal of the American Chemical Society* **2004**, *126*, 8074-8075.

- (75) Bauer, R. E.; Enkelmann, V.; Wiesler, U. M.; Berresheim, A. J.; Müllen, K. *Chemistry-A European Journal* **2002**, *8*, 3858-3864.
- (76) Moore, J. S. *Accounts of Chemical Research* **1997**, *30*, 402-413.
- (77) Andreitchenko, E. Dissertation, Johannes Gutenberg-Universität (Mainz) **2006**.
- (78) W. Diltthey, G. H., *Chemische Berichte* **1934**, *67*, 2004.
- (79) W. Diltthey, W. S., H. Dierichs, O. Trösken, *Chemische Berichte* **1933**, *66*, 1627.
- (80) Newkome, G. R.; Moorefield, C. N.; Keith, J. M.; Baker, G. R.; Escamilla, G. H. *Angewandte Chemie-International Edition* **1994**, *33*, 666-668.
- (81) Bauer, R. Dissertation, Johannes Gutenberg-Universität (Mainz) **2005**.
- (82) Halgren, T. A. *Journal of Computational Chemistry* **1996**, *17*, 490-519.
- (83) Degennes, P. G.; Hervet, H. *Journal De Physique Lettres* **1983**, *44*, L351-L360.
- (84) Mourey, T. H.; Turner, S. R.; Rubinstein, M.; Fréchet, J. M. J.; Hawker, C. J.; Wooley, K. L. *Macromolecules* **1992**, *25*, 2401-2406.
- (85) Wooley, K. L.; Klug, C. A.; Tasaki, K.; Schaefer, J. *Journal of the American Chemical Society* **1997**, *119*, 53-58.
- (86) De Backer, S.; Prinzie, Y.; Verheijen, W.; Smet, M.; Desmedt, K.; Dehaen, W.; De Schryver, F. C. *Journal of Physical Chemistry A* **1998**, *102*, 5451-5455.
- (87) Lescanec, R. L.; Muthukumar, M. *Macromolecules* **1990**, *23*, 2280-2288.
- (88) Scherrenberg, R.; Coussens, B.; van Vliet, P.; Edouard, G.; Brackman, J.; de Brabander, E.; Mortensen, K. *Macromolecules* **1998**, *31*, 456-461.
- (89) Mansfield, M. L.; Klushin, L. I. *Macromolecules* **1993**, *26*, 4262-4268.
- (90) Boris, D.; Rubinstein, M. *Macromolecules* **1996**, *29*, 7251-7260.
- (91) Rosenfeldt, S.; Dingenouts, N.; Potschke, D.; Ballauff, M.; Berresheim, A. J.; Müllen, K.; Lindner, P. *Angewandte Chemie-International Edition* **2004**, *43*, 109-112.
- (92) Wind, M.; Saalwächter, K.; Wiesler, U. M.; Müllen, K.; Spiess, H. W. *Macromolecules* **2002**, *35*, 10071-10086.
- (93) Wind, M.; Wiesler, U. M.; Saalwächter, K.; Müllen, K.; Spiess, H. W. *Advanced Materials* **2001**, *13*, 752-756.
- (94) Halgren, T. A. *Journal of Computational Chemistry* **1996**, *17*, 490-519.
- (95) Berlman, I. B. *Journal of Physical Chemistry* **1970**, *74*, 3085-3093.
- (96) Liu, D. J.; De Feyter, S.; Cotlet, M.; Stefan, A.; Wiesler, U. M.; Herrmann, A.; Grebel-Koehler, D.; Qu, J. Q.; Müllen, K.; De Schryver, F. C. *Macromolecules* **2003**, *36*, 5918-5925.
- (97) Qu, J. Q.; Liu, D. J.; De Feyter, S.; Zhang, J. Y.; De Schryver, F. C.; Müllen, K. *Journal of Organic Chemistry* **2003**, *68*, 9802-9808.
- (98) Winnik, F. M.; Winnik, M. A.; Tazuke, S.; Ober, C. K. *Macromolecules* **1987**, *20*, 38-44.
- (99) D.-P. Häder, P., Georg Thieme Verlag, Stuttgart, **1999**.
- (100) Kohn, F.; Hofkens, J.; Gronheid, R.; Cotlet, M.; Müllen, K.; Van der Auweraer, M.; De Schryver, F. C. *ChemPhysChem* **2002**, *3*, 1005-1013.
- (101) Eaton, D. F. *Pure and Applied Chemistry* **1988**, *60*, 1107-1114.
- (102) Herrmann, A.; Weil, T.; Sinigersky, V.; Wiesler, U. M.; Vosch, T.; Hofkens, J.; De Schryver, F. C.; Müllen, K. *Chemistry-A European Journal* **2001**, *7*, 4844).
- (103) Hecht, S.; Vladimirov, N.; Fréchet, J. M. J. *Journal of the American Chemical Society* **2001**, *123*, 18-25.
- (104) Zhang, J.; Campbell, R. E.; Ting, A. Y.; Tsien, R. Y. *Nature Reviews Molecular Cell Biology* **2002**, *3*, 906-918.
- (105) Taylor, D. L.; Wang, Y. L. *Nature* **1980**, *284*, 405-410.
- (106) Lakowicz, J. R. *Principles of Fluorescence Spectroscopy; 2 ed.*; Kluwer Academic/Plenum Publishers, New York, **1999**.
- (107) Eftink, M. R. in *Fluorescence Spectroscopy*; Plenum Press: New York; Vol. 2, **1991**.
- (108) Birks, J. B. in *Photophysics of Aromatic Molecules*, Wiley Interscience, London, **1970**.
- (109) Wilkinson, F. *Advanced Photochemistry* **1964**, *3*, 241.
- (110) Förster, T. *Angewandte Chemie-International Edition* **1969**, *8*, 333-&.
- (111) Förster, T. *Angewandte Chemie-International Edition* **1960**, *72*, 716-716.
- (112) Keeling-Tucker, T.; Brennan, J. D. *Chemistry of Materials* **2001**, *13*, 3331-3350.
- (113) Stevens, B.; Ban, M. I. *Transactions of the Faraday Society* **1964**, *60*, 1515-&.

-
- (114) Benschafrit, R.; Shabtai, E.; Rabinovitz, M.; Scott, L. T. *European Journal of Organic Chemistry* **2000**, 1091-1106.
- (115) Eshdat, L.; Ayalon, A.; Beust, R.; Shenhar, R.; Rabinovitz, M. *Journal of the American Chemical Society* **2000**, *122*, 12637-12645.
- (116) Eshdat, L.; Berger, H.; Hopf, H.; Rabinovitz, M. *Journal of the American Chemical Society* **2002**, *124*, 3822-3823.
- (117) Ayalon, A.; Sygula, A.; Cheng, P. C.; Rabinovitz, M.; Rabideau, P. W.; Scott, L. T. *Science* **1994**, *265*, 1065-1067.
- (118) Shenhar, R.; Wang, H.; Hoffman, R. E.; Frish, L.; Avram, L.; Willner, I.; Rajca, A.; Rabinovitz, M. *Journal of the American Chemical Society* **2002**, *124*, 4685-4692.
- (119) Bock, H.; Havlas, Z.; Gharagozloo-Hubmann, K.; Sievert, M. *Angewandte Chemie-International Edition* **1999**, *38*, 2240-2243.
- (120) Aprahamian, I.; Hoffman, R. E.; Sheradsky, T.; Preda, D. V.; Bancu, M.; Scott, L. T.; Rabinovitz, M. *Angewandte Chemie-International Edition* **2002**, *41*, 1712.
- (121) Edlund, U.; Eliasson, B. *Chemical Communications* **1982**, 950-952.
- (122) Baumgarten, M.; Müllen, K. in *Electron Transfer I, Topics in Current Chemistry*, Springer - Verlag, Berlin, **1994**, *169*, 1-103.
- (123) Schnieders, C.; Müllen, K.; Huber, W. *Tetrahedron* **1984**, *40*, 1701-1711.
- (124) Daub, J.; Engl, R.; Kurzawa, J.; Miller, S. E.; Schneider, S.; Stockmann, A.; Wasielewski, M. R. *Journal of Physical Chemistry A* **2000**, *105*, 5655-5665.
- (125) Shida, T.; Iwata, S. *Journal of the American Chemical Society* **1973**, *95*, 3473-3483.
- (126) Shida, T.; Iwata, S. *Journal of Chemical Physics* **1972**, *56*, 2858.
- (127) Shida, T.; Iwata, S. *Journal of Physical Chemistry* **1971**, *75*, 2591.
- (128) Lindow, D. F.; Cortez, C. N.; Harvey, R. G. *Journal of the American Chemical Society* **1972**, *94*, 5406.
- (129) Balk, P.; Debruijn, S.; Hoijtink, G. *Recueil des Travaux Chimiques des Pays-Bas* **1957**, *76*, 907-918.
- (130) Enomoto, M.; Aida, T. *Journal of the American Chemical Society* **1999**, *121*, 874-875.
- (131) Mitschke, U.; Bauerle, P. *Journal of Materials Chemistry* **2000**, *10*, 1471-1507.

3. BENZOPHENONE FUNCTIONALIZED POLYPHENYLENE DENDRIMERS – FROM INSIDE TO OUTSIDE

3.1 Introduction

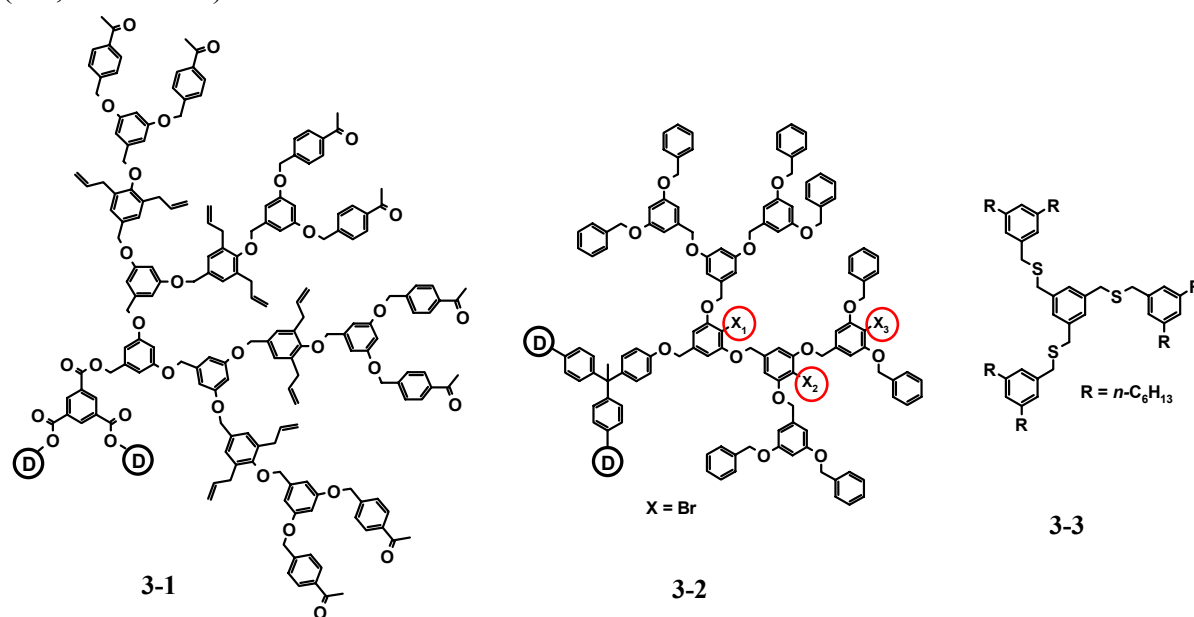
Since the TOMALIA^{1,2} and NEWKOME³ reports on dendrimers, research on these branched molecules has mainly focused on the preparation and characterization of a wide variety of dendritic macromolecules. Throughout the last years, the interest in this field has shifted toward designing functional dendrimers for specific high-end applications.⁴⁻⁷ In most cases the spatial isolation of the core and periphery has been used to tune the properties of the resulting materials. In that way many new fascinating phenomena could be studied, e.g. site isolation, host-guest chemistry, light harvesting and catalysis. However, in most cases, the dendrimer backbone was used to spatially arrange the functional moieties without bearing functions by itself.

Only few examples of a regiospecific covalent functionalization of the interior dendrimer backbone are known. Introducing functions in the interior of dendrimers can provide many new aspects to the synthesis of highly specialized nanoparticles. That way, for example, researchers synthesized multichromophore light harvesting systems providing an efficient energy-transfer from the peripherally located chromophores to the emitting core.⁸⁻¹³ Another aspect is that the interaction between multiple functional groups can enhance the non-covalent bonding of guest-molecules.¹⁴⁻¹⁶ Furthermore, instead of using only one catalytic active site in the center of the dendrimers, many catalytic centers could be embedded in a dendrimer, thereby leading to a significantly increased catalytic activity.¹⁷⁻¹⁹

Both, convergent and divergent approaches have been utilized for the construction of these new functional nanoparticles. (see also chapter 1.3). Functionalization of the inner dendrimer backbone can be done in two ways. 1. Applying a branching unit, that carries the desired function as well as additional functions that ensure the further dendrimer growth. That way, pre-functionalized branching units can be used to synthesize layered structures possessing different functional groups in neighbouring layers. 2. In a postsynthetic approach, where a dendrimer is constructed from a branching unit carrying an active function which can, after the synthesis of the dendrimer, be used as a starting point for further functionalization. The last approach offers a larger flexibility as once the dendrimer has been synthesized, the functionalization can easily be varied.

TWYMAN and coworkers have described the internal functionalization of a dendrimer possessing tertiary nitrogen groups.²⁰ When reacted with an excess of benzyl bromide, however, product mixtures were obtained, showing a nonquantitative conversion, which was attributed to steric and electronic effects. ZIMMERMAN et al. reported the postsynthetic intramolecular cross linking of internal allyl groups (**3-1**, Scheme 28).²¹ Removal of the core gave so called “cored” dendrimers, where the inner empty sphere is thought to be useful for the complexation of guest molecules. MAJORAL, CAMINADE and coworkers introduced phosphorous dendrimers, where internal aminophosphite group [P=N-P:] allowed the grafting of several functional groups in specific locations.^{22,23} Additionally, the internal reactive centers were used as starting points for the growth of new dendrons inside the dendrimer cavities. SCHLÜTER and coworkers presented FRÉCHET-type dendrimers selectively carrying

one aryl bromide functional group in the first-, second- or third-generation layer, respectively (**3-2**, Scheme 28).²⁴

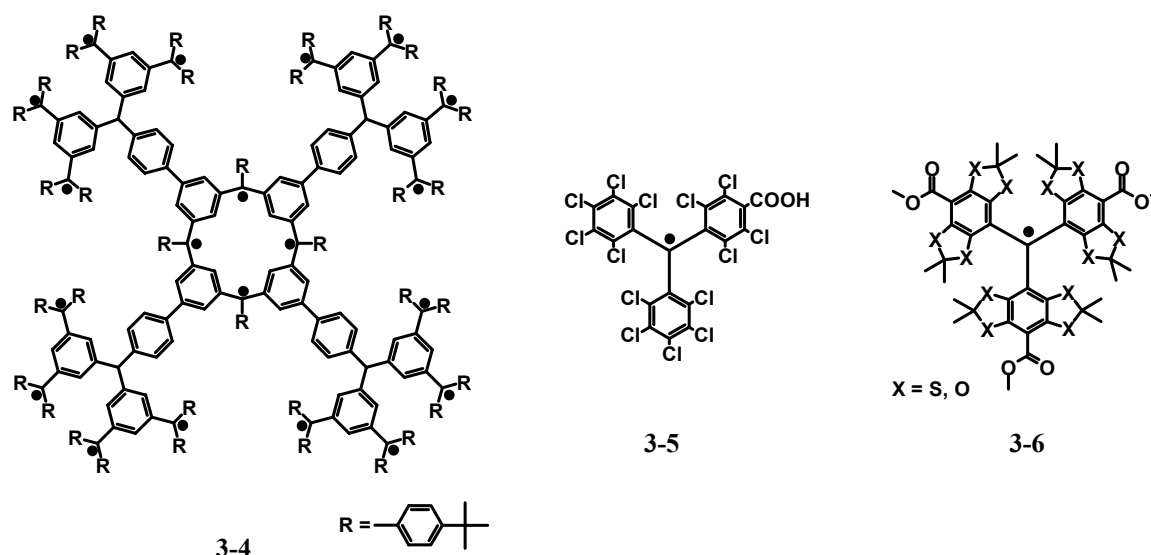


Scheme 28. Examples of a postsynthetic modification of the dendrimer interior in literature. (**3-1** ZIMMERMAN et al.,²¹ **3-2** SCHLÜTER et al.,²⁴ **3-3** CHOW et al.²⁵ **3-1**: One arm is drawn out fully. The three other arms are identical with the one shown but are abbreviated as a circled-D for ease of visualization. **3-2**: The two other arms are identical except missing bromine atoms.

These functions were accessible for SUZUKI cross-coupling reactions, showing their potential as internal anchor groups. Recently, CHOW et al. prepared oligo(dibenzylsulfide) dendrimers (**3-3**, Scheme 28).²⁵ Hydrogen peroxide oxidation of the internal dibenzyl-sulfide moieties gave the corresponding dibenzyl sulfane groups. Subsequent RAMBERG-BÄCKLUND reaction yielded an oligo(phenylvinylene) dendrimer backbone, highly interesting as this kind of building block possesses valuable liquid crystalline, photophysical, electrochemical, and electroluminescence properties.

Throughout the last years, there has been an increasing interest in the synthesis of three-dimensional architectures bearing multiple spin and/or charge carrying functions.²⁶⁻³³ Two major classes of polyradicals can be distinguished. Firstly, those with an unconjugated backbone to which stable radicals are attached as pendant groups. Secondly, the class that contains materials with conjugated backbone of the phenylacetylene type, either linked to free-radical side groups, or incorporating repeating paramagnetic centers within the backbone.

Dendritic structures with their unique properties, e.g. monodispersity and mesoscopic dimension have been functionalized with suitable groups that allowed the synthesis of novel nanoobjects. RAJCA and coworkers synthesized high-spin poly(arylmethyl) polyradicals (**3-4**, Scheme 29).^{34,35} Magnetic measurements confirmed the presence of high-spin ground states due to spatially well-defined polarized π -pins leading to organic magnetic materials on the nanoscale. However, the experimental examination and quantification of radical species is often difficult because of their high reactivity and thus short lifetime. To circumvent these problems BALLESTER et al. introduced perchlorinated triphenylmethyl radicals possessing high chemical and thermal stability (**3-5**, Scheme 29).³²



Scheme 29. Some examples of trityl radicals: (3-4 RAJCA et al.,^{34,35} 3-5 BALLESTER et al.,³² 3-6 RAWAL et al.³⁶).

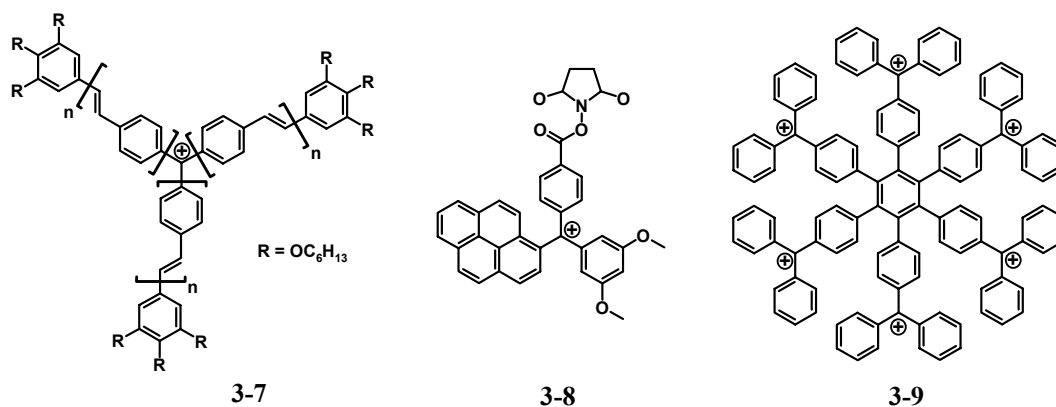
When additional carboxylic acids were attached these radicals form hydrogen-bonds and arrange in a supramolecular fashion. The aggregated trityl radicals showed to be stable even at 275 °C. Trityl radicals for EPR imaging of biological systems were introduced by RAWAL et al. (3-6, Scheme 29).³⁶ These trityl radicals were water soluble and even more, they were stable toward oxidants and reductants in biological systems, presumably because the ion pair electrons on the heteroatoms shielded the radical species.

The investigation of the monomer-dimer equilibrium of the parent triphenylmethyl radical showed that phenyl substituents are very powerful stabilizing substituents, mainly due to resonance. In addition to electronic effects, bulky substituents can produce steric hindrance keeping the radicals apart from each other.³⁷⁻⁴⁰

The highly stable triphenylmethyl (or trityl cation) and anion have been utilized in many facets of chemistry including in organic chemistry since the beginning of the twentieth century. The high stability of the trityl ions can be attributed to the extensive delocalization of the charge onto the phenyl rings via resonance. This particular property, which makes trityl ethers acid-labile, turned out to be useful, and the next few decades saw the trityl being developed into a major class of protective groups widely used in almost all fields of organic and bioorganic chemistry.

Trityl-based compounds also occupy an important niche in organic dye chemistry. MEIER and coworkers synthesized trityl cations with para-substituted oligo(1,4-phenylenevinylene)s (3-7, Scheme 30).⁴¹ Due to a far reaching charge distribution, these materials showed to be suitable as NIR-dyes with an absorption maximum of 860 nm and higher. SHCHEPINOV et al. introduced a new class of switchable fluorescent dyes in which one of the trityl phenyl rings is replaced by a fluorophore, in the case shown here pyrene (3-8, Scheme 30).⁴² Due to the trityl-type structure, their fluorescence can be reversibly switched by changing the pH.

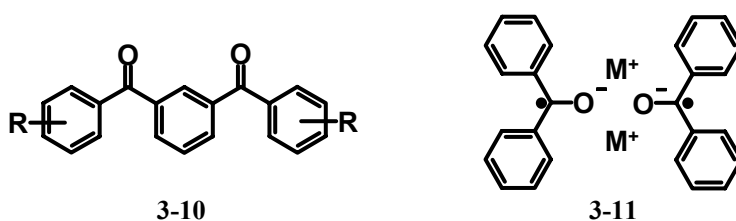
During the course of this work, RATHORE et. al reported the synthesis of a tetraphenylmethane and hexaphenylmethane moiety (3-9, Scheme 30) with peripherally attached trityl cations starting from the according polyalcohol precursors.⁴³ The multi trityl cations showed to be stable in substance at room temperature, mainly due to stabilization by resonance in the all phenyl structures.



Scheme 30. Trityl cations, some examples. (3-7 MEIER et al.,⁴¹ 3-8 SHCHEPINOV et al.,⁴² and 3-9 RATHORE et al.⁴³)

To apply a postsynthetic concept for the functionalization of dendrimers generally functional groups are required that exhibit both, a high reactivity as well as a high selectivity. Keto groups fulfil these demands, as they have been shown to be important substrates for several reactions leading to C-C bond formation e.g. Aldol- and CLAISEN-condensation or GRIGNARD-reactions.⁴⁴ As it will be shown later, in our case benzophenone was used as interior functional group for the postsynthetic modification of polyphenylene dendrimers.

Besides of chemical transformations, benzophenone has often been used to synthesize charge or spin carrying systems. For instance, the direct reduction of benzophenone with potassium is known to form the ketyl radical anion.⁴⁵⁻⁵¹ This radical species is one of the most important intermediates in the well-known photoreduction of benzophenone,⁵²⁻⁵⁵ thus its spectroscopic and electrochemical properties have been widely studied. The benzophenone “ketyl” radical anion has also received attention as a building block for the synthesis of high-spin organics and electrophores.



Scheme 31. Benzophenone radical anions in a conjugated backbone 3-10 and formation of metal bridged biradicals 3-11.

It is well established, that intramolecular high-spin systems can be designed by the incorporation of 1,3-aroylbenzene moieties into a structure with extended conjugation (3-10, Scheme 31).⁵⁶ Recent reports by HOU et al.^{57,58} have confirmed earlier conclusion arrived at by HIROTA and WEISSMAN^{49,59} on the basis of UV- and EPR-data that alkali metal aromatic ketone radical anions form strongly coupled biradicals. (3-11, Scheme 31). Therefore, the design of new high-spin systems is possible based on both, intra- and intermolecular high-spin coupling.

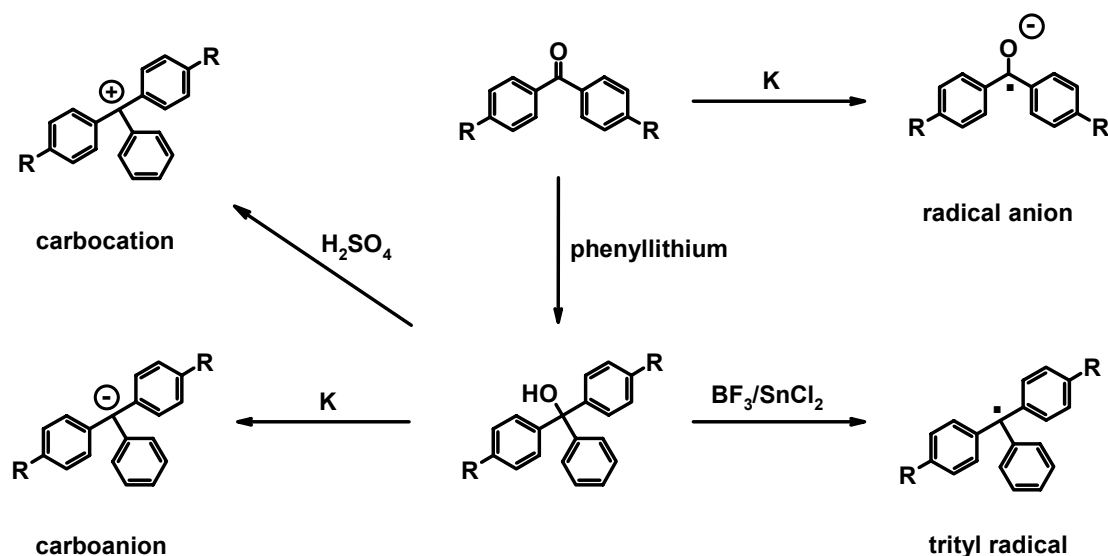
Chapter 3 deals with the functionalization of polyphenylene dendrimers with benzophenones. In the first part, chapter 3.2, multiple benzophenones were introduced in the dendritic scaffold. The promising results obtained from their postsynthetic modification are

then used to introduce benzophenones also in the core (chapter 3.3) and on the surface (chapter 3.4) of polyphenylene dendrimers. A more detailed introduction for the last two parts is given in the beginning of the according chapters.

The examples presented above suggest that a postsynthetic concept offers the possibility of conveniently altering the dendrimer interior once a suitable precursor molecule is available. As only related example R. BAUER in our group showed that ethyl esters in the inner of dendrimers could be hydrolyzed into the according acids. Furthermore, it was possible to decarboxylate the acids using CuO at 230 °C in ethylene glycol.⁶⁰

However, up to now, no topologically defined postsynthetic introduction of new functions in the scaffold of polyphenylene dendrimers is known. Especially the introduction of more complex functions, which are not stable during the DIELS-ALDER cycloaddition ($T > 150$ °C) might lead to new nanoparticles extending the scope of dendrimer functionalization of what is possible at the moment. As mentioned in the introduction polyphenylene dendrimers possess a rigid and shape persistent dendrimer backbone. This should allow defining the spatial arrangement of the introduced functions.

As suitable precursor unit, benzophenone was chosen due to its high reactivity toward lithium and GRIGNARD-reagents. The reaction of benzophenone derivatives with organo lithium-reagents yields the tertiary alcohol.



Scheme 32. Reaction pathways to spin/charge carrying derivatives starting from benzophenone.

Accordingly, benzophenone and phenyllithium give triphenylmethanol (Scheme 32). Triphenylmethanol itself can be used to synthesize carbocation, carboanion and trityl radical species. As already mentioned above, the reduction of benzophenone with alkali metals produces the radical anion. The introduction of benzophenone precursors in the polyphenylene backbone requires a branching unit that carries the benzophenones as well as active sites for the further dendrimer growth.

Once the dendrimers are synthesized postsynthetic functionalizations on the inner benzophenones will be attempted. When the term postsynthetic functionalization is used

together with macromolecules many questions arise. The most important one is maybe the question of how accessible the groups are on which the functionalization will be done. Steric hindrance can significantly influence the properties, e.g. reactivity or stability of embedded functions. The question of how accessible the inner benzophenones in the dendrimer are, is therefore of great interest and will be investigated in detail. Entrapping radicals or charged species in polyphenylene dendrons is expected to lead to a delocalization of their charge/spin into the all-phenyl backbone. Moreover, the intramolecular recombination or dimerization of radical centers should be avoided due to the hindered motion of the shape persistent dendritic arms. UV/vis, EPR, and NMR techniques will be used to investigate the role of the polyphenylene shell upon the accessibility and the chemical properties of the charge/spin carrying centers.

3.2 Multiple Benzophenones in the Dendrimer Backbone

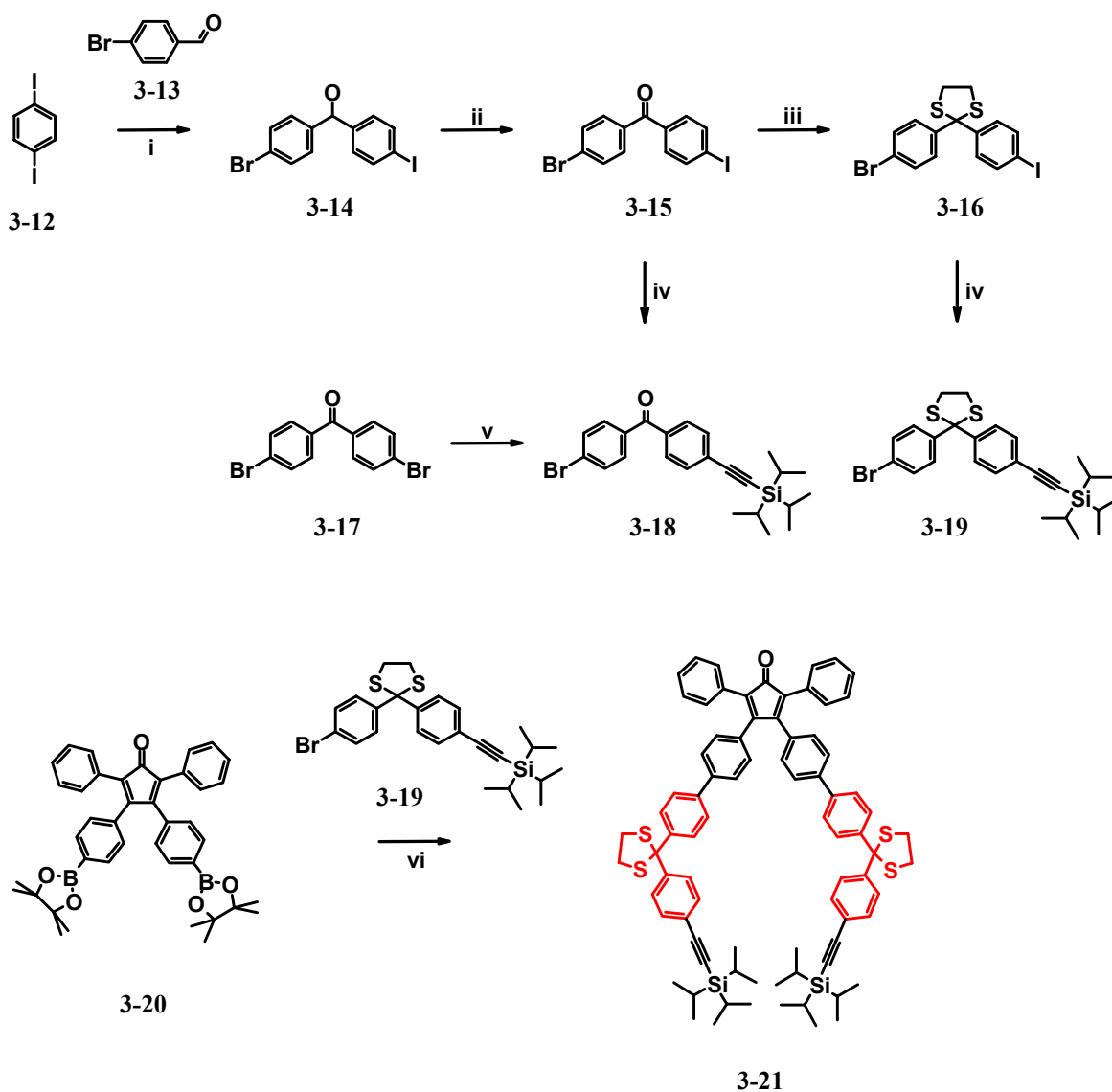
In this chapter the synthesis and characterization of dendrimers with embedded keto groups is presented. Several postsynthetic reactions in the inner of the dendrimer are performed showing the advantages of the herein described approach. Furthermore, charge or spin carrying centers were introduced in the dendrimer backbone. The investigation of their properties is one of the main topics.

3.2.1 Synthesis of the Branching Reagent

The key building block for the construction of ketone bearing polyphenylene dendrimers is a tetraphenylcyclopentadienone branching unit carrying both: the keto groups and additional ethynyl groups allowing further growth in a DIELS-ALDER cycloaddition. This concept of an inner dendrimer functionalization has first been introduced by T. WEIL in the group of Prof. MÜLLEN, where one of the two branching sites of the tetraphenylcyclopentadienone branching unit **1-35** was replaced by a perylene monoimide (PMI) moiety. Using this branching unit a PMI substituted dendritic backbone was obtained.⁶¹ One outcome of this approach was that due to the reduced number of branching sites the polyphenylene shell was less crowded, leading to relatively big voids in the dendrimer shell.

Recently we have shown that the boronic-acid functionalized tetraphenylcyclopentadienone **3-20** is an efficient building block, as bromo- or iodo-substituted aromatic compounds with the desired functionality can easily be introduced by SUZUKI cross-coupling.⁶² To apply this concept for the synthesis of a benzophenone functionalized tetraphenylcyclopentadienone, the benzophenone derivative **3-18** had to be synthesized, where the bromine can be used for the SUZUKI cross-coupling with **3-20** and the *triisopropylsilyl* protected ethynyl group ensures further dendrimer growth. In the beginning, **3-18** could be obtained by statistical HAGIHARA-SONOGASHIRA cross-coupling of the commercially available 4,4'-dibromobenzophenone (**3-17**) and (*triisopropylsilyl*)-ethyne (Scheme 33). Due to the statistical reaction and difficult chromatographic purification the overall yield of this step was only 15%.

Coupling of acetylenes with halogen benzenes using HAGIHARA-SONOGASHIRA cross-coupling reaction conditions can be done selectively on the iodo at room temperature, present bromo functions react only at higher temperatures ($\approx 60-80$ °C).⁶³ Typically, the yields for the coupling reactions with iodo benzenes are higher than those for bromo benzenes.

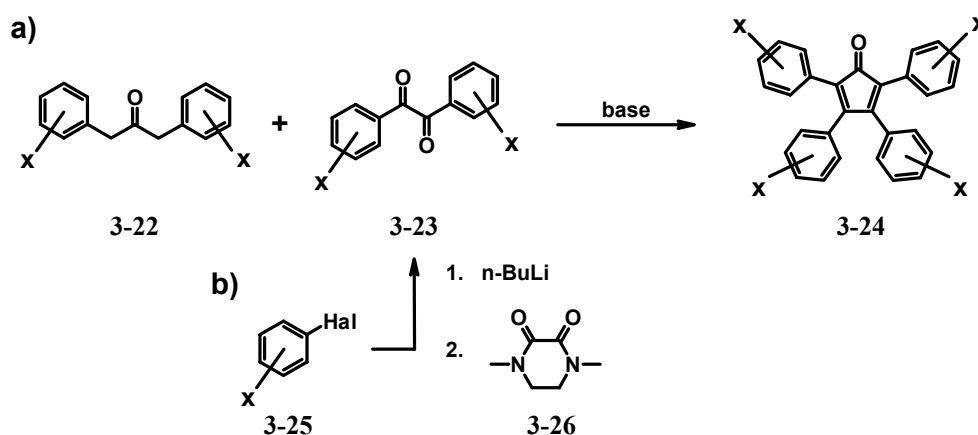


Scheme 33. Synthesis of the benzophenone functionalized branching unit 3,4-bis-[4-(2-{4-[(triisopropylsilyl)ethynyl]-ethynyl]-phenyl}-[1,3]dithiolan-2-yl)-phenyl]-2,5-diphenylcyclopentadienone (**3-21**): i) 1 eq. *n*-BuLi, 4-bromobenzaldehyde (**3-13**), THF, -78 °C, 80%; ii) Oxalylchloride, DMSO, TEA, CH₂Cl₂, -78 °C, 93%; iii) ethane-1,2-dithiole, BF₃·OAc₂, CH₂Cl₂, 95%; iv) **3-15/3-16**, (triisopropylsilyl)-ethyne, [Pd(PPh₃)₂]Cl₂, PPh₃, CuI, Toluene, TEA, 97%/96%; v) (triisopropylsilyl)-ethyne, [Pd(PPh₃)₂]Cl₂, PPh₃, CuI, Toluene, TEA, 80 °C, 15%; vi) 3 eq. **3-19**, Pd(PPh₃)₄, K₂CO₃, Toluene, EtOH, 80 °C, 78%.

The improved synthesis of **3-18** is therefore based on the 4-bromo-4'-iodo-benzophenone derivative **3-15** allowing the selective desymetrization reaction with (triisopropylsilyl)-ethyne (Scheme 33) in high yield. After successful mono-lithiation of 1,4-diiodobenzene (**3-12**), the reaction was quenched with 4-bromo-benzaldehyde (**3-13**) to afford (4-bromo-phenyl)-(4-iodo-phenyl)-methanol (**3-14**) in 80% yield.⁶⁴ Subsequent SWERN oxidation⁶⁵⁻⁶⁷ generated 4-bromo-4'-iodo-benzophenone (**3-15**) in almost quantitative yield. The desymetrization of the benzophenone assured that the following HAGIHARA-SONOGASHIRA cross-coupling^{63,68,69} with (triisopropylsilyl)-ethyne could be carried out selective on the iodo function of **3-15** to obtain a single product in high yield.

Advantages of this longer synthetic route are: high yields in every step and easy purification of the products. Thus, **3-18** could be obtained in an overall yield of 69% on the 20 gram scale. Unfortunately, the SUZUKI cross-coupling⁷⁰⁻⁷² of **3-20** with **3-18** gave the desired benzophenone functionalized tetraphenylcyclopentadienone (structure not shown) in only 20% yield, even when different catalyst/base systems were employed.⁷³⁻⁷⁵ Since the branching unit is used in excess in the DIELS-ALDER cycloaddition, a more efficient synthesis had to be developed, allowing the synthesis of the branching unit in gram-scale.

Next to a postsynthetic functionalization using the boronester functionalized building block **3-20**, substituted tetraphenylcyclopentadienones are also available by the functionalization of the 1,2-diphenyl-ethane-1,2-dione precursor (**3-23** (Scheme 34). Subsequent base-catalysed KNOEVENAGEL condensation with 1,4-diphenylpropan-2-on (**3-22**) yields the functionalized tetraphenylcyclopentadienone **3-24**. MÜLLER-WESTERHOFF introduced an alternative method for the synthesis of substituted 1,2-diphenyl-ethane-1,2-diones: halogen lithium exchange of a benzene carrying the desired function and subsequent reaction with N,N'-dimethyl-piperazin-2,3-dion (**3-26**).^{76,77}



Scheme 34. Synthesis of functionalized tetraphenylcyclopentadienones. a) base-catalyzed KNOEVENAGEL condensation, b) approach by MÜLLER-WESTERHOFF for the synthesis of substituted 1,2-Diphenyl-ethane-1,2-diones **3-23**.

To use this concept for the synthesis of a benzophenone substituted 1,2-diphenyl-ethane-1,2-dione, the benzophenone keto group had to be protected since *n*-butyllithium is used in the course of the reaction. This was accomplished by introducing a dithiolan protecting group^{78,79} yielding the benzophenone derivative **3-19**. Unfortunately, during the synthesis of the benzophenone functionalized 1,2-diphenyl-ethane-1,2-dione side products were formed which could not be separated by column chromatography. However, further experiments showed that, after the introduction of the dithiolane protecting group, the SUZUKI cross-coupling of **3-20** with **3-19** furnished the tetraphenylcyclopentadienone **3-21** in the surprisingly good yield of 78% (Scheme 33) (catalyst/base: Pd(PPh₃)₄/K₂CO₃). One reason for the significant increase of the yield (20% to 78%) might be the conjugation between the keto group and the bromine which is interrupted by the introduction of the dithiolane protecting group. Additionally, the dithiolan derivative **3-19** is better soluble than the benzophenone **3-18**.

The purity of the benzophenone functionalized tetraphenylcyclopentadienone **3-21** was checked by FD-mass spectrometry as well as by NMR spectroscopy. Figure 28a shows the FD mass spectrum of **3-21**. A major signal is displayed at a molecular weight of 1258.1 g·mol⁻¹

and can be attributed to the desired product (calculated: $1258.0 \text{ g}\cdot\text{mol}^{-1}$). Additionally, a signal for the double-charged species can be observed at $2514 \text{ g}\cdot\text{mol}^{-1}$.

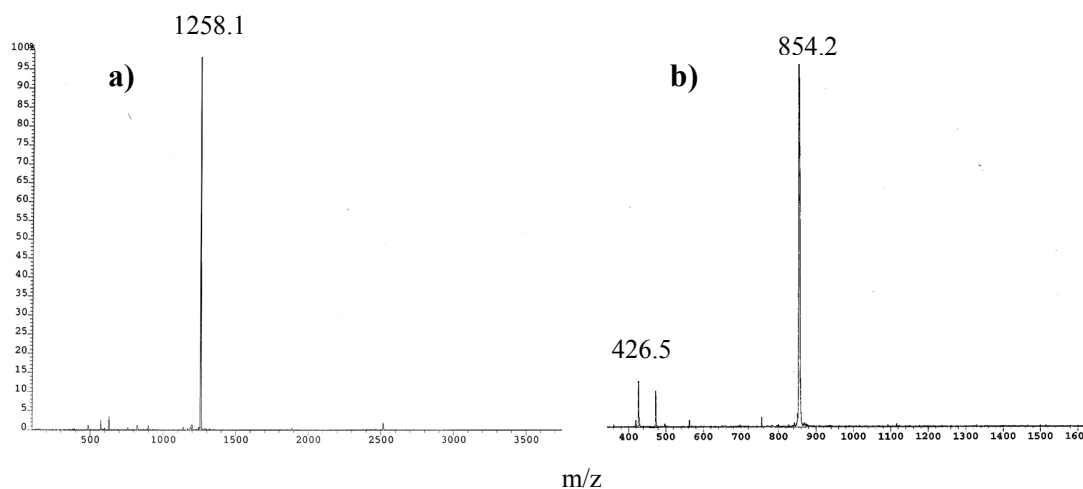


Figure 28. a) FD mass spectrum of **3-21** and b) **3-69** (calculated molecular weight: a) $1258.0 \text{ g}\cdot\text{mol}^{-1}$, b) $857.1 \text{ g}\cdot\text{mol}^{-1}$).

The ^1H NMR spectrum of the branching unit **3-21** is depicted in Figure 29. The *triisopropylsilyl* (TIPS) protons H_a and H_b showed up at $\delta = 1.12 \text{ ppm}$ as a single peak. The resonances of the dithiolan protecting groups $\text{H}_{c+c'}$ were located at $\delta = 3.42 \text{ ppm}$.

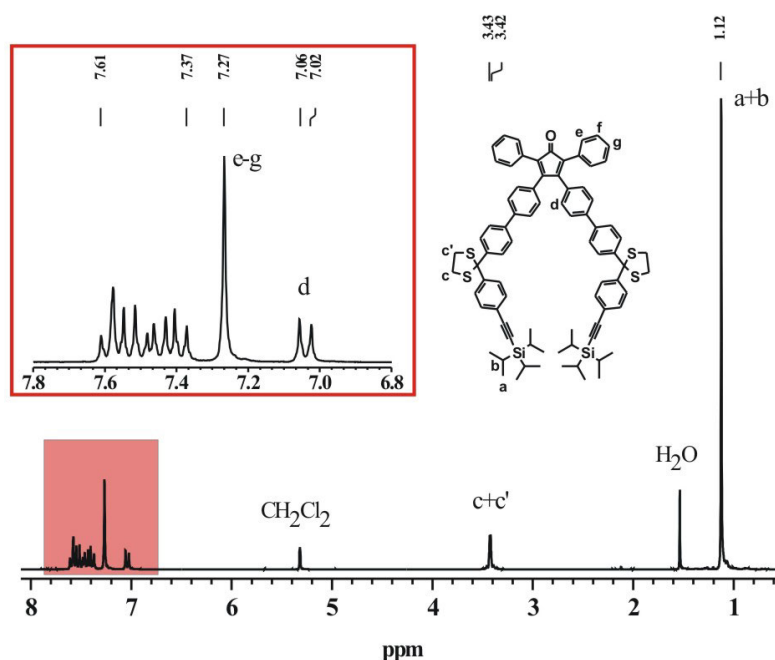


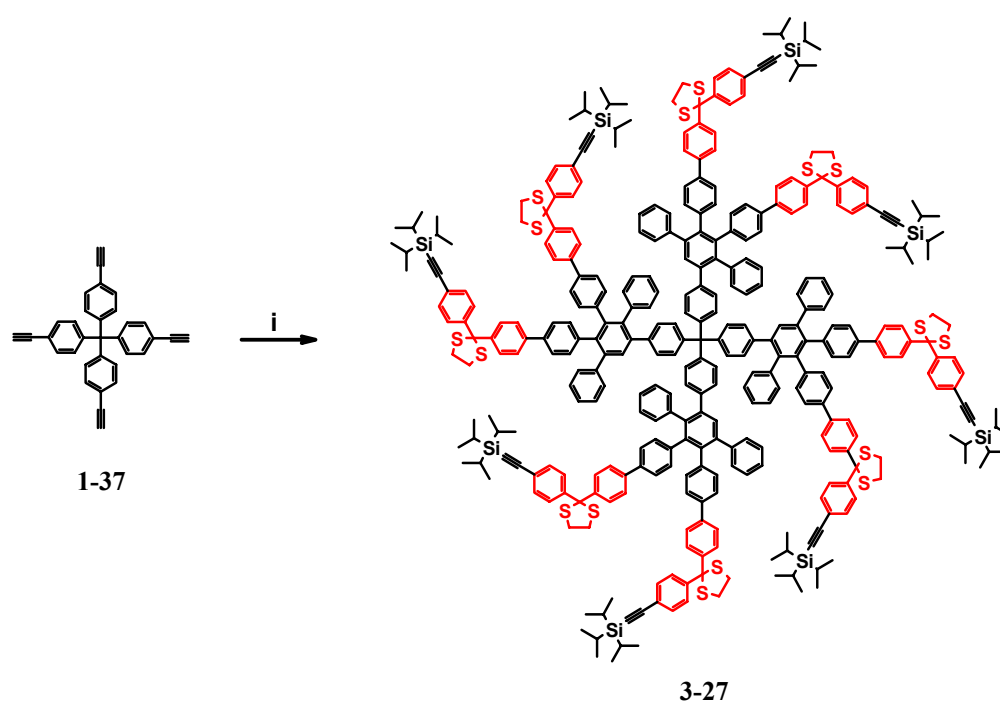
Figure 29. ^1H NMR spectrum of the benzophenone functionalized tetraphenylcyclopentadienone **3-21**. (250 MHz, CD_2Cl_2 , 300 K).

In the aromatic region the doublet at $\delta = 7.02 \text{ ppm}$ was assigned to the protons on the β -phenyl rings next to the cyclopentadienone moiety. The protons on the α -phenyl rings $\text{H}_e - \text{H}_g$ overlapped to the singlet at $\delta = 7.27 \text{ ppm}$. The other aromatic protons of the substituted benzophenones displayed as a multiplett at $\delta = 7.61 - 7.37 \text{ ppm}$.

Concluding, FD-mass spectrometry and ^1H NMR measurements prove the purity of the building block **3-21**. For a monodisperse dendrimer growth it is absolutely necessary, that the branching unit is perfectly pure. Impure materials would result in structural defects of the dendrimers, these being almost impossible to remove by chromatography.

3.2.2 Synthesis of the Dendrimers

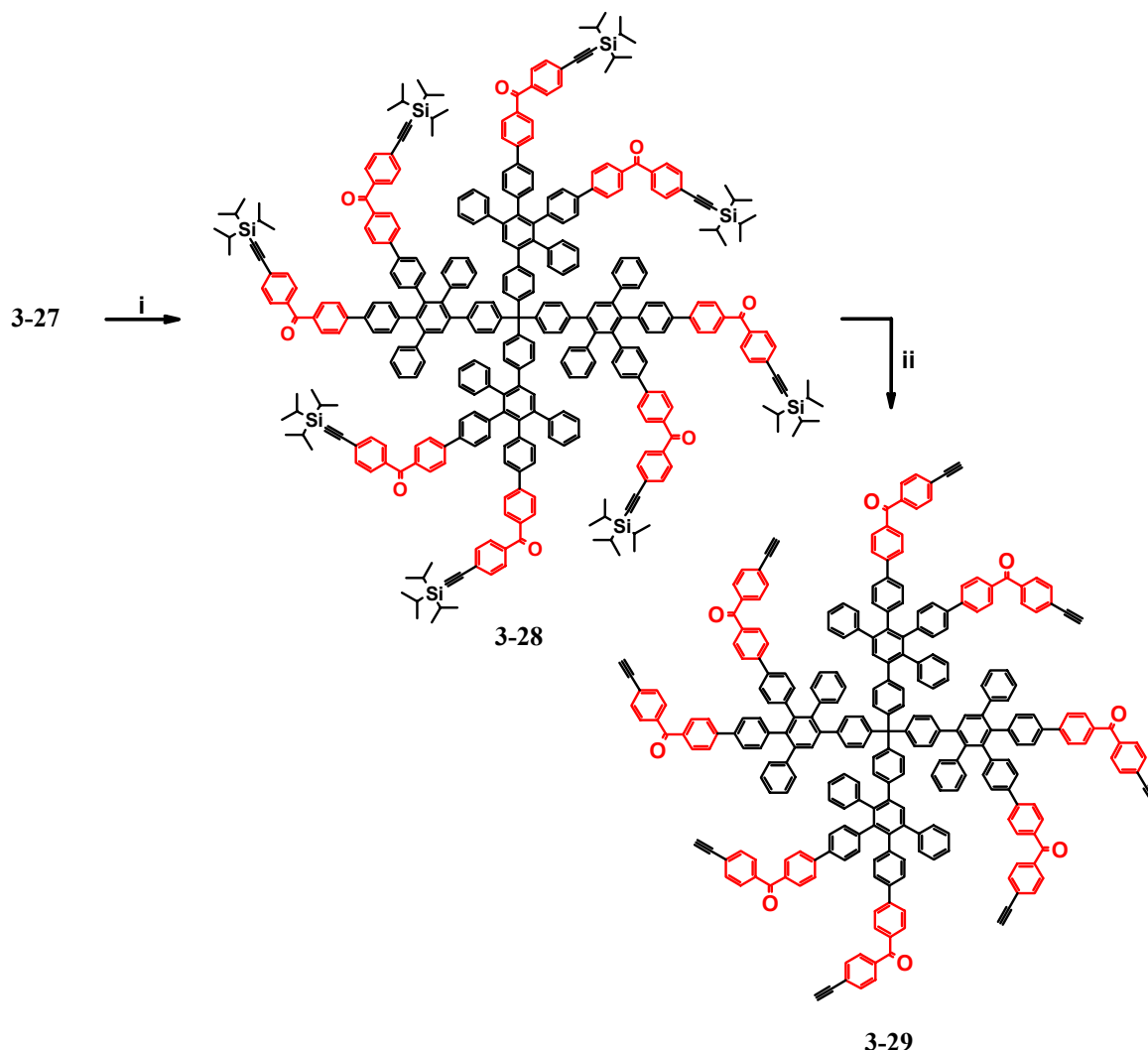
The key step in the synthesis of structurally well defined polyphenylene dendrimers is the repeated $[4 + 2]$ cycloaddition of the tetraphenylcyclopentadienone building block to an ethynyl substituted core or dendrimer and subsequent deprotection of the TIPS protected ethynyl groups which activates the molecule for further growth.^{80,81} To place the functional groups in the inner dendrimer scaffold, the benzophenone functionalized branching unit **3-21** has been used in the first step of dendrimer growth. Heating of the tetraphenylmethane core **1-37** and the branching unit **3-21** in *o*-xylene at 155 °C yields the first-generation dendrimer **3-27** (Scheme 35) in almost quantitative yield.



Scheme 35. Synthesis of the first-generation dendrimers **3-27**: i) 6 eq. **3-21**, *o*-xylene, 155 °C, 98%.

In general, the monodispersity of polyphenylene dendrimers can easily be proven by means of MALDI-TOF mass spectrometry. In the case of **3-27** no clear product mass signal could be detected due to fragmentation of the dithiolane protecting groups. Probably cleavage of ethylsulfide groups happened under the MALDI-TOF mass conditions as multiple mass signals were found, differing from each other with $62 \text{ g}\cdot\text{mol}^{-1}$.⁸² Thus, quantitative conversion of the DIELS-ALDER cycloaddition was proven by ^1H NMR spectroscopy through the absence of the ethynyl proton signal of the core **1-37**. For the synthesis of higher-generation polyphenylene dendrimers MALDI-TOF mass spectrometry is crucial, as reaction time of the growth step sometimes exceeds a few days making a careful control over the course of the reaction absolutely necessary. Dithiolane protecting groups can be removed by stirring the

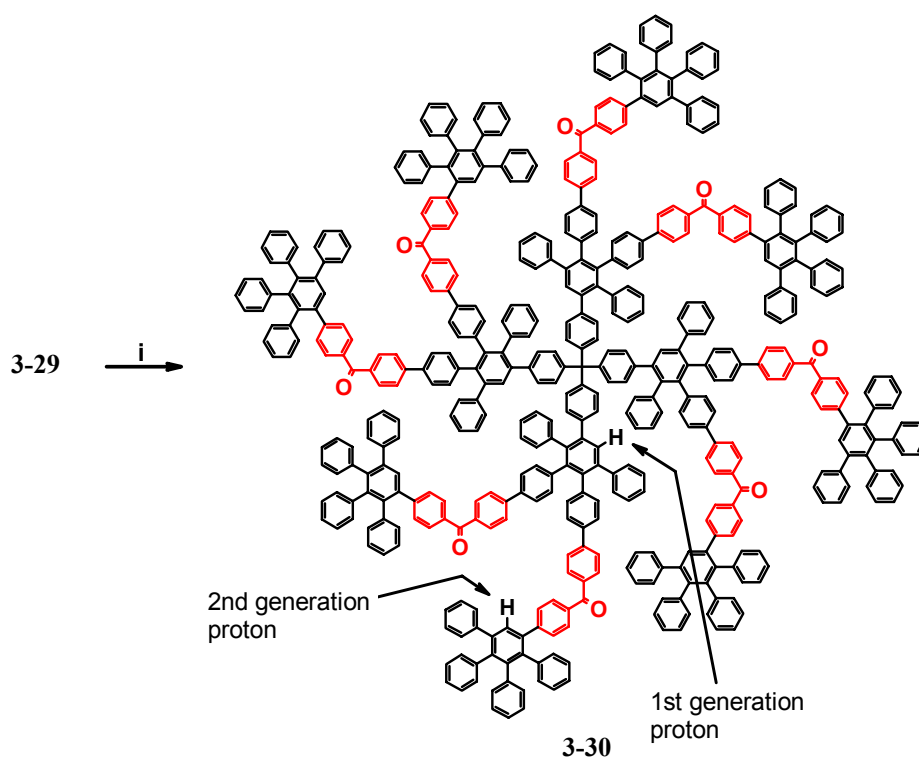
protected derivative in a mixture of DMSO and *t*-butylbromide at higher temperature.⁸³ The deprotection step, when carried out on the stage of the tetraphenylcyclopentadienone **3-21**, yielded a mixture of products containing partially degraded tetraphenylcyclopentadienone moieties. To enable anyhow MALDI-TOF mass spectrometry for the higher generation dendrimers, the deprotection of the benzophenones was therefore accomplished after the synthesis of the first-generation dendrimer **3-27**.



Scheme 36. Synthesis of the scaffold functionalized dendrimers **3-28** and **3-29**: i) *t*-butylbromide, DMSO, 75 °C, 94%; ii) TBAF, THF, 96%.

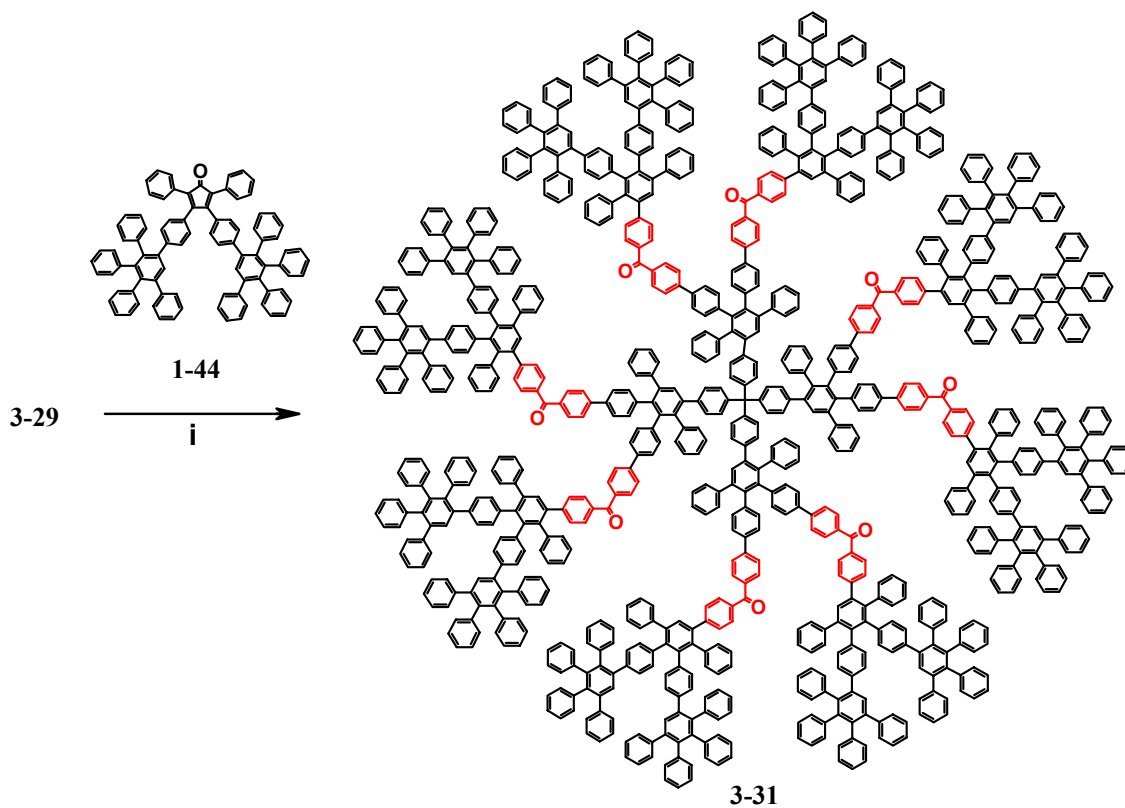
Following the deprotection procedure described above gave **3-28** in very good yield (Scheme 36). Purification of **3-28** was achieved by precipitation from MeOH and washing of the residue with water and MeOH. The ethynyl functionalized first-generation dendrimer **3-29** was obtained by subsequent quantitative desilylation of the TIPS protecting groups with tetrabutylammonium fluoride (TBAF). In the last step toward dendrimers with embedded keto groups, **3-29** and tetraphenylcyclopentadienone (**1-32**) were reacted with each other in the last step and yielded the second-generation dendrimer **3-30** in 97% yield (Scheme 37). Purification was achieved by precipitation from *n*-pentane and afterwards short column chromatography to remove small amounts of **1-32** still present after the precipitation.

The accessibility and shielding of the inner benzophenones can be varied by using different sizes of outer polyphenylene shells.



Scheme 37. Synthesis of the second-generation dendrimer **3-30**: i) 16 eq. **1-32**, *o*-xylene, 160 °C, 97%.

To increase the shielding, the first-generation dendrimer **3-29** was reacted with dendron **1-44**. Reflux in *o*-xylene overnight gave the third-generation dendrimer **3-31** (Scheme 38)



Scheme 38. Synthesis of the third-generation dendrimer **3-31**. i: 16eq. **1-44**, *o*-xylene, 180 °C, 85 %.

The herein described dendrimers possess a good solubility in common organic solvents (CH_2Cl_2 , toluene or THF, e.g. **3-28** even in hexane), which allowed their purification by column chromatography as well as their complete characterization by standard spectroscopic techniques.

^1H NMR spectroscopy showed well separated and clearly assignable signals for some of the aromatic protons as well as for the dithiolane, ethynyl, or TIPS protons. The obtained intensity ratios between aromatic and aliphatic signals corresponded well to the expected values (see Experimental part). Figure 30 displays as an example the ^1H NMR spectrum of the second-generation dendrimer **3-30**. At $\delta = 7.63$ ppm the first-generation proton H_c showed up. The second-generation protons could not be observed due to an overlap of signals, resulting in the multiplett at $\delta = 7.56$ ppm.

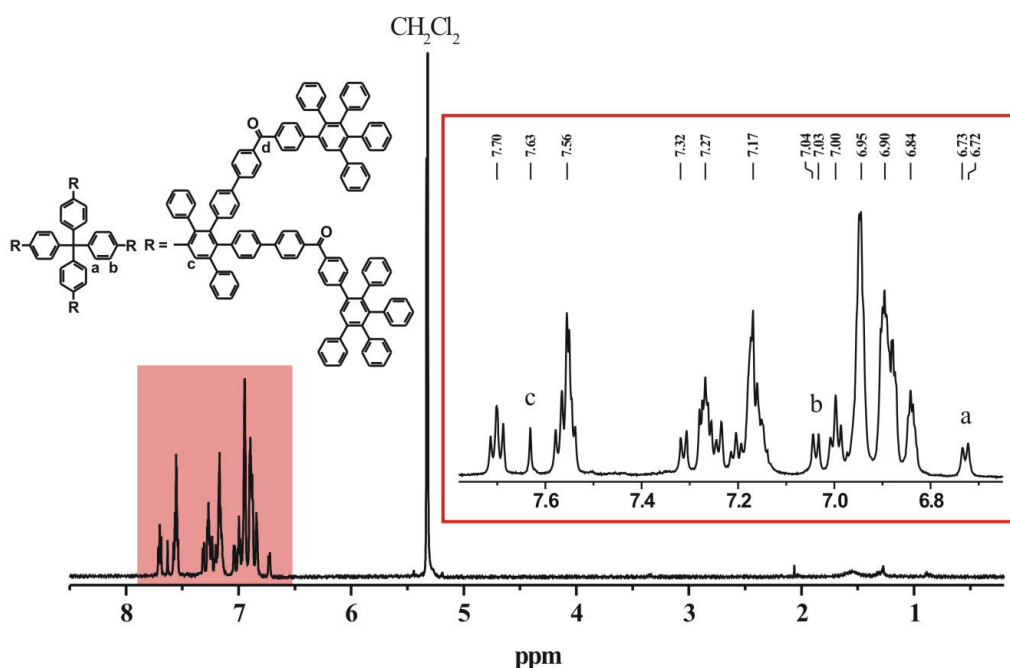


Figure 30. ^1H NMR spectrum of the second-generation dendrimer **3-30** (700 MHz, CD_2Cl_2 , 300 K).

An additional proof of structure could be derived, as significant signals of the core protons were found (see also Scheme 37). The protons H_a and H_b appeared as doublets at $\delta = 6.72$ ppm and $\delta = 7.03$ ppm, respectively. The ^{13}C NMR spectrum of **3-30** showed a single distinctive signal for the carbonyl carbon at 196 ppm.

The monodispersity of the benzophenone functionalized dendrimer **3-30** was proven using MALDI-TOF mass spectrometry, where even small amounts of unreacted species can be detected. Figure 31 shows the MALDI-TOF mass spectrum of **3-30**, measured with the addition of trifluoroacetic acid potassium salt. It showed a major signal at $6363 \text{ g}\cdot\text{mol}^{-1}$ which can be assigned to the complex of **3-30** and potassium $(\text{M}+\text{K})^+$ with a calculated molecular weight of $6367 \text{ g}\cdot\text{mol}^{-1}$. The cation of **3-30** $(\text{M})^+$ appeared as a small signal at $6325 \text{ g}\cdot\text{mol}^{-1}$, well corresponding with the calculated molecular weight of $6328 \text{ g}\cdot\text{mol}^{-1}$. An additional salt complex with silver $(\text{M}+\text{Ag})^+$ displayed at $6432 \text{ g}\cdot\text{mol}^{-1}$. The $\frac{3}{4}(\text{M})^+$ fragment at $4747 \text{ g}\cdot\text{mol}^{-1}$ and the double-charged species $(\text{M})^{2+}$ further prove the purity of **3-30**.

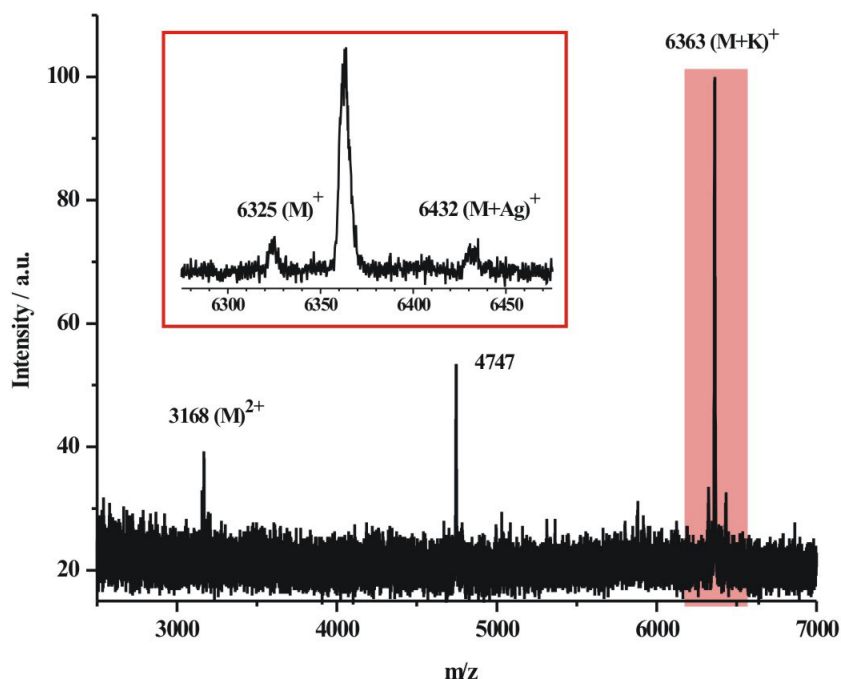


Figure 31. MALDI-TOF mass spectrum of **3-30** (calculated molecular weight: $6328 \text{ g}\cdot\text{mol}^{-1}$; matrix: dithranol).

The addition of tetraphenylcyclopentadienone (**1-32**) with the extrusion of carbon monoxide during the DIELS-ALDER cycloaddition leads to an increase of the mass of $356 \text{ g}\cdot\text{mol}^{-1}$. No signals are detected at lower or higher molecular mass thereby proving the quantitative and defectfree reaction of **1-32** with the acetylene groups of **3-29**.

3.2.3 Visualization and Simulation

To get an impression of the shape and size of the synthesized dendrimers, molecular mechanics calculations were carried out by applying the MMFF method.⁸⁴ Figure 32 shows the three-dimensional structure of the second-generation dendrimer **3-30** functionalized with eight benzophenones in its scaffold. A diameter of 5.8 nm was determined by duplicating the distance from the tetraphenylmethane center to the outer phenyl groups. For the third-generation dendrimer **3-31** a calculated diameter of 7.0 nm was found. When the parent AB_2 branching unit **1-35** is used for the growth, the second-generation dendrimer **1-40** has a diameter of 4.4 nm.⁸⁰ Due to the elongated branching arms of the benzophenone functionalized branching unit **3-21**, **3-30** possess a significantly bigger calculated diameter of 5.8 nm. The three-dimensional structure of **3-30** shows that the benzophenones (red) are located at the border between the first- and the second-generation layer.

Despite of the outer dendrimer shell the benzophenones still seem to be not shielded completely. This would allow reaction partners to approach the embedded radical centers (arrows, Figure 32) and thus hinder the radical stability. On the other hand the keto groups might therefore be accessible for chemical transformations rising the possibility of an efficient postsynthetic functionalization of the inner dendrimer.

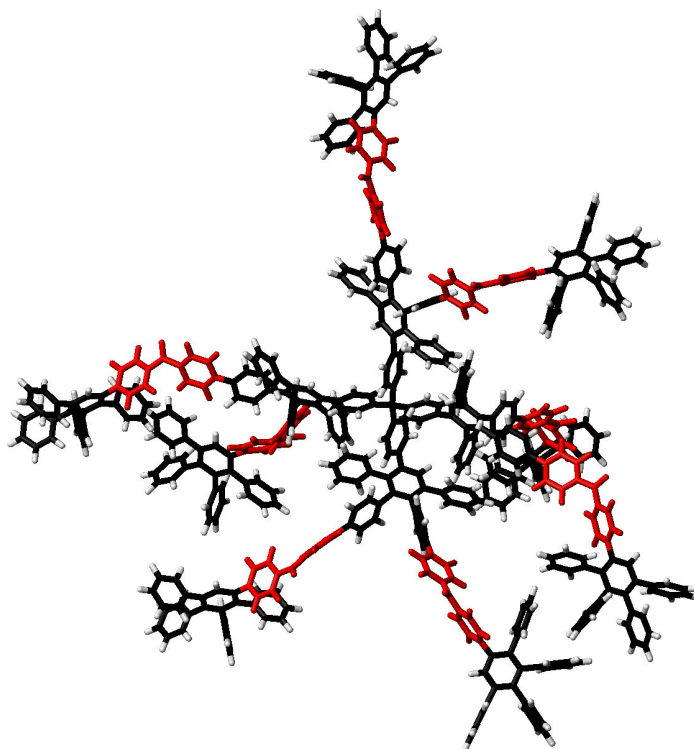


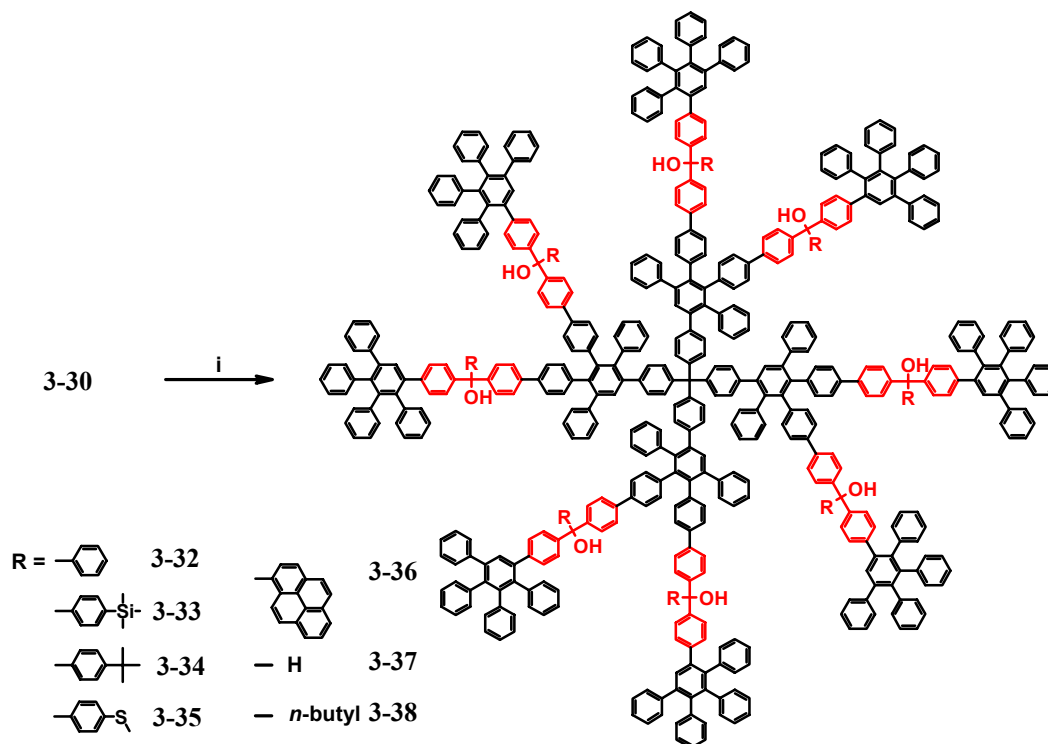
Figure 32. Three-dimensional structure of the second generation dendrimer **3-30** with 8 benzophenones (red) obtained by molecular modeling.

3.2.4 Postsynthetic Functionalizations of the Dendrimer Backbone

In this chapter, the postsynthetic modification of the backbone of polyphenylene dendrimers is described. This concept was applied to synthesize precursors, suitable for the generation of charge and/or spin carrying centers in the dendrimer interior. For reasons of clarity, synthetic aspects are exclusively described in this chapter. The in-depth characterization of the new species by different spectroscopic methods is described in the thereafter following chapters 3.2.4.1 - 3.2.6.

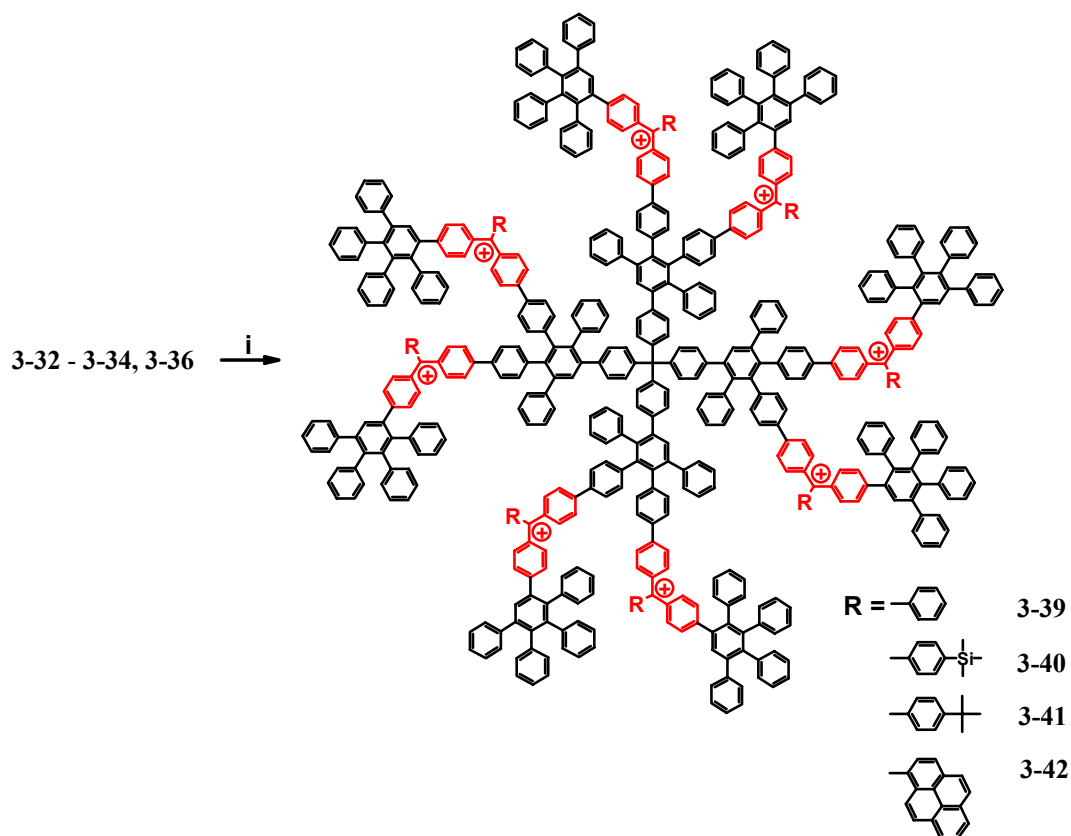
The question of how accessible the keto groups are was investigated by a large number of chemical transformations. A well documented example is the trityl cation, which is generated immediately when triphenylmethanol is reacted with a strong acid, such as tetrafluoroboric acid or trifluoroacetic acid (TFA).^{41,43,85} Since keto groups are known to be highly reactive toward lithium-reagents, multiple triphenylmethanol groups should be available by the reaction of the benzophenone bearing dendrimer **3-30** with e.g. phenyllithium. Accordingly, a large excess of phenyllithium was reacted with **3-30** in refluxing THF overnight. After hydrolysis, the eight times substituted product **3-32** was obtained in 97% yield (Scheme 39). Reactions with lithium-reagents, e.g. *n*-butyllithium are normally carried out at reduced temperature, typically -78 °C. However, the above described drastic conditions needed to be applied since the reaction of **3-30** with phenyllithium at room temperature resulted in only partial conversion. The reaction of benzophenone with nucleophiles, e.g. phenyllithium is presumably accompanied by a change in the shape of the molecule. Due to the sp^2 hybridization of the carbonyl carbon, benzophenone ideally exhibits a planar conformation. Quite contrary, after the reaction, triphenylmethanol exhibits a tetragonal shape since the central carbon atom possesses sp^3 hybridization. Applying this to the reaction of the

keto groups in dendrimer **3-30** one has to consider, that the embedded benzophenones are linked to the dendrimer backbone through their para-positions. Thus, their reaction with phenyllithium ($sp^2 \rightarrow sp^3$) is only possible, when the conformation of the whole dendrimer arm is changed. The high temperatures used might have resulted in an increased rotational motion of the dendrimer arms, thereby facilitating the reaction of the benzophenones with phenyllithium.



Scheme 39. Postsynthetic functionalization of benzophenone functionalized dendrimer **3-30**: i) **3-32**: 100 eq. C_6H_5Li , THF, 70 °C, 97%; **3-33** - **3-36**: *t*-butyllithium, THF, 70 °C, *p*-bromo-TMS-benzene (**3-33**, 96%), *p*-bromo-*t*-butylbenzene (**3-34**, 78%), 1-bromopyrene (**3-36**, 76%), *p*-bromo-thioanisol (**3-35**, %); **3-37**: 170 eq. $LiAlH_4$, THF, 70 °C, 80%; **3-38**, 100 eq. *n*-butyllithium, THF, 70 °C, 85%.

Purification of **3-32** was easily achieved by repetitive precipitation from MeOH. No side products could be observed by NMR spectroscopy, elemental analysis and mass spectrometry. However, some hydroxy groups were cleaved during the MALDI-TOF mass measurement, as indicated by small signals at lower molecular weight (see for example **3-33**, Figure 33). The ready availability of the polyalcohol precursor **3-32** made it an attractive starting point for the synthesis of a dendrimer with multiple entrapped trityl cations. When **3-32** was reacted with trifluoroacetic acid (TFA) in CH_2Cl_2 the reaction mixture immediately turned deep blue indicating the formation of the corresponding trityl cations (Scheme 40). A detailed spectroscopic characterization of the trityl cations is given in chapter 3.2.5.1. When borontrifluoride diethyl etherate ($BF_3 \cdot OEt_2$) was used as the acid,^{36,86} **3-39** could be isolated as the dark-blue trifluoroborate salt. The solid showed no degradation when stored under an argon atmosphere at room temperature for long time. Hydrolysis of **3-39** led back to the triphenylmethanol precursor indicated as the NMR spectrum of the product was identical to that of **3-32**.

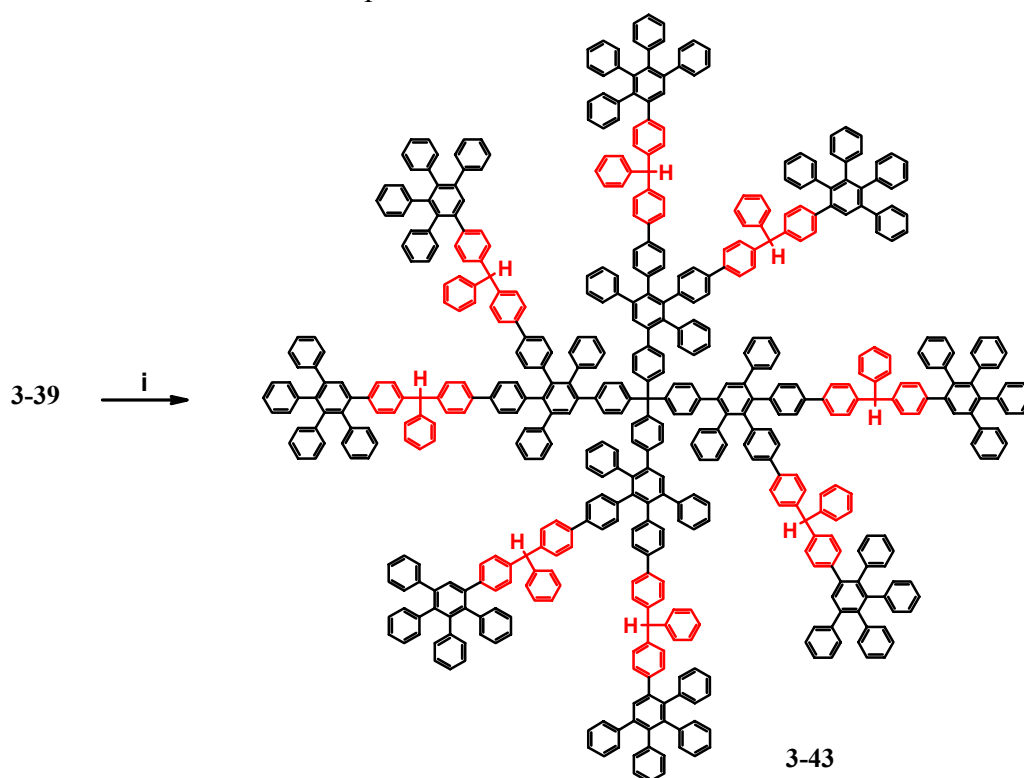


Scheme 40. Synthesis of the trityl cation bearing dendrimers **3-39** - **3-42** and hydride abstraction from triethylsilane to **3-43**: i) TFA/BF₃·OEt₂, respectively, CH₂Cl₂.

To achieve an independent proof of structure the reduction of **3-39** was carried out using triethylsilane as a hydride donor^{86,87} (Scheme 41). When a solution of **3-39** in CH₂Cl₂ at 0 °C was reacted with triethylsilane, the blue color of the trityl cation species faded away immediately. After aqueous workup and precipitation from MeOH, the desired triphenylmethyl derivative **3-43** could be verified by spectroscopic methods as well as by MALDI-TOF mass spectrometry, thereby proving the eightfold functionalization of the dendrimer backbone with trityl cations.

The stability and therefore easy handling of the trityl cation functionalized dendrimer **3-39** should make it an ideal candidate for the synthesis of a dendrimer bearing multiple trityl radicals. A variety of procedures involving the reduction of a triarylmethyl carbenium ion and the thermal or photolytic decomposition of a suitable precursor are known.^{36,88} Polyphenylene dendrimers with their stiff and shape persistent dendrimer backbone should fix the radicals in defined positions in the dendritic sphere. Since the radicals are therefore expected to be spatially separated, recombination or disproportionation reactions, possible reactions that radicals can undergo, should be suppressed. The recombination of the triphenylmethyl(trityl) radical is known to be inhibited by bulky para-substituents,⁸⁹ e.g. the tris(*p-t*-butylphenyl)methyl radical is thought to be fully dissociated in solution.⁹⁰ However, the fact that crystalline head-to-head dimers can be obtained from solutions of tris(2,6-di-*t*-butyl-4-diphenyl)methyl radicals⁹¹ and of tris(3,5-di-*t*-butyl-4-diphenyl)methyl radicals⁸⁹ raises the possibility of head-to-head association in solution. To further suppress the possible recombination of the dendrimer embedded trityl radicals a bulky para-substituent was introduced, blocking the one free para-position. Both other para-positions are connected to the

dendrimer backbone, therefore being not available for side reactions of the radical. 1-bromo-4-*t*-butyl-benzene was converted via halogen-metal exchange into its lithium-reagent and reacted with **3-30** in the same way as described before, to give the monodisperse dendrimer **3-34** (Scheme 39). Similar as to **3-32**, **3-34** was converted into its corresponding trityl cation derivative **3-41**. The subsequent formation of the trityl radical species is described in detail in chapter 3.2.5.2.



Scheme 41. Hydride abstraction from triethylsilane. i) **3-39**, triethylsilane, CH_2Cl_2 , $0\text{ }^\circ\text{C}$, 90%.

An important feature of the introduced keto groups is the possibility of a regiospecific postsynthetic functionalization of the interior dendrimer backbone as we have demonstrated with the synthesis of **3-32** and **3-34**. To show the possibility of a more challenging functionalization, a trimethylsilyl (TMS) group was introduced analogously to the above described *p-t*-butyl group to give **3-33** (Scheme 39). TMS groups can easily be converted into iodines,⁹²⁻⁹⁴ which would allow further functionalization of the inner dendritic structure via SUZUKI or HAGIHARA-SONOGASHIRA cross-coupling reaction. The reaction of iodine monochloride with **3-33**, however, did not proceed quantitatively, even when longer reaction times and an excess of iodine monochloride were applied.

Though the inner keto groups turned out to be accessible for reaction partners like phenyllithium, the outer polyphenylene shell was nevertheless expected to restrict the permeation of bigger nucleophiles. The reaction with larger nucleophiles should for that reason be more difficult or even impossible. We chose the chromophore pyrene as the sterically demanding nucleophile. Pyrene is one of the most studied chromophores with well known fluorescence properties.^{95,96} When two pyrene molecules are in close proximity excimers are formed which leads to a characteristic emission in the UV/vis spectrum (Figure 20).⁹⁷ Based upon this fact pyrene has been used before to study aggregation phenomena.^{98,99} (see also chapter 2.1) Accordingly, the UV/vis spectra of a

monodisperse dendrimer bearing multiple pyrene units in its inner dendritic scaffold should give information about the spatial arrangement of the introduced pyrenes. 1-bromopyrene was lithiated and reacted with the keto groups in the second-generation dendrimer **3-30** (Scheme 39). After prolonged reaction time the eightfold functionalization of **3-36** could be proven by ^1H NMR spectroscopy and MALDI-TOF mass measurements. This shows that the outer polyphenylene shell is not able to efficiently exclude the penetration of a larger molecule like pyrene. The prolonged reaction time was probably not only a result of a restricted diffusion of the nucleophile but also of the delocalization of the negative charge in the pyrene moiety thus reducing its nucleophilicity. The UV/vis spectrum of **3-36** is discussed later (chapter 3.2.4.1). Additionally, **3-33** and **3-36** were converted into their corresponding trityl cation derivatives **3-40** and **3-42** similarly to the before described **3-39** (Scheme 40). Their characterization is described in chapter 3.2.5.1.

To show further possibilities that arise from encapsulated benzophenone functions we tried to reduce the keto groups via hydrogenation. The reaction of **3-30** with an excess of LiAlH_4 ^{100,101} was carried out in refluxing THF and afforded after hydrolysis and precipitation from MeOH **3-37** as single product in good yield (Scheme 39). In spite of the rigorous reaction conditions no degradation of the dendrons was observed underlining the chemical inertness of polyphenylene dendrimers.

The internal voids of dendrimers can be used as pockets for the defined inclusion of guest molecules, e.g. chromophores or metals. One interesting application born from this concept is the synthesis of dendrimer encapsulated metal nanoparticles possessing a narrow size-distribution.^{102,103} Generally, in a first step, metal ions are complexed at specific binding sites in the inner of the dendrimer. Secondly, the metal ions are chemically reduced. Subsequent growth of the nanoparticles and extraction from the dendrimer yields metal nanoparticles with a defined diameter. However, when flexible dendrimers, such as poly(amidoamine) dendrimers are used, a large amount of stabilizer (e.g. *n*-hexanethiol) is often needed to prevent aggregation of the nanoparticles within the dendrimer in order to achieve a narrow size distribution of extracted metal particles.¹⁰⁴ U. M. WIESLER synthesized polyphenylene dendrimers with peripheral thiomethyl groups. The precipitation of gold nanoparticles in the presence of these dendrimers resulted in a bimodal size distribution of the gold particles with an average size of 3.7 nm. Due to the shape-persistence of the dendrimer backbone, polyphenylene dendrimers possess internal voids with a defined shape and size. This should allow a better control over the size distribution of the grown metal particles and might lead to smaller diameters of the particles due to steric restrictions. For the complexation of e.g. gold ions sulfur anchor groups in the dendrimer interior are needed. Following the postsynthetic approach, *p*-bromo-thioanisol was therefore lithiated and reacted with the benzophenone bearing dendrimer **3-30** (Scheme 39). MALDI-TOF mass spectrometry as well as NMR spectroscopy proved the eightfold introduction of the thioanisol moieties in dendrimer **3-35**. Metal complexation experiments with gold is an ongoing project, however, no results can yet be reported. Nevertheless, dendrimer **3-35** demonstrates the versatility of the presented postsynthetic functionalization concept.

Up to this point, aromatic lithium-reagents were used for the postsynthetic functionalization of the dendrimer backbone. To extend this approach to aliphatic lithium-reagents would allow using a wide range of commercially available compounds for the functionalization. Furthermore, aliphatic halogen derivatives can easily be transferred into the corresponding lithium-reagents by halogen-lithium exchange using e.g. *n*-butyllithium. These species can then also be used for the functionalization of the dendrimer interior. To test

the herein presented concept for aliphatic lithium-reagents, the benzophenone functionalized dendrimer **3-30** was reacted with a large excess of *n*-butyllithium in refluxing THF. After hydrolysis and precipitation from MeOH the eight times substituted product **3-38** could be verified using NMR spectroscopy and MALDI-TOF mass spectrometry.

The above presented postsynthetic functionalizations allows the introduction of a large diversity of functions starting with single phenyl rings up to polyaromatic hydrocarbons like pyrene. Further, substituted phenyls as well as aliphatic lithium-reagents could be reacted quantitatively with the benzophenones in the interior of the dendrimer backbone.

The monodispersity of the products obtained by the postsynthetic functionalization was verified by MALDI-TOF mass spectrometry. Figure 33 shows the MALDI-TOF mass spectrum of **3-33**, obtained after hydrolysis and precipitation from MeOH. A molecular mass of $7519 \text{ g}\cdot\text{mol}^{-1}$ was detected for **3-33** which is in very good agreement with the calculated molecular weight of $7520 \text{ g}\cdot\text{mol}^{-1}$. Signals at lower molecular weight can be assigned to either the cleavage of a hydroxy group ($(\text{M-OH})^+$, $7503 \text{ g}\cdot\text{mol}^{-1}$) or to typical fragmentation ($5656 \text{ g}\cdot\text{mol}^{-1}$, $\frac{3}{4} (\text{M})^+$), both induced by laser irradiation during the measurement. Due to their positive charge and high stability, trityl cation species possess high desorption rates in mass spectrometry. Therefore, they can be used as mass-tags even in complex mixtures, which is of interest especially in combinatorial synthesis. Due to the high desorption ability of the trityl cations, it is likely to say that the amount of dendrimer with cleaved hydroxy group (25%, inset in Figure 33) is overrated. The signal at a molecular weight of $6881 \text{ g}\cdot\text{mol}^{-1}$ does not belong to any unreacted species but could not be clearly assigned yet.

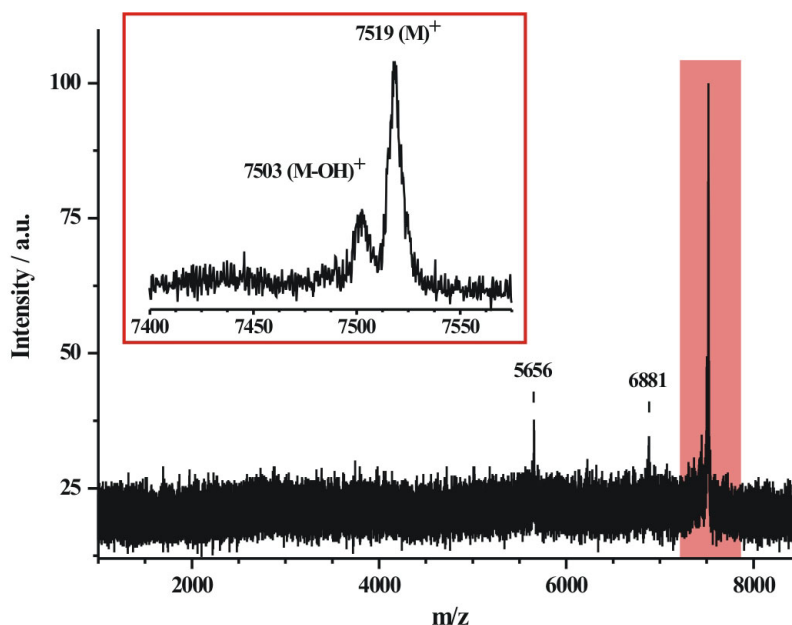


Figure 33. MALDI-TOF mass spectrum of **3-33** (calculated mass: $7520 \text{ g}\cdot\text{mol}^{-1}$; matrix: dithranol).

In addition to MALDI-TOF mass spectrometry, NMR spectroscopy can give quantitative information about the purity of the dendrimers obtained from the postsynthetic functionalization. Figure 34 shows the ^1H NMR spectrum of **3-33** as typical example. Well separated signals for some of the aromatic protons as well as for the protons of the TMS and hydroxy groups were observed. The TMS groups appeared as two overlapped singlets at $\delta = 0.24 \text{ ppm}$ ($\text{H}_{\text{e}+\text{e}}$). Reason for this is that the branching of the dendritic scaffold takes place

in the three- and four-position of the first-generation pentaphenylbenzene units, therefore being unsymmetrical. Protons located in the outer dendrimer shell therefore exhibit a different chemical and electronic environment. This resulted in unequal shifts in the ^1H NMR spectrum e.g. as before mentioned the TMS groups ($\text{H}_{e+e'}$) displayed as two singlets. The same applied to the protons $\text{H}_{c+c'}$ of the hydroxy groups appearing as two singlets at $\delta = 2.78$ ppm. In the aromatic region, one could observe the generation protons H_b (first-generation) and $\text{H}_{d+d'}$ (second-generation) at $\delta = 7.60$ ppm and $\delta = 7.52$ ppm, respectively (see also chapter 2.3.2). The protons $\text{H}_{d+d'}$ appeared as two overlapped singlets for the same reason as described above. At lower field ($\delta = 6.69$ ppm) the resonances of the core protons H_a displayed as a doublet.

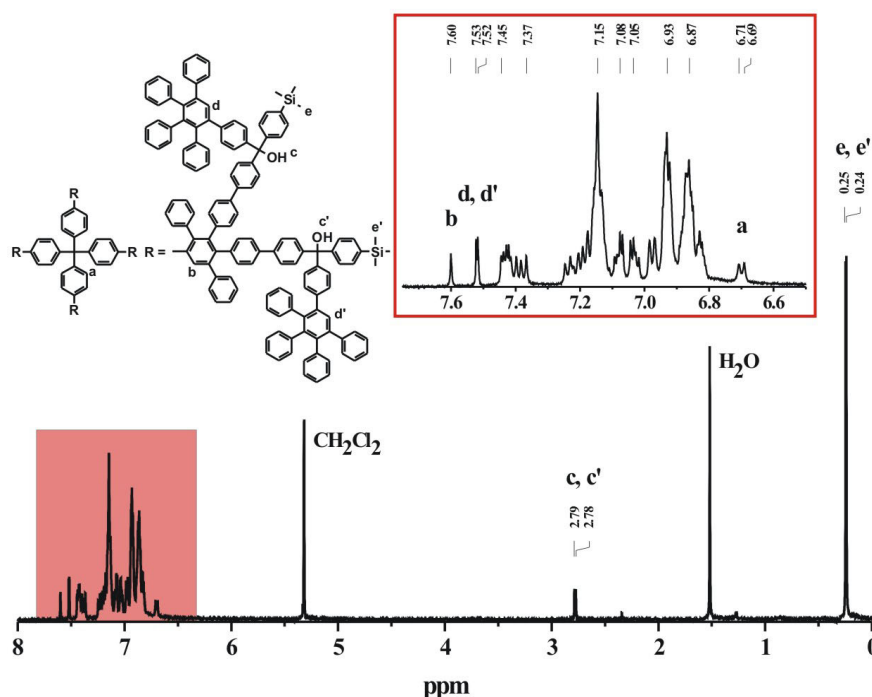


Figure 34. ^1H NMR spectrum of **3-33** (500 MHz, CD_2Cl_2 , 300 K).

Further signal assignments were not possible due to an inherent overlap of the aromatic protons of the polyphenylene dendrimer backbone. However, distinctive proton resonances of the dendrimer backbone ($\text{H}_a - \text{H}_d$) and of the introduced TMS benzene groups (H_e) and the relation of their intensities (see Experimental Part) prove the quantitative introduction of eight TMS-substituted benzenes in the interior of the dendrimer. This is also verified as in the ^{13}C NMR spectra the signal of the keto groups ($\delta = 196$ ppm) disappeared and a single distinctive signal of the triphenylmethanol carbon showed up at $\delta = 81.8$ ppm.

3.2.4.1 Pyrenyl Functionalized Dendrimer Backbone

Following the postsynthetic approach, the dendritic scaffold of dendrimer **3-36** has been functionalized with eight pyrene chromophores (Scheme 39). The characteristic excimer formation of pyrene⁹⁷⁻⁹⁹ (see also Figure 20) was used as an indicator for the spatial arrangement of the chromophores in the dendrimer. Absorption and emission spectra of **3-36** (bottom part) and unsubstituted pyrene (top part) in CH_2Cl_2 are shown in Figure 35.

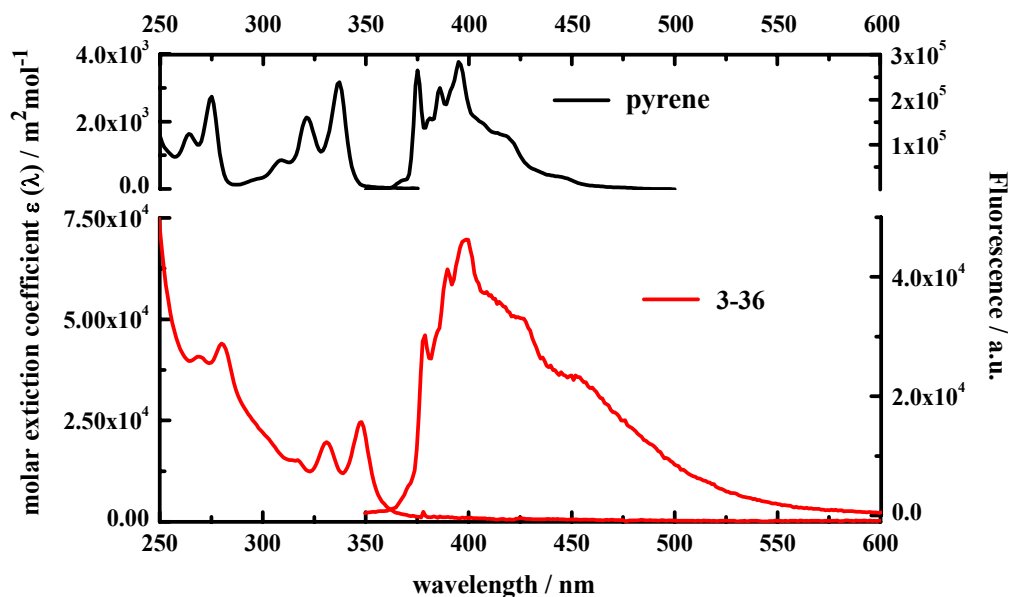


Figure 35. Absorption and emission spectra of **3-36** (bottom part) and unsubstituted pyrene (top part) in CH_2Cl_2 solution, respectively.

The absorption spectrum of **3-36** displayed maxima at $\lambda = 269, 280, 317, 331,$ and 348 nm, respectively, which can be ascribed to the absorption of the introduced pyrenes as seen when compared with the absorption spectrum of unsubstituted pyrene (top spectrum in Figure 35). The intense absorption of **3-36** at short wavelengths belongs to the dendritic polyphenylene backbone.¹⁰⁵ Compared with unsubstituted pyrene, the absorption spectrum of **3-36** showed a red-shift of 11 nm. As the introduced pyrenes are bound via a sp^3 carbon, the conjugation between them and the polyphenylene dendrons was interrupted thus only small bathochromic shifts of the pyrene absorption were induced. This is in contrast to e.g. 1,3,6,8-tetraphenylpyrene ($\Delta\lambda_{\text{max}} = 43$ nm).¹⁰⁶ The extinction coefficient $\epsilon(\lambda)$ of **3-36** ($2.47 \cdot 10^4 \text{ m}^2 \text{ mol}^{-1}$, 348 nm) was roughly the eightfold value as for monomer pyrene ($3.17 \cdot 10^3 \text{ m}^2 \text{ mol}^{-1}$, 337 nm). This supports besides of the standard spectroscopic measurements like NMR or mass spectrometry the eightfold incorporation of pyrene into the dendritic backbone of **3-36**. The fluorescence spectrum of **3-36** in CH_2Cl_2 showed maxima at $\lambda = 379, 389$ and 398 nm, respectively, which are only ≈ 3 nm red-shifted compared to the emission of monomer pyrene (Figure 35, top spectrum). When **3-36** was excited at the absorption wavelength of the polyphenylene dendrons (270 nm), an emission of the incorporated pyrenes was observed. One can attribute this to an energy transfer from the polyphenylene backbone to the entrapped pyrenes. The broken conjugation between the pyrene moieties and the dendrimer backbone suggests a pure through-space mechanism similarly to the one observed for encapsulated pyrene in chapter 2.5.1.

In concentrated solutions, pyrene shows strong characteristic excimer fluorescence at 475 nm which arises from the close proximity of two pyrene molecules (compare also Figure 20). No excimer fluorescence could be observed for the embedded pyrenes in **3-36**. A spatially separated arrangement of the pyrene moieties inside the dendrimer backbone can therefore be considered, mainly due to the stiff and shape persistent polyphenylene dendrons.¹⁰⁷⁻¹⁰⁹

3.2.5 Characterization of Charge/Spin Carrying Dendrimers

In the following part the in-depth spectroscopic characterization of the charge and spin carrying dendrimers is presented. UV/vis, NMR, and EPR techniques were applied to determine the influence of the polyphenylene dendrons upon the physical properties of the therein embedded new functions.

3.2.5.1 Trityl Cations

High resolution ^1H and ^{13}C NMR data for **3-39** - **3-42** were recorded in order to quantify the number of charged centers. Single distinctive peaks for the positively charged carbon of **3-39** - **3-42** were found in the ^{13}C NMR spectra proving the quantitative conversion of all eight triphenylmethanol groups into the corresponding trityl cations. Figure 36 displays ^{13}C NMR spectra of the triphenylmethanol precursors **3-32** - **3-34**, **3-36** (right side), and of the trityl cations **3-39** - **3-42** (left side) showing the signal of the central triphenylmethyl carbon.

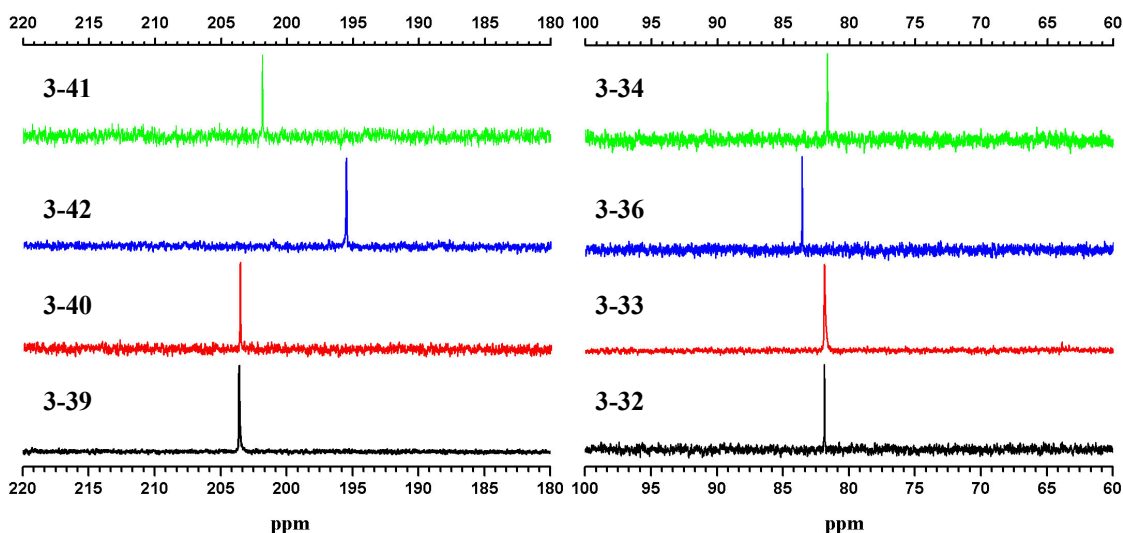


Figure 36. ^{13}C NMR spectra (selected regions) of the triphenylmethanol precursors **3-32** - **3-34**, **3-36** (triphenylmethanol carbon, right side) as well as of the trityl cation bearing dendrimers **3-39** - **3-42** (positively charged trityl carbon, left side). (**3-32** - **3-34**, **3-36**: 500 MHz, CD_2Cl_2 , 300 K; **3-39** - **3-42**: 500 MHz, $\text{CD}_2\text{Cl}_2/\text{d-TFA}$, 300 K)

Shifts of $\Delta\delta = 121.8$ ppm (C-OH, 81.8 ppm; C^+ , 203.6 ppm) for **3-39** and **3-40** and $\Delta\delta = 120.1$ ppm (C-OH, 81.7 ppm; C^+ , 201.8 ppm) for **3-41** were detected. For the pyrenyl substituted dendrimer **3-42** a down-field shift of $\Delta\delta = 112.0$ ppm (C-OH, 83.6 ppm; C^+ , 195.6 ppm) was found. The transformation of the reference triphenylmethanol into the corresponding trityl cation induces a down-field shift of the methyl carbon of $\Delta\delta = 134.4$ ppm (C-OH, 77.2 ppm; C^+ , 211.6 ppm).¹¹⁰ The smaller down-field shift of the trityl cations embedded in the dendritic structures **3-39** - **3-41** as compared to the parent trityl cation can be attributed to the delocalization of the positive charge into neighboring phenyl rings of the polyphenylene dendrons. **3-42** showed the smallest down-field shift due to the conjugated π -system of pyrene. The shift was even lower than for the reference

(1-pyrenyl)diphenylmethyl cation $\Delta\delta = 117.5$ ppm (C-OH, 83.9 ppm; C⁺, 201.4 ppm),¹¹¹ indicating the additional resonance impact of the polyphenylene dendrons in **3-42**.

Characterization of the octatryl cations **3-39** - **3-42** by ¹H NMR spectroscopy displayed well separated signals for the aromatic triphenylmethyl protons. Figure 37 shows as an example the ¹H NMR spectrum of **3-41**.

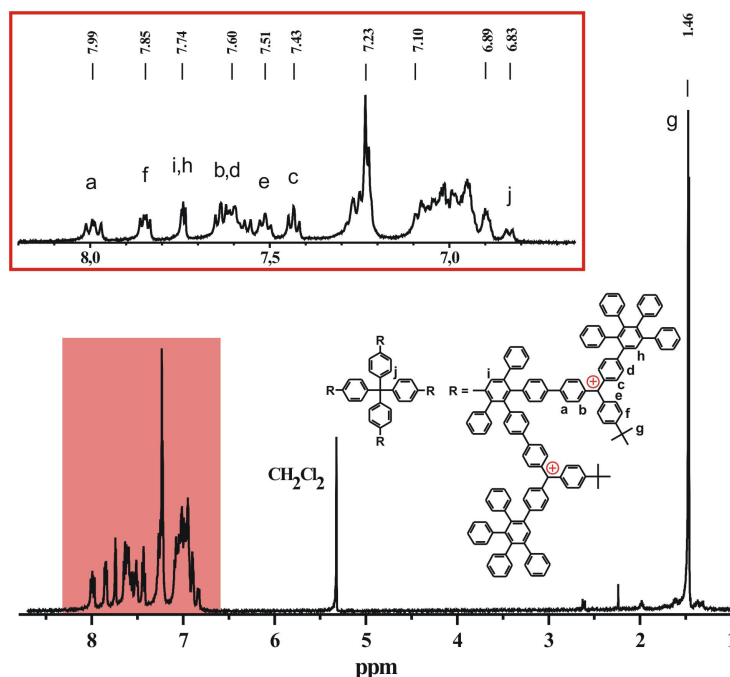


Figure 37. ¹H NMR of **3-41** (500 MHz, CD₂Cl₂/d-TFA, 300 K).

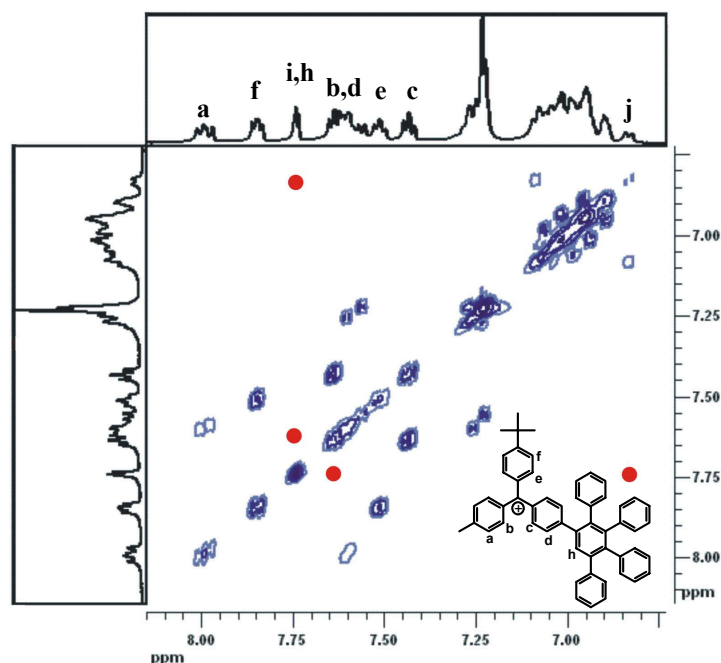


Figure 38. H,H COSY of **3-41** (500 MHz, CD₂Cl₂/d-TFA, 300 K). Red dots: NOE couplings.

Proton H_a appeared as an overlap of two doublets at 7.99 ppm for the same reason as already described for the ¹H NMR spectrum of **3-33** (Figure 34). The overlap is due to the specific branching of this type of polyphenylene dendrimers, which takes place in the 3- and 4-position of the pentaphenylbenzene units. Thus, protons on the two dendritic arms in the

second-generation dendrimer shell (“after” the branching) exhibit a different chemical environment. This resulted in unequal chemical shifts in the ^1H NMR spectra, making e.g. proton H_a (Figure 37 and Table 7) appear as two doublets with different chemical shift. The same is the case for proton H_f with a chemical shift of 7.85 ppm, appearing as two overlapped doublets. The generation protons H_i and H_h displayed as a multiplett at 7.74 ppm. A further proof of structure is derived, since specific signals for the core protons H_j ($\delta = 6.83$ ppm) as well as for the protons of the *t*-butyl groups ($\delta = 1.46$ ppm) were detected, possessing the expected intensities. The signals were assigned using H,H COSY and H,H NOESY experiments. Figure 38 displays as an example the H,H COSY spectrum of **3-41**. Many couplings were observed in the aromatic region, allowing the full assignment of all protons of the trityl moieties. Additionally, a coupling of proton H_f and the neighboring *t*-butyl group could be detected in the NOE spectrum of **3-41**. The NOE spectrum further showed the coupling of H_d with the second-generation proton H_h (Figure 38, red dots) as well as the coupling of the first-generation proton H_i with the core protons H_j (compare also Figure 37).

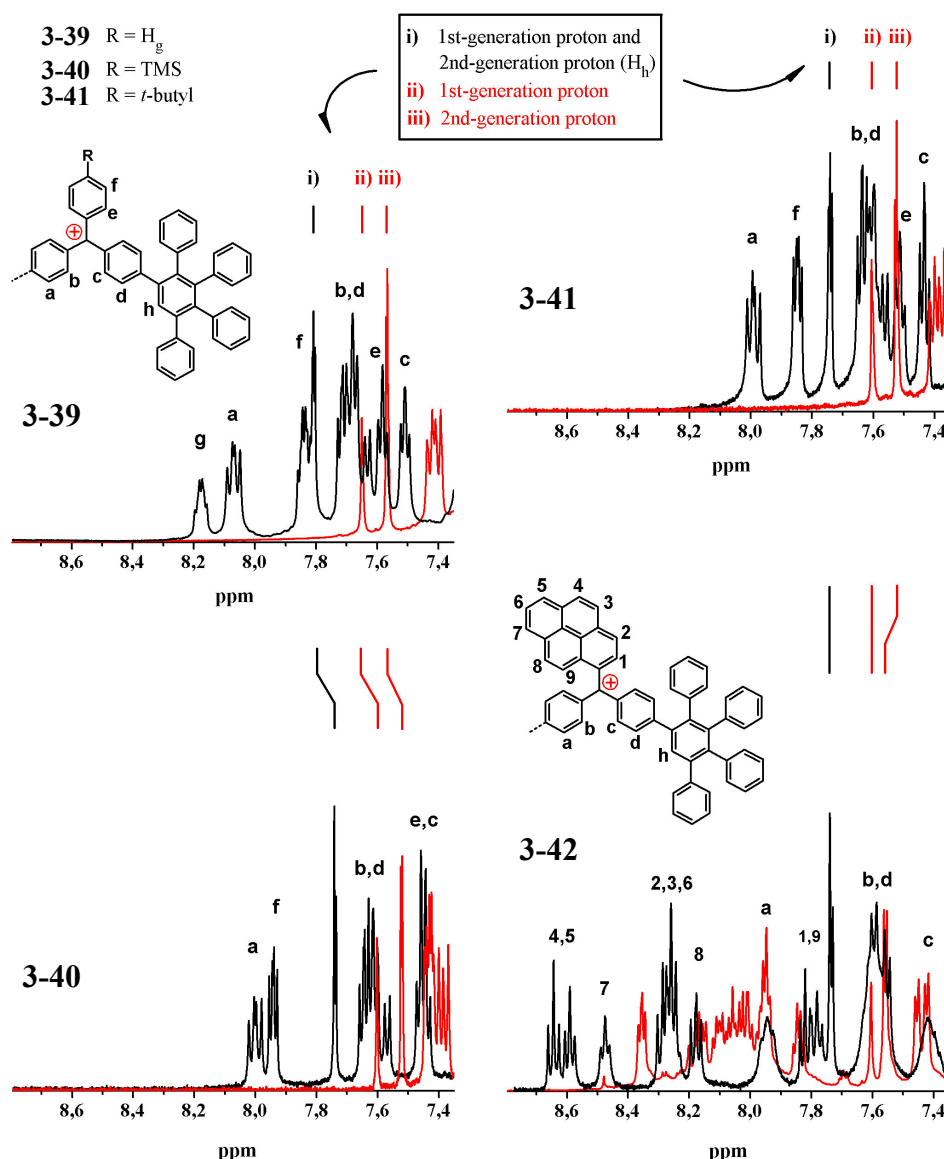


Figure 39. ^1H NMR spectra of **3-39** - **3-42** trifluoroacetic acid salts (black line & assignment) and of their corresponding precursors **3-32** - **3-34**, **3-36** (red line & assignment) (500 MHz, $\text{CD}_2\text{Cl}_2/\text{d-TFA}$, 300 K).

The ^1H NMR spectra of the other trityl cation bearing dendrimers **3-39**, **3-40**, and **3-42** are shown in Figure 39. The according signal assignments are listed in Table 7. For comparison, the spectra of the polyalcohol precursors **3-32** - **3-34**, **3-36** are shown as well. A generation-dependent chemical shift of the protons located on the central benzene of the pentaphenylbenzene unit of the polyalcohol precursors **3-32** - **3-34**, **3-36** was observed (Figure 39). Singlets displayed for the protons of the first-generation at $\delta = 7.65$ ppm (**3-32**) and $\delta = 7.60$ ppm (**3-33**, **3-34**, **3-36**), respectively. The protons of the second-generation were located at $\delta = 7.58$ ppm (**3-32**), $\delta = 7.52$ ppm (**3-33**, **3-34**) and $\delta = 7.56$ ppm (**3-36**).

Table 7. Comparison of the ^1H NMR chemical shifts (δ / ppm) of the octatryl cations **3-39** - **3-42**. (500 MHz, $\text{CD}_2\text{Cl}_2/\text{d-TFA}$, 300 K).

proton	3-39 δ / ppm	3-40 δ / ppm	3-41 δ / ppm	3-42 δ / ppm
g	8.18, 8.17 (2t, 8H)			
a	8.08, 8.06 (2d, 16H)	8.01, 7.99 (2d, 16H)	8.00, 7.98 (2d, 16H)	7.91 (m, 16H)
f	7.84, 7.83 (m, 16H)	7.95, 7.94 (2d, 16H) 7.74 (s, 8H), 7.73	7.85, 7.84 (2d, 16H)	
h + generation 1	7.81-7.80 (m, 12H)	(s, 4H)	7.75-7.73 (m, 12H)	7.70, 7.69 (m, 12H)
d, b	7.73-7.62 (m)	7.66-7.56 (m)	7.65-7.55 (m)	7.57-7.51 (m)
e	7.59, 7.57 (2d, 16H)	7.47 (2d, 16H)	7.51 (2d, 16H)	
c	7.52, 7.50 (2d, 16H)	7.43 (2d, 16H)	7.42 (2d, 16H)	7.37 (m, 16H)

Generating the octatryl cations **3-39** - **3-42** resulted in a down-field shift of the first- and second-generation proton resonances (H_i and H_h). The first-generation protons were shifted by $\Delta\delta = 0.14$ ppm (**3-39** - **3-41**) and $\Delta\delta = 0.13$ ppm (**3-42**) as compared to the polyalcohol precursors **3-32** - **3-34** and **3-36**. As compared to **3-39** - **3-42**, the second-generation protons were more down-field shifted ($\Delta\delta = 0.22$ ppm, **3-39** - **3-41** and $\Delta\delta = 0.18$ ppm, **3-42**) than the corresponding first-generation protons. Probably, this is due to the smaller distance between the positively charged carbon and the second-generation proton of ≈ 6.6 Å, whereas ≈ 12.3 Å were found for the distance to the first-generation proton.^a The large distance (more than three phenyl rings) between the trityl cation and the shifted first-generation proton indicates an efficient delocalization of the charge which supports the results from the ^{13}C NMR spectroscopy. The delocalization of the charge is expected to be hampered due to the twist of the benzene rings ($\approx 50^\circ$) in the polyphenylene dendrons.^{108,112} However, also structural changes during the formation of the trityl cation (tetragonal, $\text{sp}^3 \rightarrow$ planar, sp^2) have to be considered. The peak assignment for the protons of the pyrenyl units in dendrimer **3-42** agreed with published data¹¹¹ and is given as inset in Figure 39. The signal pattern of the triphenylmethyl units of **3-39** - **3-41** were similar to those of tetra- and hexatryl cations, obtained by RATHORE et al.⁴³ as well as to those of the parent trityl cation.¹¹³

^a Distances were derived from three-dimensional structures of **3-39** - **3-42** calculated by the MMFF method.

In difference to high resolution NMR data, the optical absorption spectra of **3-39** - **3-42** were quite similar and are shown in Figure 40. They exhibited similar absorbance spectra with a maximum at ≈ 600 nm red shifted as compared to the parent trityl cation (twin band, $\lambda_{\text{max}} = 410$ and 432 nm).¹¹⁴ The strong absorption at short wavelengths (≈ 250 nm) can be attributed to the absorption of the polyphenylene dendrons.¹⁰⁵ The bathochromic shift of the dendrimer embedded trityl cations **3-39** - **3-42** indicated a delocalization of the positive charge in the polyphenylene dendrons which supported the results from the ^1H and ^{13}C NMR measurements. UV/vis spectra with similar absorption bands were found for highly conjugated systems consisting of a central triphenylmethyl cation with attached oligo(1,4-phenylenevinylene)s.⁴¹ Likewise the reference (1-pyrenyl)diphenylmethyl cation, the pyrenyl substituted dendrimer **3-42** displayed a strong additional absorption band at $\lambda = 742$ nm.⁴²

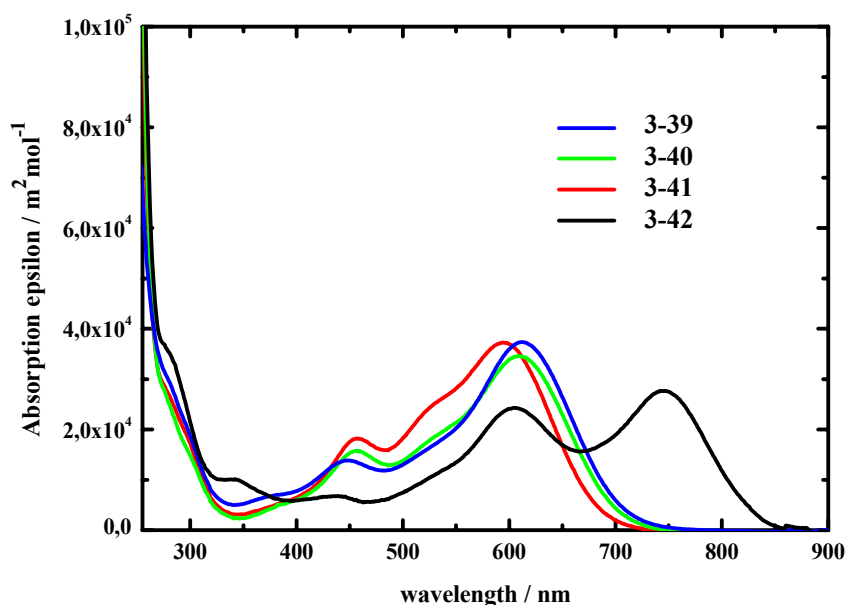


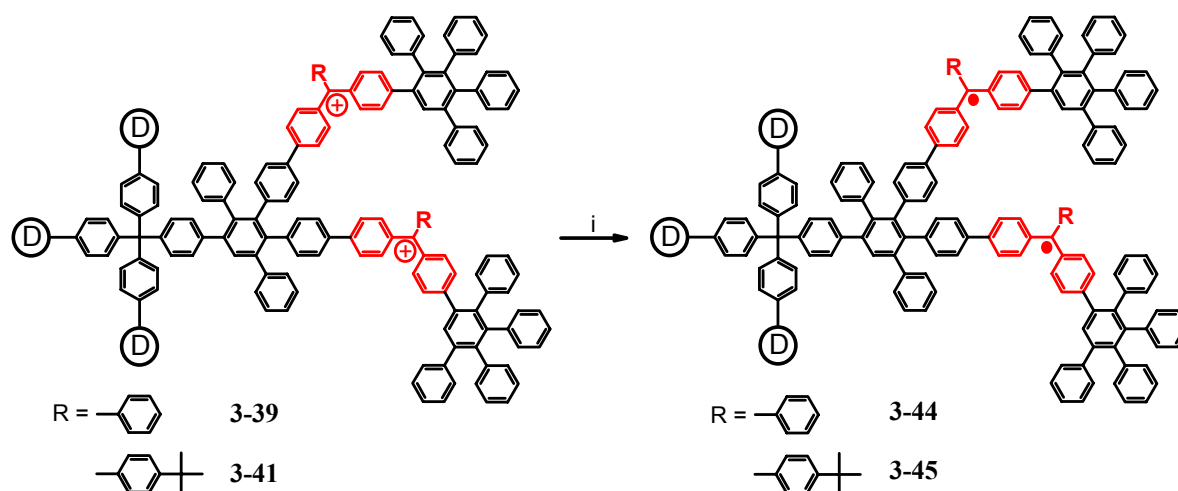
Figure 40. Absorption spectra of octatrityl cations **3-39** - **3-42** in CH_2Cl_2 .

In conclusion, high resolution ^1H and ^{13}C NMR spectroscopy have proven the quantitative functionalization of the dendrimer backbone with eight trityl cations. This further supports the result from the hydride abstraction experiment where the trityl cation derivative **3-39** was cleanly converted into the triphenylmethyl derivative **3-43**, thereby proving its former eightfold functionalization (Scheme 41). NMR and UV/vis spectroscopy indicated an efficient delocalization of the charge into the polyphenylene dendrons, which is the main reason for the great stability of the trityl cation bearing dendrimers.

3.2.5.2 Trityl Radicals

The stable trityl cation bearing dendrimers **3-39** and **3-41** have been used as starting materials for the synthesis of polyphenylene dendrimers containing multiple trityl radicals in the dendritic scaffold (Scheme 42). In a first attempt, it was tried to generate the radical species in situ. For that, the according triphenylmethanol derivative **3-32** or **3-34** were dissolved in CH_2Cl_2 under argon atmosphere. The trityl cation species was generated using TFA like described before (chapter 3.2.4). After a few minutes SnCl_2 was added, whereupon the reaction mixture turned light green which indicated the formation of trityl radicals.

However, a few seconds later the green color of the solution faded away resulting in a colorless reaction mixture.



Scheme 42. Reduction of the trityl cation dendrimers **3-39** and **3-41** yielding the trityl radical bearing dendrimers **3-44** and **3-45**, respectively: i) CH_2Cl_2 , SnCl_2 . One arm is drawn out fully. The three other arms are identical with the one shown but are abbreviated as a circled-D for ease of visualization.

Probably there were still traces of impurities e.g. water present leading to further reactions thereby destroying the radical species. To overcome these problems, the trityl cation bearing dendrimer **3-39** was dissolved in CH_2Cl_2 in a multichamber sealed glass tube under high vacuum and reacted with SnCl_2 . The reactions were followed using UV/vis and EPR spectroscopy. After some hours of mixing, the blue solution of the trityl cations started to become green and a strong absorption band at $\lambda = 400$ nm showed up in the UV/vis spectra (Figure 41a).

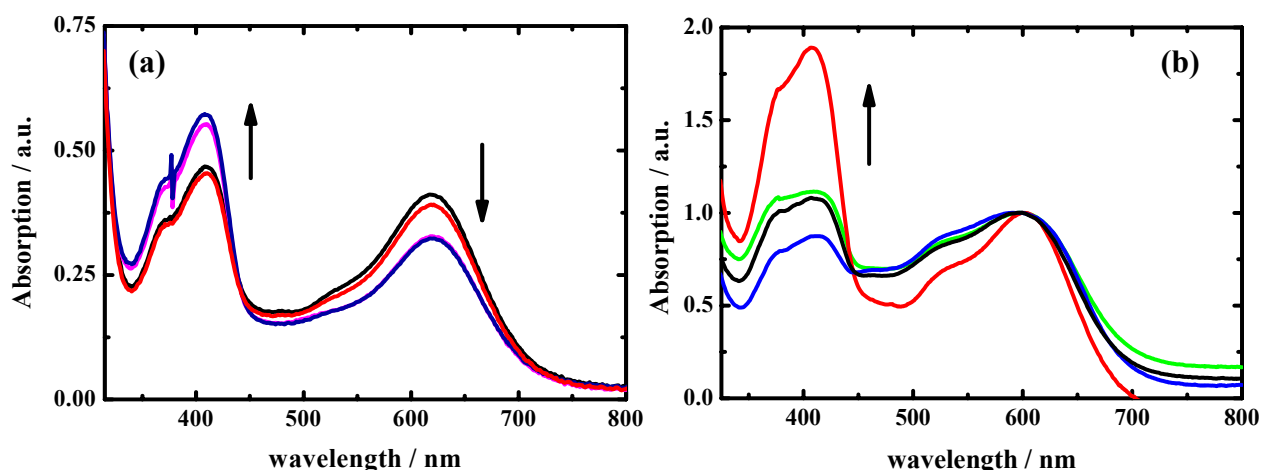


Figure 41. UV/vis absorption spectra of (a) **3-44** and (b) **3-45** in CH_2Cl_2 measured during the radical formation. The UV/vis spectra of **3-45** are normalized to the absorption band at 600 nm.

Compared with the parent trityl radical possessing two absorption maxima ($\lambda_{\text{max}} = 332, 515$ nm)^{115,116} only the first absorption maximum could clearly be detected,

while the one at longer wavelength (≈ 570 nm) was hidden in the strong absorption of the octacation. The first absorption of **3-44** was bathochromically shifted by $\Delta\lambda_{\max} = 70$ nm as compared to the parent trityl radical, similarly to other phenyl substituted trityl radicals e.g. 4,4'-diphenyltrityl ($\Delta\lambda_{\max} = 55$ nm).³⁹ Thus for **3-44** an efficient delocalization of the spin into the all-phenyl dendrimer backbone can be suggested which verified the stabilizing effect of the polyphenylene dendrons similarly to the results for the embedded trityl cations **3-39** - **3-42** and the benzophenone radical anions discussed later. As SnCl_2 is not soluble in CH_2Cl_2 , the heterogeneous reduction proceeded very slowly. Even after prolonged reaction time of several days, the absorption band of the octatrityl cation **3-39** ($\lambda_{\max} = 620$ nm) decreased upon reduction but did not disappear. It might be suggested that the remaining cation absorption band still hampered the detection of the bathochromically shifted second absorption band of the polyphenylene substituted trityl radicals. The same behavior was found for the trityl radical derivative **3-45** (Figure 41b). For reasons of clarity, the UV/vis spectra of **3-45** were normalized to the absorption band at 600 nm. After long time (≈ 2 weeks) the reaction mixtures became colorless, likely due to the reaction with impurities, however still some absorption at $\lambda = 600$ nm could be detected. The EPR spectrum of **3-44** showed a signal of at least 15 lines ($a_{\text{H}} \approx 0.09$ mT) between the two maxima (Figure 42).

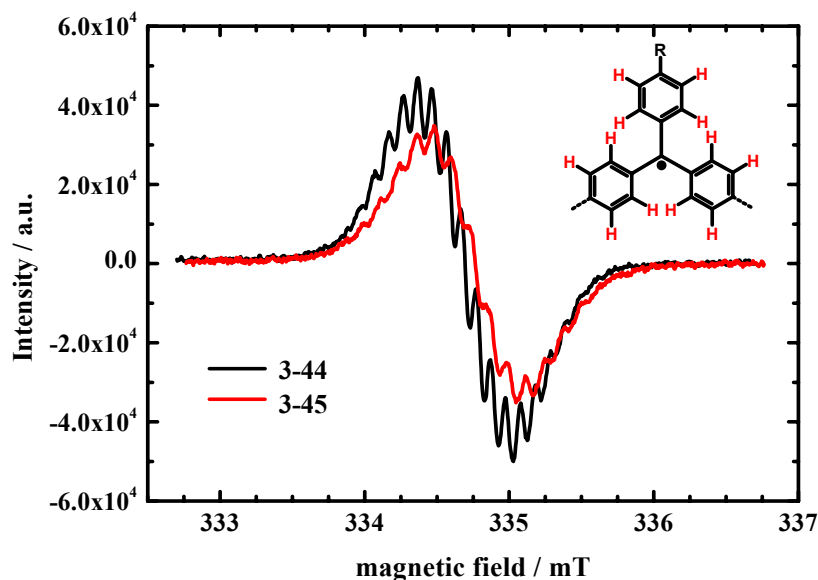


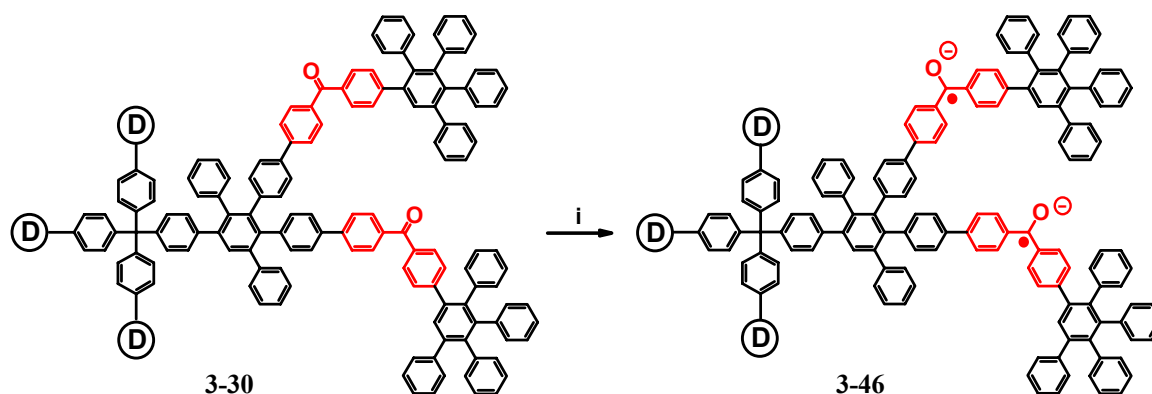
Figure 42. EPR spectra of **3-44** and **3-45** in CH_2Cl_2 at room temperature.

For a triphenylmethyl radical a 7 line signal was expected due to the coupling of the unpaired electron with 6 ortho-protons. The observed large number of couplings might result from the coupling with e.g. the free para-proton of the 4,4'-disubstituted trityl radical, the meta-protons, and may be other dendritic hydrogen's in close vicinity. The three phenyl groups of the trityl radicals **3-44** and **3-45** are differently para-substituted, therefore further complicating the analysis of the EPR spectra. However, as the para-position of the trityl radicals in **3-45** is blocked by a *t*-butyl-group, its EPR spectrum showed a reduced number of 13 lines ($a_{\text{H}} \approx 0.12$ mT). From the recorded UV/vis and EPR spectra it became evident that dendrimer entrapped trityl cations have been converted into their analogous trityl radicals. Upon standing, however, the initial green solutions became colorless. Similarly, the green color faded away immediately when the sealed glass tubes were opened. Obviously, the presented multitryl systems **3-44** and **3-45** are less stable than e.g. the perchlorinated triphenylmethyl radicals (compare **3-5**, Scheme 29).³² In these systems, the chlorine atoms

produce a very high steric congestion around the central carbon atom, thereby preventing the access of even small molecules like water or oxygen.

3.2.5.3 Benzophenone Radical Anions

Many studies have been performed on the formation of stable radical anions by the reaction of ketones and aldehydes with reducing metals.^{45-51,117} Therefore, the reduction of benzophenones being embedded in the dendritic structure should also be possible. The shielding of the inner keto groups turned out to be minor, since we have already shown their accessibility for various chemical transformations. The benzophenone bearing polyphenylene dendrimer **3-30** was reduced on a potassium mirror under high vacuum in THF solution (Scheme 43) using a technique previously described^{118,119} (compare also chapter 2.6.1)



Scheme 43. Formation of multiple ketyl radical anion bearing dendrimer **3-46**: i) rt, K, THF. One arm is drawn out fully. The three other arms are identical with the one shown but are abbreviated as a circled-D for ease of visualization.

This technique was used as it provides very clean reaction conditions together with a highly active potassium mirror. Furthermore, due to the multichamber setup also the comproportionation reaction of a reduced compound with neutral starting material is possible thereby allowing a good control over the state of the reduction. The reduction of the dendrimer entrapped benzophenones was followed using UV/vis and EPR spectroscopy.

Upon contact of a solution of the benzophenone bearing dendrimer **3-30** with the potassium mirror two increasing absorption bands at $\lambda = 410$ and 950 nm were observed in the UV/vis spectra (Figure 43a). They can be assigned to the formation of the eightfold radical anion of benzophenone in the dendritic scaffold. The bathochromic shift compared to the parent benzophenone ketyl ($\lambda_{\text{max}} = 336$ and 560 nm)¹¹⁴ can be attributed to some delocalization of the charge/spin into the adjacent phenyl rings of the polyphenylene dendrons. At a maximum intensity of these bands, the EPR spectra displayed a broad signal with 5 shoulders ($a_{\text{H}} \approx 0.27$ mT) (Figure 43b). Their hyperfine coupling can be assigned to the 4 ortho-protons carrying the largest spin density while the para-positions of the benzophenone radical monoanion are blocked by further phenyl rings (inset in Figure 43b).

Upon continued reduction on the potassium mirror the absorption bands of the radical monoanion ($\lambda_{\text{max}} = 410$ and 950 nm) disappeared and two new absorption bands at $\lambda = 575$ and 800 nm were displayed. They can be attributed to the bathochromic shifted absorption bands of the benzophenone dianions in the dendrimer.⁵⁶ Further, an isosbestic point was

observed at $\lambda = 1013$ nm indicating that the radical monoanions were transformed into the corresponding dianions without any side reactions.

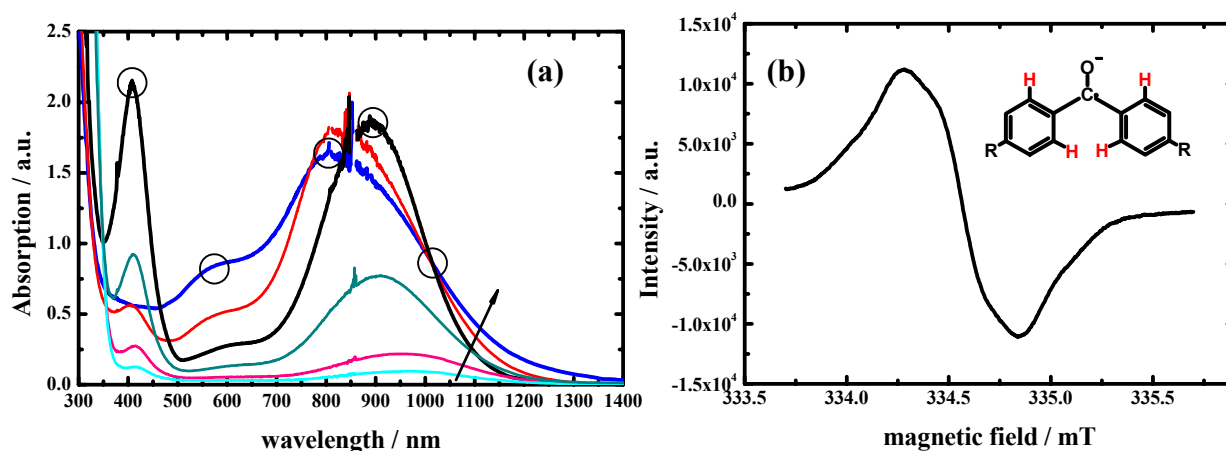


Figure 43. (a) UV/vis absorption spectra of the reduction of dendrimer **3-30** in THF (1-6) in the order of further reduction. Circles highlight significant points of the spectra. (b) EPR spectra at the maximum intensity of the radical monoanion absorption band of **3-46** ($\lambda = 950$ nm) in THF at 300 K.

EPR spectroscopy showed a signal of very low intensity, however, no complete diamagnetic state could be achieved even after extended reaction time. UV/vis signals broadened after prolonged contact time. These findings can be explained by additional charging of the polyphenylene shell, where these extra charges are not localized on any defined bi- or triphenyl units¹²⁰⁻¹²⁴ (compare also chapter 2.6.1), but just delocalize by electron hopping over many phenylene units. Thus, while the ketyl species could be generated quantitatively, a well defined reduction to the benzophenone dianions was not possible, before charging of the polyphenylene shell resulted in dendrimers possessing differently charged species.

Recently HOU et al.^{46,57,58} have confirmed earlier observations by HIROTA and others^{49,56,125,126} that alkali radical anions form metal bridged dimers, which can be identified as biradicals in the triplet state. Therefore, at maximum intensity of radical monoanion, frozen state EPR spectra were recorded. They displayed large zero field splittings of $2D = 15-17$ mT and $2D = 30$ mT (Figure 44), which are of similar size as usually found for benzophenone anion dimers ($2D \approx 18 - 20$ mT).^{49,59} In addition to the typical signals for the zero-field splittings, which exceeded the spectral width of the anisotropic hyperfine interaction of the monoradicals, also a relatively strong half-field transition at $g \approx 4$ was found ($\Delta_{ms} = 2$, inset in Figure 44), further demonstrating the triplet character of these biradicals.

According to a point dipole evaluation,⁴⁴ the observed zero-field splittings correspond to a distance of 0.55 - 0.57 nm between the radical centers. The intramolecular distances between two benzophenones in the dendritic structure, on the other hand, were found to be 1.2 - 1.5 nm and should therefore give only small zero-field splittings of $2D < 3.2$ mT for intramolecularly interacting radicals in **3-46**. Such tiny splittings could unfortunately not be resolved due to the broad radical monoanion signal. Thus, the large zero-field splittings can only be explained by intermolecular penetration of dendritic arms, arranging the ketyl radicals in such a close proximity that metal bridged biradicals are formed.

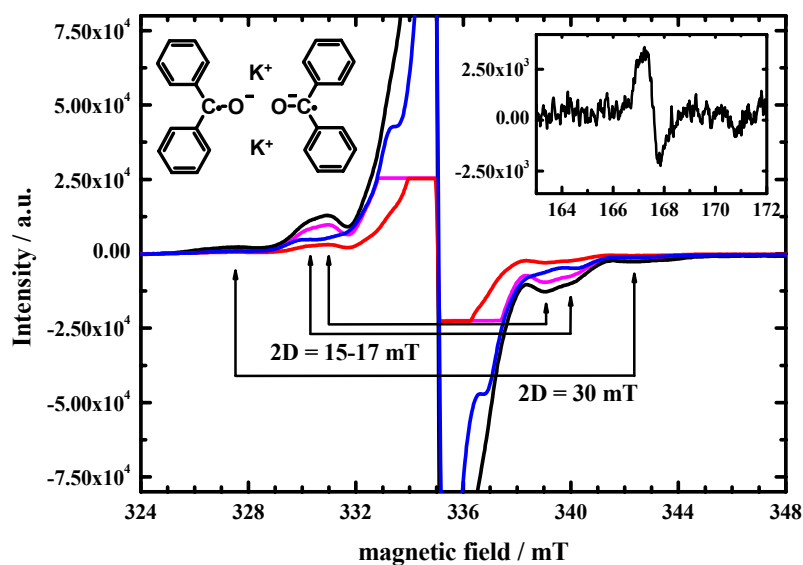


Figure 44. EPR spectra of the eightfold radical anion **3-46** in THF at ≈ 120 K, zero field-splittings indicated by arrows and half field transition (inset).

Figure 45 shows a schematic illustration of a three-dimensional network formed by intermolecular biradical formation. The single dendrimers were obtained via a force-field optimisation.

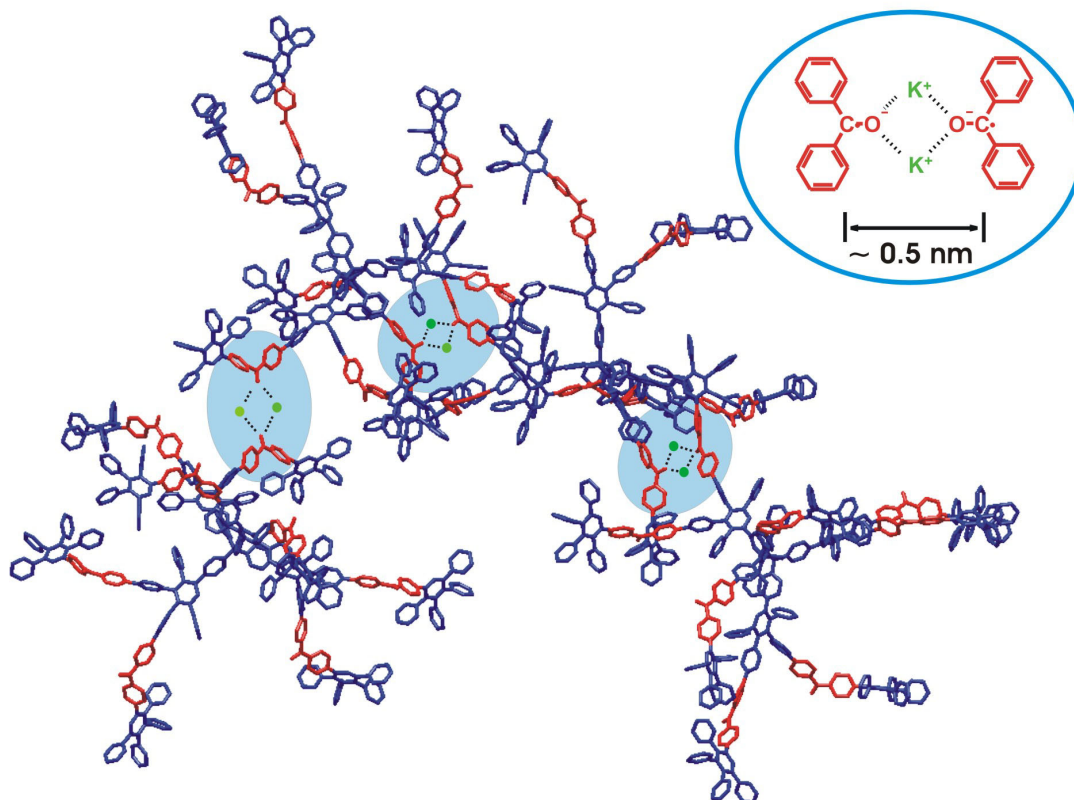
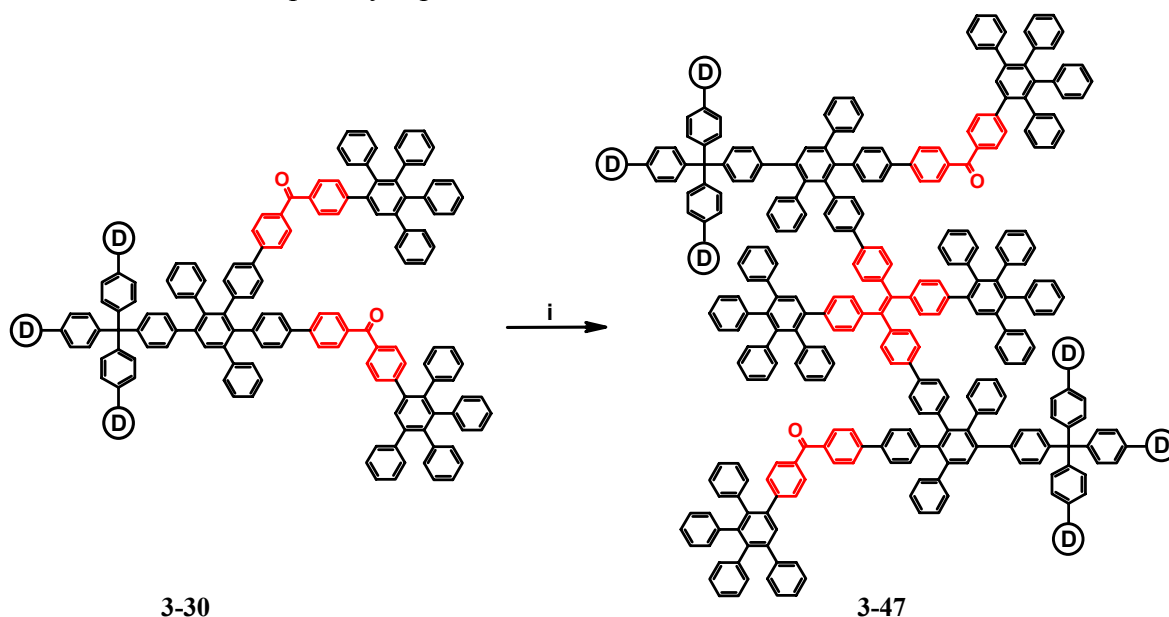


Figure 45. Schematic illustration of a radical network constructed from intermolecular potassium bridged biradicals. The structures of the single dendrimers were obtained from a force-field optimization.

For further insights into this phenomenon, one would have to investigate the influence of the concentration upon the biradical formation, which unfortunately was not possible with the experimental setup that we used. For example, the addition of complexating agents like crown ethers is known to inhibit biradical formation by removing the potassium ions from the system.¹²⁷

3.2.6 Further Postsynthetic Reactions

An additional proof for the existence of intermolecular interpenetrated dendrimer arms was derived from the MCMURRY coupling reaction^{128,129} of the dendrimer-embedded benzophenones in dendrimer **3-30**. The MCMURRY reaction of benzophenone with itself yields 1,1,2,2-tetraphenylethylene in high yield.¹³⁰ Accordingly, if penetration of dendritic arms exists in solution, the intermolecular reaction of dendrimer **3-30** should lead to multiple dendrimers, covalently connected to each other via tetraphenylethylene units (Scheme 44). The shape persistent dendrimer backbone should prevent an intramolecular MCMURRY coupling reaction of the benzophenones by fixing them at defined positions thereby keeping them spatially separated. This can be suggested as no pyrene excimer formation was observed for the pyrenyl bearing dendrimer **3-36** (see chapter 3.2.4.1). Thus, also the benzophenones in **3-30** are assumed to be spatially separated.



Scheme 44. MCMURRY reaction of **3-30** with itself. i) TiCl_4 , LiAlH_4 , THF, 60 °C. One arm is drawn out fully. The three other arms are identical with the one shown but are abbreviated as a circled-D for ease of visualization.

The $\text{Ti}(0)$ species required for the MCMURRY reaction was formed in situ from TiCl_4 with LiAlH_4 as the reducing agent.¹³⁰ Subsequently, a solution of **3-30** was added to the $\text{Ti}(0)$ solution which resulted in the extrusion of hydrogen as indicated by extensive bubbling. After complete addition, the reaction mixture was heated to 60 °C for two days. Hydrolysis with diluted hydrochloric acid and extraction with CHCl_3 yielded a green solid possessing green fluorescence, even in the bulk. Figure 46a shows the MALDI-TOF mass spectrum of **3-47**. Products with a molecular weight of up to $\approx 50000 \text{ g}\cdot\text{mol}^{-1}$ could be detected. The obtained mass signals were consistent with multiple mass of the monomer **3-30** ($6328 \text{ g}\cdot\text{mol}^{-1}$).

Since multiple molecular weights can also be seen due to cluster formation during the mass measurement, **3-47** was also characterized by Gel Permeation Chromatography (GPC). The GPC spectrum of **3-47** is depicted in Figure 46b and was measured with THF as solvent and polystyrene as standard. With an elution volume of ≈ 25.7 mL and a molecular weight of ≈ 6300 g \cdot mol $^{-1}$ still some monomer was detected in the product mixture. The next maximum (elution volume 24.5 mL) possesses a molecular weight of ≈ 12000 g \cdot mol $^{-1}$, which can be attributed to the dimer of **3-47** formed during the reaction.

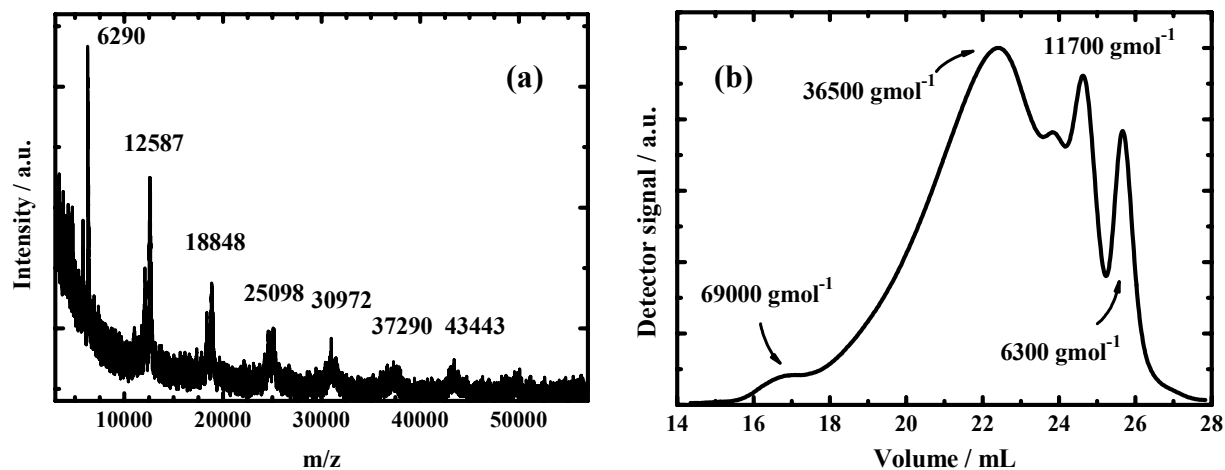


Figure 46. (a) MALDI-TOF mass spectrum of **3-47** (matrix: dithranol) and (b) GPC spectrum of **3-47**. Eluent THF, Polystyrene standard.

Further signals can be attributed to the trimer or higher homologues. The main peak with an average molecular weight of 36500 g \cdot mol $^{-1}$, six times the molecular weight of the monomer **3-30**, was very broad. The peak with the smallest elution volume showed a molecular weight of ≈ 69000 g \cdot mol $^{-1}$, which is about ten times the molecular weight of the monomer. An overall polydispersity of 3.6 was calculated from the obtained spectrum.

Both used analytical techniques showed independently the formation of high molecular weight products. However, these methods can give no information about the structure of the polydisperse products. A question would be if the MCMURRY reaction produces a linear “chain of dendrimers” with a maximum number of two linking points per dendrimer or if branching occurs due to multiple linking points which would lead to a kind of network. A suggestion can be made from the shape of the GPC spectrum. The trimer is the first oligomer which can have a linear or a nonlinear conformation. These different structures should lead to different hydrodynamic radii and thereby to different elution times in the GPC. For a linearly connected product, it can be expected that the signal for the trimer possesses an intensity which is in line with the intensities of the dimer and the tetramer, either following an increasing or a decreasing trend. In the case of **3-47**, the signal, which was attributed to the trimer, is not following this trend. Probably, this comes from different conformations being present in the mixture, which suggests the existence of branches along the “dendrimer chain”. However, the fact that monomer was still detectable, recommends to increase the reaction time. This type of “polymerization” follows in principle the rules for a polyaddition reaction, thus products with a high molecular weight can only be obtained with high conversion.

Since the two-dimensional structure of **3-47** as shown in Scheme 44 only provides an insufficient impression of the spatial arrangement, molecular mechanics calculations were carried out by applying the MMFF method. The optimized structures of dendrimers **3-30** were

connected with each other using preoptimized tetraphenylethylene units. Final overall refinement gave the three-dimensional structure as depicted in Figure 47. The obtained structure indicates a high similarity with the structure obtained for the radical anion bearing dendrimers intermolecularly linked via multiple potassium bridged biradicals (chapter 3.2.5.3).

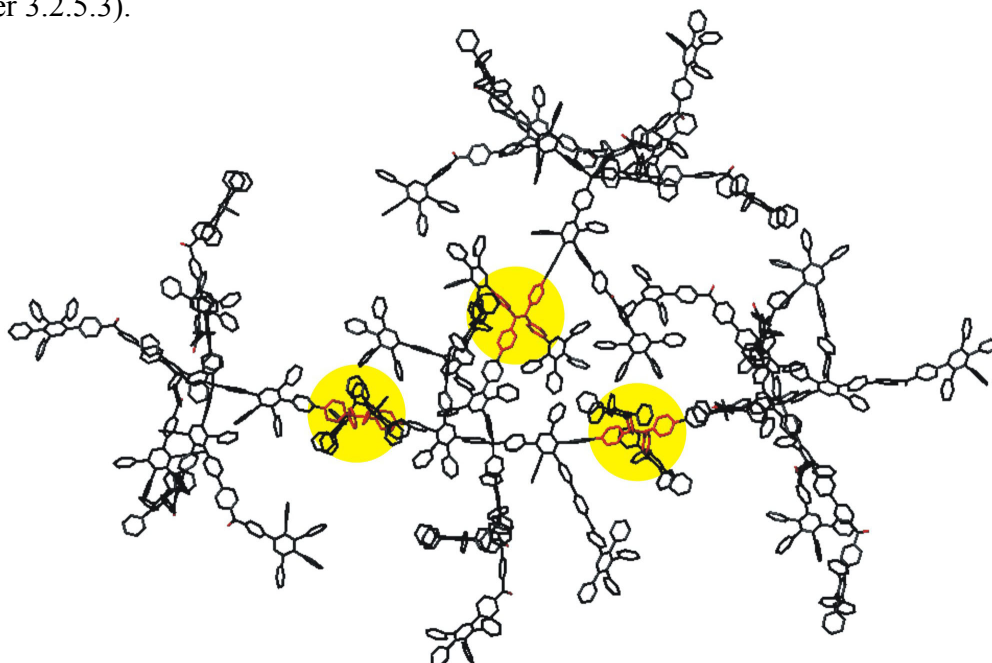


Figure 47. Three-dimensional structure of a dendrimer network consisting of four connected dendrimers as obtained by molecular mechanics calculations.

In both cases, the interdigitation of dendritic arms seems not to be hindered by the outer polyphenylene dendrimer shell. Therefore, it can be suggested that three intermolecular linkages (or even more) are in general possible on one dendrimer, which would lead to some kind of network of the dendrimers themselves. As already mentioned, the obtained products exhibited an intense green fluorescence. Figure 48 shows the absorption and emission spectrum of **3-47**.

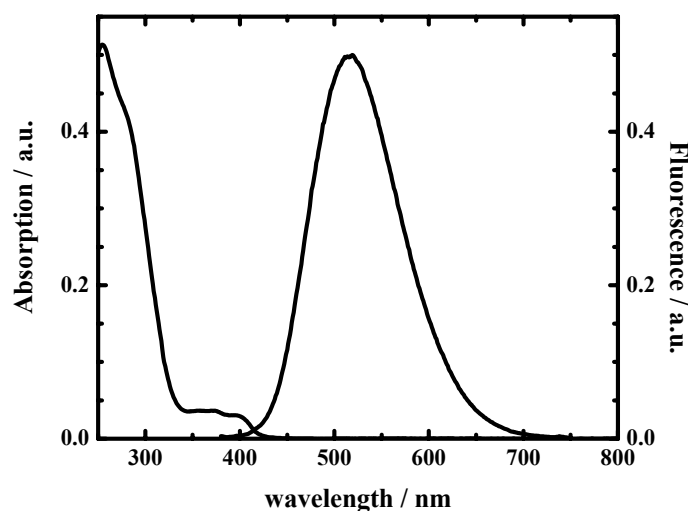


Figure 48. Absorption and fluorescence spectra of **3-47** in CHCl₃. Excitation wavelength: 280 nm.

An intense absorption displayed at short wavelengths (250 - 300 nm) which can be ascribed to the absorption of the polyphenylene dendrons.¹⁰⁵ The small absorption band between 350 and 400 nm is due to the absorption of the tetraphenylethylene branching points, bathochromically shifted as compared to parent tetraphenylethylene ($\lambda_{\text{max}} = 320$ nm). The emission spectrum displayed a single band with a maximum at 518 nm, bathochromically shifted as compared to tetraphenylethylene (451 nm). Since the tetraphenylethylene units are linked to the dendrimers via their para-positions an efficient through-bond coupling can be assumed thereby leading to the observed large red-shifted emission.

In the first part, chapter 3.2, the functionalization of the dendrimer backbone has been described. For that, the benzophenone substituted tetraphenylcyclopentadienone **3-21** was synthesized, carrying next to the attached benzophenones additional ethynyl groups thereby allowing the further dendrimer growth. Postsynthetic modifications with a large variety of reagents could be carried out in a quantitative manner. However, it thus became obvious that benzophenone units only shielded by one dendrimer generation are highly accessible to many chemical transformations even with bulk substituents. To investigate the properties of more efficiently shielded keto groups, a benzophenone was placed as the core of polyphenylene dendrimers which is described in the following second part, chapter 3.3.

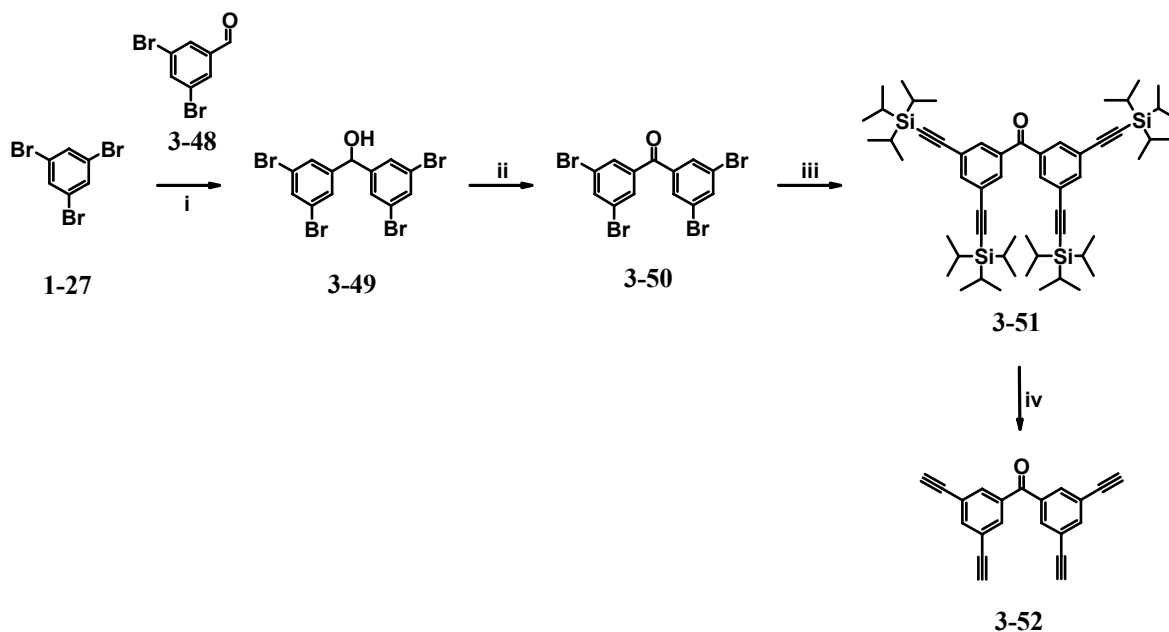
3.3 Benzophenone as Core

As already pointed out in the introduction of the first chapter, a functional core has often been used in dendrimer history to probe the amount of steric congestion coming from the surrounding dendrimer shell. In most cases, redox¹³¹⁻¹³³ and/or photoactive¹³⁴⁻¹³⁶ cores were chosen. The degree of encapsulation applied to a core depends strongly on the number and the nature of the branching units attached. That allows altering for example the density, the polarity and the flexibility of the dendrimers shell. However, during the photophysical investigation of dendronized pyrenes (chapter 2.5), fluorescence quenching experiments displayed a size-dependent penetration of molecules into the polyphenylene shell (chapter 2.5.3). This suggests that the density of the dendrimer shell is a major factor that controls the accessibility of the core. Impressive results were obtained from postsynthetic functionalizations in the scaffold of polyphenylene dendrimers (chapter 3.2.4). Up to now, however, only one example of a postsynthetic functionalization of a core or focal point of a dendrimer is reported. TWYMAN et al. presented the postsynthetic modification at the focal point of a hyperbranched polyester making use of a selective aminolysis reaction.¹³⁷ However, no quantitative conversion could be achieved. Recently, FRÉCHET et al presented a benzophenone, which was used as dendritic core surrounded by an aliphatic ester shell.¹³⁸ Light-driven catalysis based on the [4+2]cycloaddition of singlet oxygen to cyclopentadiene in methanol was chosen as a model system to show the catalytic activity of the dendrimers. An increased conversion was observed with increasing dendrimer-generation. This was attributed to the hydrophobic interior of the dendrimer which led to a high local concentration of the substrate near the catalytic active site.

To extend the previously presented synthetic concept for the functionalization of the dendrimer core, an ethynyl substituted benzophenone was synthesized and used as core for the construction of the dendrimers. Contrary to benzophenones in the dendrimer scaffold, the accessibility of an encapsulated single keto group should significantly be reduced due to steric hindrance coming from the surrounding polyphenylene shell.

3.3.1 Synthesis of a Benzophenone Core

To ensure a dense and therefore highly shielding polyphenylene shell around the benzophenone core, a high number of starting points for the dendrimer growth is desired. After mono-lithiation of 1,3,5-tribromo-benzene (**1-27**) the reaction was quenched with 3,5-dibromo-benzaldehyde (**3-48**) to afford bis-(3,5-dibromo-phenyl)-methanol (**3-49**) (Scheme 45).



Scheme 45. Synthesis of the benzophenone core **3-52**. i) 1 eq. *n*-BuLi, 3,5-dibromobenzaldehyde (**3-48**), THF, -78 °C, 80%; ii) Oxalylchloride, DMSO, TEA, CH₂Cl₂, 85%; iii) (triisopropylsilyl)-ethyne, Pd(PPh₃)₂Cl₂, CuI, PPh₃, Toluene, TEA, 80 °C, 60%; iv) TBAF, THF, 67%.

Subsequent SWERN-oxidation⁶⁵⁻⁶⁷ generated the according benzophenone derivative **3-50**. The introduction of the triple bonds necessary for polyphenylene dendrimer growth was achieved by HAGIHARA-SONOGASHIRA cross-coupling^{63,68,69} with triisopropylsilylethyne to give compound **3-51**. After deprotection of the TIPS protecting groups with TBAF, the desired core bis-(3,5-diethynyl-phenyl)-methanone **3-52** was obtained. The surprisingly bad yield in the TIPS deprotection step (normally > 90%) is probably due to side reactions between fluoride ions and the keto group. One would therefore use better trimethylsilyl (TMS) protecting groups next time which can be removed more smoothly using K₂CO₃ as base.

Figure 49 shows the ¹H NMR and FD mass spectra of the core **3-52**. The ¹H NMR spectrum of **3-52** was quite simple to interpret as the aromatic protons of the benzophenone moiety appeared as a singlet at 7.82 ppm. The ethynyl protons displayed at 3.77 ppm, also as a singlet. The intensities (see Experimental Part) were in line with the expected values proving the defect free substitution of the benzophenone core with four ethynyl groups.

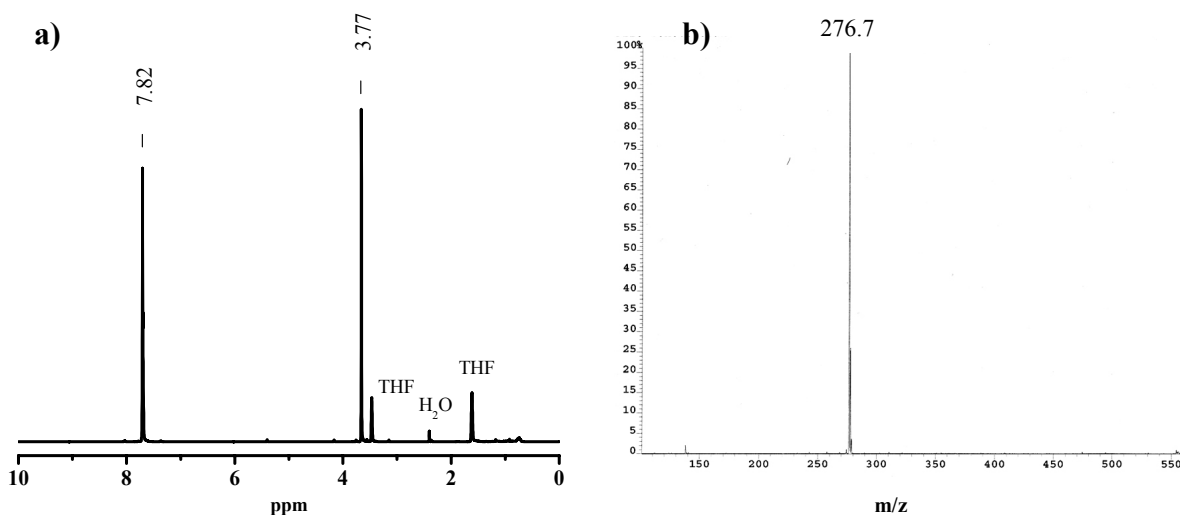
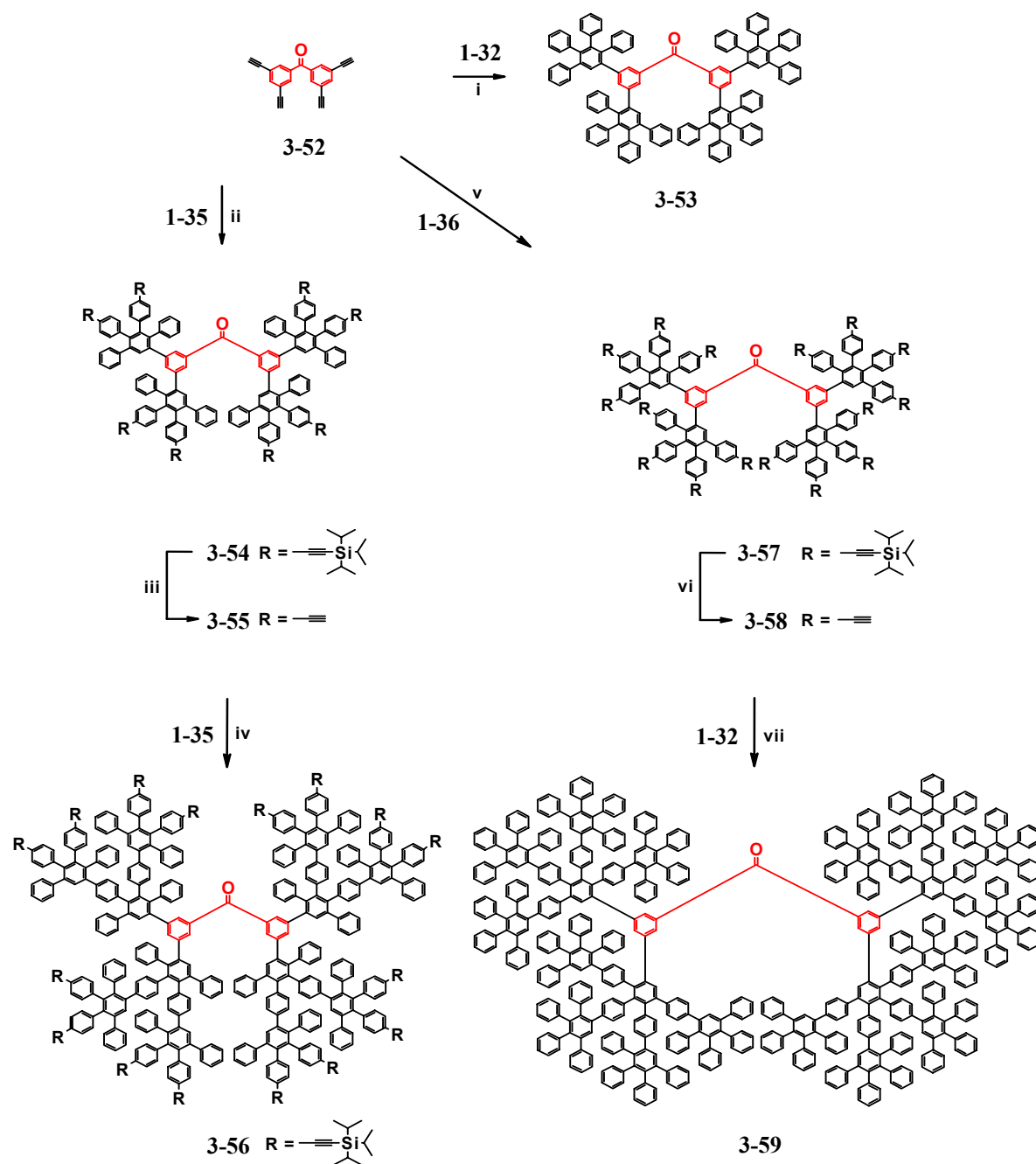


Figure 49. a) ¹H NMR (250 MHz, CD₂Cl₂, 300 K) and b) FD mass spectrum of the benzophenone core **3-52** (calculated molecular mass: 278.3 g·mol⁻¹).

The FD mass spectrum of **3-52** showed a major signal with a mass of 276.7 g·mol⁻¹, which can be assigned to the desired product with a calculated molecular weight of 278.3 g·mol⁻¹.

3.3.2 Synthesis of the Dendrimers

The first-generation dendrimer **3-53** was obtained from the DIELS-ALDER cycloaddition of tetraphenylcyclopentadienone (**1-32**) with the benzophenone core **3-52**. Scheme 46 shows the synthesis of the first- and second-generation dendrimers **3-53**, **3-56**, and **3-59**, respectively. Since the high steric shielding of the benzophenone core was one goal within this approach, a second-generation dendrimer **3-59** was synthesized using the AB₄-branching unit **1-36**. This building block possesses four reactive sites for further dendrimer growth and provides therefore a significantly denser dendrimer shell than if the corresponding AB₂ branching unit **1-35** is used.⁸⁰ DIELS-ALDER cycloaddition of **3-52** and **1-36** gave the first-generation dendrimer **3-57**, decorated with 16 TIPS protected ethynyl groups. Subsequent deprotection of the TIPS protecting groups with TBAF generated the first-generation dendrimer **3-58** with 16 terminal ethynyl groups. The reaction of **3-58** with tetraphenylcyclopentadienone (**1-32**) yielded the second-generation dendrimer **3-43** in 85% yield. When the AB₄ branching unit **1-36** is used, a dendrimer growth is only possible up to the second-generation due to the inherent spatial congestion (compare also chapter 1.4.2). Attaching a third-generation dendrimer shell around the benzophenone core was expected to lead to a larger diameter of the nanoparticles and coming from that, to a higher steric shielding of the core. The DIELS-ALDER cycloaddition of **3-52** with **1-35** gave the first-generation dendrimer **3-54**, possessing 8 TIPS protected ethynyl groups. Desilylation with TBAF generated dendrimer **3-55** with 8 peripheral ethynyl groups. Subsequent DIELS-ALDER cycloaddition with **1-35** yielded the second-generation dendrimer **3-56**. Desilylation of the TIPS protecting groups would lead to the ethynyl substituted second-generation dendrimer, from where the third-generation would be accessible. However, these last steps were not carried out, since further investigations focused on the first- and second-generation dendrimers **3-53** and **3-59**, respectively.



Scheme 46. Synthesis of polyphenylene dendrimers with a benzophenone core: i) 6 eq. **1-32**, *o*-xylene, 150 °C, 77%; ii) 6 eq. **1-35**, *o*-xylene, 160 °C, 47%; iii) TBAF, THF, 95%; iv) 16 eq. **1-35**, *o*-xylene, 170 °C, 90%; v) 6 eq. **1-36**, *o*-xylene, 160 °C, 76%; vi) TBAF, THF, 78%; vii) 48 eq. **1-32**, *o*-xylene, 170 °C, 85%.

Anyhow, a question to be investigated in the future, however, would then be how the difference in the dendrimer shell densities influences the accessibility of the benzophenone core, for example for small reagents.

Due to the good solubility in common organic solvents the above described dendrimers were all characterized using NMR and mass techniques. The MALDI-TOF spectrum of the second-generation dendrimer **3-59** displayed a single distinctive peak with a molecular mass of $7792 \text{ g}\cdot\text{mol}^{-1}$, which is in perfect agreement with its calculated molecular weight. The ^1H NMR spectrum of the unfunctionalized second-generation dendrimer **3-59** allowed only

assigning some of the aromatic signals, e.g. the generation protons, the other signals could not be assigned due to strong overlapping. For the TIPS or ethynyl substituted dendrimers, the intensity ratios between aliphatic and aromatic signals agreed with the calculated values. Further proof for the purity of the final products was derived from ^{13}C NMR spectroscopy and elemental analysis.

3.3.3 Visualisation and Simulation

To get an impression of the shape and size of the synthesized dendrimers molecular mechanics calculations were carried out by applying the MMFF method.⁸⁴ Figure 50 shows the three-dimensional structures of the first- and second-generation dendrimers **3-53** and **3-59**, respectively.

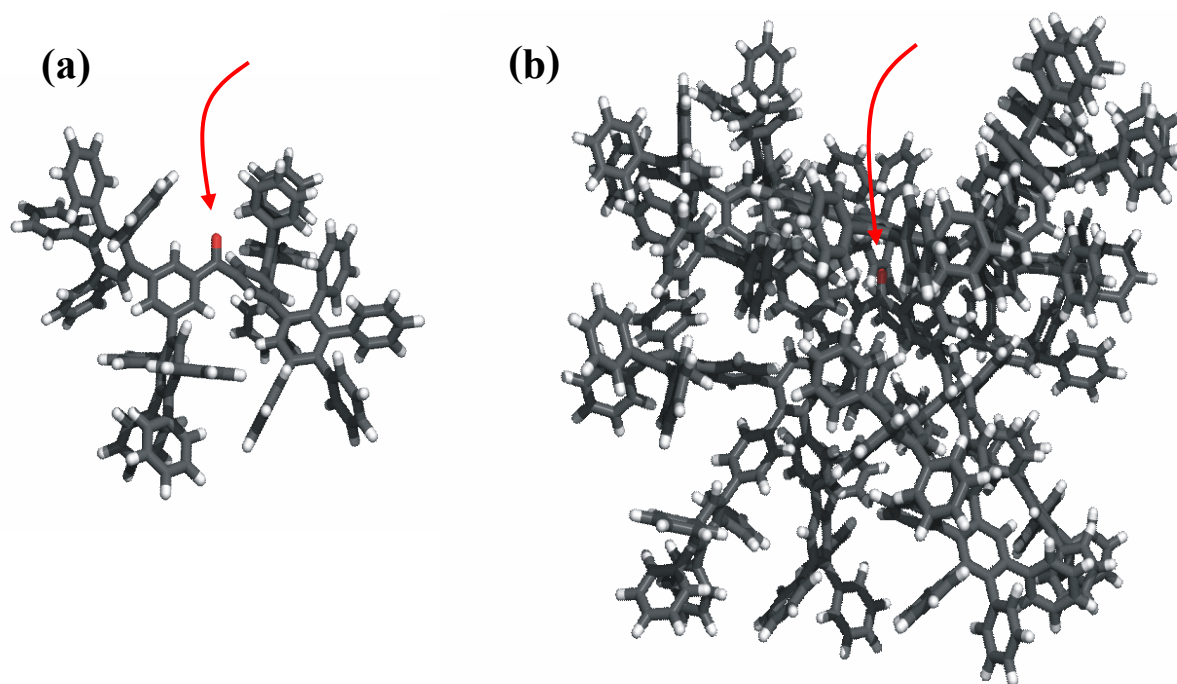


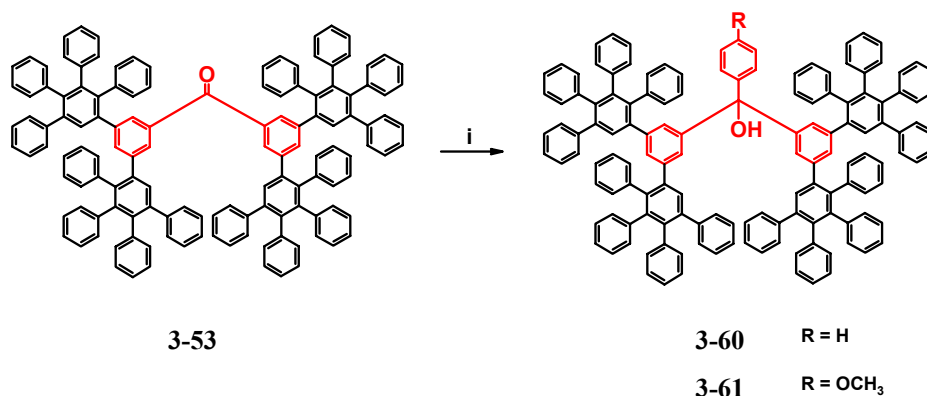
Figure 50. Molecular model of (a) the first-generation dendrimer **3-53** and (b) the second-generation dendrimer **3-59** (red = keto group).

In the first-generation dendrimer **3-53**, the shape of the dendrimer is strongly influenced by the substitution pattern on the benzophenone core, resulting in a bended dumb-bell like structure. The benzophenone core seems not to be shielded completely, as larger voids are observed. This would allow reaction partners to approach the reactive keto group. However, the second-generation dendrimer **3-59** possesses a more spherical shape, due to the dense polyphenylene shell provided by the AB_4 branching unit **1-36**. It is hard to even see the embedded benzophenone in the three-dimensional structure which suggests an isolated shielded core. The diameters of the spherical objects were determined to be 2.2 nm for **3-53** and 3.6 nm for **3-59**.

3.3.4 Postsynthetic Functionalizations in the Core

The postsynthetic functionalization of the dendrimers possessing a reactive benzophenone core has been carried out parallel to the before described reactions carried out on the scaffold

functionalized dendrimer **3-30** (see Scheme 39). Accordingly, **3-53** was reacted with a large excess of phenyllithium in refluxing THF to give compound **3-60** (Scheme 47).



Scheme 47. Postsynthetic functionalization of the first-generation dendrimer **3-53**: i) **3-60**: 60 eq. phenyllithium, THF, 70 °C, 70%; **3-61**: 25 eq. 4-methoxy-phenylmagnesiumbromide, THF, 70 °C, 66%.

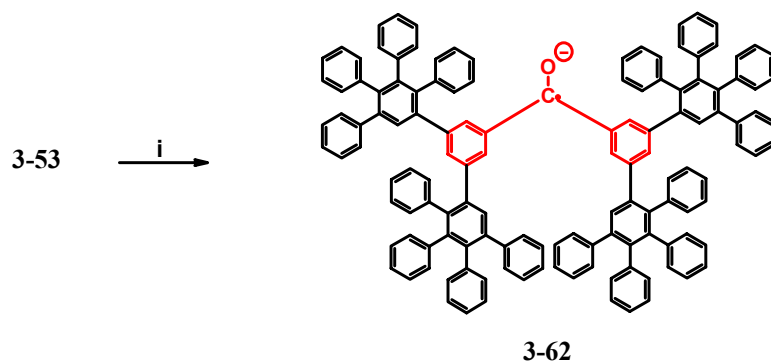
No addition products could be detected when larger nucleophiles e.g. lithium-biphenyl (obtained from halogen-lithium exchange of 4-bromo-biphenyl) were reacted with **3-53**. The FD-mass spectrum of quenched reaction mixtures, however, showed that the halogen-lithium exchange reaction was successful, since unsubstituted biphenyl was detected after hydrolysis. An introduction of substituted benzenes was achieved, when GRIGNARD reagents were used e.g. 4-methoxy-phenylmagnesiumbromide. In all cases of the postsynthetic functionalization of the first-generation dendrimer **3-53**, however, some starting material was detected in the reaction mixture, making a chromatographic separation necessary to yield the clean product. This is in contrast to the postsynthetic functionalizations carried out in the scaffold of the polyphenylene dendrimer **3-30** (chapter 3.2.4). Reason for this is probably the higher steric congestion around the benzophenone in the case of **3-52** with four meta-substituents contrary as to two para-substituents in the case of dendrimer **3-30**.

To check the accessibility of a higher shielded benzophenone core the second-generation dendrimer **3-59** was reacted with phenyllithium in the same way as described for the first-generation dendrimer **3-53**. Due to the higher steric congestion around the core, the reaction time needed to be prolonged to three days in refluxing THF. MALDI-TOF mass spectrometry showed the formation of the desired product. However, similarly to the first-generation dendrimer **3-53**, some starting material was still present even after longer reaction time. Unfortunately, the separation from the starting material using column chromatography was not possible in the case of the second-generation dendrimer due to only small differing polarity of the two species.

Similarly to dendrimer **3-30** with the benzophenones placed in the scaffold, the first-generation dendrimer **3-53** was reacted in a MCMURRY reaction with itself. After hydrolysis and chromatographic purification, the reaction of **3-53** with itself yielded a white material of which unfortunately no meaningful mass spectrum could be measured. NMR spectroscopy resulted in no further clues. However, one effort to be made in the future will be to receive an indirect structure proof, e.g. by the hydroboration of the assumed double bond of the tetraphenylethylene. The hydroboration product should then display explicit protons signals in the ¹H NMR spectrum.

3.3.5 Reduction of the Dendronized Benzophenone Core

The reduction of the first- and second-generation dendrimers was carried out similarly to dendrimer **3-30** possessing eight benzophenones in its scaffold (chapter 3.2.6.3). For this, a solution of **3-53** and **3-59** in THF was reacted with a potassium mirror under high vacuum in a sealed glass apparatus (Scheme 48). UV/vis and EPR spectroscopy were applied to follow the reaction.



Scheme 48. Formation of the ketyl radical anions **3-62** starting from dendrimer **3-53**. i) rt, K, THF.

Upon contact of a solution of the dendrimer **3-53** with the potassium mirror two increasing absorption bands at $\lambda \approx 350$ and 825 nm were observed in the UV/vis spectra (Figure 51a).

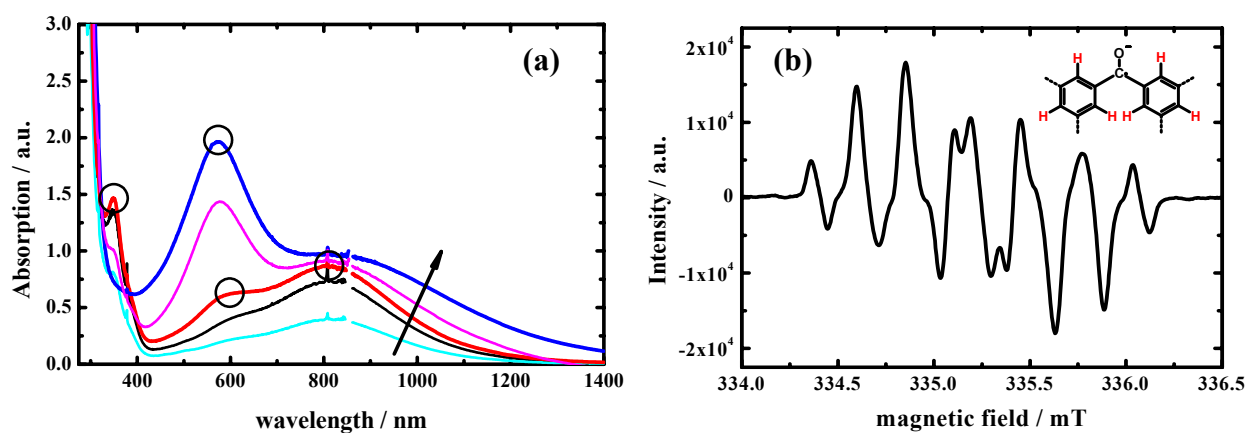


Figure 51. (a) UV/vis absorption spectra of the reduction of dendrimer **3-53** in THF in the order of further reduction. (b) EPR spectra at the maximum intensity of the radical monoanion absorption band of **3-62** ($\lambda = 825$ nm) in THF at 300 K.

They can be assigned to the formation of the radical anion of the benzophenone core in dendrimer **3-62**. The maxima were bathochromically shifted as compared to the parent benzophenone radical anion ($\lambda_{\text{max}} = 336$ and 560 nm),¹¹⁴ mainly due to the delocalization of the charge/spin into the neighboring phenyl rings. The absorption maxima of the benzophenone radical anion in **3-62** were less bathochromically shifted compared to the absorption maxima of the radical anion of para-phenyl substituted benzophenone in **3-46** ($\lambda_{\text{max}} = 410$ and 950, Figure 43). This can be attributed to the less efficient delocalization of the charge/spin into the neighboring phenyl rings in the case of the meta-phenyl substituted benzophenone core.

At a maximum intensity of these bands, the EPR spectra (Figure 51b) of **3-62** displayed a resolved signal with a high number of couplings. The signal consists of more lines than that observed in the case of the reduction of the eightfold benzophenone bearing dendrimer **3-30** (compare Figure 43b). The hyperfine coupling in **3-62** may be assigned to the four ortho-protons and the two para-protons carrying the largest spin-density while further phenyl rings block the meta-positions of the benzophenone radical monoanion. (inset in Figure 51b).

At maximum concentration of the radical monoanion the frozen state EPR spectra were recorded and showed characteristic zero-field splittings of $2D = 16$ mT (Figure 52a) which are of similar size as usually found for metal bridged benzophenone anion dimers ($2D \approx 18$ -20 mT).^{49,59}

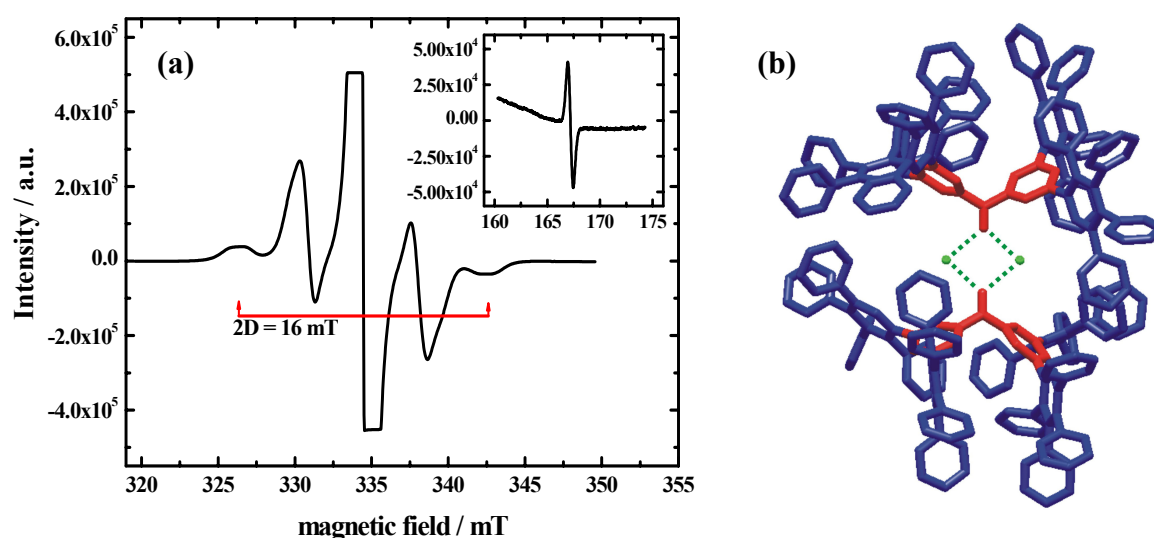
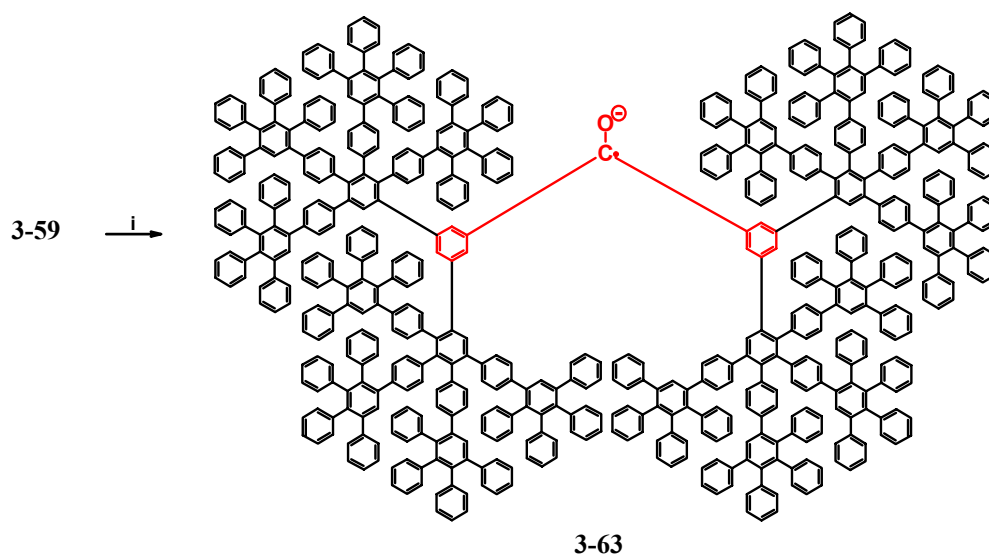


Figure 52. (a) EPR spectra of the reduction of **3-62** in THF at ≈ 120 K, zero-field-splittings and half-field transition (inset). (b) Three-dimensional structure of the potassium bridged biradical of **3-62**, obtained from a force-field optimization. Potassium: green, benzophenone: red.

In addition to the typical signal for the zero-field splittings ($\Delta m_s = 1$) also a relatively strong half-field transition at $g \approx 4$ was found ($\Delta m_s = 2$), further demonstrating the triplet character of these biradicals (inset in Figure 52a). Figure 52b shows a three-dimensional structure of the potassium bridged biradical of the first-generation dendrimer **3-62**, obtained from a force-field optimization. One gets the impression that the first-generation shell of **3-62** still provides enough space around the benzophenone core allowing the biradical formation. Due to the bended conformation of the benzophenone core, especially the oxygen is well accessible for e.g. the herein described dimerization reaction. Upon continued reduction on the potassium mirror the absorption bands of the radical monoanion **3-62** ($\lambda_{\max} = 350$ and 825 nm) disappeared and a new absorption band at $\lambda = 575$ nm increased in intensity (Figure 51a). This band can be attributed to the bathochromic shifted absorption band of the benzophenone dianion, being located at $\lambda = 340$ and 680 nm.⁵⁶ The EPR spectrum of this sample showed an unresolved signal of very low intensity ($< 1\%$ of monoanion signal). Even longer contact of the dendrimer solution with the potassium mirror, however, did not lead to a diamagnetic state, as still an EPR signal of small intensity could be observed. Additionally, the UV/vis spectra of the solution became more and more unresolved. Upon further reduction, the increase of an intense sharp EPR signal was observed which can be attributed to highly

mobile extra charges in the polyphenylene shell similarly as already observed for polyphenylene dendronized pyrenes (chapter 2.6.1).



Scheme 49. Formation of the ketyl radical anions **3-63** starting from dendrimer **3-59**. i) rt, K, THF.

For the second-generation dendrimer **3-59** reduction experiments have been performed under the same conditions (Scheme 49) to give the corresponding dendrimer **3-63** with a benzophenone radical monoanion as core. UV/vis and EPR spectra were similar to those measured during the reduction of the first-generation dendrimer **3-53**. Contrary as to **3-62**, the frozen state EPR spectra of **3-63** displayed no zero-field splittings and half-field transition, ruling out the formation of biradicals. One can attribute this to two reasons: firstly, the diameter of **3-63** is significantly larger than that of **3-62** thus keeping the radical centers more separated. Secondly, the use of the AB₄ branching-unit during the synthesis of **3-59** afforded a very dense polyphenylene shell. This led to some shape persistence and prevented the interdigitation of dendritic arms which could have resulted in a reduced distance between the radical centers and dimer formation. To show the non-destructive nature of the reduction process, a reoxidation experiment has been performed. When the sealed glass tubes were opened, the color of the reduction solutions immediately faded away due to the reaction with oxygen. In the case of dendrimer **3-53**, benzophenones as core, both spectra, before and after reduction, are in good agreement, suggesting a reversible charging process. However, in the case of dendrimer **3-30** with multiple benzophenones in the dendritic scaffold, the absorption band at 310 nm lost intensity as compared to the absorption of the polyphenylene shell at 250 nm during the reduction process.

In this chapter, chapter 3.3, the benzophenone core **3-52** has been used for the construction of polyphenylene dendrimers. Postsynthetic modifications were only possible with smaller reagents, mainly due to the increased spatial congestion around the keto group. In the following third part, chapter 3.4, benzophenones were used for the functionalization of the dendrimer surface.

3.4 Multiple Benzophenones on the Dendrimer Surface

During the first years of dendrimer history, most of functionalization has been performed on the dendrimer surface. Examples, like the benzophenone bearing dendrimers **3-30** and **3-53** described herein and examples from others show that the scope of interest is now directed toward the synthesis of dendrimers bearing multiple functions in all different places (core, scaffold and surface), mostly having a specialized application in mind. However, the functionalization of the dendrimer surface remains fascinating. Reason for this are the relative ease of functionalization since most functions can be introduced in the last step either by a polymeranalogous reaction or by using the accordingly functionalized endcapping reagent. Furthermore, the dendrimer surface represents the border to the surrounding medium and plays therefore an important role for the physical properties of the materials, e.g. their solubility as well as for their bulk behavior in heterogeneous matrices.

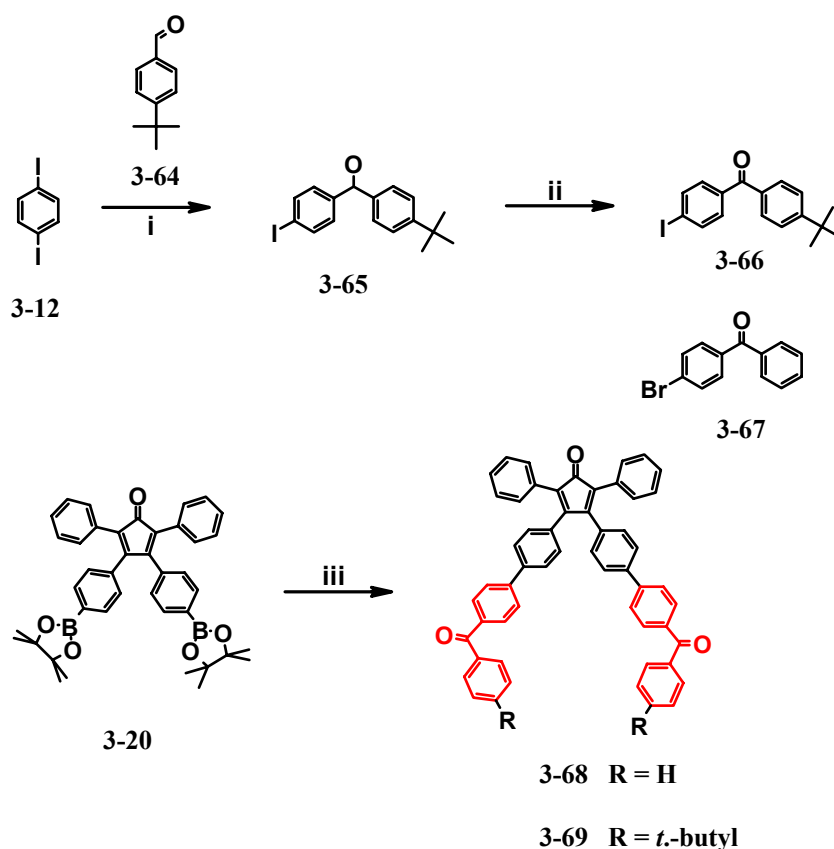
The surface of polyphenylene dendrimers has been functionalized following two synthetic approaches. Firstly, by using a functionalized tetraphenylcyclopentadienone endcapping reagent and secondly, by a postsynthetic procedure which involved simple derivatizations like ester or ether cleavage. In these cases, monodisperse products could be obtained after extended reaction time. However, also electrophilic substitution was used in a postsynthetic manner, e.g. bromination and sulfonation has been carried out with polyphenylene dendrimers. There, polydisperse products were obtained with no possibility of purification. Postsynthetic functionalizations, carried out on a polyphenylene dendrimer with benzophenones in its scaffold, have been described in chapter 3.2.4. Monodisperse products were obtained in high yield after an easy purification method. To use the synthetic potential of the benzophenones for the functionalization of the dendrimer surface, a benzophenone substituted tetraphenylcyclopentadienone endcapping reagent is required. All postsynthetic functionalizations, e.g. the introduction of charge or spin carrying centers, should also be possible on the dendrimer surface. Furthermore, these benzophenone substituted dendrimers might be a suitable starting material for a diverse library of easily accessible surface functionalized dendrimers.

The synthesis of a benzophenone substituted tetraphenylcyclopentadienone as well as the synthesis of the according dendrimers is described on the following pages.

3.4.1 Synthesis of the Endcapping Reagent

Similar to the branching unit **3-21**, which was used for the functionalization of the dendrimer scaffold, the termination agent **3-69**, used for the functionalization of the dendrimer surface, was synthesized via a SUZUKI cross-coupling reaction⁶² (Scheme 50 iii). In a first synthetic approach, the benzophenone substituted tetraphenylcyclopentadienone **3-68** was synthesized in one step from the boronic ester substituted tetraphenylcyclopentadienone **3-20** and the commercially available 4-bromobenzophenone (**3-67**). **3-68** turned out to be hardly soluble in common organic solvents, therefore being difficult to purify. Furthermore, also a first-generation dendrimer prepared from **3-68** was expected to be almost insoluble. Thus, in the improved approach solubilizing *t*-butyl groups were introduced. The *t*-butyl substituted benzophenone **3-66** was prepared in the same manner as already the before described benzophenone derivatives **3-21** and **3-52**. After halogen lithium exchange of 1,4-diiodo-benzene (**3-12**) with *n*-butyllithium the reaction was quenched with 4-*t*-butyl-benzaldehyde (**3-64**) yielding 4-*t*-butyl-4'-iodo-diphenylmethanol (**3-65**).

Subsequent SWERN oxidation⁶⁵⁻⁶⁷ gave 4-iodo-4'-*t*-butyl-benzophenone (**3-66**) in almost quantitative yield. The Suzuki cross-coupling reaction⁶² of **3-20** with **3-66** furnished the benzophenone substituted endcapping reagent **3-69** in 45% yield.

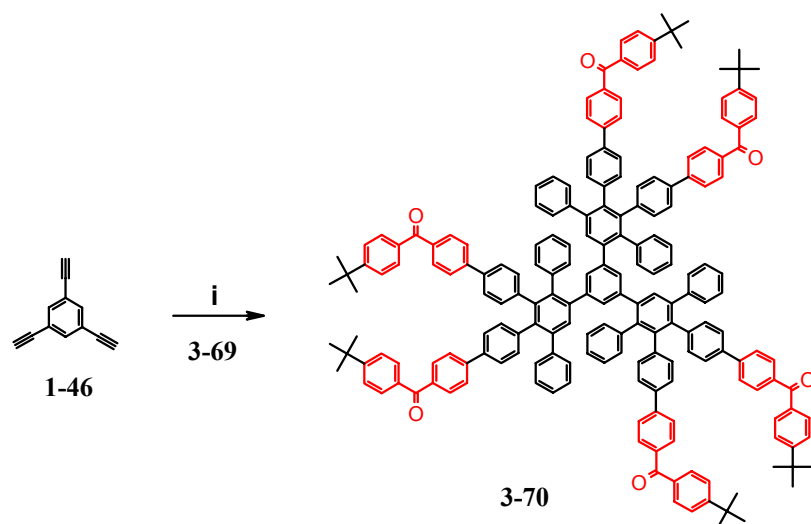


Scheme 50. Synthesis of the endcapping reagent **3-69**. i) 1 eq. *n*-BuLi, 4-*t*-butylbenzaldehyde (**3-64**), THF, -78 °C, 80%; ii) Oxalylchloride, DMSO, TEA, CH₂Cl₂, 98%; iii) 3 eq. **3-67** or **3-66**, respectively, Pd(PPh₃)₄, K₂CO₃, toluene, ethanol, 80 °C, 30% or 45%, respectively.

Contrary to **3-21**, no dithiolan groups had to be introduced in order to increase the yield of the cross-coupling step, probably because the herein used iodine possesses a higher reactivity than the former used bromine (compare also chapter 3.2.1). The purity of **3-69** was checked using NMR spectroscopy as well as mass spectrometry.

3.4.2 Synthesis of the Dendrimers

The DIELS-ALDER cycloaddition of the commercially available 1,3,5-triethynylbenzene core **1-46** with the endcapping reagent **3-69** yielded the first-generation dendrimer **3-70**, possessing 6 benzophenone groups on its surface (Scheme 51). Purification of **3-70** by column chromatography was difficult due to almost similar *r_f* values of **3-69**, which was used in an excess, and the product **3-70**. With the eluent mixture toluene/MeOH (100:1) a separation could be achieved, however, some material was lost lowering the yield.



Scheme 51. Synthesis the first-generation dendrimer **3-70** with a benzophenone decorated surface: i) 12 eq. **3-69**, *o*-xylene, 150 °C, 16 h, 47%.

The purity of **3-70** was checked by NMR spectroscopy and MALDI-TOF mass measurements.

3.4.3 Visualisation and Simulation

To get an impression of the shape and size of the synthesized dendrimer, molecular mechanics calculations were carried out by applying the MMFF method.⁸⁴ Figure 53 shows the three-dimensional structures of the first-generation dendrimer **3-70**.

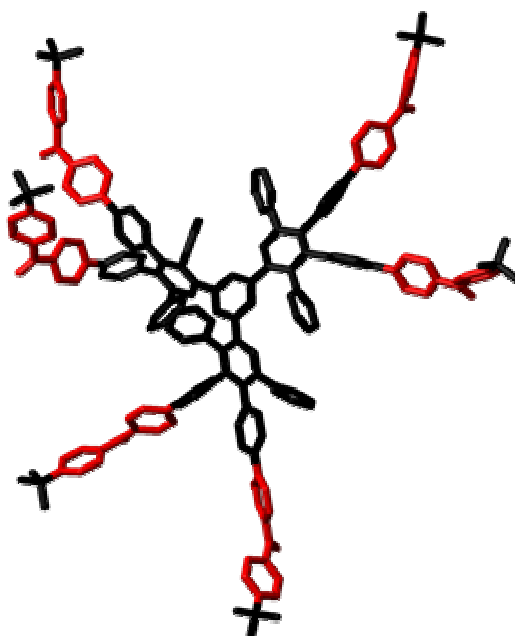


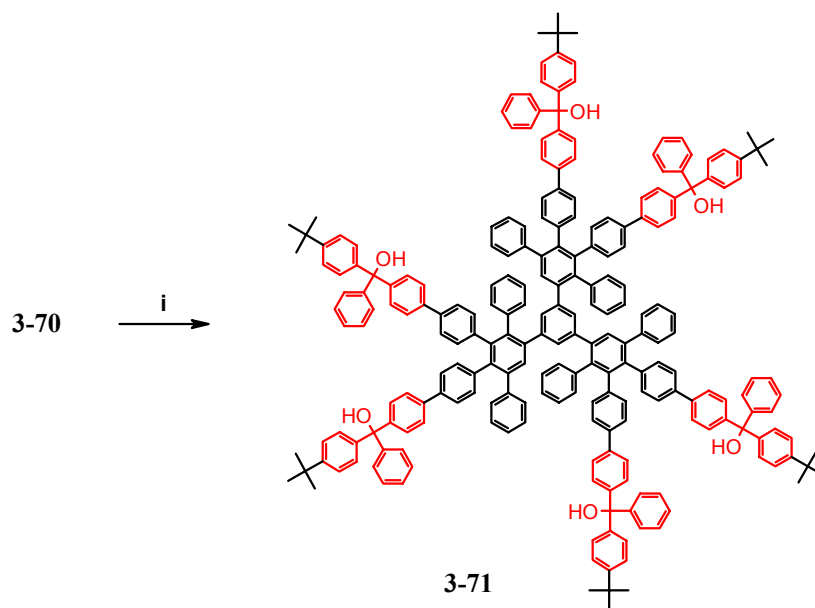
Figure 53. Molecular model of the first-generation dendrimer **3-70** (red = benzophenone).

The simulated structure clearly shows that the benzophenone groups are located on the surface of the dendrimer. Contrary to the second-generation dendrimer **3-30**, where multiple benzophenones were placed in the dendrimer backbone, the benzophenone groups in **3-70** are easily accessible. Thus, the postsynthetic introduction of even larger nucleophiles than pyrene

should be possible. The diameter of **3-70** was determined from the simulated structure to be ≈ 3.9 nm.

3.4.4 Postsynthetic Functionalizations on the Dendrimer Surface

Similar to the postsynthetic functionalization of the core or the scaffold of polyphenylene dendrimers, dendrimer **3-70** was used for the postsynthetic functionalization of the dendrimer surface. Scheme 52 shows as an example the test reaction of **3-70** with phenyllithium in refluxing THF.



Scheme 52. Postsynthetic functionalization of the first-generation dendrimer **3-70**: i) 100 eq. phenyllithium, THF, 70 °C, 76%.

After hydrolysis and precipitation from MeOH the according triphenylmethanol group bearing dendrimer **3-71** was obtained as a white solid in good yield. The MALDI-TOF mass spectrum of **3-71** displayed a major peak with multiple signals at lower molecular weight (Figure 54). No more starting material could be detected at $2640 \text{ g}\cdot\text{mol}^{-1}$. The major peak displayed at a molecular mass of $3088 \text{ g}\cdot\text{mol}^{-1}$, fitting with the calculated molecular weight of **3-71** ($3106 \text{ g}\cdot\text{mol}^{-1}$), if a hydroxy group has been cleaved off. Further signals at lower molecular weight differed from each other with a mass of $17 \text{ g}\cdot\text{mol}^{-1}$, exactly the mass of a hydroxyl group. Probably, by laser irradiation during the MALDI-TOF mass measurements, hydroxyl groups are cleaved off to form the stable trityl cation species. The same has been observed before for **3-33**, possessing eight triphenylmethanol groups in its interior. Further, the sodium and potassium complex $(M+\text{Na})^+$ and $(M+\text{K})^+$ were observed.

^1H NMR measurements proved the purity of the obtained product **3-71** and showed signal patterns similar to those of the triphenylmethanol derivative **3-34** with triphenylmethanol groups in its inner scaffold.

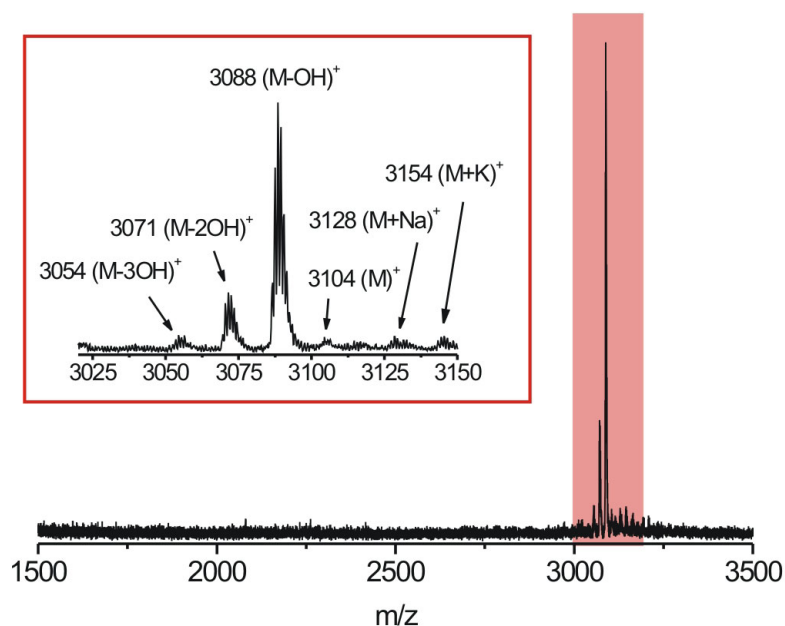


Figure 54. MALDI-TOF spectrum of 3-71 (calculated molecular mass: $3106 \text{ g}\cdot\text{mol}^{-1}$).

This test reaction has shown that dendrimer **3-70** represents a valuable precursor for the functionalization of the dendrimer surface. Further reactions with more sophisticated reagents are planned, especially the introduction of temperature labile components (DIELS-ALDER cycloaddition $\approx 430 \text{ K}$), is of great interest. Starting from **3-70**, an object of future research could be the synthesis of a dendrimer with a trityl cation decorated surface similarly as to dendrimer **3-9**, introduced by RATHORE et al.⁴³ Additionally, since the benzophenones on the dendrimer surface are freely accessible, the MCMURRY coupling reaction of **3-70** with itself should lead to an dendrimer network with increased density and molecular weight as compared to the network obtained from dendrimer **3-30**, bearing the benzophenones in its inner (chapter 3.2.6.4).

3.5 Conclusion

In this chapter, benzophenone moieties were introduced in polyphenylene dendrimers and used as universal precursors for further functionalizations. Starting from benzophenone as core enabled the synthesis of new spherical nanoparticles with a single keto group in their center. Applying a benzophenone substituted branching unit, polyphenylene dendrimers possessing multiple keto groups in the dendrimer backbone became accessible. Furthermore, by utilizing a benzophenone substituted endcapping reagent the surface of polyphenylene dendrimers was functionalized with a defined number of keto groups.

In the first part of this chapter, the functionalization of the dendrimer backbone has been described. For that, the benzophenone substituted tetraphenylcyclopentadienone **3-21** was synthesized carrying next to the attached benzophenones additional ethynyl groups thereby allowing the further dendrimer growth. Second- and third-generation dendrimers could be obtained, possessing eight keto groups in the first-generation layer. Irrespective of the surrounding higher generation dendrimer shell, the keto groups turned out to be still accessible for a large variety of reagents. Lithium-reagents, ranging from *n*-butyllithium to multiple substituted benzenes, were reacted with the dendrimer under relatively harsh reaction

conditions (THF, reflux). Nevertheless, a versatile and defect free postsynthetic functionalization of the dendritic scaffold could be achieved by this. Even eight pyrenyl moieties have been introduced quantitatively allowing for the modification of the dendrimer backbone also with larger substituents. Further proof for the accessibility of the inner keto groups was achieved as trityl cations, trityl radicals and ketyl species could be generated throughout the dendritic scaffold. Thereby, the stiff and shape-persistent polyphenylene dendrons ensured the investigation of spatially separated and thus stabilized functions. However, only the trityl cation derivatives were stable under atmospheric conditions.

The radical anion bearing dendrimer turned out to be of particular interest since it displayed intermolecular biradical formation in the frozen state. Thus, the existence of intermolecular interdigitating dendrimer arms could be shown, suggesting a radical network of the dendrimers themselves. Further proof for the ability of dendrimer arms to interlock was obtained from the MCMURRY coupling reaction of the benzophenones embedded in the dendrimer. High molecular weight products were obtained due to a network of polyphenylene dendrimers, with the dendrimers covalently linked to each other via multiple tetraphenylethylene units.

In the second part of this chapter, we focused on the synthesis of polyphenylene dendrimers with the benzophenone core **3-52**. The variation of the dendrimer generation and the density of the surrounding dendrimer shell generated a defined amount of encapsulation around the core. Postsynthetic functionalizations, similarly as for the scaffold functionalized dendrimers, were carried out using lithium- and GRIGNARD-reagents. However, monodisperse products could only be obtained for the reaction with small molecules, mainly due to the increased spatial congestion around the core. Remember in this context, that the benzophenones in the dendritic scaffold were embedded in the dendrimer backbone via their para-positions, whereas the benzophenone core is linked to the four dendrons via its meta-positions resulting in an obviously increased shielding of the core. Similarly to the above described dendrimer with benzophenones in its scaffold, the first- and second-generation dendrimers with benzophenone as core were reduced on a potassium mirror to yield the according radical anion species. Only the first-generation dendrimer displayed biradical formation, mainly due to the higher steric congestion in the case of the second-generation dendrimer, thereby suppressing both radical centers from approaching each other.

Going one-step further, the benzophenone carrying tetraphenylcyclopentadienone **3-69** has been synthesized, which was used as an endcapping reagent for the functionalization of the dendrimer surface. A first postsynthetic reaction was reported to give monodisperse products in high yield. Further work in that area is planned.

3.6 References

- (1) Tomalia, D. A.; Baker, H.; Dewald, J.; Hall, M.; Kallos, G.; Martin, S.; Roeck, J.; Ryder, J.; Smith, P. *Polymer Journal* **1985**, *17*, 117.
- (2) Tomalia, D. A.; Baker, H.; Dewald, J.; Hall, M.; Kallos, G.; Martin, S.; Roeck, J.; Ryder, J.; Smith, P. *Macromolecules* **1986**, *19*, 2466.
- (3) Newkome, G. R.; Baker, G. R.; Saunders, M. J.; Russo, P. S.; Gupta, V. K.; Yao, Z. Q.; Miller, J. E.; Bouillion, K. *Chemical Communications* **1986**, 752.
- (4) Newkome, G. R.; Moorefield, C. N.; Vögtle, F., *Dendrimers and Dendrons: Concepts, Syntheses, Application*; Wiley-VCH: Weinheim **2001** and references therein.
- (5) Tomalia, D. A.; Naylor, A. M.; Goddard, W. A. *Angewandte Chemie-International Edition* **1990**, *29*, 138.

- (6) Fréchet, J. M. J. *Journal of Polymer Science, Part A* **2003**, *41*, 3713.
- (7) Caminade, A. M.; Majoral, J. P. *Accounts of Chemical Research* **2004**, *37*, 341.
- (8) Gilat, S. L.; Adronov, A.; Fréchet, J. M. J. *Angewandte Chemie-International Edition* **1999**, *38*, 1422.
- (9) Adronov, A.; Fréchet, J. M. J. *Chemical Communications* **2000**, 1701.
- (10) Gong, L. Z.; Hu, Q. S.; Pu, L. *Journal of Organic Chemistry* **2001**, *66*, 2358.
- (11) Choi, M. S.; Aida, T.; Yamazaki, T.; Yamazaki, I. *Chemistry-A European Journal* **2002**, *8*, 2668.
- (12) Hahn, U.; Gorka, M.; Vogtle, F.; Vicinelli, V.; Ceroni, P.; Maestri, M.; Balzani, V. *Angewandte Chemie-International Edition* **2002**, *41*, 3595.
- (13) Balzani, V.; Ceroni, P.; Maestri, M.; Vicinelli, V. *Current Opinion in Chemical Biology* **2003**, *7*, 657.
- (14) Pittelkow, M.; Christensen, J. B.; Meijer, E. W. *Journal of Polymer Science Part A* **2004**, *42*, 3792.
- (15) Teobaldi, G.; Zerbetto, F. *Journal of the American Chemical Society* **2003**, *125*, 7388.
- (16) Baars, M.; Meijer, E. W. in *Dendrimers II, Topics in Current Chemistry* **2000**; *210*, 131.
- (17) Oosterom, G. E.; Reek, J. N. H.; Kamer, P. C. J.; van Leeuwen, P. *Angewandte Chemie-International Edition* **2001**, *40*, 1828.
- (18) Kreiter, R.; Kleij, A. W.; Gebbink, R.; van Koten, G. in *Dendrimers IV, Topics in Current Chemistry* **2001**; *217*, 163.
- (19) Twyman, L. J.; King, A. S. H.; Martin, I. K. *Chemical Society Reviews* **2002**, *31*, 69.
- (20) Twyman, L. J. *Tetrahedron Letters* **2000**, *41*, 6875.
- (21) Schultz, L. G.; Zhao, Y.; Zimmerman, S. C. *Angewandte Chemie-International Edition* **2001**, *40*, 1962.
- (22) Larre, C.; Bressolles, D.; Turrin, C.; Donnadieu, B.; Caminade, A. M.; Majoral, J. P. *Journal of the American Chemical Society* **1998**, *120*, 13070.
- (23) Galliot, C.; Larre, C.; Caminade, A. M.; Majoral, J. P. *Science* **1997**, *277*, 1981.
- (24) Bo, Z. S.; Schäfer, A.; Franke, P.; Schlüter, A. D. *Organic Letters* **2000**, *2*, 1645.
- (25) Chow, H. F.; Ng, M. K.; Leung, C. W.; Wang, G. X. *Journal of the American Chemical Society* **2004**, *126*, 12907.
- (26) Ziessel, R.; Stroh, C. *Synthesis* **2003**, 2145.
- (27) Kaneko, T.; Makino, T.; Miyaji, H.; Teraguchi, M.; Aoki, T.; Miyasaka, M.; Nishide, H. *Journal of the American Chemical Society* **2003**, *125*, 3554.
- (28) Lahti, P. M. in *Magnetic Properties of Organic Materials*, Marcel-Dekker, New-York, **1999**.
- (29) Nishide, H.; Miyasaka, M.; Tsuchida, E. *Angewandte Chemie-International Edition* **1998**, *37*, 2400.
- (30) Rajca, A. *Chemical Reviews* **1994**, *94*, 871.
- (31) Miller, J. S.; Epstein, A. J. *Angewandte Chemie-International Edition*. **1994**, *33*, 385.
- (32) Ballester, M. *Accounts of Chemical Research* **1985**, *18*, 380.
- (33) Skotheim, T. A. *Handbook of Conducting Polymers*, Marcel Dekker, New York, **1986**.
- (34) Rajca, S.; Rajca, A.; Wongsriratanakul, J.; Butler, P.; Choi, S. M. *Journal of the American Chemical Society* **2004**, *126*, 6972.
- (35) Rajca, A.; Wongsriratanakul, J.; Rajca, S.; Cerny, R. *Angewandte Chemie-International Edition* **1998**, *37*, 1229.
- (36) Reddy, T. J.; Iwama, T.; Halpern, H. J.; Rawal, V. H. *Journal of Organic Chemistry* **2002**, *67*, 4635.
- (37) Viehe, H. G.; Janousek, Z.; Merényi, R. *Substituent Effects in Radical Chemistry NATO ASI Series Dordrecht*, **1986**; Vol. 189.
- (38) Neumann, W. P.; Uzick, W.; Zarkadis, A. K. *Journal of the American Chemical Society* **1986**, *108*, 3762.
- (39) Neumann, W. P.; Penenory, A.; Stewen, U.; Lehnig, M. *Journal of the American Chemical Society* **1989**, *111*, 5845.
- (40) Janzen, E. G. *Accounts of Chemical Research* **1969**, *2*, 279.
- (41) Meier, H.; Kim, S. *European Journal of Organic Chemistry* **2001**, 1163.
- (42) Shchepinov, M. S.; Korshun, V. A.; Egeland, R. D.; Southern, E. M. *Tetrahedron Letters* **2000**, *41*, 4943.

- (43) Rathore, R.; Burns, C. L.; Guzei, I. A. *Journal of Organic Chemistry* **2004**, *69*, 1524.
- (44) Ashby, E. C.; Laemmle, J.; Neumann, H. M. *Accounts of Chemical Research* **1974**, *7*, 272.
- (45) Kawai, A.; Hirakawa, M.; Abe, T.; Obi, K.; Shibuya, K. *Journal of Physical Chemistry Part A* **2001**, *105*, 9628.
- (46) Hou, Z. M.; Jia, X. S.; Fujita, A.; Tezuka, H.; Yamazaki, H.; Wakatsuki, Y. *Chemistry-A European Journal* **2000**, *6*, 2994.
- (47) Molander, G. A. *Accounts of Chemical Research* **1998**, *31*, 603.
- (48) Skrydstrup, T. *Angewandte Chemie-International Edition* **1997**, *36*, 345.
- (49) Hirota, N. *Journal of the American Chemical Society* **1967**, *89*, 32.
- (50) Schlenck, W.; Weichel, T. *Berichte* **1911**, 1182.
- (51) Beckman, F.; Paul, T. *Annalen der Chemie* **1891**, 266, 1.
- (52) Takeda, K.; Kajii, Y.; Shibuya, K.; Obi, K. *Journal of Photochemistry and Photobiology A* **1998**, *115*, 109.
- (53) Bewick, A.; Jones, V. W.; Kalaji, M. *Electrochimica Acta* **1996**, *41*, 1961.
- (54) Redmond, R. W.; Scaiano, J. C.; Johnston, L. J. *Journal of the American Chemical Society* **1990**, *112*, 398.
- (55) Hiratsuka, H.; Yamazaki, T.; Maekawa, Y.; Hikida, T.; Mori, Y. *Journal of Physical Chemistry* **1986**, *90*, 774.
- (56) Baumgarten, M.; Gherghel, L.; Wehrmeister, T. *Chemical Physics Letters* **1997**, *267*, 175.
- (57) Hou, Z. M.; Miyano, T.; Yamazaki, H.; Wakatsuki, Y. *Journal of the American Chemical Society* **1995**, *117*, 4421.
- (58) Hou, Z. M.; Fujita, A.; Yamazaki, H.; Wakatsuki, Y. *Journal of the American Chemical Society* **1996**, *118*, 2503.
- (59) Hirota, N.; Weissman, S. I. *Journal of the American Chemical Society* **1964**, *86*, 2538.
- (60) Bauer, R.; Dissertation Johannes Gutenberg Universität (Mainz), **2005**.
- (61) Weil, T.; Dissertation Johannes Gutenberg Universität (Mainz), **2001**.
- (62) Weil, T.; Wiesler, U. M.; Herrmann, A.; Bauer, R.; Hofkens, J.; De Schryver, F. C.; Müllen, K. *Journal of the American Chemical Society* **2001**, *123*, 8101.
- (63) Sonogashira, K.; Tohda, Y.; Hagihara, N. *Tetrahedron Letters* **1975**, 4467.
- (64) Tour, J. M.; Rawlett, A. M.; Kozuki, M.; Yao, Y.; Jagessar, R. C.; Dirk, S. M.; Price, D. W.; Reed, A. M.; Zhou, C.-W.; Chen, J.; Wang, W.; Wenyong, I. C. *Chemistry-A European Journal* **2001**, *23*, 5118.
- (65) Omura, K.; Swern, D. *Tetrahedron* **1978**, *34*, 1651.
- (66) Mancuso, A. J.; Brownfain, D. S.; Swern, D. *Journal of Organic Chemistry* **1979**, *44*, 4148.
- (67) Mancuso, A. J.; Huang, S.-L.; Swern, D. *Journal of Organic Chemistry* **1978**, *43*, 2480.
- (68) Dieck, H. A.; Heck, F. R. *Journal of Organometallic Chemistry* **1975**, *93*, 259.
- (69) Sonogashira, K.; Takahashi, S. *Journal of Synthetic Organic Chemistry Japan* **1993**, *51*, 1053.
- (70) Ishiyama, T.; Murata, M.; Miyaura, N. *Journal of Organic Chemistry* **1995**, *60*, 7508.
- (71) Miyaura, N.; Suzuki, A. A. *Chemistry Reviews* **1995**, *95*, 2457.
- (72) Watanabe, J. *Chemical Communications* **1994**, 467.
- (73) Jong, S. J.; Fang, J.-M. *Journal of Organic Chemistry* **2001**, *66*, 3522.
- (74) Mathews, C. J.; Smith, P. J.; Welton, T. *Chemical Communication* **2000**, 1249.
- (75) Wolfe, J. P.; Singer, R. A.; Yang, B. H.; Buchwald, S. L. *Journal of the American Chemical Society* **1999**, *121*, 9550.
- (76) Mueller-Westerhoff, U. T.; Zhou, M. *Tetrahedron Letters* **1993**, *34*, 571.
- (77) Mueller-Westerhoff, U. T.; Zhou, M. *Journal of Organic Chemistry* **1994**, *59*, 4988.
- (78) Fieser, F. L. *Journal of the American Chemical Society* **1954**, *76*, 1945.
- (79) Sondej, S. C.; Katzenellenbogen, J. A. *Journal of Organic Chemistry* **1986**, *51*, 3508.
- (80) Wiesler, U. M.; Berresheim, A. J.; Morgenroth, F.; Lieser, G.; Müllen, K. *Macromolecules* **2001**, *34*, 187.
- (81) Morgenroth, F.; Müllen, K. *Tetrahedron* **1997**, *53*, 15349.
- (82) Pretsch, E.; Clerc, T.; Seibl, J.; Simon, W. *Tabellen zur Strukturaufklärung organischer Verbindungen mit spektroskopischen Methoden*; Springer: Heidelberg, **1986**.
- (83) Olah, G. A.; Mehrotra, A. K.; Narang, S. C. *Synthesis* **1982**, *2*, 151.
- (84) Halgren, T. A. *Journal of Computational Chemistry* **1996**, *17*, 490.

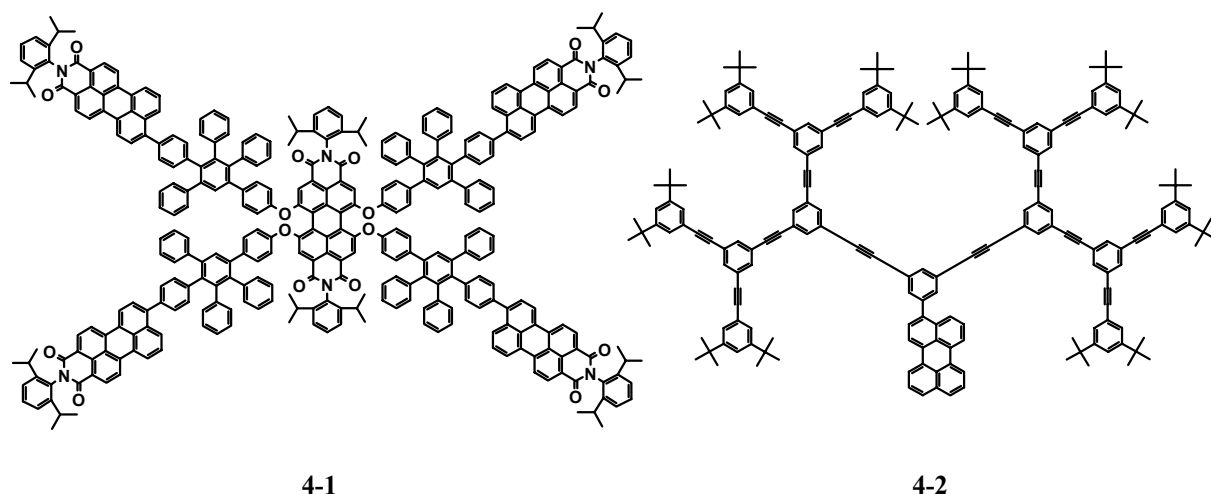
- (85) Abarca, B.; Asensio, G.; Ballesteros, R.; Varea, T. *Journal of Organic Chemistry* **1991**, *56*, 3224.
- (86) Badejo, I. T.; Karaman, R.; Fry, J. L. *Journal of Organic Chemistry* **1989**, *54*, 4591.
- (87) Carey, F. A.; Tremper, H. S. *Journal of the American Chemical Society* **1968**, *90*, 2578.
- (88) Forrester, A. R.; Hay, J. M.; Thomson, R. H. *Organic Chemistry of Stable Free Radicals*; Academic Press: New York, **1968**.
- (89) Kahr, B.; Vanengen, D.; Mislow, K. *Journal of the American Chemical Society* **1986**, *108*, 8305.
- (90) Colle, K. S.; Glaspie, P. S.; Lewis, E. S. *Chemical Communications* **1975**, 266.
- (91) Stein, M.; Winter, W.; Rieker, A. *Angewandte Chemie-International Edition* **1978**, *17*, 692.
- (92) Felix, G.; Dunoques, J.; Piscioti, F.; Calas, R. *Angewandte Chemie-International Edition* **1977**, *16*, 488.
- (93) Funk, R. L.; Vollhardt, K. P. C. *Chemical Communications* **1976**, 833.
- (94) Aalbersberg, W. G. L.; Barkovich, A. J.; Funk, R. L.; Hillard, R. L.; Vollhardt, K. P. C. *Journal of the American Chemical Society* **1975**, *97*, 5600.
- (95) Carmichael, I.; Hug, G. L. *Handbook of Photochemistry*, 2nd ed.; Marcel Dekker: New York, **1993**.
- (96) Winnik, F. M. *Chemical Reviews* **1993**, *93*, 587.
- (97) Förster, T. *Angewandte Chemie-International Edition* **1969**, *8*, 333.
- (98) Birks, J. B. *Photophysics of Aromatic Molecules*; Wiley Interscience: London, **1970**.
- (99) Thomas, A.; Polarz, S.; Antonietti, M. *Journal of Physical Chemistry B* **2003**, *107*, 5081.
- (100) Umland, J. B.; Jefraim, M. I. *Journal of the American Chemical Society* **1956**, *78*, 2788.
- (101) Nystrom, R. F.; Brown, W. G. *Journal of the American Chemical Society* **1947**, *69*, 1197.
- (102) Scott, R. W. J.; Wilson, O. M.; Crooks, R. M. *Journal of Physical Chemistry B* **2005**, *109*, 692.
- (103) Crooks, R. M.; Zhao, M. Q.; Sun, L.; Chechik, V.; Yeung, L. K. *Accounts of Chemical Research* **2001**, *34*, 181.
- (104) Taubert, A.; Wiesler, U. M.; Müllen, K. *Journal of Materials Chemistry* **2003**, *13*, 1090.
- (105) Liu, D. J.; De Feyter, S.; Cotlet, M.; Stefan, A.; Wiesler, U. M.; Herrmann, A.; Grebel-Koehler, D.; Qu, J. Q.; Müllen, K.; De Schryver, F. C. *Macromolecules* **2003**, *36*, 5918.
- (106) Berlman, I. B. *Journal of Physical Chemistry* **1970**, *74*, 3085.
- (107) Zhang, H.; Grim, P. C. M.; Foubert, P.; Vosch, T.; Vanoppen, P.; Wiesler, U. M.; Berresheim, A. J.; Müllen, K.; De Schryver, F. C. *Langmuir* **2000**, *16*, 9009.
- (108) Wind, M.; Saalwachter, K.; Wiesler, U. M.; Müllen, K.; Spiess, H. W. *Macromolecules* **2002**, *35*, 10071.
- (109) Rosenfeldt, S.; Dingenouts, N.; Potschke, D.; Ballauff, M.; Berresheim, A. J.; Müllen, K.; Lindner, P. *Angewandte Chemie-International Edition* **2004**, *43*, 109.
- (110) Ray, G. J.; Kurland, R. J.; Colter, A. K. *Tetrahedron* **1971**, *27*, 735.
- (111) Hansen, P. E.; Spanget-Larsen, J.; Laali, K. K. *Journal of Organic Chemistry* **1998**, *63*, 1827.
- (112) Wind, M.; Wiesler, U. M.; Saalwächter, K.; Müllen, K.; Spiess, H. W. *Advanced Materials* **2001**, *13*, 752.
- (113) Farnum, D. G. *Journal of the American Chemical Society* **1964**, *86*, 934.
- (114) Shida, T. *Electronic Absorption Spectra of Radical Ions*, Physical Science data 34; Elsevier Science Publishers B.V: Netherlands, **1935**.
- (115) Maki, A. H.; Allendoe R. D.; Danner, J. C.; Keys, R. T. *Journal of the American Chemical Society* **1968**, *90*, 4225.
- (116) Bromberg, A.; Schmidt, K. H.; Meisel, D. *Journal of the American Chemical Society* **1985**, *107*, 83.
- (117) Ashby, E. C.; Argyropoulos, J. N.; Meyer, G. R.; Goel, A. B. *Journal of the American Chemical Society* **1982**, *104*, 6788.
- (118) Baumgarten, M.; Huber, W.; Müllen, K. *Advances in Physical Organic Chemistry* **1993**, *28*, 1.
- (119) Baumgarten, M.; Müllen, K. in *Electron Transfer I, Topics in Current Chemistry* **1994**; *169*, 1-103.
- (120) Shida, T.; Iwata, S. *Journal of Physical Chemistry* **1971**, *75*, 2591.
- (121) Shida, T.; Iwata, S. *Journal of Physical Chemistry* **1972**, *56*, 2858.
- (122) Shida, T.; Iwata, S. *Journal of the American Chemical Society* **1973**, *95*, 3473.

-
- (123) Lindow, D. F.; Cortez, C. N.; Harvey, R. G. *Journal of the American Chemical Society* **1972**, *94*, 5406.
- (124) Balk, P.; Debruijn, S.; Hoijtink, G. J. *Recueil des Travaux Chimique des Pays-Bas* **1957**, *76*, 907.
- (125) Baumgarten, M. *Molecular Crystals and Liquid Crystals Science and Technology Section A* **1995**, *271*, 109.
- (126) Takui, T.; Sato, K.; Shiomi, D.; Nakazawa, S.; Yano, M.; Kinoshita, T.; Abe, K.; Itoh, K.; Nakamura, T.; Momose, T.; Shida, T. *Molecular Crystals and Liquid Crystals Science and Technology Section A* **1997**, *306*, 353.
- (127) Shohoji, M.; Franco, M.; Lazana, M. C. R.; Sato, K.; Takui, T.; Itoh, K. *Molecular Crystals and Liquid Crystals Science and Technology Section A-Molecular Crystals and Liquid Crystals* **1997**, *305*, 353.
- (128) Ephritikhine, M. *Chemical Communications* **1998**, 2549.
- (129) Villiers, C.; Ephritikhine, M. *Angewandte Chemie-International Edition* **1997**, *36*, 2380.
- (130) Dams, R.; Malinowski, M.; Geise, H. J. *Bulletin Des Societes Chimiques Belges* **1981**, *90*, 1141.
- (131) Dandliker, P. J.; Diederich, F.; Gross, M.; Knobler, C. B.; Louati, A.; Sanford, E. M. *Angewandte Chemie-International Edition* **1994**, *33*, 1739.
- (132) Weyermann, P.; Gisselbrecht, J. P.; Boudon, C.; Diederich, F.; Gross, M. *Angewandte Chemie-International Edition* **1999**, *38*, 3215.
- (133) Gorman, C. B.; Smith, J. C. *Accounts of Chemical Research* **2001**, *34*, 60.
- (134) Devadoss, C.; Bharathi, P.; Moore, J. S. *Journal of the American Chemical Society* **1996**, *118*, 9635.
- (135) Jiang, D. L.; Aida, T. *Journal of the American Chemical Society* **1998**, *120*, 10895.
- (136) Jin, R. H.; Aida, T.; Inoue, S. *Chemical Communications* **1993**, 1260.
- (137) Gittins, P. J.; Twyman, L. J. *Journal of the American Chemical Society* **2005**, *127*, 1646.
- (138) Hecht, S.; Fréchet, J. M. J. *Journal of the American Chemical Society* **2001**, *123*, 6959.

4. TRIPHENYLAMINE (TPA) PERYLENEMONOIMIDE (PMI) DONOR-ACCEPTOR SYSTEMS

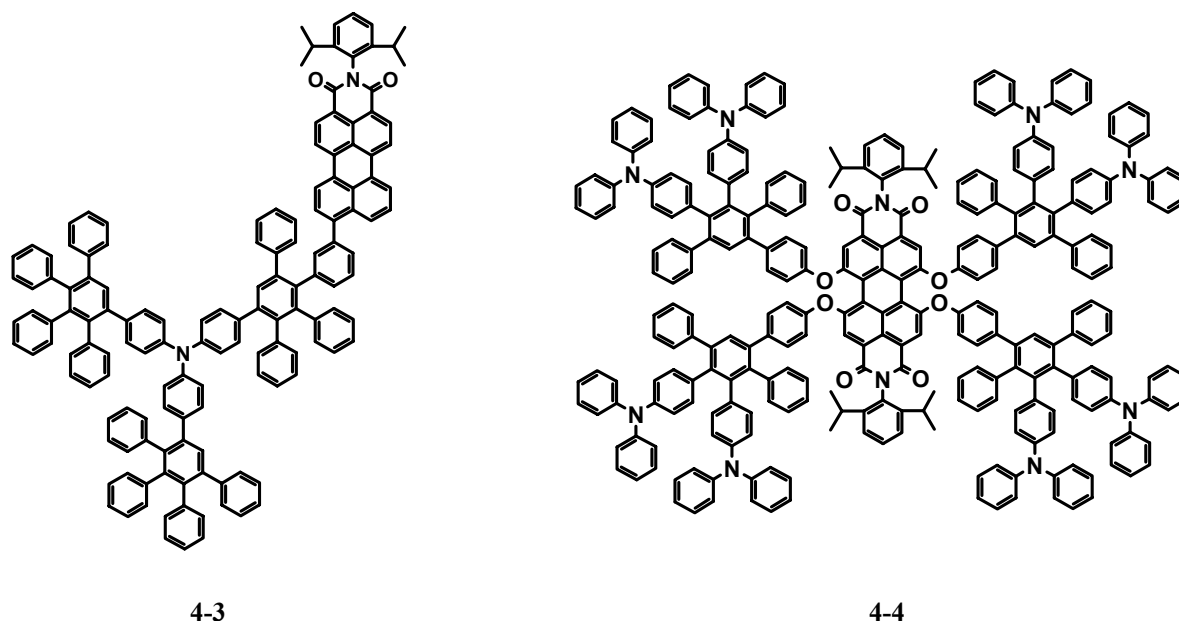
4.1 Introduction

During the last years, the synthesis of multichromophoric molecules has reached an unprecedented high level.¹⁻⁴ These sophisticated structures are mainly used for two reasons: firstly, to mimic biological systems linked to processes in photosynthesis or secondly, in fundamental research to study the energy transfer mechanism between different chromophores. Since the spatial orientation of the chromophores plays an important role in the energy transfer process, rigid dendritic structures exhibit some unbeatable advantages. Firstly, dendrimers can be synthesized monodisperse by a repeated activation growth procedure thereby the size of the resulting nanoparticles can be controlled. Secondly, especially rigid dendritic structures allow to engineer nanostructures with the chromophores placed on defined positions. Polyphenylene dendrimers with their shape persistent dendrimer backbone gain more and more attraction as the basis of well-defined multichromophor systems. Recent progress in dendrimer synthesis enabled scientists to functionalize the core, the dendritic scaffold as well as the dendrimer surface with various chromophores.



Scheme 53. Multichromophor systems. **4-1**, four PMI donors and a TDI acceptor,⁵⁻⁷ **4-2**, *t*-butyl groups as donors and perylene as acceptor.⁸

A demonstration of chromophore coupling and energy funnelling is dendrimer **4-1** with four perylene monoimide (PMI) donor chromophores on the rim and a terylene diimide (TDI) acceptor chromophore in the core (Scheme 53).⁵⁻⁷ Energy transfer between the chromophores and donor-acceptor bleaching could be observed in the emission spectra of **4-1**. An earlier example of a dendritic donor-acceptor system is **4-2**, introduced by MOORE and coworkers,⁸ where the conjugated dendrimer backbone provided an excellent through-bond energy transfer (Scheme 53). Recent examples from our group are polyphenylene dendrimers with triphenylamine (TPA) as donor and perylene monoimide (PMI) as acceptor part (Scheme 54).



Scheme 54. Multichromophore systems **4-3**^{9,10} and **4-4**¹¹ based on perylene monoimide (PMI) and triphenylamine (TPA).

Upon excitation of **4-3** at the absorption wavelength of the TPA donor, a fast charge separation was observed indicating efficient electron transfer.^{9,10} Furthermore, a thermally activated back reaction occurred in solution at room temperature. The unique properties of this triphenylamine perylene donor-acceptor systems allowed the photophysical investigation of **4-3** even on the single molecule level.⁹ Contrary to **4-3** with its one donor – one acceptor array, **4-4** possesses multiple TPA moieties arranged around the perylene diimide chromophore core.¹¹ The influence of molecular oxygen and the motion of the surrounding polymer matrix on the optical properties of **4-4** could be demonstrated.¹²

Single molecule spectroscopy has attracted much attention throughout the last ten years including a large number of different classes from simple dye molecules to fluorescent proteins investigated so far.¹³⁻¹⁶ Normally, spectroscopic measurements yield results, that are rendered over an ensemble of molecules. Contrary, single molecule spectroscopy allows to discover the whole range of photophysical properties, such as fluorescence intensity, fluorescence lifetime etc. on just one molecule. Single molecule spectroscopy offers some more advantages. For inhomogeneous systems, ensemble measurements can only give a mean value of a quantity without being able to provide the distribution of a molecular property. With single molecule spectroscopy, these distributions can be determined.

Therefore, single molecules studies with biological systems provided new insights into e.g. the dynamics of protein folding processes. One problem in single molecule spectroscopy is that due to repetitive excitations by a laser beam photoinduced artefacts of the investigated molecules are created. This “photo-bleaching” process therefore often hampers to record the behavior of a single molecule over long periods of time. Perylene chromophores are in this respect ideally suited for single molecule spectroscopy, since because of their high photochemical stability, trajectories on the minute timescale can be recorded. In most cases, the molecules to be investigated are immersed in a polymer matrix from which thin films on quartz substrates are prepared. From this follows another problem in single molecule spectroscopy, which is that the polymer matrix strongly influences the optical properties of

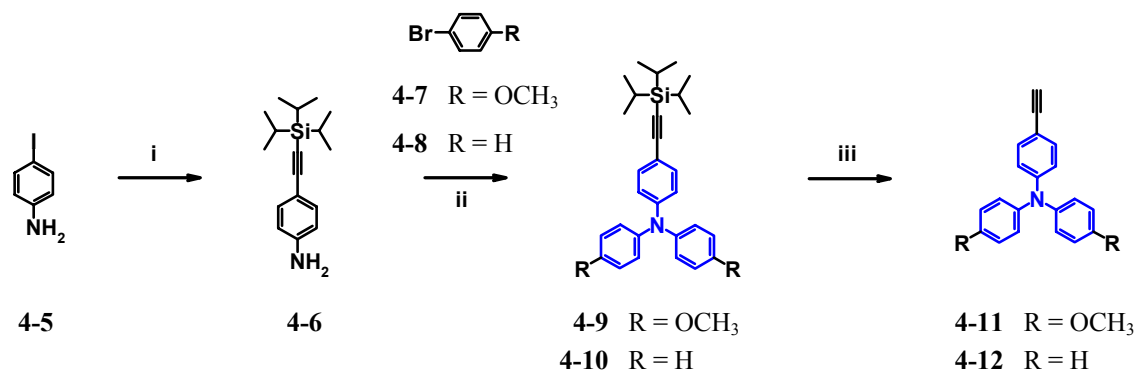
the embedded molecules. The motion of the polymer chains can affect “off” periods, periods in which no photon can be detected during the emission of a single molecule that undergoes electron transfer.¹⁷ Furthermore, the multiple nano-environments present in the polymer matrix can limit detailed spectroscopic investigations.¹⁸

To overcome the above mentioned problems the herein presented approach is directed towards the synthesis of electron-transfer systems which can be studied at the single molecule level without being embedded in a disturbing polymer matrix. To attach the single molecules in defined positions on a quartz substrate, they were thought to be fixed making use of non-covalent bonding motifs. Carboxy groups are used as the anchor functions as they can be linked to unmodified silicon hydroxide as well as to a modified quartz substrate possessing positively charged ammonium groups. In the last case, the strong counter ion attraction should even enforce the surface binding properties. As pointed above, the photophysical properties of other TPA-PMI electron transfer systems have already been well investigated in cooperation with Prof. De SCHRYVER, Katholieke Universiteit Leuven (Belgium). In the approach described herein, a single donor and single acceptor array are used as this represents the most simple donor-acceptor system which should simplify the study of relationships between molecular structure and optical properties. Before attaching the dendrimers on the surface, the photophysical properties of suitable model compounds will have to be investigated in solution and at the single molecule level.

4.2 Synthesis

4.2.1 Synthesis of the TPA Cores

Substituted triphenylamines (TPAs) can be obtained in good yield from the BUCHWALD cross-coupling reaction of an aniline derivative with substituted bromo benzenes.^{19,20} The synthesis of the amine derivative 4-(*triisopropylsilyl*-ethynyl)-aniline (**4-6**) was accomplished by HAGIHARA-SONOGASHIRA coupling of 4-iodo-aniline (**4-5**) with (*triisopropylsilyl*)-ethyne (Scheme 55).²¹



Scheme 55. Synthesis of the TPA dendrimer cores **4-11** and **4-12**. i) (*triisopropylsilyl*)-ethyne, [Pd(OAc)₂], PPh₃, CuI, toluene/TEA, 96%; ii) 3 eq. **4-7/4-8**, Pd₂dba₃, sodium *t*-butoxide, tri-*t*-butylphosphine, toluene, 80 °C, 73% (**4-9**), 99% (**4-10**); iii) TBAF, THF, 95% (**4-11**), 88% (**4-12**).

Subsequent BUCHWALD reaction of **4-6** with 4-bromo-anisol (**4-7**) using the catalyst/ligand system palladium dibenzoyl acetone/tri-*t*-butylphosphine gave bis-(4-methoxy-phenyl)-{4-[(triisopropylsilyl)-ethynyl]-phenyl}-amine (**4-9**) in 73% yield as a brown oil. Cleavage of the TIPS protecting groups furnished the ethynyl group functionalized core (4-ethynyl-phenyl)-bis-(4-methoxy-phenyl)-amine (**4-11**) in an overall yield of 90 %, ready for the synthesis of polyphenylene dendrimers using the DIELS-ALDER cycloaddition.

Ethers are electron-donating groups. Therefore, when combined with an electron acceptor the TPA core **4-11** should be a better electron donor compared to unsubstituted TPA. To vary the electron donor capacity of the TPA moiety, the core (4-ethynyl-phenyl)diphenyl-amine) **4-12** was synthesized (Scheme 55). As **4-12** possesses hydrogen atoms instead of methoxy groups, its electron donating power should be reduced compared to **4-11**. The TIPS protected precursor **4-10** was obtained by the BUCHWALD reaction of 4-(triisopropylsilyl-ethynyl)-aniline (**4-6**) with bromobenzene (**4-8**). Subsequent deprotection of the TIPS protecting group yielded the desired product **4-12**.

Purity of TPA cores **4-11** and **4-12** was checked by mass spectrometry as well as by NMR spectroscopy. Figure 55 shows the FD mass spectrum of the TPA cores **4-11** and **4-12**.

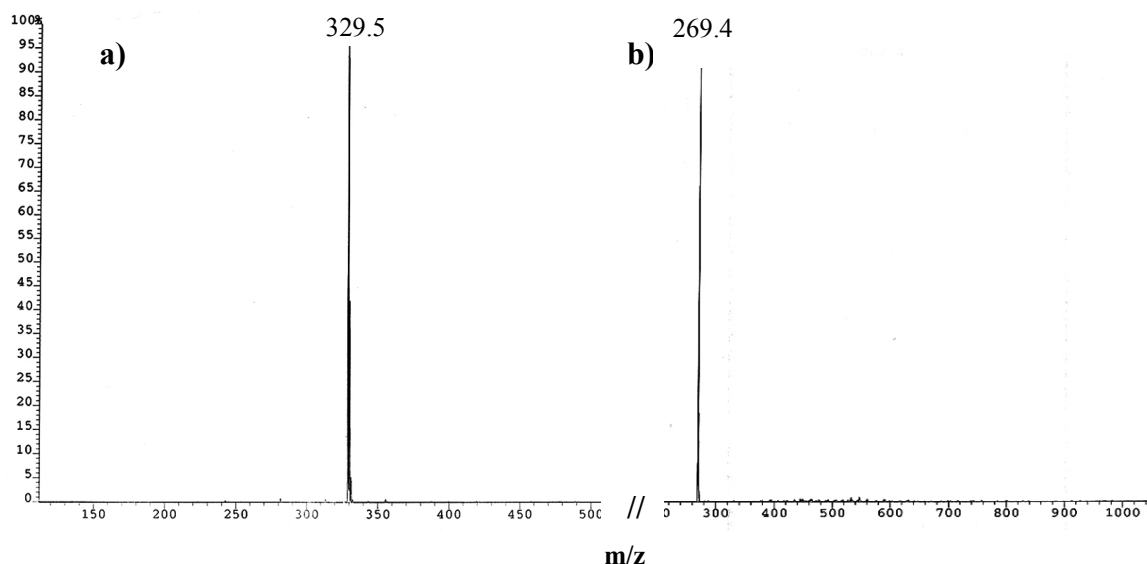


Figure 55. FD mass spectrum of the TPA cores a) **4-11** and b) **4-12** (calculated mass: **4-11**: 329.4 g·mol⁻¹, **4-12**: 269.4 g·mol⁻¹).

Exclusive mass signals at the expected molecular weight indicated a quantitative cleavage of the TIPS protecting groups and purity of the products. Figure 56 shows the ¹H NMR of the core **4-11**. The aromatic protons H_b - H_c of the TPA unit displayed doublet signal patterns between δ = 7.26 and 6.75 ppm. At δ = 3.78 ppm the protons of the methoxy groups H_f appeared as a singlet. The ethynyl proton H_a showed a resonance at δ = 3.03 ppm.

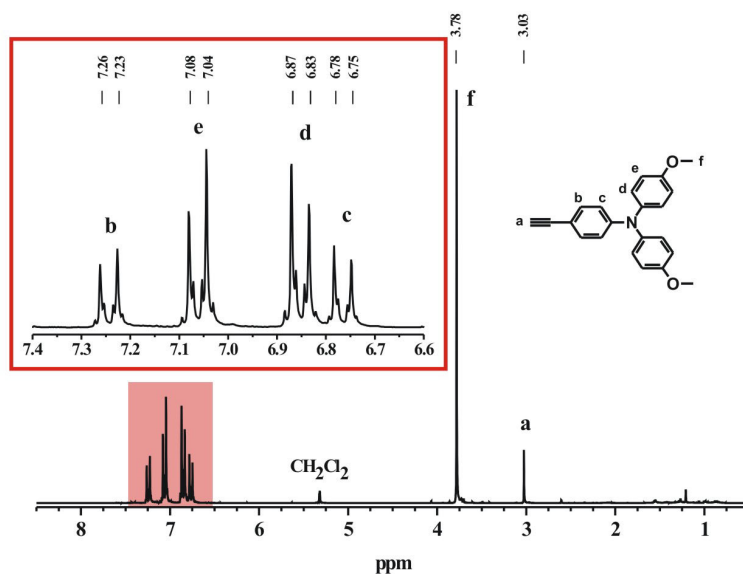
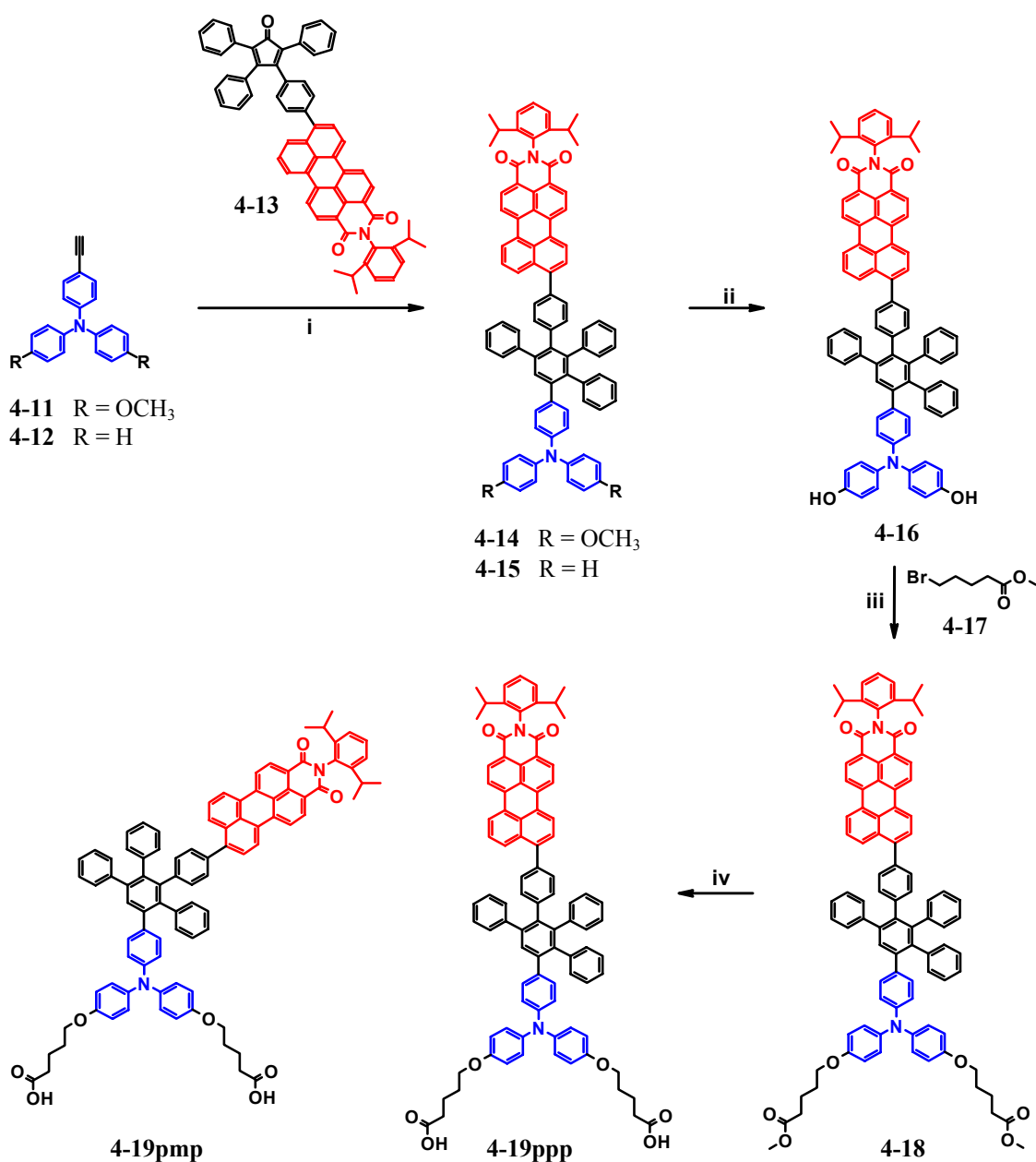


Figure 56. ^1H NMR spectrum of the TPA core **4-11** (250 MHz, CD_2Cl_2 , 300 K).

4.2.2 Synthesis of the Dendrimers

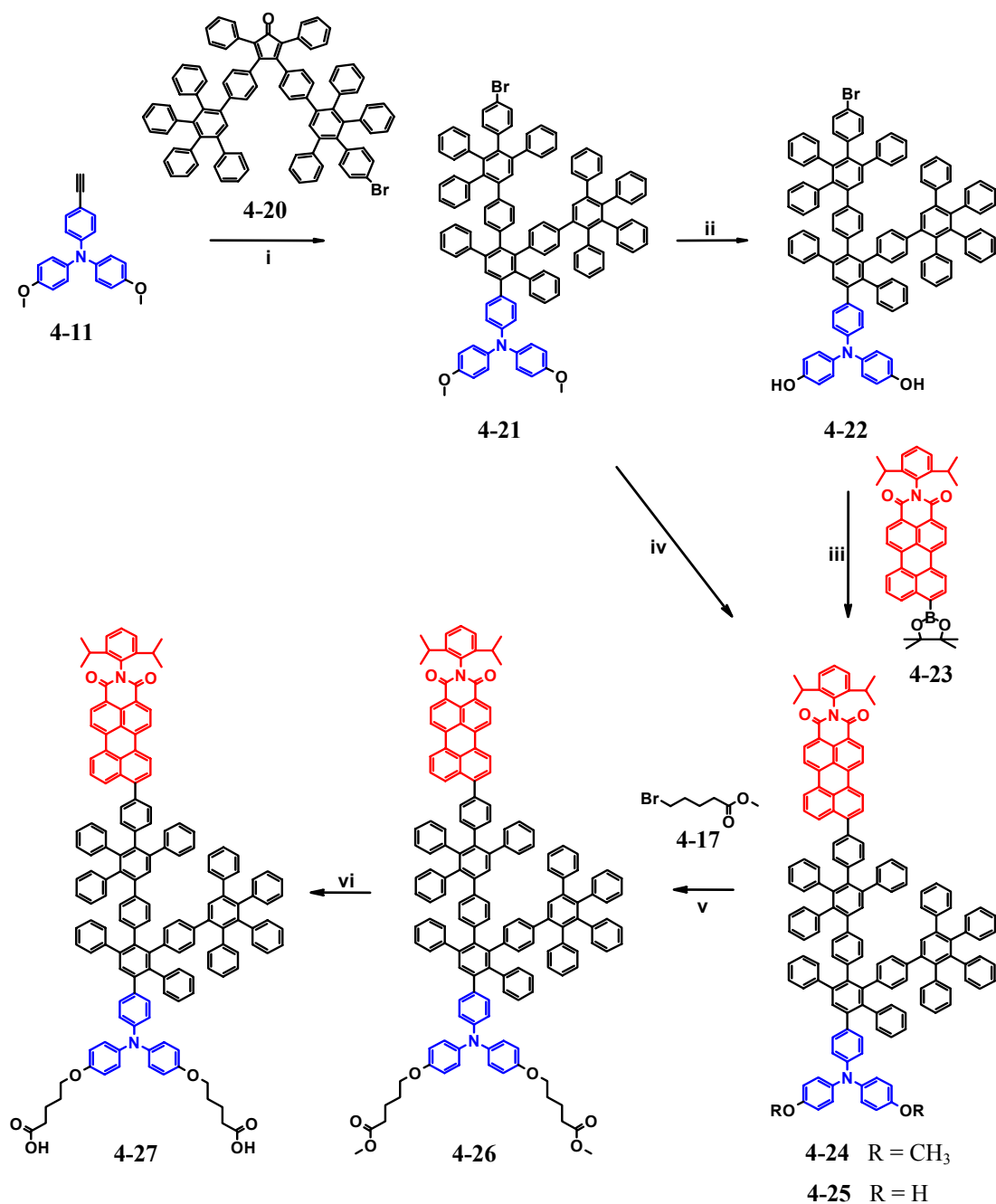
DIELS-ALDER cycloaddition of the ethynyl substituted TPA core **4-11** with the perylene monoimide (PMI) functionalized tetraphenylcyclopentadienone **4-13** in refluxing *o*-xylene gave the desymetrized first-generation dendrimer **4-14** in 90% yield as a red solid (Scheme 56). During the DIELS-ALDER cycloaddition step two isomers are formed (compare also Scheme 58). Consequently, all following products represent an isomeric mixture. For example, the two product isomers are depicted in Scheme 56, denoted as **4-19pmp** and **4-19ppp**. The reason for this denotation and the influence of this isomerism on the photophysical behavior of the TPA-PMI dendrimers as well as the visualization of the two isomers is presented in chapter 4.3 in detail. The building block **4-13** was firstly introduced by T. WEIL allowing the introduction of a perylene chromophore on the dendrimer surface in the last step of the dendrimer synthesis.^{22,23} The next step in the synthesis of **4-19** was the demethylation of the methoxy groups in order to get the hydroxy derivative **4-16**, suitable for the attachment of α -bromo alkyl chains using WILLIAMSON ether synthesis. In literature the demethylation of methoxy group bearing TPA moieties is described using $\text{BBr}_3 \cdot \text{S}(\text{CH}_3)_2$ under reflux in dichloro ethane.²⁴ With substrate **4-14**, even after short reaction time, mono- and dibrominated products were found in the FD mass spectra of the reaction mixtures. Unfortunately, the sideproducts could not be separated by column chromatography. Further experiments with BBr_3 at -78°C showed no bromination. Following this method the hydroxy substituted TPA dendrimer **4-16** could be obtained in good yield. Subsequent base-catalyzed reaction with bromovalerianacid methylester (**4-17**) for four days gave dendrimer **4-18** (Scheme 56). Base promoted hydrolysis of the ester groups was achieved using sodium hydroxide (NaOH). After purification by column chromatography the first-generation TPA-PMI dendrimer **4-19** with carboxy anchor groups could be obtained as a red solid in a high overall yield of 44%.



Scheme 56. Synthesis of the first-generation TPA dendrimers **4-14**, **4-15**, and **4-19**. i) *o*-xylene, 160 °C, 90% (**4-14**), 49% (**4-15**); ii) **4-14**, BBr₃, CH₂Cl₂, 66%; iii) 4.4 eq. **4-17**, K₂CO₃, acetone, 60 °C, 85%; iv) NaOH, MeOH, THF, 88%.

To study the influence of the donor capacity on the electron transfer process the model compound **4-15** without attached methoxy groups was synthesized. Following the above presented synthetic concept presented above (Scheme 56), the TPA core **4-12** was reacted with the PMI functionalized cyclopentadienone **4-13** to yield the desired product **4-15**.

As described in chapter 2.5.1 the distance between donor and acceptor strongly influences the electron transfer efficiency. To test this distance dependence for the TPA-PMI donor-acceptor system, the second-generation dendrimer **4-27** was synthesized as well (Scheme 57). It provides a larger donor-acceptor distance thus electron transfer efficiency should be reduced compared to the first-generation dendrimer **4-19**. The synthesis of **4-27** followed in principle the same route as for the first-generation dendrimer **4-19**.



Scheme 57. Synthesis of dendrimers **4-24** and **4-27**. i) 1.5 eq. **4-20**, *o*-xylene, 160 °C, 97%; ii) BBr₃, CH₂Cl₂, 66%; iii) 2 eq. **4-23**, Pd(PPh₃)₄, K₂CO₃, toluene, ethanol, H₂O, 80 °C, 44%; iv) 2 eq. **4-23**, Pd(PPh₃)₄, K₂CO₃, toluene, ethanol, H₂O, 80 °C, 44% v) **4-25**, 5 eq. **4-17**, acetone, DMF, 60 °C, 80%; vi) NaOH, MeOH, THF, 76%.

The only difference is that the first step was the DIELS-ALDER cycloaddition of the core **4-11** with mono-bromo dendron **4-20**. This building block has been used before in the convergent synthesis of polyphenylene dendrimers.²² In combination with a partially activated core, it allowed the synthesis of second-generation polyphenylene dendrimers carrying only a single functional group on their surface (see also chapter 1.3.2).²² Similarly, the second-generation dendrimer **4-21** could be constructed in only one step. Further functionalization of the dendrimer surface was ensured by the single bromo function (Scheme 57). Subsequent cleavage of the methoxy groups using BBr₃ gave **4-22** in good yield.

In the next step the perylene monoimide moiety was introduced by the Suzuki cross-coupling reaction of **4-22** with the boronic ester functionalized PMI derivative **4-23**. The introduction of a PMI moiety via SUZUKI cross-coupling showed to be a powerful tool not only for the synthesis of PMI functionalized building blocks like **4-13**. A second-generation triphenylamine dendrimer functionalized with a single PMI (e.g. **4-24**) would also be available by the DIELS-ALDER cycloaddition of the core **4-11** with a PMI functionalized dendron. However, the following synthetic steps were carried out parallel to the before mentioned synthesis of the first-generation TPA-PMI dendrimer **4-19**. In the end the acid group carrying second-generation TPA-PMI dendrimer **4-27** was obtained in an overall yield of 17%. The yield is significantly lower than for the first-generation dendrimer **4-19**, mainly due to the fact that the PMI moiety in **4-27** was introduced via a SUZUKI cross-coupling reaction (44% yield) and not via a DIELS-ALDER reaction as for **4-19** (90% yield). As already pointed out for the first-generation dendrimer **4-19**, also **4-27** exists as an isomeric mixture. This point is discussed in chapter 4.3 in detail considering dendrimer **4-14** as example.

Before attaching the acid functionalized dendrimers **4-19** and **4-27** on a surface suitable for single molecule spectroscopy, the photophysical properties of TPA-PMI dendrimers with additionally attached donating groups were planned to be investigated in solution. As suitable model compound for the first-generation dendrimer **4-19** we chose the methoxy substituted precursor **4-14**. The electronic properties of the TPA core were expected to be relatively invariant towards extending the alkyl chains of the donating ether groups. Accordingly, as model compound for the second-generation dendrimer **4-27**, the methoxy group substituted dendrimer **4-24** was synthesized. For that, **4-21** was reacted with the boronic ester functionalized PMI derivative **4-23** in a SUZUKI cross-coupling reaction to give model compound **4-24**. Characterization of the acid functionalized TPA-PMI dendrimers was accomplished using NMR spectroscopy and mass spectrometry.

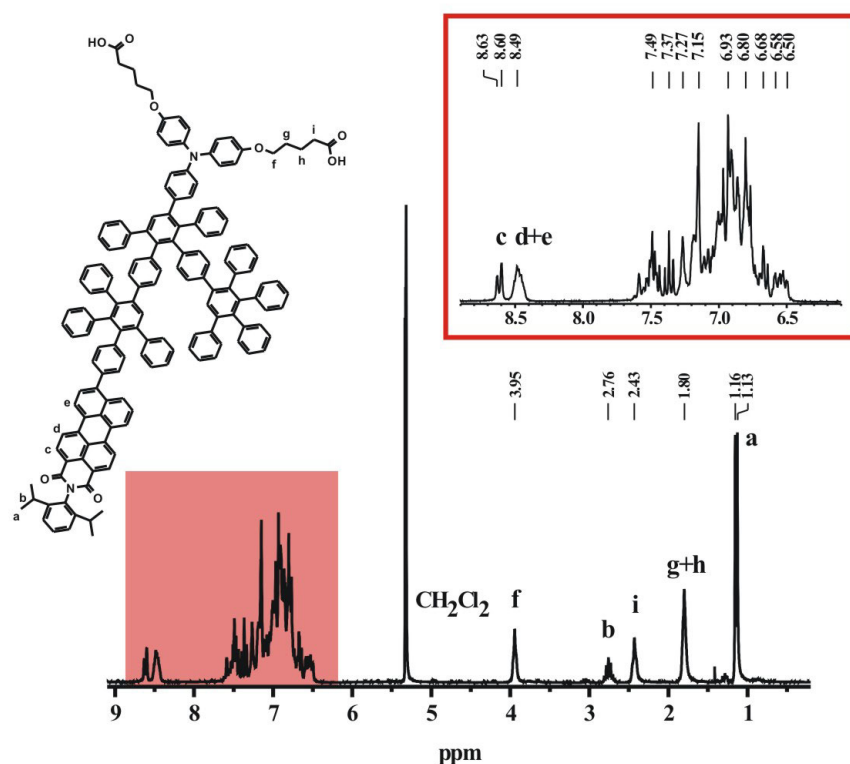


Figure 57. ^1H NMR spectrum of **4-27** (250 MHz, CD_2Cl_2 , 300 K).

Figure 57 shows as example the ^1H NMR spectrum of the second-generation dendrimer **4-27**. In the aliphatic region the protons of the isopropyl groups on the perylene moiety (H_a and H_b) appeared at $\delta = 1.13$ ppm and $\delta = 2.76$ ppm, respectively. The protons of the alkyl chains H_f - H_i showed up between $\delta = 3.95$ ppm and $\delta = 1.80$ ppm. At high field ($\delta = 8.63$ - 8.49 ppm) resonances of the aromatic protons H_c - H_e of the perylene unit could be observed. Further assignments were not possible due to overlapped signals of the aromatic protons of the dendrimer backbone.

The MALDI-TOF mass spectrum of **4-27** is displayed in Figure 58. A mass signal with a high intensity appeared at a molecular mass of $2099 \text{ g}\cdot\text{mol}^{-1}$, perfectly agreeing with the calculated mass of **4-27**. At a molecular mass of $2136 \text{ g}\cdot\text{mol}^{-1}$ the corresponding cluster with potassium $(\text{M}+\text{K})^+$ showed up. Another small signal at $2009 \text{ g}\cdot\text{mol}^{-1}$ can be attributed to a missing alkyl chain. Since ^1H and ^{13}C NMR spectroscopy did not show a reasonable amount of this possible side product, it is likely to say that fragmentation occurred during the mass measurement. Furthermore, desorption of molecules in MALDI-TOF mass spectrometry is strongly dependent on the applied laser power. A very minor content of a side product can give an intense mass signal, when it possesses a higher desorption rate than the major product. Thus, no quantitative information can in general be extracted from a MALDI-TOF spectrum.

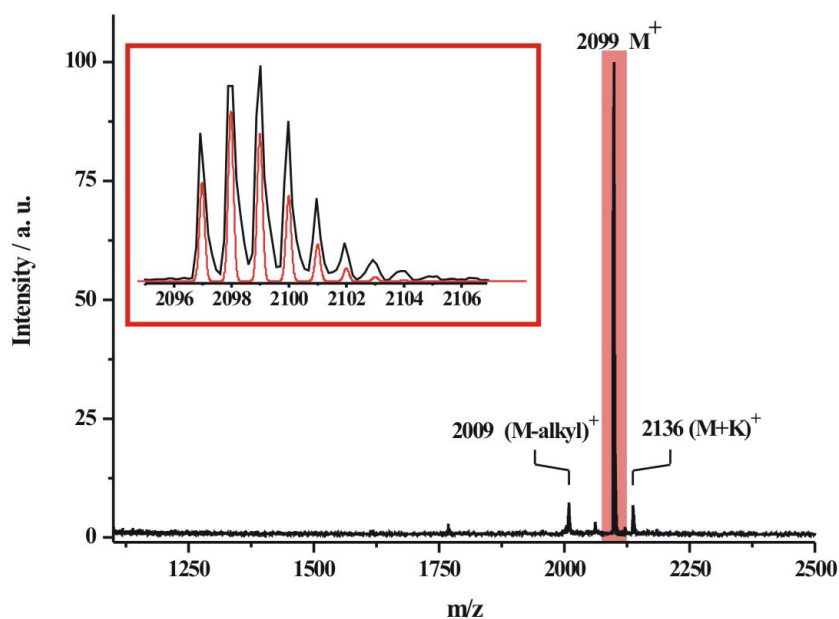


Figure 58. MALDI-TOF mass spectrum of **4-27** (calculated mass: $2099 \text{ g}\cdot\text{mol}^{-1}$; matrix: dithranol). Inset: isotopically resolved mass spectra, experimental (black) and calculated (red).

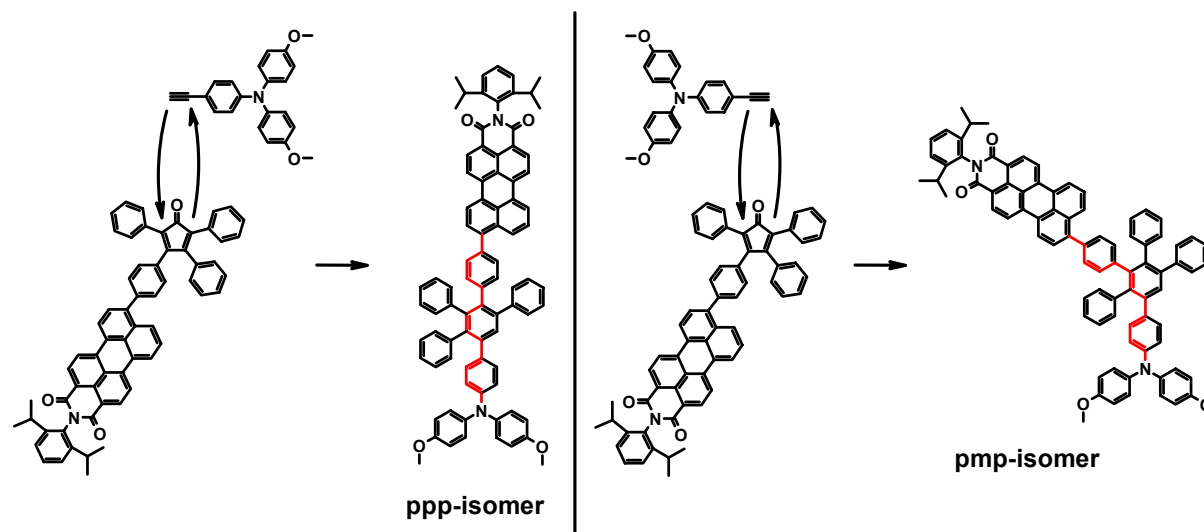
However, an eventually small amount of dendrimers, carrying only one acid functionalized alkyl chain should not have a significant influence on the surface binding properties. The inset in Figure 58 shows the isotopically resolved mass signal of **4-27** at $2099 \text{ g}\cdot\text{mol}^{-1}$ (black line). The signal pattern matches perfectly with the curve derived from calculation (red line), further proving the purity of dendrimer **4-27**.

4.3 Visualization and Simulation

The DIELS-ALDER cycloaddition of a PMI substituted tetraphenylcyclopentadienone with a terminal ethynyl bond leads to two constitutional isomers of **4-14** (Scheme 58). Separation of the two isomers of **4-14** was tried using chiral High-Performance-Liquid-chromatography

(HPLC) on a chiral column. The investigation of the individual photophysical properties of the separated isomers should give new information of how the spatial orientation of donor and acceptor influences the electron transfer properties. Two peaks with a slight different elution time displayed in the HPLC spectrum, however, no base line separation could be achieved.

One differentiates between the ppp (para-para-para) isomer and the pmp (para-meta-para) isomer. Para-para-para means that the three phenyl rings between the nitrogen of the TPA unit and the perylene moiety are linked via their para-positions (red line in Scheme 58).



Scheme 58. Constitutional isomers of the first-generation dendrimer **4-14**. Red: through-bond distance between donor (TPA) and acceptor (PMI).

In the para-meta-para isomer, the central phenyl ring of the pentaphenyl benzene connects the TPA core and the perylene via a meta link.

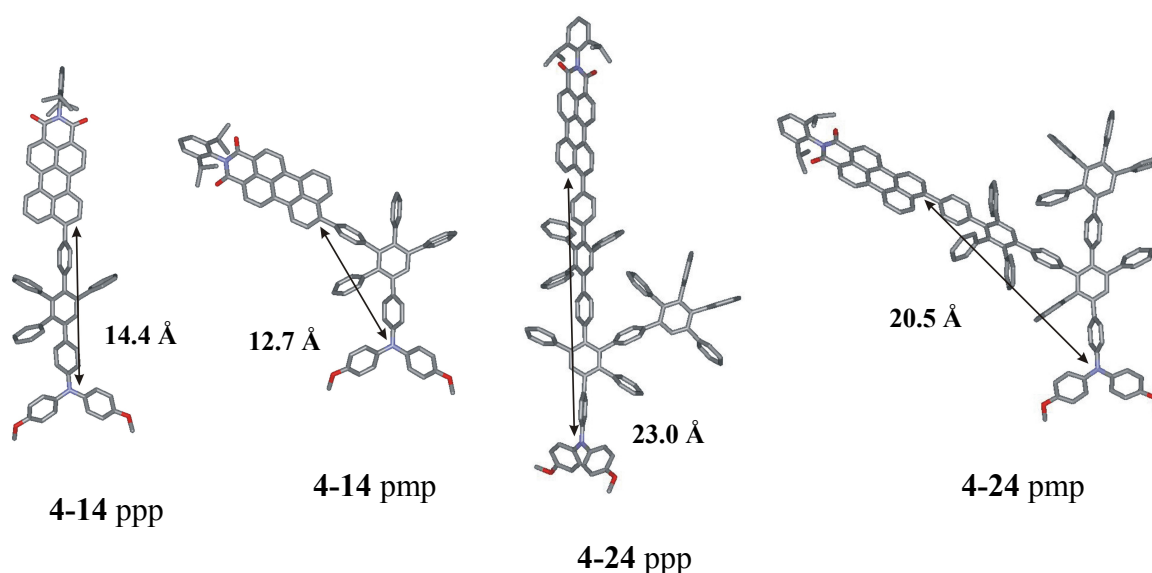
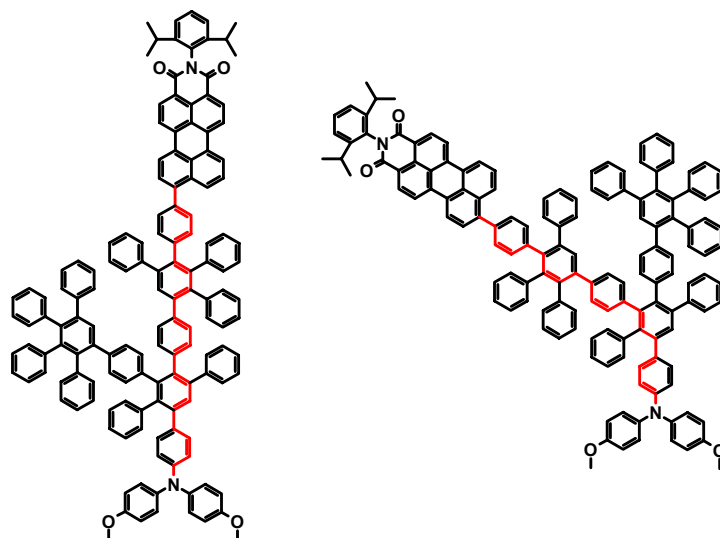


Figure 59. Three-dimensional structures of the ppp and pmp isomers of the first-generation dendrimer **4-14** and the second-generation dendrimer **4-24** (nitrogen: blue, oxygen: red). Distances were measured between the nitrogen of the TPA and the first carbon of the PMI moiety.

The isomers of **4-14** are characterized by different through-space distances (ppp isomer: 14.4 Å, pmp isomer: 12.7 Å) and different through-bond distances (ppp isomer: 13 bonds, pmp isomer: 12 bonds). The through-space distances were estimated from the three-dimensional structures of the two isomers, obtained by molecular modeling (blue and red cross, Figure 59).



Scheme 59. Constitutional isomers of the second-generation dendrimer **4-24**. Red: through bond distance between donor (TPA) and acceptor (PMI).

For the two constitutional isomers of the second-generation dendrimer **4-24**, through-space distances of 23.0 Å (ppp isomer) and 20.5 Å (pmp isomer) were found (blue and red cross, Figure 59). Like for the first-generation dendrimer **4-14**, the through-bond distances for the second-generation dendrimer **4-24** differ with one bond between the ppp isomer (21 bonds) and the pmp isomer (20 bonds) (Scheme 59).

4.4 Photophysical Investigations

The photophysical properties of the herein synthesized TPA-PMI dendrimers are currently investigated in close cooperation with the group of Prof. De SCHRYVER, Katholieke Universiteit Leuven (Belgium). The results obtained up to now are presented in the following chapters.

4.4.1 Ensemble Measurements

Steady state UV/vis measurements of the first- and second-generation dendrimers were performed. Figure 60a shows the absorption and emission spectra of the acid functionalized dendrimers **4-19** and **4-27** in CHCl_3 . The strong absorption at ≈ 504 and 524 nm can be attributed to the absorption of the PMI moiety, bathochromically shifted as compared to unsubstituted PMI (≈ 485 and 507 nm), which is due to the enlarged π -system induced by attaching a polyphenylene dendron to the chromophore moiety. The shoulder at ≈ 330 nm displays the absorption of the TPA core. The intense absorption at short wavelengths (≈ 260 nm) belongs to the absorption of the polyphenylene dendrons.²⁵ Accordingly, the intensity of this band is strongly increased for **4-27**, possessing the larger polyphenylene dendron as compared to **4-19**.

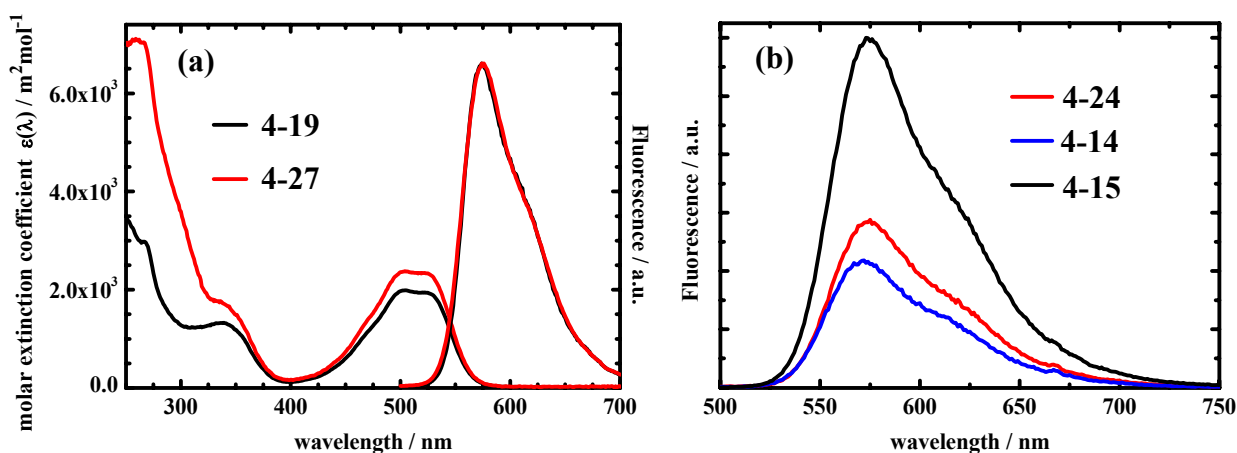


Figure 60. a) Absorption and emission spectra of **4-19** and **4-27** in CHCl_3 , Excitation: 334 nm. b) Emission spectra of dendrimer **4-14**, **4-15**, and **4-24** in CHCl_3 . Excitation: 334 nm. The emission spectra are normalized to the absorption at the excitation wavelength of the TPA (334 nm).

The emission spectra of **4-19** and **4-27** were recorded after excitation at the absorption maximum of the TPA core (334 nm) and displayed a single band with its maximum at 567 nm, almost not shifted as compared to unsubstituted perylene (544 and 579 nm).

In the framework of the FÖRSTER equation (chapter 2.5.1, eq. 1 and 2), electron transfer efficiency is decreasing with larger distance between donor and acceptor. To investigate this, the second-generation dendrimer **4-27** has been synthesized. Experiments included absorption and emission spectra of model compounds **4-24** and **4-14**. Figure 60b displays the fluorescence spectrum of **4-24**, when excited at the wavelength of the TPA core (334 nm). As compared to **4-14**, the fluorescence intensity of **4-24** was slightly increased. This can be explained from the kinetic model shown in Scheme 60, which was developed from these measurements and based on further experiments described later. Applying that model, the large distance between the TPA donor and the PMI acceptor in **4-24** leads to a smaller forward electron transfer constant and a decreased efficiency of the charge-separation process from the locally excited state (LE) to the charge separated state (CS). This makes direct fluorescence from the LE state the favored emission process. Contrary, in the case of **4-14**, the smaller distance between TPA and PMI led to an increased forward charge transfer. As a result, delayed fluorescence by reverse electron transfer and, in this case more important, nonradiative charge recombination to the ground state (GS) were observed. In summary, the fluorescence intensity of **4-14** is significantly decreased as compared to **4-24**.

Another object of interest was how the varying donor capacity of the TPA core influences the fluorescence behavior of the dendrimers. As part of the Förster-equation (chapter 2.5.1, eq. 1 and 2), the spectral overlap J of the donor emission spectrum and the acceptor absorption spectrum influences the electron transfer efficiency. To test this for the differently substituted TPA cores, absorption and emission spectra of the TPA cores **4-11** and **4-12** were recorded (Excitation: 334 nm) and correlated with the absorption profile of the according dendrimers **4-14** and **4-15**, respectively. Figure 61a/b show the resulting overlapped spectra. The TPA core **4-12** without methoxy groups has an emission maximum at 416 nm, the TPA core **4-11** with methoxy groups attached has its absorption maximum at 474 nm. This is a bathochromic shift of almost 60 nm, induced by the introduction of the electron-donating methoxy groups. As a result, the spectral overlap of the emission spectrum of the TPA core

4-11 and the absorption spectrum of **4-14** is almost three times bigger than the spectral overlap in the case of dendrimer **4-15** constructed from the core **4-12**. An increased charge transfer efficiency can therefore be suggested for the first-generation dendrimer **4-14** with methoxy groups attached to the donor. A proof for this was derived from the emission spectra of the differently substituted dendrimers **4-14** and **4-15**, recorded after excitation at 334 nm (Figure 60b). The emission maximum of **4-15** (573 nm) is bathochromically shifted by only 2 nm compared to **4-14** (571 nm). On the other side, the fluorescence intensity (integrated emission spectrum) of **4-15** is almost three times higher as compared to **4-14**.

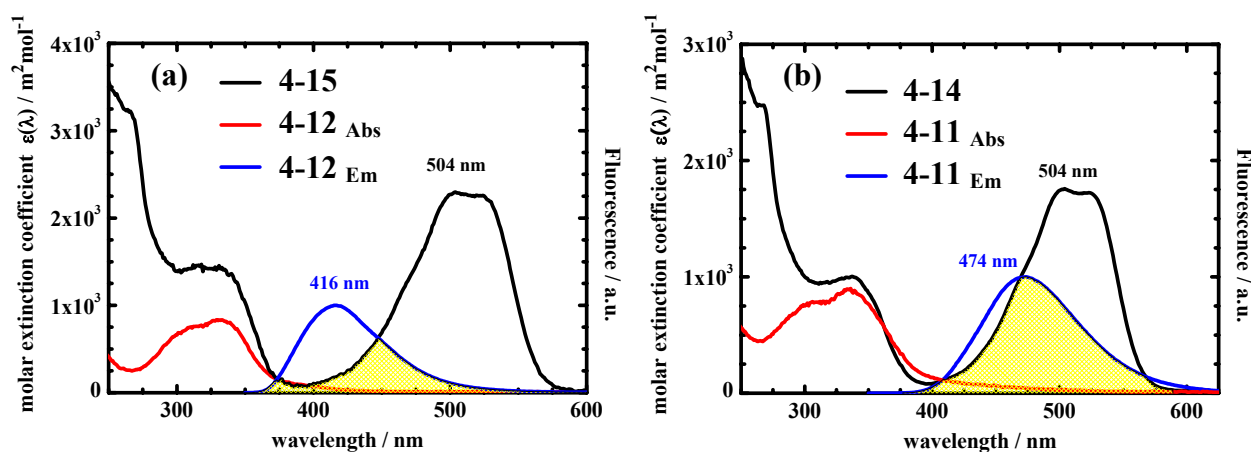


Figure 61. a) Absorption and emission spectra of the TPA core **4-12** and absorption spectrum of **4-15** in CHCl_3 , b) Absorption and emission spectra of the TPA core **4-11** and absorption spectrum of **4-14** in CHCl_3 . The fluorescence spectra are normalized to the absorption at the excitation wavelength (334 nm).

Almost similar to the above described effect for varying the donor-acceptor distance, this different fluorescence behavior can be explained from the kinetic model shown in Scheme 60. The high fluorescence intensity found for **4-15** is then due to a low efficiency of the forward electron transfer process, leading to more fluorescence from the LE state for **4-15** as compared to **4-14**. The donating power of the methoxy groups is obviously the reason for the significantly decreased fluorescence intensity of **4-14**.

Since the CS state is expected to be stabilized by more polar solvents, a further point of interest was how the polarity of the solvent influences the electron transfer properties. Therefore, absorption and emission spectra of **4-14** in solvents of different polarity were recorded. (Figure 62). In MCH, the absorption spectrum displayed maxima at 486 and 514 nm red-shifted compared to the absorption maxima of unsubstituted PMI similarly to the spectra obtained from CHCl_3 solution. The emission spectrum of **4-14** in MCH showed maxima at 540 and 579 nm. Upon changing from MCH as solvent to the more polar toluene, the emission maximum displayed a bathochromic shift of 18 nm. Furthermore, with increasing solvent polarity, the fluorescence quantum yield dropped from 0.96 in MCH to 0.90 for toluene and 0.05 in DEE (Table 8), indicating an efficient quenching mechanism in polar solvents. Aerated toluene solution of **4-14** showed a fluorescence quantum yield of 0.78, however, degassing led to the value of 0.90. This behavior has earlier been observed for triphenylamine dendrimers like **4-3** and **4-4** (Scheme 54). HOFKENS and DESCHRYVER et al. found that increased oxygen concentration resulted in slowed decay of the CS state to the LE state by enhancing intersystem crossing to the triplet charge separated state (compare also Scheme 60).¹² Deactivation therefore happens radiationless through charge recombination to

the GS state thereby lowering the fluorescence quantum yield. The same seems to hold true for the herein described dendrimer **4-14**.

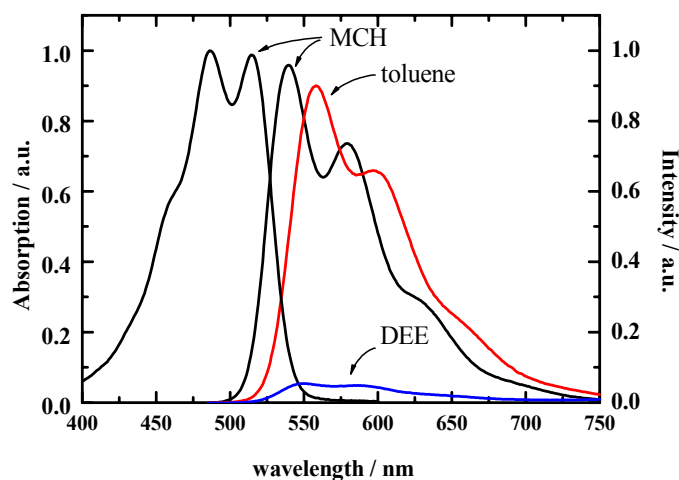


Figure 62. Absorption spectra of **4-14** recorded in methylcyclohexane (MCH) and corrected fluorescence spectra of **4-14** recorded in cyclohexane, toluene and diethylether (DEE). Excitation wavelength: 470 nm. The absorption and fluorescence intensities have been normalized to 1.0 at their respective maxima, and the emission spectra then scaled according to the fluorescence quantum yield of **4-14** in the according solvent.

To further investigate the photophysics of **4-14**, the fluorescence decays were determined using time-correlated single photon counting (TCSPC) measurements. Complex results were obtained, due to the presence of the ppp and pmp isomers (Table 8).

Table 8. Ensemble fluorescence data of **4-14**: solvent polarizability (ϵ_r), fluorescence quantum yield (Φ_{flu}), decay times (τ_{flu}) and electron transfer rate constants (k_{fwd} and k_{rev}). Excitation wavelength: 485 nm.

Solvent	ϵ_r	Φ_{flu}	$\tau_{\text{flu}} / \text{ns}^*$	$k_{\text{ET}} / \text{s}^{-1}$
MCH	2.0	0.96	4.0 (100%)	-
Toluene	2.4	0.90	0.19 (27%)	$3.0 \cdot 10^9$ (k_{fwd})
			10.1 (18%)	$2.2 \cdot 10^9$ (k_{rev})
			4.2 (55%)	-
DEE	4.3	0.05	0.03 (39%)	$3.5 \cdot 10^{10}$ (k_{fwd})
			0.07 (56%)	$1.5 \cdot 10^{10}$ (k_{rev})

* The values in parentheses give the amount in which the decay time contributes to the fluorescence intensity.

In MCH, a mono-exponential decay with a decay time of 4.0 ns was observed which is in the same time range as found for unsubstituted perylene monoimide (4.2 ns in aerated and 4.7 ns in deoxygenated diethylether). Obviously, both isomers do not undergo electron transfer in MCH. In toluene, a three-exponential decay was necessary to fit the fluorescence decay. The long decay time of 10.1 ns can be attributed to delayed fluorescence, the short decay time of 0.19 ns to the quenched direct fluorescence of the perylene monoimide. Additionally, the third decay time of 4.2 ns belongs to the unquenched fluorescence of

perylene monoimide. The three decay times can be attributed to the presence of the two isomers depicted in Scheme 58. It can be suggested that one of the isomers undergoes photo-induced electron transfer leading to the decay times of 10.1 ns and 0.19 ns, whereas the other isomer seemed to be inactive thus contributing the decay time of 4.2 ns. The amount in which the two isomers contributed to the fluorescence intensity was roughly 1:1 (45% isomer active in electron transfer, 55% isomer inactive) showing that both isomers were present in roughly equal proportions. In the polar solvent DEE, **4-14** exhibited fluorescence decay times of 0.03 and 0.07 ns indicating that both isomers are electron transfer active. This results in an almost completely quenched fluorescence ($\Phi_{\text{flu}} = 0.05$). The observed results are somewhat contrary to the TPA-PMI dendrimer **4-3** (Scheme 54) where a mono-exponential fluorescence decay ($\tau_{\text{flu}} = 4.1$ ns) was found for toluene as solvent. This indicated that no electron transfer occurred for **4-3** in toluene. The fact, that **4-14** on the other side undergoes electron transfer in toluene can be attributed to the better electron donor capacity of the TPA core provided by the additionally attached methoxy groups.

Femtosecond transient absorption measurements were performed in order to investigate the photophysics of **4-14** in toluene more closely. A fast decrease of the absorption band at ≈ 550 nm was displayed which can be attributed to the decrease of the S^1 - S^n absorption band of the perylene chromophore (Figure 63). In the same time-range, a new absorption band appeared at ≈ 650 nm and can be attributed to the radical anion absorption band of perylene monoimide,⁹ proving the occurrence of electron transfer processes. The decay of the absorption band at 650 nm could be described by a multi-exponential function. Global analysis resulted in three kinetic components: a 6 ps, a 180 ps and a nanosecond component. As mentioned above, the nanosecond component can be attributed to delayed fluorescence. The 180 ps component is due to the formation of the PMI radical anion and is in good agreement with the determined fluorescence decay times from the TCSPC experiments (Table 8). The 6 ps component can be attributed to vibrational relaxation of the molecule.

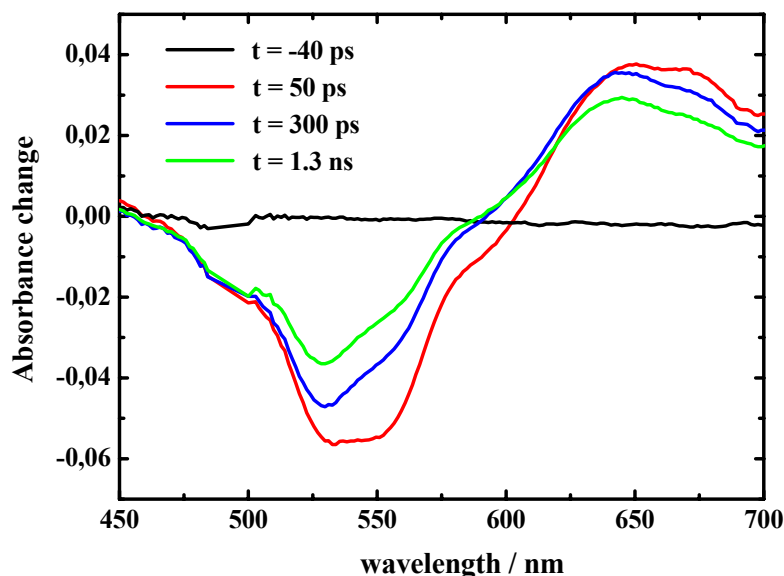
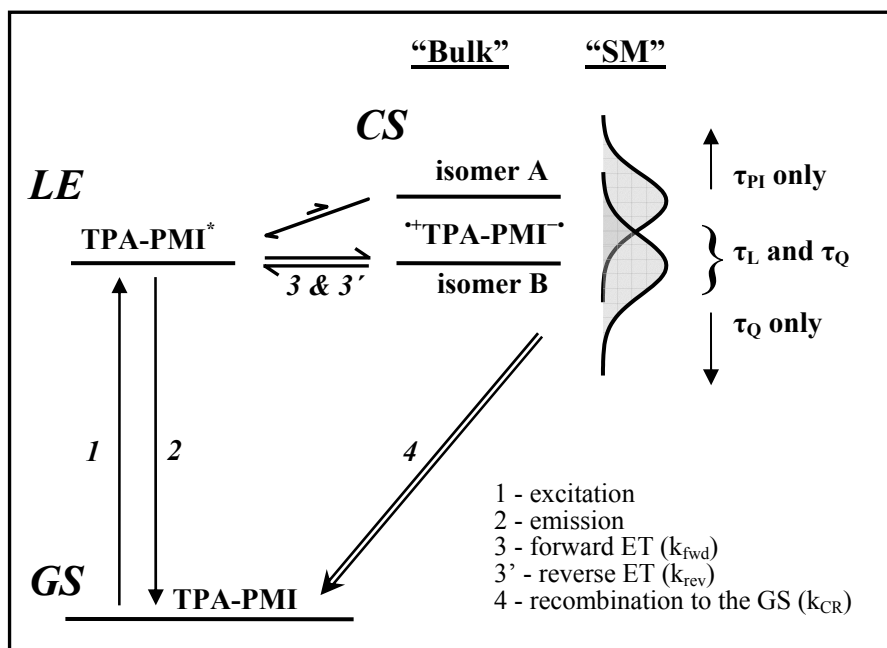


Figure 63. Transient absorption spectra of **4-14** in toluene recorded at discrete time intervals after the arrival of an 80 fs pulse of 488 nm light.

The investigation of the ensemble fluorescence behavior of **4-14** yielded a kinetic model (Scheme 60) with the photophysical behavior in solution displayed under the “bulk” heading.

Excitation of **4-14** results in the population of the locally excited state (LE). Forward electron transfer from the TPA donor to the PMI acceptor leads to the charge separated state (CS). This occurs only for one of the two possible constitutional isomers of **4-14** in a reasonable amount, assigned as isomer B in Scheme 60.



Scheme 60. Scheme of the excited states of the TPA-PMI dendrimer **4-14**. GS: ground state, LE: locally-excited state, CS: charge-separated state. Bulk: Energy levels in solution. SM: Energy levels from single-molecule measurements in a polystyrene film.

The other isomer (isomer A) exhibits an energy level higher than that of the LE, therefore the driving force for the forward electron transfer is lower. Accordingly, the reverse electron transfer from the CS state to the LE level is strongly enhanced for isomer A. Charge recombination can occur in two different ways, by reverse electron transfer to the LE state or by nonradiative recombination to the ground state (GS). At the moment, it is not yet clear which isomer is electron transfer active in toluene and which not. On one hand, the pmp isomer has a greater driving force for electron-transfer, ΔG^0_{CS} (free energy for the charge separation) as it possesses the smaller through-space distance between the two chromophores TPA and PMI (Figure 59). On the other hand, for two chromophores linked by a conjugated backbone, para-links provide an increased through-bond coupling compared to a meta-linked backbone. Therefore, it can be expected that the ppp isomer possesses the more efficient through-bond coupling compared to the pmp isomer.

The rate constants for the forward and reverse electron transfer in **4-14** were calculated using the decay time and pre-exponential factors extracted from the TCSPC fluorescence decay profile.²⁶ For the active isomer of **4-14** in toluene k_{fwd} and k_{rev} are $3.0 \cdot 10^9 \text{ s}^{-1}$ and $2.2 \cdot 10^9 \text{ s}^{-1}$, respectively, yielding a K_{CS} of 1.36 and a ΔG^0_{CS} of $-0.75 \text{ kJ} \cdot \text{mol}^{-1}$. The value of k_{CR} was found to be $2 \cdot 10^6 \text{ s}^{-1}$. This means that charge recombination to the ground state is about a factor of 1000 slower than the electron transfer between the locally excited state (LE) and the charge separated (CS) state (Scheme 60). Thus, emission occurs mainly radiatively from the LE state, resulting in the high fluorescence quantum yield ($\Phi_{flu} = 0.90$) observed for **4-14** in toluene.

Ensemble measurements of the acid functionalized TPA-PMI dendrimer **4-19** yielded results comparable to those described above for the model compound **4-14**. In degassed toluene a three-exponential fit was necessary to describe the fluorescence decay of **4-19**. Decay times of $\tau_1 = 11.1$ ns, $\tau_2 = 4.4$ ns and $\tau_3 = 0.22$ ns were determined. This can again be attributed to the presence of the two constitutional isomers (ppp and pmp) of **4-19** resulting in a delayed (τ_1) and a prompt (τ_3) fluorescence for the electron transfer active isomer as well as fluorescence of the acceptor PMI (τ_2) for the electron transfer inactive isomer. Rate constants were determined to be $k_{\text{fwd}} = 2.8 \cdot 10^9 \text{ s}^{-1}$ and $k_{\text{rev}} = 1.6 \cdot 10^9 \text{ s}^{-1}$. From this K_{CS} was calculated to be 1.36 yielding a ΔG^0_{CS} of $-0.32 \text{ kJ} \cdot \text{mol}^{-1}$ comparable to the methoxy substituted model compound **4-14**.

4.4.2 Single Molecule Spectroscopy

For single molecule spectroscopy **4-14** was immersed in polystyrene with a narrow molecular weight distribution. Polystyrene was chosen as it possesses a polarizability comparable to toluene (ϵ_r toluene: 2.4, ϵ_r polystyrene: ≈ 2.5). Thin films of the resulting solution were prepared by spin-coating on quartz substrates. The studied single molecules showed large variations in their fluorescence behavior. To get a better overview, the molecules were grouped by their decay times. Fluorescence decay times were determined by binning every 5000 photon during the course of the trajectory. Decay times of 4 ± 1 ns were attributed to the fluorescence of the PMI moiety (τ_{PMI}). Decay times of longer than 5 ns (τ_{L}) were considered as delayed fluorescence and decay times of less than 3 ns were considered as quenched fluorescence (τ_{Q}). Additionally, the number of molecules in each class possessing “long-off” times was determined as well. Periods of longer than 20 ms without a detected photon were considered to be “long-off”. Figure 64 displays the result of the grouping process. For further clarification the fluorescence trajectories as well as the according decay times for significant classes of molecules are shown in Figure 65.

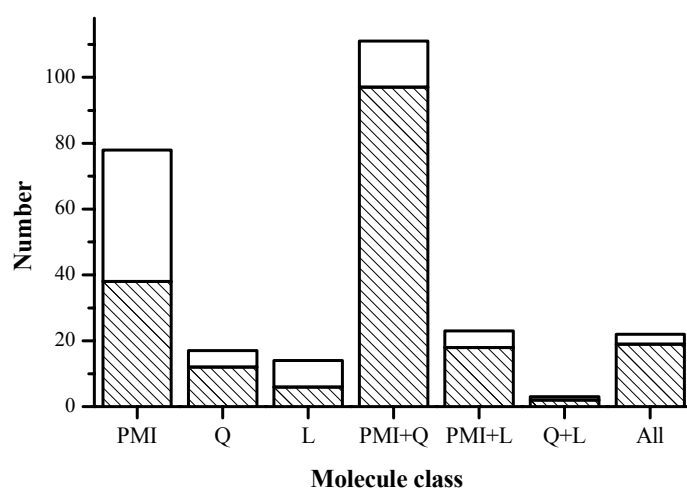


Figure 64. Grouping of molecules of **4-14** investigated at the single molecule level. PMI = $3 \text{ ns} < \tau_{\text{flu}} < 5 \text{ ns}$, Q = $\tau_{\text{flu}} < 3 \text{ ns}$, L = $\tau_{\text{flu}} > 5 \text{ ns}$ as well as combinations of the three. Shaded parts represent number of molecules showing “long-off” times.

Two main groups resulted from the grouping process (Figure 64). One group was the one with “ τ_{PMI} - only” molecules, the other group contained molecules showing quenched decay times, τ_{Q} , as well as periods of τ_{PMI} . Examples of these two major groups are molecule a and b

in Figure 65. A class of molecules showed extended decay times τ_L such as molecule c in Figure 65. Molecule d in Figure 65 is an example for the class of molecules showing all three different kinds of decay times. Only few molecules showed bi-exponential fluorescence kinetics with both decay times τ_{PMI} and τ_Q being present (molecule e).

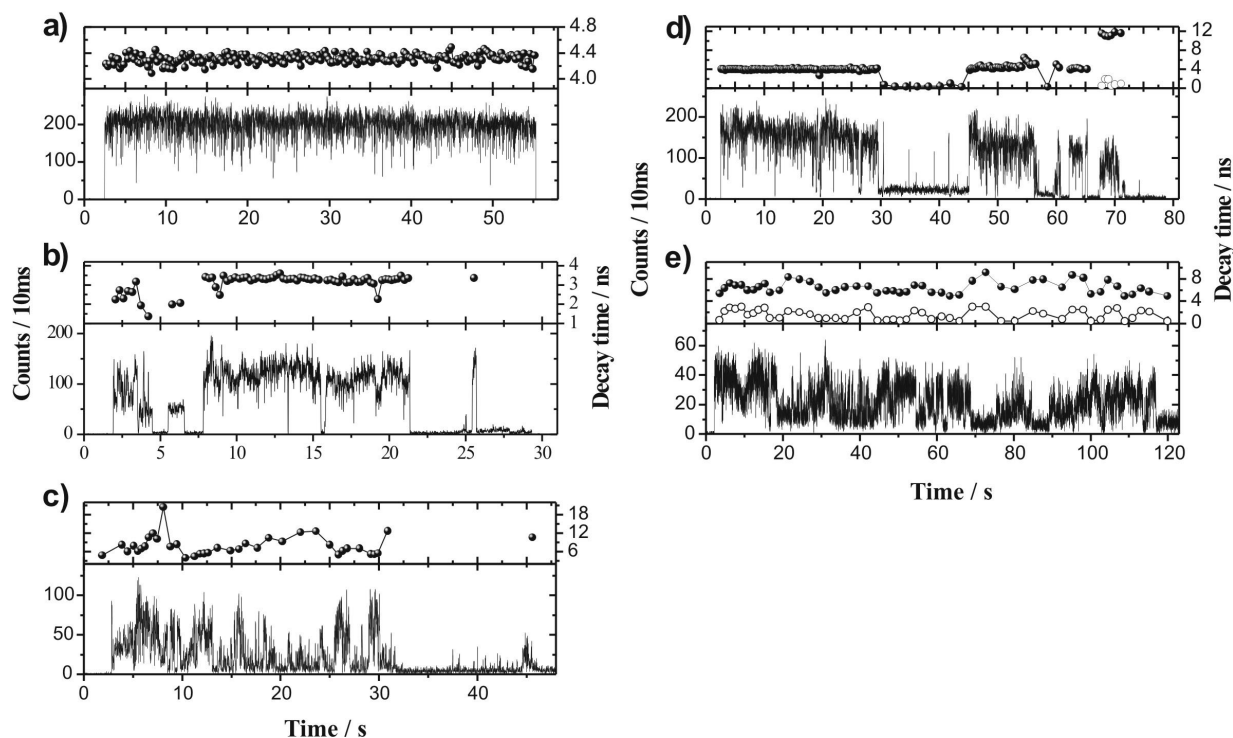


Figure 65. Fluorescence trajectories (lower panels) and decay times (upper panels) for example molecules a - e of **4-14** in a polystyrene film at the single molecule level.

The observation of bi-exponential fluorescence behavior strongly indicates that the electron transfer processes observed in the ensemble measurements are also present at the single molecule level in polystyrene. However, the wide range of fluorescence behaviors at the single molecule level hampered the distinction between the two isomers. Reason for this is the variety of nanoenvironments in the polystyrene film and their influence on the electron transfer processes. Of importance in this respect is also the mobility of the polymer chains in the film, leading to fluctuations in the emission properties of the immersed single molecules. This situation is illustrated by the Gaussian-shaped envelopes in Scheme 60 under the “SM” heading representing the energy values that the charge separated state can possess. Further single molecule studies with **4-14** and other donor-acceptor systems in different polymer films are performed at the moment to learn more about how the physical properties (e.g. polarity) of the polymer matrix influence the electron transfer process at the single molecule level.

Throughout all the grouped classes of molecules a large amount of molecules showed “long-off” times during the single molecule measurements (Figure 64). The presence of so-called “dim” states (partly attenuated fluorescence intensity) or “off-time” states (reduced fluorescence intensity to the background level) at the single molecule level could be explained using the kinetic model shown in Scheme 60. During the “dim” state (molecule b in the first two seconds, Figure 65) the population of the excited state is decreased by both, radiative emission and nonradiative charge recombination to the ground state. When the rate for the forward electron transfer (k_{fwd}) is much larger than for the reverse electron transfer rate (k_{rev}), this results in a lowered fluorescence quantum yield (Φ_{flu}) at the single molecule level leading

to a “dim” state. During the “off-time” states (molecule d, Figure 65) this happens to such an extent that emission can no more be detected. However, with a signal/noise ratio of 20:1 from the given experimental setup, it is expected that some emitted photons stay undetected. Thus, such molecules seem to be dark, even though emission from the locally excited state still occurs.

4.5 Cyclovoltammetry

In the group of Prof. MÜLLEN, C. HAMPEL investigated the encapsulation of a triphenylamine core in polyphenylene dendrimers using cyclovoltammetry.²⁷ She found an attenuated electron transfer to the core with increasing dendrimer generation which was attributed to the steric shielding of the core. Similar results were observed for polyphenylene dendronized terylene diimide by T. WEIL.²⁸ During the course of this work (compare also chapter 2.6.2) comparable results were obtained for dendronized pyrene. The fluorescence behavior of the TPA-PMI dendrimer **4-14** showed how an electron transfer process between a donor and an acceptor can be enhanced by increasing the donor power. To further investigate this fact, cyclovoltammetry was used to determine the energy levels of the donor-acceptor pair **4-14**. The experiments were carried out together with J. W. F. ROBERTSON: A standard three-electrode format was used with a platinum wire counter electrode and a silver (Ag/Ag^+) reference electrode calibrated with the ferrocene (Fc/Fc^+) redox couple at 4.8 eV below vacuum. E^{on} values were estimated as the average between the forward sweep and the reverse sweep. All measurements were performed in 0.1 M tetrabutylammonium perchlorate in acetonitrile with ≈ 5 mM electroactive species and acquired at 100 mV/s. For comparison, also the TPA-PMI derivative **4-15** without additional methoxy groups was investigated. Figure 66 displays the obtained spectra.

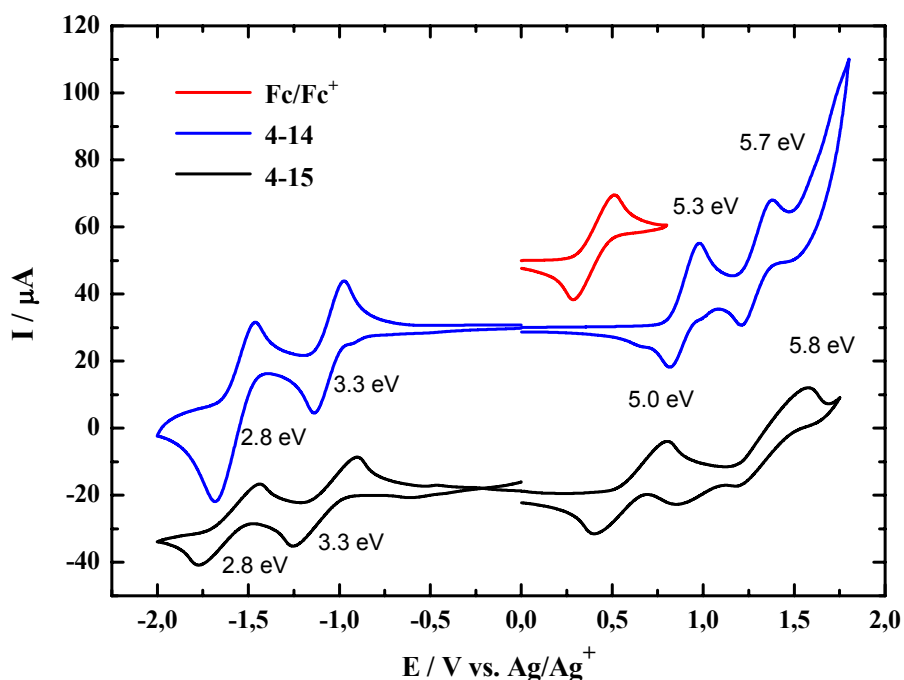


Figure 66. Cyclovoltammetry spectra of **4-14** (blue line) and **4-15** (black line) as well as of the reference ferrocene (red line, 4.8 eV in vacuum).

For both substances, **4-14** and **4-15**, well-resolved spectra were obtained showing two oxidation- and reduction-steps, respectively. The spectrum of **4-15** looks more “stretched” probably due to slower kinetics. Maybe an irreversible reaction followed or some conformation change occurred during the oxidation and reduction cycle. The HOMO-LUMO gap for **4-15** was calculated to be 1.7 eV, which is significantly smaller than for **4-14** (2 eV). This can be attributed to the electron donating methoxy groups in **4-14**.

4.6 Conclusion

As already mentioned, stiff polyphenylene dendrimers showed to be useful for arranging chromophores in defined positions in respect to each other. Additionally, by attaching polyphenylene dendrimer arms to a central chromophore, the self-aggregation of the dye was efficiently suppressed because of spatial shielding.²⁹ (see also 2.5).

This concept of encapsulation did not play a role in the herein presented approach. Therefore, a single polyphenylene dendrimer arm could be used to arrange a triphenylamine (TPA) donor and a perylene monoimide (PMI) acceptor moiety in a defined distance. This array of a single donor and a single acceptor part simplified the photo physical investigations. Additionally, carboxy acid groups have been attached to the TPA core to enable surface binding of the dendrimers. Two conformational isomers were formed during the DIELS-ALDER cycloaddition step, possessing a different through-bond and through-space distance between the TPA and the PMI. Since the donor-acceptor distance is of crucial importance for the efficiency of electron transfer processes and since this was one task to investigate, also a second-generation dendrimer was synthesized arranging the donor and the acceptor in an increased distance. Accordingly, also the second-generation dendrimers consists of two isomers.

First photo-physical investigations of model compound **4-14** showed encouraging results. Upon excitation, a photo induced electron transfer was observed at the ensemble level in toluene leading to a fast charge separation and a long-lived ion-pair state. Electron transfer in polyaryl bridged TPA-PMI systems in such an unpolar solvent was uncommon and can be attributed to the donating nature of the methoxy groups attached to the TPA core. The two isomers (ppp and pmp) of the model compound **4-14** could be assigned in the ensemble state since one isomer seemed to be active in electron transfer and the other one not. By now, it is not yet fully clear which isomer showed which behavior. Emission from the charge-separated state happened in two ways. Firstly, by reverse electron transfer to the locally excited state and subsequent fluorescence or secondly, by nonradiative charge recombination to the ground state.

In single molecule spectroscopy, the two isomers of the methoxy substituted **4-14** could not be resolved anymore, probably due to disturbing effects coming from the polymer matrix used for embedding the molecules. Long “dim-states” and “off-states” were observed for the majority of the single molecules and could be explained with the kinetic model developed. Summarizing, the ensemble and single molecule measurements of model compound **4-14** showed that the herein presented donor-acceptor systems are highly promising for the investigation of electron transfer processes. However, up to now only **4-14** has been studied at the single molecule level. Future work will be to attach the acid functionalized donor-acceptor systems on a suitable surface. Object of interest will be for example how the fluorescence properties of the dendrimers attached on the surface change, when different solvents are applied. Furthermore, without the polymer matrix it should be possible to distinguish between the two isomers even at the single molecule level.

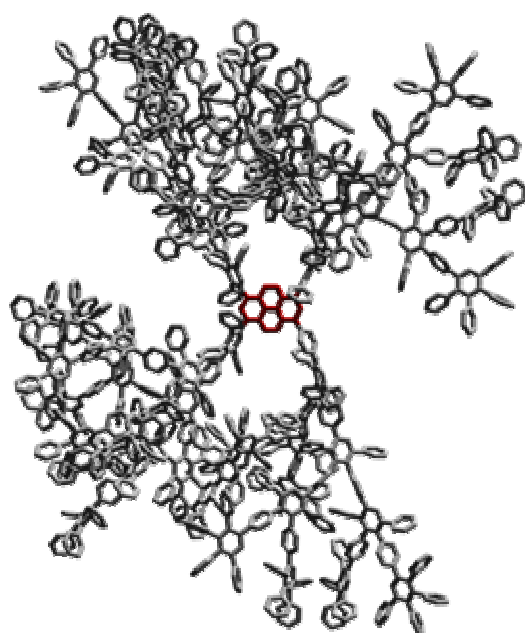
4.7 References

- (1) Shortreed, M. R.; Swallen, S. F.; Shi, Z. Y.; Tan, W. H.; Xu, Z. F.; Devadoss, C.; Moore, J. S.; Kopelman, R. *Journal of Physical Chemistry B* **1997**, *101*, 6318.
- (2) Serin, J. M.; Brousmiche, D. W.; Frechet, J. M. J. *Chemical Communications* **2002**, 2605.
- (3) Weil, T.; Reuther, E.; Müllen, K. *Angewandte Chemie-International Edition* **2002**, *41*, 1900.
- (4) Grimsdale, A. C.; Vosch, T.; Lor, M.; Cotlet, M.; Habuchi, S.; Hofkens, J.; De Schryver, F. C.; Müllen, K. *Journal of Luminescence* **2005**, *111*, 239.
- (5) Schweitzer, G.; Gronheid, R.; Jordens, S.; Lor, M.; De Belder, G.; Weil, T.; Reuther, E.; Müllen, M.; De Schryver, F. C. *Journal of Physical Chemistry A* **2003**, *107*, 3199.
- (6) Jordens, S.; De Belder, G.; Lor, M.; Schweitzer, G.; Van der Auweraer, M.; Weil, T.; Reuther, E.; Müllen, L.; De Schryver, F. C. *Photochemical & Photobiological Sciences* **2003**, *2*, 177.
- (7) Gronheid, R.; Hofkens, J.; Kohn, F.; Weil, T.; Reuther, E.; Müllen, K.; De Schryver, F. C. *Journal of the American Chemical Society* **2002**, *124*, 2418.
- (8) Xu, Z. F.; Moore, J. S. *Acta Polymerica* **1994**, *45*, 83.
- (9) Lor, M.; Jordens, S.; De Belder, G.; Schweitzer, G.; Fron, E.; Viaene, L.; Cotlet, M.; Weil, T.; Müllen, K.; Verhoeven, J. N.; Van der Auweraer, M.; De Schryver, F. C. *Photochemical & Photobiological Sciences* **2003**, *2*, 501.
- (10) Lor, M.; Thielemans, J.; Viaene, L.; Cotlet, M.; Hofkens, J.; Weil, T.; Hampel, C.; Müllen, K.; Verhoeven, J. W.; Van der Auweraer, M.; De Schryver, F. C. *Journal of the American Chemical Society* **2002**, *124*, 9918.
- (11) Qu, J. Q.; Pschirer, N. G.; Liu, D. J.; Stefan, A.; De Schryver, F. C.; Müllen, K. *Chemistry-A European Journal* **2004**, *10*, 528.
- (12) Cotlet, M.; Masuo, S.; Lor, M.; Fron, E.; Van der Auweraer, M.; Müllen, K.; Hofkens, J.; De Schryver, F. *Angewandte Chemie-International Edition* **2004**, *43*, 6116.
- (13) Xie, X. S.; Trautman, J. K. *Annual Review of Physical Chemistry* **1998**, *49*, 441.
- (14) Tamarat, P.; Maali, A.; Lounis, B.; Orrit, M. *Journal of Physical Chemistry A* **2000**, *104*, 1.
- (15) Kulzer, F.; Orrit, M. *Annual Review of Physical Chemistry* **2004**, *55*, 585.
- (16) Peterman, E. J. G.; Sosa, H.; Moerner, W. E. *Annual Review of Physical Chemistry* **2004**, *55*, 79.
- (17) Izquierdo, M. A.; Bell, T. D. M.; Habuchi, S.; Fron, E.; Pilot, R.; Vosch, T.; De Feyter, S.; Verhoeven, J.; Jacob, J.; Müllen, K.; Hofkens, J.; De Schryver, F. C. *Chemical Physics Letters* **2005**, *401*, 503.
- (18) Bell, T. D. M.; Stefan, A.; Masuo, S.; Vosch, T.; Lor, M.; Cotlet, M.; Hofkens, J.; Bernhardt, S.; Müllen, K.; van der Auweraer, M.; Verhoeven, J. W.; De Schryver, F. C. *ChemPhysChem* **2005**, *6*, 942.
- (19) Wolfe, J. P.; Buchwald, S. L. *Journal of Organic Chemistry* **2000**, *65*, 1144.
- (20) Wolfe, J. P.; Tomori, H.; Sadighi, J. P.; Yin, J. J.; Buchwald, S. L. *Journal of Organic Chemistry* **2000**, *65*, 1158.
- (21) Anderson, S. *Chemistry-A European Journal* **2001**, *7*, 4706.
- (22) Weil, T.; Wiesler, U. M.; Herrmann, A.; Bauer, R.; Hofkens, J.; De Schryver, F. C.; Müllen, K. *Journal of the American Chemical Society* **2001**, *123*, 8101.
- (23) Gensch, T.; Hofkens, J.; Herrmann, A.; Tsuda, K.; Verheijen, W.; Vosch, T.; Christ, T.; Basché, T.; Müllen, K.; De Schryver, F. C. *Angewandte Chemie-International Edition* **1999**, *38*, 3752.
- (24) Williard, P. G.; Fryhle, C. B. *Tetrahedron Letters* **1980**, *21*, 3731.
- (25) Liu, D. J.; De Feyter, S.; Cotlet, M.; Stefan, A.; Wiesler, U. M.; Herrmann, A.; Grebel-Koehler, D.; Qu, J. Q.; Müllen, K.; De Schryver, F. C. *Macromolecules* **2003**, *36*, 5918.
- (26) Gronheid, R.; Stefan, A.; Cotlet, M.; Hofkens, J.; Qu, J. Q.; Müllen, K.; Van der Auweraer, M.; Verhoeven, J. W.; De Schryver, F. C. *Angewandte Chemie-International Edition* **2003**, *42*, 4209.
- (27) Hampel, C.; Dissertation Johannes Gutenberg Universität (Mainz), **2001**.
- (28) Weil, T.; Dissertation Johannes Gutenberg Universität (Mainz), **2001**.
- (29) Herrmann, A.; Weil, T.; Sinigersky, V.; Wiesler, U. M.; Vosch, T.; Hofkens, J.; De Schryver, F. C.; Müllen, K. *Chemistry-A European Journal* **2001**, *7*, 4844.

5. CONCLUSION AND OUTLOOK

As introduced earlier in the motivation, the main goals of this work were the design, synthesis, and characterization of new functional polyphenylene dendrimers. These new functional nanoparticles were highly interesting as well from the point of view of fundamental research (looking into the optic, and electronic properties of such unique shape persistent structures) as from the point of view of their potential application as tailor-made nonmaterials in the field of optoelectronics.

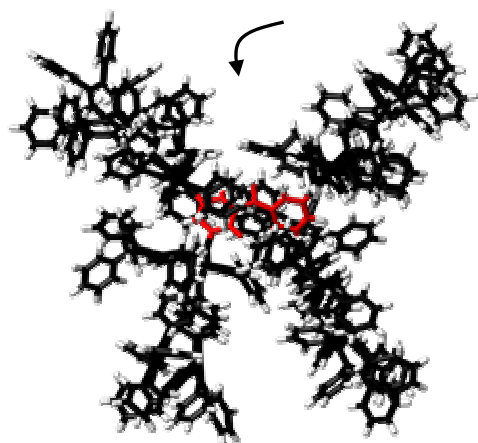
The first chapter presented the successful synthesis of polyphenylene dendrimers, starting from a tetraethynyl substituted pyrene core. Next to the routine characterization of the new compounds, the focus of the investigations was upon the shielding efficiency of dendritic



shells of different generations upon the pyrene-functionality in the core. It could be observed, that for all generations, the suppressed aggregation of the chromophore resulted in highly fluorescent nanoparticles with a defined emission spectrum. The influence of the dendrimer shell upon the optical properties of the core was further investigated using fluorescence quenching experiments and temperature fluorescence spectroscopy. Fluorescence quenching experiments displayed an increased quenching for quenchers of smaller size, indicating a size exclusion effect provided by the dendrimer shell. Temperature dependent fluorescence spectroscopy showed that excimer formation of the pyrene core can be suppressed by a second-generation dendrimer shell. Even more, the emission

properties were almost invariant from the temperature, suggesting a stiff and shape-persistent dendrimer shell. Further evidence for an efficient encapsulation was derived from the reduction of the pyrene dendrimers on a potassium mirror, as well as from cyclovoltametry experiments. In the first case, a hampered electron transfer to the core could be seen when comparing the reduction process of a second- and a fourth-generation dendrimer shell. Cyclovoltametry showed slowed electron transfer kinetics with increasing dendrimer generation. Combining a shape-persistent dendrimer shell with a chromophore core yielded spherical nanoparticles with improved optical properties. These properties are rendering this new class of polyphenylene dendrimers as potential candidates in applications on the field of nanoelectronics.

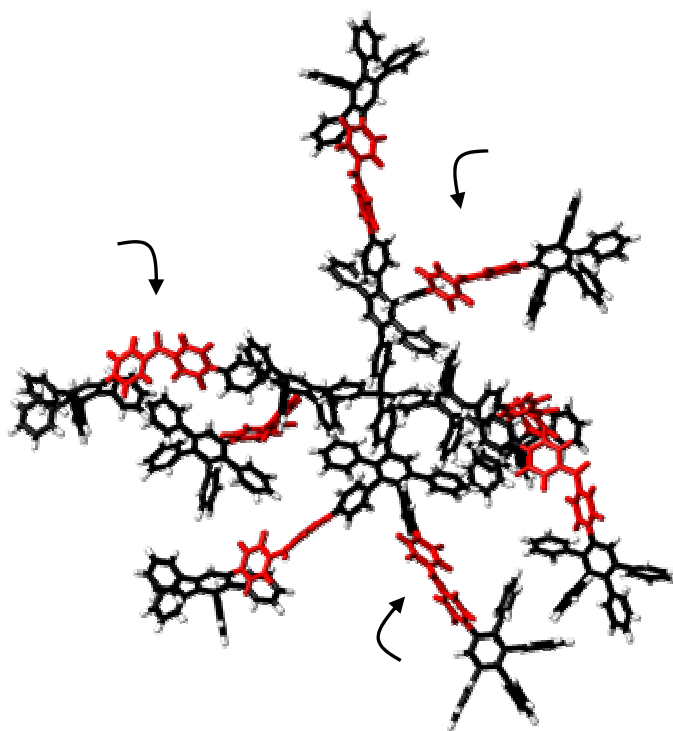
The defined functionalization of polyphenylene dendrimers often requires a great synthetic effort, since for every desired function the appropriate building block has to be synthesized. To overcome these disadvantages, a new functionalization concept has been developed. This new concept has been applied for the functionalization of the dendritic core, the dendrimer shell, and the dendrimer surface.



Starting from a tetraethynyl substituted benzophenone core (red), dendrimers were obtained with a single encapsulated reactive keto group. Varying the dendrimer generation and the density of the dendrimer shell resulted in a defined amount of shielding of the benzophenone core. For the postsynthetic functionalization of the core, the dendrimers were reacted with lithium and GRIGNARD reagents. Monodisperse products could only be obtained for the reaction with small molecules, mainly due to spatial congestion. To further evaluate the amount of shielding, the alkali metal reduction of the

first-generation dendrimer was carried out. The according ketyl radical anion species could be obtained, displaying potassium-bridged biradicals in the solid-state EPR measurements. Contrary, the second-generation dendrimer shell suppressed the biradical formation by keeping the radical centers separated.

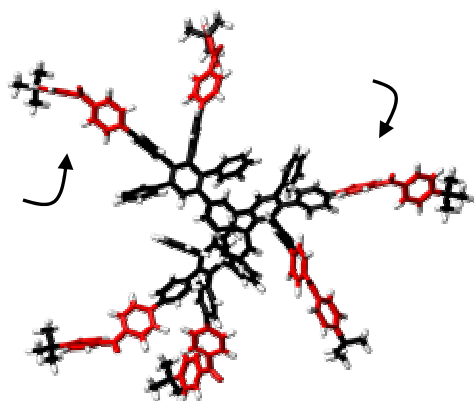
Going one step further, multiple benzophenones were placed in the dendrimer shell. For that, the benzophenone substituted tetraphenyl-cyclopentadienone **3-21** was synthesized carrying next to the attached benzophenones additional ethynyl groups thereby allowing the further dendrimer growth. Second- and third-generation dendrimers could be obtained, possessing eight keto groups (red) in the first-generation layer. Irrespective of the surrounding higher generation dendrimer shell, a versatile and defect free postsynthetic functionalization of the dendritic scaffold could be achieved by reacting the dendrimer with lithium-reagents, ranging from *n*-butyllithium to multiple substituted benzenes. Furthermore, spin and/or charge carrying centers like ketyl radical anions, trityl cations, and trityl radicals were generated in the inner of the dendrimers. The stiff and shape persistent dendrimer backbone stabilized these reactive species, thus allowing their full characterization.



The accessibility of the inner keto groups even allowed the interdigitation of dendritic arms as indicated by the formation of intermolecular bridged biradicals from the corresponding ketyl radical anion species. Further, the MCMURRY cross-coupling reaction of the embedded benzophenones yielded polymeric networks.

To use keto groups for the postsynthetic functionalization of the dendrimer surface, a benzophenone substituted endcapping reagent was synthesized. It allowed the introduction of a defined number of reactive sites (red) to the dendrimer periphery. A first example of a postsynthetic functionalization was carried out and gave the monodisperse product.

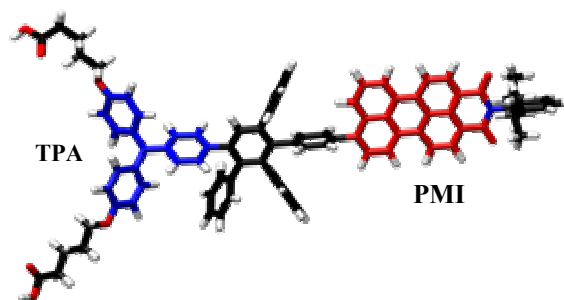
The herein described benzophenone carrying building blocks a) core b) branching and c) endcapping reagent are expected to play a key role for the functionalization of polyphenylene dendrimers in the future. They afford a wide spectrum of possible reagents that



can be introduced. Especially, it should enable the introduction of functionalities, which are not stable under the conditions of the DIELS-ALDER cycloaddition ($T \approx 430$ K). Furthermore, the introduced benzophenones may be used to easily alter the properties of the dendrimers in a systematic way. For example, introducing differently polar groups in the core, in the scaffold and on the surface of a dendrimer should lead to some kind of polarity gradient throughout the dendrimer shell. Another possibility is that the same precursor can be used to

introduce complementary functional groups on the dendrimer surface (e.g. acid and base) without the need of synthesizing the accordingly functionalized tetraphenylcyclopentadienones. The interaction of these dendrimers in solution and in the bulk can then be investigated in a systematic manner, as the postsynthetic approach allows easy modification of the interacting surface groups. These are just two possible examples, where benzophenone bearing dendrimers can be used as valuable precursors; for the investigation of nanoscopic properties upon varying functional groups.

The combination of the synthetic protocols of core and surfacefunctionalization resulted in a new type of functional molecules, highly interesting from the point of electron transfer processes. According to this, a polyphenylene dendron was used to arrange a donor (blue = TPA) and an acceptor (red = PMI) moiety in a defined spatial distance. The in-depth photophysical investigation of a first model compound was reported. Two constitutional isomers, formed during the DIELS-ALDER cycloaddition step, showed different electron transfer behavior at the ensemble level. In single molecule spectroscopy, long “dim-states” and “off-states” were observed and could be explained with the kinetic model developed. Further surface binding carboxylic acid groups were introduced in order to attach these electron transfer systems on a surface. This would allow to investigate their photophysical properties at the single molecule level without embedding them in a disturbing polymer matrix.



The herein presented functionalized dendrimers give an impression of the wide range of defined functional nanoparticles originating from polyphenylene dendrimers. Classical as well as new synthetic concepts are available for the target-oriented dendrimer design. Thereby, the investigation of structure – property relationships remains to be the most challenging task.

6. EXPERIMENTAL PART

6.1 General Procedures

All starting materials were obtained from commercial suppliers (Aldrich, Fluka, Fischer, Strem, Acros) and were used without purification. Solvents were used in HPLC grade purity as purchased. All atmosphere-sensitive reactions were performed under argon using Schlenk techniques. Analytical thin-layer chromatography (TLC) was performed on commercial Merck plates coated with silica gel F-254. Visualization was accomplished with UV light. Flash chromatography was carried out with silica gel 60 (230-400 mesh) from E. Merck. ^1H and ^{13}C NMR Spectrum spectra were recorded on a Bruker AMX250 spectrometer, a Bruker AC300 spectrometer, a Bruker AMX500 NMR Spectrum spectrometer and a Bruker 700Ultrasield NMR Spectrum spectrometer by using the residual proton resonance of the solvent or the carbon signal of the deuterated solvent as the internal standard. Chemical shifts are reported in parts per million. FD mass spectra were performed with a VG-Instruments ZAB 2-SE-FDP. MALDI-TOF mass spectra were measured with a Bruker Reflex II and dithranol as matrix (molar ratio dithranol/sample 250:1). The mass peaks with the lowest isotopic mass are reported. UV/vis absorption spectra were recorded on a Perkin Elmer Lambda 9 spectrophotometer, fluorescence spectra on a SPEX Fluorolog2 spectrometer. EPR spectra were recorded on a CW X-band ESP 300 equipped with an NMR Spectrum gauss meter (Bruker ER 035), a frequency counter (Bruker ER 041 XK) and a variable temperature control continuous flow N_2 cryostat (Bruker B-VT 2000). The elemental analysis was carried out by the Microanalytical Laboratory of the University of Mainz, Mainz, Germany.

Because of the high carbon content in some molecules, the combustion may have been incomplete (sooting) resulting in lower values than expected for the carbon content. Another reason for wrong values can be the inclusion of solvent molecules in large dendrimers, difficult to remove by vacuum.

6.2 Synthetic Procedures

6.2.1 General Synthetic Procedures

6.2.1.1 Diels-Alder-Cycloaddition of Ethynyl- and Tetraphenylcyclopentadiene

Derivatives.

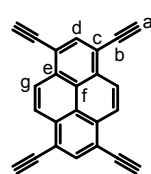
A mixture of the ethynyl derivative and tetraphenylcyclopentadiene derivative was refluxed in *o*-xylene or diphenyl ether under an argon atmosphere. When **1-32** was used as the endcapping reagent, the cooled reaction mixture was poured into *n*-pentane to remove the excess of tetraphenylcyclopentadienone. The precipitated product was filtered and the filter washed with pentane until the filtrate became colorless. All crude products were purified by column chromatography (silica gel). Reactions were monitored by MALDI-TOF mass spectrometry to ensure their completeness.

6.2.1.2 Desilylation of Tri-iso-propylsilylethynyl Derivatives.

The tri-*iso*-propylsilylethynyl derivative was dissolved in dry THF and 1 equivalent of tetrabutylammonium fluoride hexahydrate (dissolved in THF) per tri-*iso*-propylsilylethynyl group was added under argon atmosphere. The end of the reaction (\approx 5-15 min) was determined by TLC (silica gel). The reaction was quenched with H₂O, and extracted with H₂O and CH₂Cl₂. The organic phase was separated and dried over MgSO₄. Having removed the solvent under reduced pressure, the crude product was purified by column chromatography on silica gel.

6.2.2 Special Synthetic Procedures

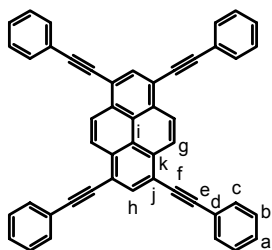
1,3,6,8-Tetraethynyl-pyrene (2-10)



2-15 (1 g, 1.7 mmol) was suspended in 100 mL of MeOH. K₂CO₃ (1.9 g, 13.6 mmol) was added and the reaction mixture stirred over night and then poured in 500 mL of water and the precipitate filtered off. The residue was washed with H₂O until the filtrate was neutral to afford **2-10** as a slight brown solid.

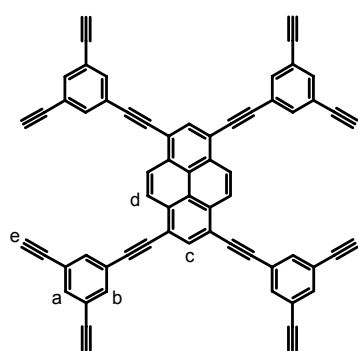
Yield: 480 mg (1.61 mmol), 95%. ¹H NMR Spectrum Spectrum (300 MHz, d⁸-THF, 300K) δ [ppm] = 8.70 (s, 4H, H_g), 8.36 (s, 2H, H_d), 4.31 (s, 4H, H_a). ¹³C NMR Spectrum Spectrum (75 MHz, d⁸-THF, 300 K) δ [ppm] = 135.6 (C_d), 133.1 (C_c), 127.7 (C_g), 124.4 (C_f), 119.2 (C_e), 86.2 (C_b), 81.8 (C_a). FD Mass Spectrum (8kV) m/z = 298.08 (100%, (M)⁺) (calcd. 298.35). Elemental Analysis for C₂₄H₁₀ Calcd.: C, 96.62; H, 3.38 Found: C, 92.07; H, 3.65.

1,3,6,8-Tetrakis-phenylethynyl-pyrene (2-11)



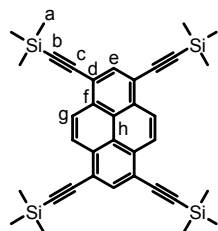
2-14 (314 mg, 61 μ mol) was suspended in 15 mL of TEA and 5 mL of toluene. Bis(triphenylphosphine)-palladium(II) dichloride (130 mg, 0.18 mmol), copper(I) iodide (45 mg, 0.24 mmol), and triphenylphosphine (64 mg, 0.24 mmol) were added. The flask was evacuated and flushed with argon several times. The reaction mixture was heated to 60 °C under stirring and phenylacetylene (0.56 mL, 4.8 mmol) was injected through a septum. After 15 min of stirring at this temperature the reaction mixture was heated to 80 °C and stirred over night under argon atmosphere. The reaction mixture was cooled down and the orange precipitate filtered off. The residue was thoroughly washed with CH₂Cl₂ and acetone to give **2-11** as a yellow solid.

Yield: 340 mg (56.4 μ mol), 92%. ¹H NMR Spectrum (250 MHz, CD₂Cl₂, 300 K) δ [ppm] = 7.78-7.69 (m, 6H, H_{pyrene}), 7.56-7.02 (m, 20H, H_{arom.}). ¹³C NMR Spectrum (125 MHz, C₂D₂Cl₄, 373 K) δ [ppm] = 134.1 (C_j), 132.2 (C_k), 132.1 (C_c), 128.9 (C_b), 128.7 (C_b), 127.2 (C_h), 124.5 (C_i), 123.6 (C_d), 119.5 (C_g), 96.8 (C_e), 88.1 (C_f). FD Mass Spectrum (8kV) m/z = 603.1 (100%, (M)⁺), 301.7 (20%, (M)²⁺) (calcd. 602.7). Elemental Analysis for C₄₈H₂₆ Calcd.: C, 95.65; H, 4.35. Found: C, 93.36; H, 3.93.

1,3,6,8-Tetrakis-(3,5-diethynyl-phenylethynyl)-pyrene (2-12)

2-33 (0.5 g, 0.24 mmol) was dissolved in 250 mL of dry THF under argon atmosphere and reacted with TBAF (920 mg, 0.37 mmol) following the general desilylation procedure. After 5 min reaction time the product started to precipitate from the solution. The end of the reaction was determined using MALDI-TOF mass spectrometry. The suspension was poured into 1000 mL of water and stirred for 30 min. The solid was filtered off and the residue washed H₂O to give **2-12** as an orange solid.

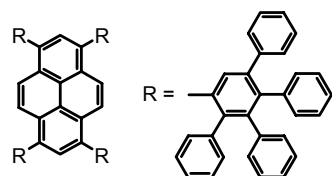
Yield: 184 mg (0.23 mmol), 95%. ¹H NMR Spectrum (700 MHz, C₂D₂Cl₄, 393 K) δ [ppm] = 8.91 (s, 4H, H_d), 8.55 (s, 2H, H_c), 7.88 (s, 8H, H_b), 7.64 (s, 4H, H_a), 3.78 (s, 8H, H_e). MALDI TOF Mass Spectrum m/z = 795 (100%, (M)⁺), calcd. for C₆₄H₂₆ (749.9).

1,3,6,8-Tetrakis-trimethylsilanylethynyl-pyrene (2-15)

2-14 (0.5 g, 0.97 mmol) was suspended in 20 mL of TEA and 3 mL of toluene. Bis(triphenylphosphine)palladium(II) dichloride (136 mg, 0.19 mmol), copper(I) iodide (73 mg, 0.39 mmol), and triphenylphosphine (101 mg, 0.39 mmol) were added and the flask evacuated and flushed with argon several times. The reaction mixture was heated to 60 °C while stirring and trimethylsilylethyne (0.8 mL, 5.8 mmol) was injected through a septum. After 15 min stirring at this temperature, the reaction was

heated to 80 °C and stirred over night under argon atmosphere. The reaction mixture was cooled to RT and extracted CH₂Cl₂/H₂O. The organic phase was dried over MgSO₄, the solvent removed under reduced pressure and the crude product purified by column chromatography (silica gel, PE) to afford **2-15** as an orange solid.

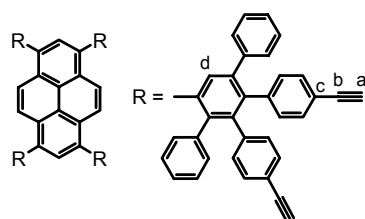
Yield: 470 mg (0.8 mmol), 83%. ¹H NMR Spectrum Spectrum (250 MHz, CD₂Cl₂, 300K) δ [ppm] = 8.59 (m, 4H, H_g), 8.27 (s, 2H, H_e), 0.39 (s, 36H, H_a). ¹³C NMR Spectrum Spectrum (75 MHz, CD₂Cl₂, 300 K) δ [ppm] = 134.7 (C_e), 132.3 (C_d), 127.3 (C_g), 123.8 (C_h), 119.1 (C_f), 102.8 (C_c), 102.1 (C_b), 0.1 (C_a). FD Mass Spectrum (8kV) m/z = 587.24 (100%, (M)⁺) (calcd. 587.08). Elemental Analysis for C₃₆H₄₂Si₄ Calcd.: C, 73.65; H, 7.21. Found: C, 73.14; H, 7.55.

2-16

2-10 (0.2 g, 0.67 mmol) and **1-32** (1.55 g, 4.03 mmol) were reacted in 20 mL of *o*-xylene for 12 h at 160 °C under argon atmosphere. The reaction mixture was poured in MeOH and the precipitated product filtered off. **2-16** was purified by multiple reprecipitation from EtOH until the red color of the tetraphenylcyclopentadienone had disappeared.

Yield: 480 mg (1.61 mmol), 95%. ¹H NMR Spectrum (700 MHz, C₂D₂Cl₄, 373K) δ [ppm] = 7.86-7.40 (m, 6H, H_{pyrene}), 7.24-6.52 (m, 84H, H_{arom.}). ¹³C NMR Spectrum (75 MHz, CD₂Cl₂, 300 K) δ [ppm] = 142.1, 141.7, 141.1, 141.0, 140.7, 140.5, 140.3, 139.9, 131.9, 131.8, 131.3, 131.0, 130.3, 128.3, 128.2, 128.1, 127.5, 127.4, 126.9, 126.6, 126.4, 126.2, 125.6, 125.3, 125.2, 125.1. FD Mass Spectrum (8kV) m/z = 1725 (100%, (M)⁺) (calcd. 1724). Elemental Analysis for C₁₃₆H₉₀ Calcd.: C, 94.74; H, 5.26. Found: C, 93.75; H, 5.56.

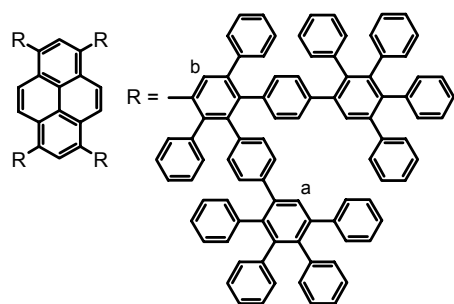
2-18



2-20 (1.43 g, 0.45 mmol) was dissolved in 30 mL of dry THF and reacted with TBAF (1.14 g, 3.6 mmol) following the general desilylation procedure. Purification was performed by column chromatography (silica gel, PE/CH₂Cl₂ 2:3) to afford **2-18** as a yellow solid.

Yield: 0.8 g, (0.42 mmol), 93%. ¹H NMR Spectrum (250 Mhz, CD₂Cl₂, 300K) δ [ppm] = 7.89-7.73 (m, 6H, H_{pyrene}), 7.53-7.43 (m, 4H, H_d), 7.17-6.60 (m, 80H, H_{arom.}), 3.02 (m, 8H, H_a). ¹³C NMR Spectrum (75 MHz, d⁸-THF, 300 K) δ [ppm] = 142.3, 142.2, 142.1, 141.9, 141.8, 141.7, 141.6, 141.6, 141.5, 141.5, 141.3, 141.3, 141.2, 141.2, 141.1, 140.9, 140.8, 140.7, 140.6, 140.6, 140.5, 140.4, 140.3, 140.2, 139.9, 139.6, 139.5, 139.5, 139.4, 139.4, 139.3, 137.3, 137.3, 137.3, 137.1, 136.9, 136.8, 136.5, 136.4, 136.1, 134.8, 134.6, 134.4, 134.2, 133.9, 132.7, 132.5, 132.3, 131.9, 131.6, 131.3, 130.7, 130.6, 130.1, 129.6, 128.9, 128.9, 128.7, 128.5, 128.1, 127.5, 127.3, 126.8, 126.5, 126.5, 126.3, 126.1, 126.0, 125.9, 125.5, 125.4, 125.2, 125.1, 125.0 (all Ar-C), 121.0, 120.6 (all C_c), 84.2 (C_b), 78.7, 78.6 (all C_a). MALDI TOF Mass Spectrum m/z = 1916 (100%, (M)⁺) (calcd. 1916). Elemental Analysis for C₁₅₂H₉₀ Calcd.: C, 95.27; H, 4.73. Found: C, 94.61; H, 4.91.

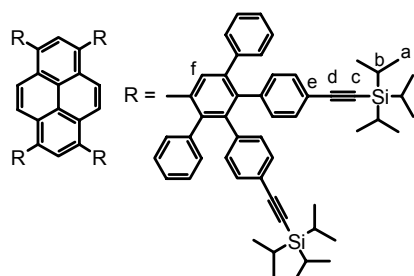
2-19



2-18 (200 mg, 104 μ mol) and **1-32** (640 mg, 1.67 mmol) were dissolved in 10 mL of *o*-xylene and reacted for 16 h at 160 °C under argon atmosphere. Purification was performed by column chromatography (silica gel, PE/CH₂Cl₂ 3:2) to afford **2-19** as a yellow solid.

Yield: 360 mg (76 μ mol), 73%. ¹H NMR Spectrum (250 MHz, CD₂Cl₂, 300 K) δ [ppm] = 7.78-7.61 (m, 6H, H_{pyrene}), 7.43-7.35 (m, 12H, H_{a+b}), 7.16-6.53 (m, 232H, H_{arom.}). ¹³C NMR Spectrum (75 MHz, d⁸-THF, 300 K) δ [ppm] = 142.8, 142.7, 142.0, 141.7, 141.4, 141.3, 141.1, 141.0, 140.1, 140.1, 140.0, 139.7, 139.4, 139.2, 138.9, 132.4, 132.0, 130.6, 129.5, 129.2, 129.1, 128.3, 127.6, 127.3, 126.9, 126.3, 126.0 (all Ar-C). MALDI TOF Mass Spectrum m/z = 4768 (100%, (M)⁺) (calcd 4768). Elemental Analysis for C₃₇₆H₂₅₀ Calcd.: C, 94.72; H, 5.87. Found: C, 94.00; H, 5.87.

2-20

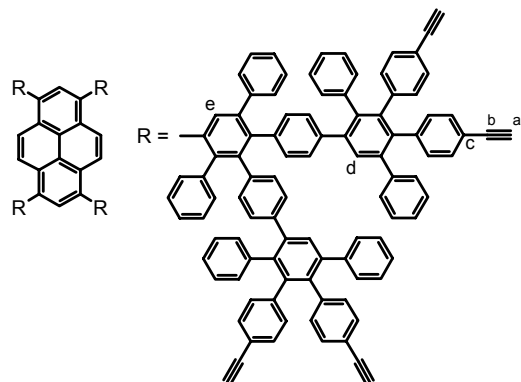


2-10 (250 mg, 0.84 mmol) and **1-35** (3.0 g, 4.03 mmol) were reacted in 30 mL of *o*-xylene for 12 h at 160 °C under argon atmosphere. Purification was performed by column chromatography (silica gel, PE/CH₂Cl₂ 5:1) to afford **2-20** as a yellow solid.

Yield: 1.88 g (0.59 mmol), 71%. ¹H NMR Spectrum (250 MHz, CD₂Cl₂, 300 K) δ [ppm] = 8.02-7.57 (m, 6H, H_{pyrene}), 7.42 (m, 4H, (H_f), 7.19-6.61 (m, 72H, H_{arom.}), 1.10 (s, 215H, H_{a+b}). ¹³C NMR Spectrum (75 MHz, d⁸-THF, 300 K) δ [ppm] = 142.3, 142.2, 141.9, 141.9, 141.7, 141.8, 141.7, 141.6, 141.6, 141.6, 141.6, 141.5, 141.5, 141.4, 141.3, 141.3, 141.2, 141.1, 140.9, 140.9, 140.7, 140.6, 140.5, 140.4, 140.4, 139.9, 139.6, 139.6, 139.5, 139.4, 139.4, 139.3, 137.4, 137.3, 137.2, 137.1, 136.8, 136.5, 136.0, 132.4, 132.4, 131.6,

131.3, 130.7, 130.6, 130.7, 129.7, 129.0, 128.9, 128.8, 128.7, 128.4, 128.0, 127.5, 127.2, 126.5, 126.0, 125.2 (all Ar-C), 121.7, 121.4 (all C_e), 108.5 (C_d), 90.2, 90.0 (C_c), 19.0 (C_a), 12.2 (C_b). MALDI TOF Mass Spectrum m/z = 3166 (100%, (M)⁺) (calcd. 3167). Elemental Analysis for C₂₂₄H₂₅₀Si₈ Calcd.: C, 84.95; H, 7.96. Found: C, 83.56; H, 8.09.

2-21

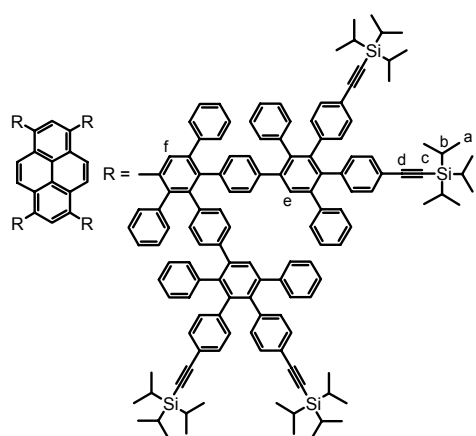


2-22 (0.8 g, 104 μmol) was dissolved in 15 mL of dry THF and reacted with TBAF (518 mg, 1.67 mmol) following the general desilylation procedure. Purification was performed by column chromatography (silica gel, PE/CH₂Cl₂ 1:1) to afford **2-21** as a yellow solid.

Yield: 0.49 g (95 μmol), 91%. ¹H NMR Spectrum (250 MHz, CD₂Cl₂, 300K) δ [ppm] = 7.78-7.61 (m, 6H, H_{pyrene}), 7.46-7.32 (m, 12H, H_{d+e}), 7.18-6.54 (m, 216H, H_{arom.}), 3.02 (m, 16H, H_a).

¹³C NMR Spectrum (75 MHz, d⁸-THF, 300 K) δ [ppm] = 141.6, 141.3, 141.1, 139.5, 139.4, 139.0, 138.8, 138.5, 131.8, 131.5, 131.2, 130.8, 130.2, 129.0, 128.6, 128.1, 127.9, 127.4, 126.9, 126.2 (all Ar-C), 119.7, 119.4 (all C_c), 83.8 (C_b), 77.3 (C_a). MALDI TOF Mass Spectrum m/z = 5147 (100%, (M)⁺) (calcd. 5153). Elemental Analysis for C₄₀₈H₂₅₀ Calcd.: C, 95.11; H, 4.89. Found: C, 94.38; H, 5.76.

2-22

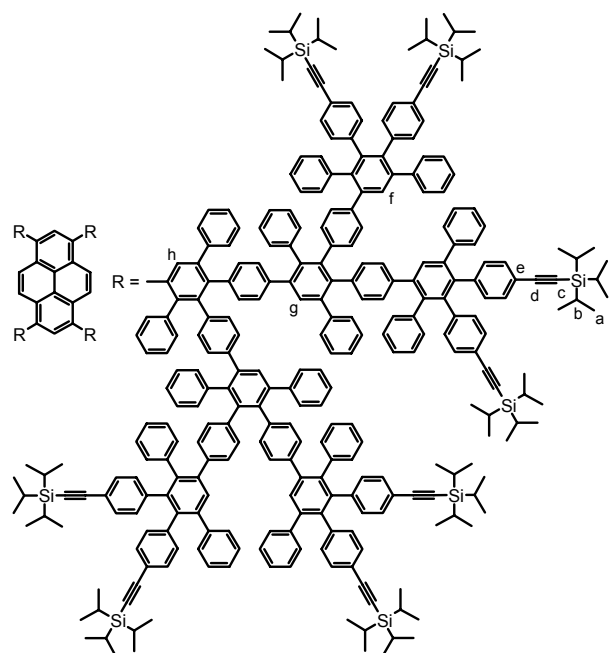


2-18 (300 mg, 0.16 mmol) and **1-35** (1.4 g, 1.88 mmol) were dissolved in 10 mL of *o*-xylene and reacted for 20 h at 150 °C under argon atmosphere. Purification was performed by column chromatography (silica gel, PE/CH₂Cl₂ 7:1) to afford **2-22** as a yellow solid.

Yield: 0.91 g (0.12 mmol), 76%. ¹H NMR Spectrum (250 MHz, CD₂Cl₂, 300 K) δ [ppm] = 7.78-7.61 (m, 6H, H_{pyrene}), 7.42-7.31 (m, 12H, H_{e+f}), 7.18-6.40 (m, 216H, H_{arom.}), 1.09 (s, 336H, H_{a+b}). ¹³C NMR Spectrum (75 MHz, d⁸-THF, 300 K) δ [ppm] = 142.6, 142.4, 141.9, 141.9, 141.8, 141.7, 141.4, 141.2, 141.0, 140.6, 140.5, 140.1, 140.0, 140.4, 140.3, 139.6, 139.5,

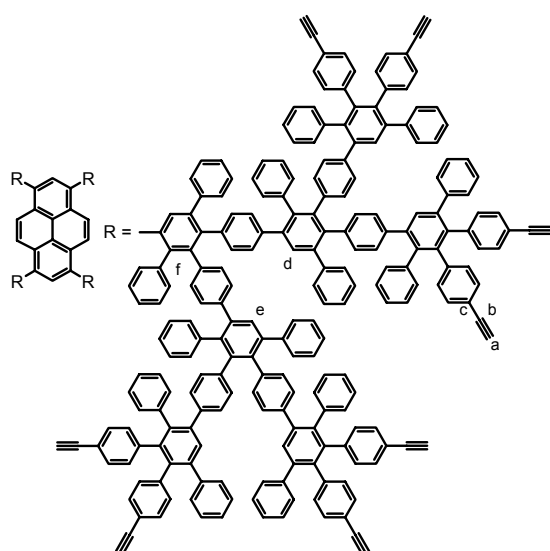
139.2, 139.2, 138.9, 137.4, 136.9, 136.6, 136.2, 136.9, 132.3, 131.5, 131.2, 130.8, 130.6, 130.1, 129.5, 129.2, 128.8, 128.5, 128.3, 127.8, 127.2, 127.0, 126.7, 126.7, 126.5, 123.8, 121.6, 121.3 (all Ar-C), 108.5, 108.5 (all C_d), 90.2, 90.0 (all C_c), 19.0 (C_a), 12.2 (C_b). MALDI TOF Mass Spectrum m/z = 7657 (100%, (M)⁺) (calcd. 7654). Elemental Analysis for C₅₅₂H₅₇₀Si₁₆ Calcd.: C, 86.62; H, 7.51. Found: C, 86.94; H, 7.61.

2-23



137.4, 136.9, 132.3, 132.0, 131.5, 131.2, 130.7, 130.6, 130.1, 129.4, 129.1, 128.5, 128.3, 127.8, 127.2, 126.7, 126.5, 126.9 (all Ar-C), 121.6, 121.3 (all C_e), 108.5 (C_d), 90.2, 90.0 (all C_c), 19.0 (C_a), 12.2 (C_b). MALDI TOF Mass Spectrum $m/z = 16640$ (100%, (M)⁺) (calcd. 16628). Elemental Analysis for C₁₂₀₈H₁₂₁₀Si₃₂ Calcd.: C, 87.26; H, 7.33. Found: C, 86.22; H, 7.79.

2-24



132.4, 132.0, 131.5, 131.2, 130.7, 130.6, 129.4, 129.1, 128.5, 128.3, 127.8, 127.2, 127.0, 126.9, 126.7, 126.5 (all Ar-C), 120.9, 120.6 (all C_c), 84.2 (C_b), 78.6 (C_a). MALDI TOF Mass Spectrum $m/z = 11618$ (100%, (M)⁺) (calcd. 11625). Elemental Analysis for C₉₂₀H₅₇₀ Calcd.: C, 95.06; H, 4.94. Found: C, 93.11; H, 6.90. (sooting or incorporated solvent)

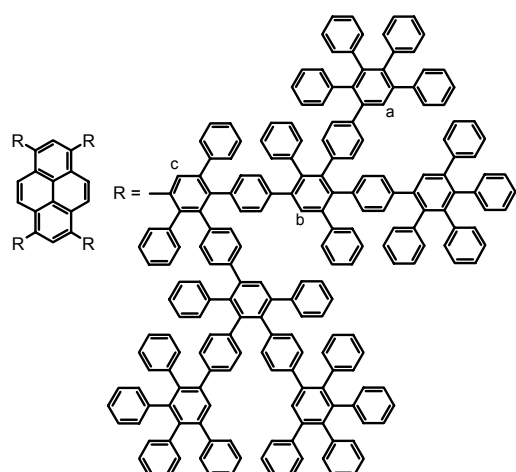
2-22 (200 mg, 39 μmol) and **1-35** (0.93 g, 1.25 mmol) were dissolved in 10 mL of *o*-xylene and reacted for 20 h at 160 °C under argon atmosphere. Purification was performed by column chromatography (silica gel, PE/CH₂Cl₂ 2:1) to afford **2-23** as a yellow solid.

Yield: 0.55 g (33 μmol), 85%. ¹H NMR Spectrum (250 MHz, CD₂Cl₂, 300 K) δ [ppm] = 7.78-7.59 (m, 6H, H_{pyrene}), 7.40-7.27 (m, 28H, H_{f-h}), 7.17-6.38 (m, 504H, H_{arom.}), 1.08 (s, 672H, H_{a+b}). ¹³C NMR Spectrum (75 MHz, d⁸-THF, 300 K) δ [ppm] = 142.8, 142.7, 142.7, 142.4, 141.9, 141.9, 141.8, 141.7, 141.4, 141.0, 140.9, 140.6, 140.1, 140.0, 139.9, 139.8, 139.5, 139.3, 139.2, 139.2, 139.1, 139.0, 138.8,

2-23 (0.4 g, 24.1 μmol) was dissolved in 15 mL of dry THF and reacted with TBAF (243 mg, 0.77 mmol) following the general desilylation procedure. Purification was performed by column chromatography (silica gel, PE/CH₂Cl₂ 1:1) to afford **2-24** as a yellow solid.

Yield: 250 mg (21.5 μmol), 89.2%. ¹H NMR Spectrum (250 MHz, CD₂Cl₂, 300K) δ [ppm] = 7.77-7.59 (m, 6H, H_{pyrene}), 7.42 (m, 8H, H_e), 7.38 (m, 16H, H_d), 7.31-7.29 (m, 4H, H_f), 7.13-6.44 (m, 504H, H_{arom.}), 3.04-2.00 (m, 32H, H_a). ¹³C NMR Spectrum (75 MHz, d⁸-THF, 300 K) δ [ppm] = 142.8, 142.7, 142.3, 141.9, 141.8, 141.8, 141.7, 141.4, 141.0, 140.9, 140.5, 140.0, 139.9, 139.4, 139.3, 139.2, 139.2, 139.0, 138.8,

2-25

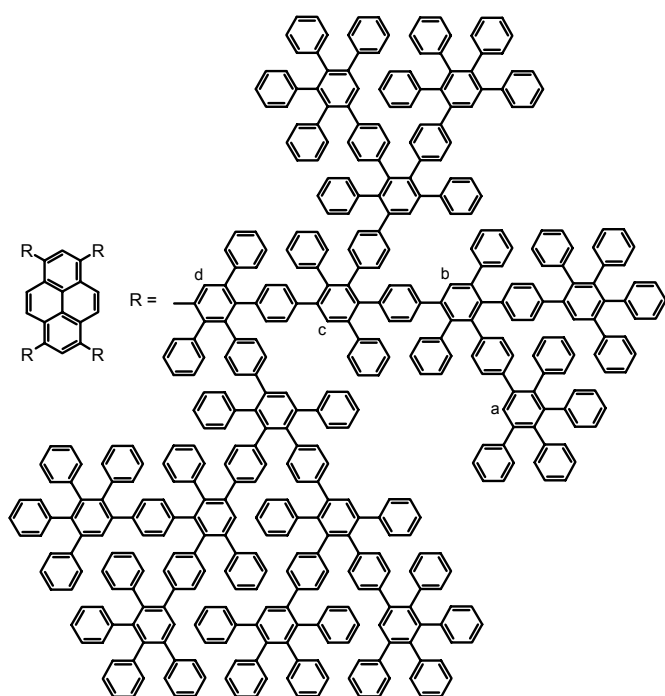


141.4, 141.3, 141.1, 141.0, 140.2, 140.1, 140.0, 140.0, 139.7, 139.5, 139.4, 139.4, 139.2, 138.9, 132.4, 132.0, 130.6, 129.6, 129.5, 129.2, 128.9, 128.3, 127.6, 127.3, 126.9, 126.5, 126.3, 126.3, 126.0 (all Ar-C). MALDI TOF Mass Spectrum $m/z = 10837$ (100%, $(M)^+$) (calcd. 10856). Elemental Analysis for $C_{856}H_{570}$ Calcd.: C, 94.71; H, 5.29. Found: C, 94.50; H, 5.24.

2-21 (100 mg, 52 μmol) and **1-32** (950 mg, 0.83 mmol) were dissolved in 10 mL of *o*-xylene and reacted for 2 days at 170 °C under argon atmosphere. The solvent was removed under reduced pressure and the crude product was purified by column chromatography (silica gel, PE/ CH_2Cl_2 1:1) to afford **2-25** as a yellow solid.

Yield: 310 mg (29 μmol), 55%. ^1H NMR Spectrum (250 MHz, CD_2Cl_2 , 300 K) δ [ppm] = 7.76-7.60 (m, 6H, H_{pyrene}), 7.41 (m, 8H, H_b), 7.37 (m, 16H, H_a), 7.32-7.29 (m, 4H, H_c), 7.13-6.44 (m, 536H, $H_{\text{arom.}}$). ^{13}C NMR Spectrum (75 MHz, d^8 -THF, 300 K) δ [ppm] = 142.8, 142.7, 142.0, 141.7, 141.4,

2-26

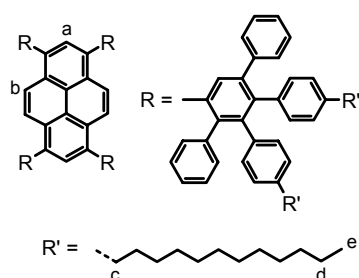


129.2, 129.1, 128.3, 127.6, 127.3, 126.9, 126.3, 126.0 (all Ar-C). MALDI TOF Mass Spectrum $m/z = 23019$ (100%, $(M)^+$) (calcd. 23031). Elemental Analysis for $C_{1816}H_{1210}$ Calcd.: C, 94.70; H, 5.30. Found: C, 94.58; H, 5.37.

2-24 (100 mg, 8.6 μmol) and **1-32** (420 mg, 0.56 mmol) were dissolved in 8 mL of diphenyl ether and reacted for 5 days at 190 °C under argon atmosphere. Purification was performed by column chromatography (silica gel, PE/ CH_2Cl_2 2:1) to afford **2-26** as a yellow solid.

Yield: 170 mg (7.3 μmol), 85%. ^1H NMR Spectrum (250 MHz, CD_2Cl_2 , 300 K) δ [ppm] = 7.79-7.59 (m, 6H, H_{pyrene}), 7.41-7.30 (m, 58H, H_{a-d}), 7.14-6.42 (m, 1146H, $H_{\text{arom.}}$). ^{13}C NMR Spectrum (75 MHz, d^8 -THF, 300 K) δ [ppm] = 142.8, 142.7, 142.0, 141.7, 141.4, 141.3, 141.1, 141.0, 140.1, 140.1, 140.0, 139.7, 139.4, 139.2, 138.9, 132.4, 132.0, 130.6, 129.5,

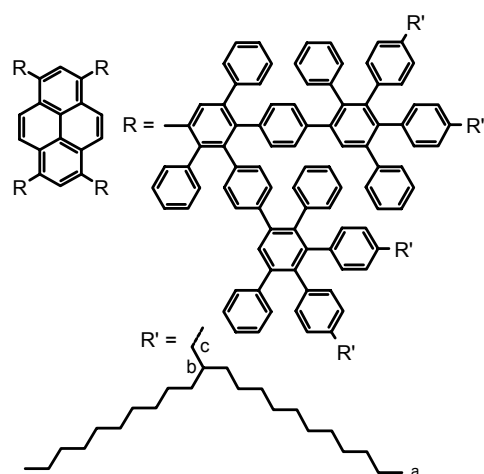
2-27



2-10 (150 mg, 0.5 mmol) and **2-28** (2.15 g, 3.02 mmol) were dissolved in 15 mL of *o*-xylene and reacted for 24 h at 150 °C under argon atmosphere. The solvent was removed under reduced pressure. Purification was performed by column chromatography (silica gel, PE/CH₂Cl₂ 5:1) to afford **2-27** as a yellow solid.

Yield: 1.2 g (0.39 mmol), 78%. **¹H NMR Spectrum** (500 MHz, CD₂Cl₂, 300 K) δ [ppm] = 7.91-7.74 (m, 4H, H_b); 7.54-7.39 (m, 2H, H_a); 7.14 (m, 22H, H_{arom.}); 6.83-6.57 (m, 54H, H_{arom.}); 2.45-2.35 (m, 16H, H_c); 1.48-1.13 (m, 160H, H_{alkyl}); 0.90 (m, 24H, H_d). **¹³C NMR Spectrum** (125 MHz, CD₂Cl₂, 300 K) δ [ppm] = 142.3, 142.3, 142.3, 142.2, 142.2, 142.1, 142.1, 142.1, 142.0, 141.1, 141.0, 141.0, 141.0, 140.8, 140.8, 140.7, 140.6, 140.6, 140.6, 140.5, 140.3, 140.3, 140.1, 140.1, 140.0, 139.9, 139.9, 139.8, 139.7, 139.6, 139.5, 139.5, 139.4, 139.3, 138.2, 138.1, 137.9, 137.9, 137.1, 137.0, 136.8, 136.4, 136.4, 136.1, 133.6, 133.4, 133.3, 133.2, 133.0, 132.9, 132.8, 131.8, 131.7, 131.6, 130.4, 130.3, 127.7, 127.7, 127.2, 127.0, 126.9, 126.4, 125.6, 125.6, 125.5, 125.4 (all Ar-C), 35.7, 35.6 (all C_c), 32.3, 31.6, 31.6, 30.1, 30.0, 29.9, 29.7, 29.3, 29.1 (all-CH₂-), 23.1 (C_d), 14.2 (C_e). **FD Mass Spectrum** (8kV) m/z = 3072.4 (100%, (M)⁺) (calcd. 3071). **Elemental Analysis** for C₂₃₂H₂₈₂ Calcd.: C, 91.10; H, 8.90. Found: C, 90.20; H, 9.20.

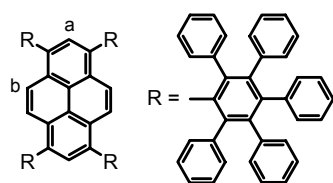
2-30



2-18 (18 mg, 9.4 μmol) and **2-29** (140 mg, 132 μmol) were dissolved in 4 mL of diphenyl ether and reacted for 16 h at 220 °C under argon atmosphere. Purification was performed by column chromatography (silica gel, PE/CH₂Cl₂ 1:1) to afford **2-30** as a yellow oil.

Yield: 60 mg (5.9 μmol), 63%. **¹H NMR Spectrum** (500 MHz, CD₂Cl₂, 300 K) δ [ppm] = 7.80-6.42 (m, 234H, H_{arom.}), 2.31 (m, 16H, H_b), 1.27-1.19 (m, 672H, H_{alkyl}), 0.88-0.87 (m, 96H, H_a). **¹³C NMR Spectrum** (125 MHz, CD₂Cl₂, 300 K) δ [ppm] = 168.2, 168.0, 156.9, 156.3, 142.8, 142.7, 142.5, 141.9, 141.7, 141.4, 141.4, 141.2, 141.0, 140.9, 140.9, 140.8, 140.2, 140.1, 139.9, 139.8, 139.6, 139.4, 139.3, 138.9, 138.7, 138.7, 138.5, 138.2, 135.6, 134.3, 133.9, 133.6, 133.3, 133.2, 133.0, 132.8, 132.3, 131.9, 131.8, 131.7, 131.5, 131.4, 131.4, 131.1, 130.7, 130.6, 130.4, 130.4, 130.3, 130.3, 130.2, 123.0, 129.9, 129.8, 129.5, 129.4, 129.3, 129.3, 129.2, 129.0, 128.9, 128.7, 128.6, 128.5, 128.4, 128.2, 128.0, 128.0, 127.9, 127.7, 127.6, 127.4, 126.6, 126.0, 125.6 (all Ar-C), 120.5, 41.21, 40.77, 40.63, 40.22, 40.19, 39.71, 39.64, 39.51, 39.44 (all C_{b+c}), 33.71, 33.62, 34.17, 34.00, 32.52, 30.65, 30.29, 30.25, 29.92, 27.10, 27.13, 23.23 (all-CH₂-), 14.33 (C_a). **MALDI TOF Mass Spectrum** m/z = 10161 (100%, (M)⁺), calcd. for C₇₆₀H₁₀₁₈ (10155).

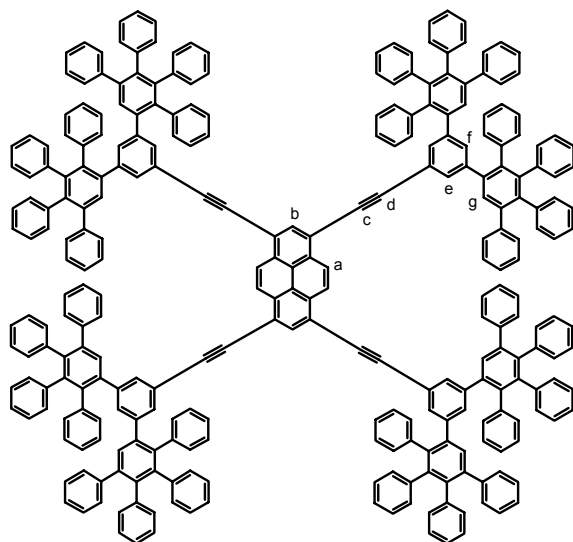
2-31



2-11 (79 mg, 0.13 mmol) and **1-32** (300 mg, 0.78 mmol) were dissolved in 5 mL of diphenyl ether and reacted for 24 h at 230 °C under argon atmosphere. Purification was performed by column chromatography (silica gel, PE/CH₂Cl₂ 2:1) to afford **2-31** as a yellow solid.

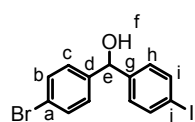
Yield: 170 mg (7.3 μmol), 85%. ¹H NMR Spectrum (500 MHz, C₂D₂Cl₄, 373 K) δ [ppm] = 7.31 (d, ³J(H,H) = 6 Hz, 2H, H_a), 7.23 (d, ³J(H,H) = 5.5 Hz, 4H, H_b), 6.81-6.75 (m, 80H, H_{arom.}), 6.52 (m, 20H, H_{arom.}). ¹³C NMR Spectrum (500 MHz, C₂D₂Cl₄, 373 K) δ [ppm] = 141.6, 141.3, 140.8, 140.7, 138.6, 134.8, 134.0, 131.9, 131.8, 131.4, 126.6, 126.5, 126.3, 125.1, 125.0. FD Mass Spectrum (8kV) m/z = 2031.4 (100%, (M)⁺) (calcd. 2028.6). Elemental Analysis for C₁₆₀H₁₀₆ Calcd.: C, 94.73; H, 5.27. Found: C, 93.90; H, 5.52.

2-36



2-12 (25 mg, 31.4 μmol) and **1-32** (190 mg, 0.49 mmol) were dissolved in 4 mL of toluene and reacted for 3-4 days at 120 °C under argon atmosphere. Purification was performed by column chromatography (silica gel, PE/CH₂Cl₂ 3:2) to afford **2-36** as a yellow solid.

Yield: 32 mg (8.8 μmol), 28%. ¹H NMR Spectrum (500 MHz, CD₂Cl₂, 300 K) δ [ppm] = 8.51 (s, 4H, H_a), 8.18 (s, 2H, H_b), 7.28, (2s, 8H, H_c), 7.24 (s, 8H, H_g), 7.16 (m, 40H, H_{arom.}), 7.11 (m, 4H, H_f), 6.94-6.83 (m, 120H, H_{arom.}). ¹³C NMR Spectrum (500 MHz, CD₂Cl₂, 300 K) δ [ppm] = 142.1, 142.1, 142.0, 141.3, 140.7, 140.4, 140.2, 140.0, 139.9, 139.6, 134.2, 132.9, 131.9, 131.8, 131.8, 131.5, 131.4, 130.3, 127.9, 127.5, 127.2, 127.1, 126.9, 126.7, 126.3, 126.0, 125.7, 121.9, 119.2, 96.4 (C_d), 87.2 (C_c). MALDI TOF Mass Spectrum m/z = 3647 (100%, (M)⁺), calcd. for C₂₈₈H₁₈₆ (3647).

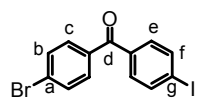
4-Bromo-4'-iodo-diphenylmethanol (**3-14**)

1,4-Diiodo-benzene (**3-12**) (50 g, 0.152 mol) was placed in 300 mL of dry diethyl ether at -78 °C under argon atmosphere. Within 60 min n-butyllithium (94.7 mL, 0.152 mol, 1.6 M in hexane) were added drop wise and the solution stirred for 2 h at this temperature. 4-Bromo-benzaldehyde (**3-13**) (30.9 g, 0.178 mol) were dissolved in 90 mL of diethyl ether and added to the solution within 5 min. The reaction mixture was stirred for another 2 h at -78 °C and then allowed to reach room temperature. 100 mL of H₂O were added, the solution stirred for 30 min and then extracted with diethyl ether. The organic layer was concentrated under reduced pressure and the crude product purified by column chromatography (silica gel, PE/CH₂Cl₂ 1:2) to afford **3-14** as a white solid.

Yield: 43 g (0.11 mol), 73 %. Mp: 122 °C. ¹H NMR Spectrum (250MHz, CD₂Cl₂, 300 K) δ [ppm] = 7.69-7.66 (d, ³J = 8.5 Hz, 2H, H_i), 7.51-7.48 (d, ³J = 8.5 Hz, 2H, H_b), 7.25-7.22

(d, $^3J = 8.5$ Hz, 2H, H_h), 7.13-7.09 (d, $^3J = 8.2$ Hz, 2H, H_c), 5.72 (s, 1H, H_f), 2.48 (s, 1H, H_e). ^{13}C NMR Spectrum (62.9 MHz, CD_2Cl_2 , 300 K) δ [ppm] = 143.7, 143.0, 137.9 (C_i), 131.9 (C_b), 128.8, 128.6, 121.8 (C_a), 93.4 (C_j), 75.2 (C_e). FD Mass Spectrum (8kV) $m/z = 389.1$ (100%, (M)⁺) (calcd. 389.0). Elemental Analysis For C₁₃H₁₀BrIO Calcd.: C, 40.14; H, 2.59. Found: C, 38.86; H, 2.31.

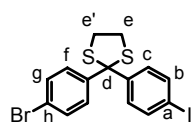
4-Bromo-4'-iodo-benzophenone (3-15)



10 mL of dry CH_2Cl_2 were placed in a flask under argon atmosphere and cooled to -78 °C under argon. Oxalyl chloride (0.24 mL, 2.83 mmol) was added through a septum and the solution was stirred for 15 min. Afterwards DMSO (0.4 mL, 5.65 mmol), dissolved in 2 mL of CH_2Cl_2 , was added and after 15 min of stirring **3-14** (1 g, 2.57 mmol), dissolved in 2 mL of CH_2Cl_2 was added and the solution stirred for another 15 min. Thereafter, TEA (1.81 mL, 12.9 mmol) was added and the solution allowed to warm to room temperature. Subsequent extraction with brine, 1% H_2SO_4 , H_2O and 5% NaHCO_3 gave the crude product which could be purified by recrystallisation from EtOH to give **3-15** as a white solid.

Yield: 920 mg (2.4 mmol), 93 %. Mp: 202 °C. ^1H NMR Spectrum (300MHz, CD_2Cl_2 , 300 K) δ [ppm] = 7.90-7.86 (d, $^3J(\text{H,H}) = 8.5$ Hz, 2H, H_c); 7.65 (s, 4H, H_{e+f}); 7.50-7.47 (d, $^3J(\text{H,H}) = 8.5$ Hz, 2H, H_b). ^{13}C NMR Spectrum (62.9 MHz, CD_2Cl_2 , 300 K) δ [ppm] = 194.9 (C_d), 138.1, 136.9, 136.3, 132.1, 131.8, 131.6, 127.9 (C_a), 100.5 (C_g). FD Mass Spectrum (8kV) $m/z = 387.3$ (100%, (M)⁺) (calcd. 387.0). Elemental Analysis for C₁₃H₈BrIO Calcd.: C, 40.35; H, 2.08. Found: C, 39.05; H, 2.42.

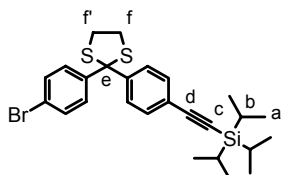
2-(4-Bromo-phenyl)-2-(4-iodo-phenyl)-[1,3]dithiolane (3-16)



3-15 (30 g, 77.5 mmol) was placed together with $\text{BF}_3 \cdot \text{OAc}_2$ in 300 mL of dry CH_2Cl_2 under argon atmosphere. Ethane-1,2-dithiol (13 mL, 0.145 mol) was added through a septum and the solution stirred for 20 min. Subsequent dilution with CH_2Cl_2 and extraction with H_2O , saturated NaHCO_3 , 15% NaOH and brine gave the crude product, which was purified by column chromatography (silica gel, PE/ CH_2Cl_2 3:1) to afford **3-16** as a white solid.

Yield: 31.9 g (68.9 mmol), 94 %. Mp: 93 °C. ^1H NMR Spectrum (250 MHz, CD_2Cl_2 , 300 K) δ [ppm] = 7.64-7.61 (d, $^3J(\text{H,H}) = 8.5$ Hz, 2H, H_b), 7.49-7.39 (m, 4H, H_{f+g}), 7.35-7.32 (d, $^3J(\text{H,H}) = 8.5$ Hz, 2H, H_c), 3.41 (s, 4H, H_{e+e'}). ^{13}C NMR Spectrum (62.9 MHz, CD_2Cl_2 , 300 K) δ [ppm] = 144.7, 143.9, 137.4, 131.4, 130.6, 130.4, 121.6 (C_h), 93.4 (C_a), 75.7 (C_d), 40.9 (C_{e+e'}). FD Mass Spectrum (8kV) $m/z = 463.0$ (100%, (M)⁺) (calcd 463.2). Elemental Analysis for C₁₅H₁₂BrIS₂ Calcd.: C, 38.90; H, 2.61. Found: C, 37.90; H, 2.73.

{4-[2-(4-Bromo-phenyl)-[1,3]dithiolan-2-yl]-phenylethynyl}-tris(isopropyl)silane (3-19)

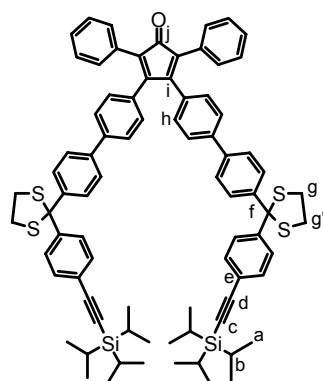


3-16 (5.0 g, 10.8 mmol) was suspended in 90 mL TEA and 20 mL toluene. Bis(triphenylphosphine)-palladium(II) dichloride (0.38 g, 0.54 mmol), copper(I) iodide (0.21 g, 0.11 mmol), and triphenylphosphine (0.28 g, 0.11 mmol) were added and the flask evacuated and flushed with argon several times. The reaction mixture was heated to 60 °C and triisopropylsilylethyne (2.9 mL, 12.9 mmol) was injected through a septum. After 15 min stirring at this temperature the reaction was heated to 80 °C and stirred over night under argon atmosphere. After cooling the reaction mixture was diluted with CH_2Cl_2 and 200 ml of H_2O and 100 mL of 2N HCl were added. The organic phase was

extracted with CH_2Cl_2 , saturated NH_4Cl , H_2O and dried over MgSO_4 to give the product **3-19** as a colorless oil.

Yield: 5.41 g (10.5 mmol), 97%. ^1H NMR Spectrum (250 MHz, CD_2Cl_2 , 300 K) δ [ppm] = 7.54-7.36 (m, 8H, $\text{H}_{\text{arom.}}$), 3.41 (s, 4H, $\text{H}_{\text{f+f'}}$), 1.13 (s, 21H, $\text{H}_{\text{a+b}}$). ^{13}C NMR Spectrum (62.9 MHz, CD_2Cl_2 , 300 K) δ [ppm] = 145.0, 144.2, 132.0, 131.4, 130.5, 128.5, 123.0, 121.7, 107.0 (C_d), 91.7 (C_c), 76.3 (C_e), 41.0 ($\text{C}_{\text{f+f'}}$), 18.9 (C_b), 11.8 (C_a). FD Mass Spectrum (8kV) m/z = 518.0 (100%, $(\text{M})^+$), calcd. for $\text{C}_{26}\text{H}_{33}\text{BrS}_2\text{Si}$ (517.7).

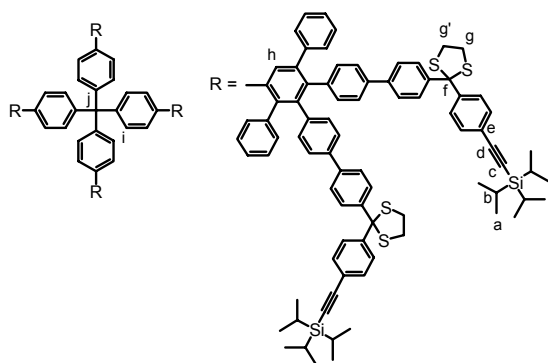
3,4-Bis-[4-(2-{4-[(triisopropylsilylethynyl)-ethynyl]-phenyl}-[1,3]dithiolan-2-yl)-phenyl]-2,5-diphenylcyclopentadienone (**3-21**)



3-20 (138 mg, 0.21 mmol) and **3-19** (250 mg, 0.48 mmol) were dissolved in 7.5 mL of toluene. 0.5 mL of EtOH and 2.5 mL of a solution of 0.8 g K_2CO_3 in H_2O (2.3M) were added and the reaction mixture was flushed with argon. $\text{Pd}(\text{PPh}_3)_4$ catalyst (110 mg, 0.095 mmol) was added and the reaction mixture was stirred at 80 °C for 16 h. The resulting solution was washed three times with $\text{CH}_2\text{Cl}_2/\text{H}_2\text{O}$. The organic layer was separated and dried over MgSO_4 . The crude product was purified by column chromatography (silica gel, PE/ CH_2Cl_2 3:2) to give **3-21** as a brown solid.

Yield: 0.21 g (0.17 mmol), 78 %. Mp: 172 °C. ^1H NMR Spectrum (250 MHz, CD_2Cl_2 , 300 K) δ [ppm] = 7.62-7.37 (m, 20H, $\text{H}_{\text{arom.}}$), 7.06-7.02 (d, 4H, H_h), 7.27 (s, 10H, $\text{H}_{\text{arom.}}$), 3.50-3.35 (m, 8H, $\text{H}_{\text{g+g'}}$), 1.13 (s, 42 H, $\text{H}_{\text{a+b}}$). ^{13}C NMR Spectrum (62.9 MHz, CD_2Cl_2 , 300 K) δ [ppm] = 200.4 (C_j), 154.5 (C_i), 145.5, 144.2, 140.6, 139.4, 132.6, 131.9, 131.4, 130.6, 130.4, 129.0, 128.4, 127.9, 126.7, 126.1, 122.7 (C_e), 107.0 (C_d), 91.5 (C_c), 76.5 (C_f), 40.8 ($\text{C}_{\text{g+g'}}$), 18.8 (C_b), 11.7 (C_a). FD Mass Spectrum (8kV) m/z = 1258 (100%, M^+) (calcd. 1258). Elemental Analysis for $\text{C}_{81}\text{H}_{84}\text{OS}_4\text{Si}_2$ Calcd.: C, 77.34; H, 6.73. Found: C, 78.33; H, 6.52.

3-27

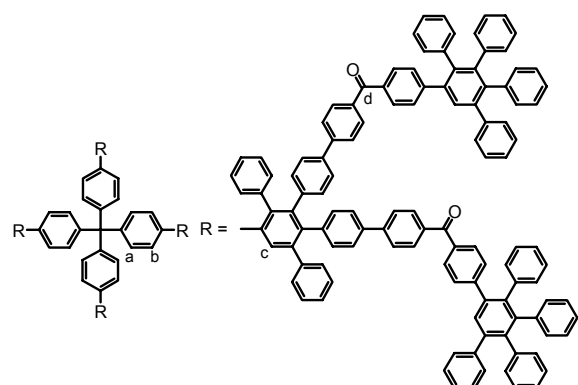


A mixture of **1-37** (33 mg, 79 μmol) and **3-21** (0.59 g, 0.47 mmol) was dissolved in 7 mL of *o*-xylene and refluxed for 16 hrs at 155 °C under argon atmosphere. The solvent was removed under reduced pressure and the crude product purified by column chromatography (silica gel, PE/ CH_2Cl_2 1:1) to afford **3-27** as a white solid.

Yield: 0.41 g (77 μmol), 97%. Mp: 295 °C (decomposition). ^1H NMR Spectrum (250 MHz, CD_2Cl_2 , 300 K) δ [ppm] = 7.61 (s, 4H, H_h), 7.55-

7.49 (m, 32H, $\text{H}_{\text{arom.}}$), 7.40-7.34 (m, 32H, $\text{H}_{\text{arom.}}$), 7.24-7.15 (m, 32H, $\text{H}_{\text{arom.}}$), 6.99-6.88 (m, 48H, $\text{H}_{\text{arom.}}$), 6.72-6.68 (d, $^3\text{J}(\text{H,H}) = 8.5$ Hz, 8H, H_i), 3.40 (s, 32H, $\text{H}_{\text{g+g'}}$), 1.12 (s, 168H, $\text{H}_{\text{a+b}}$). ^{13}C NMR Spectrum (75 MHz, CD_2Cl_2 , 300 K) δ [ppm] = 145.6, 145.0, 143.6, 143.6, 142.2, 141.7, 141.4, 141.3, 140.5, 140.3, 140.2, 134.0, 139.9, 139.8, 139.4, 137.7, 137.5, 133.0, 132.5, 132.5, 132.4, 132.3, 132.1, 131.9, 131.4, 130.8, 130.4, 129.2, 128.9, 128.9, 128.6, 128.1, 127.3, 127.0, 126.8, 126.6, 126.6, 126.1, 125.8, 125.5, 122.8 (C_e), 107.2 (C_d), 91.5 (C_c), 76.7 (C_f), 63.9 (C_j), 40.8 ($\text{C}_{\text{g+g'}}$), 18.9 (C_b), 11.8 (C_a). Elemental Analysis for

3-30

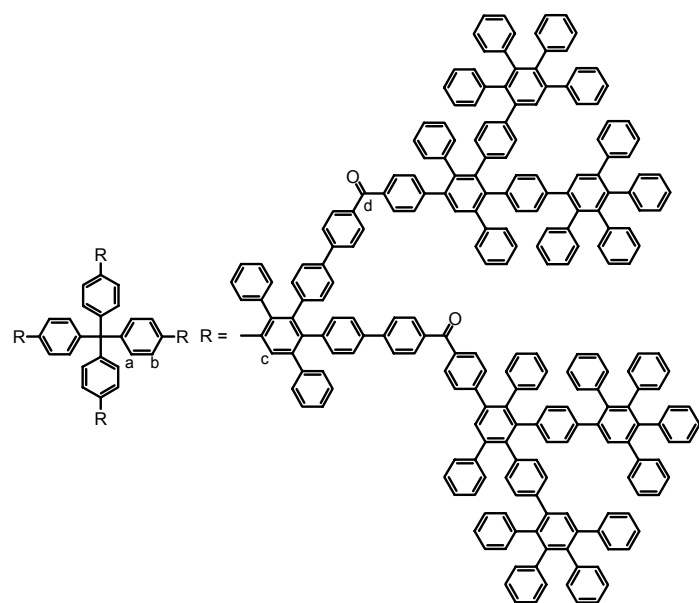


A mixture of **3-29** (75 mg, 21.3 μmol) and **1-32** (620 mg, 0.34 mmol) was dissolved in 6 mL of *o*-xylene and refluxed for 48 hrs at 160 $^{\circ}\text{C}$ under argon atmosphere. The solvent was removed under reduced pressure and the crude product purified by column chromatography (silica gel, PE/ CH_2Cl_2 1:1) to afford **3-30** as a white solid.

Yield: 131 mg (20.7 μmol), 97%. Mp: > 300 $^{\circ}\text{C}$. ^1H NMR Spectrum (250 MHz,

CD_2Cl_2 , 300 K) δ [ppm] = 7.73-7.68 (m, 16H, $\text{H}_{\text{arom.}}$), 7.64 (s, 4H, H_c), 7.59-7.54 (m, 40H, $\text{H}_{\text{arom.}}$), 7.33-7.17 (m, 90H, $\text{H}_{\text{arom.}}$), 7.04-7.03 (d, $^3\text{J}(\text{H,H}) = 8.1$ Hz, 8H, H_b), 7.01-6.87 (m, 166H, $\text{H}_{\text{arom.}}$), 6.74-6.71 (d, $^3\text{J}(\text{H,H}) = 8.5$ Hz, 8H, H_a). ^{13}C NMR Spectrum (175 MHz,
 CD_2Cl_2 , 300 K) δ [ppm] = 195.9 (C_d), 146.6, 145.1, 144.7, 142.5, 142.2, 141.6, 141.5, 141.5, 141.2, 140.8, 140.5, 140.3, 140.2, 140.0, 139.9, 139.3, 137.5, 137.2, 136.8, 136.0, 132.7, 132.7, 132.2, 132.0, 131.9, 131.9, 131.6, 131.4, 130.8, 130.5, 130.4, 130.3, 129.7, 129.3, 128.2, 128.1, 127.5, 127.4, 127.3, 127.1, 126.8, 126.8, 126.3, 126.2, 125.9 (all Ar-C). MALDI TOF Mass Spectrum $m/z = 6327$ (20%, $(\text{M})^+$), 4748 (100%, $(3/4\text{M})^+$), 3169 (50%, $(\text{M})^{2+}$) (calcd. 6328). UV/Vis (CHCl_3) λ [nm] = 313. Elemental Analysis for $\text{C}_{489}\text{H}_{324}\text{O}_8$ Calcd.: C, 92.82; H, 5.35. Found: C, 92.06; H, 6.03.

3-31



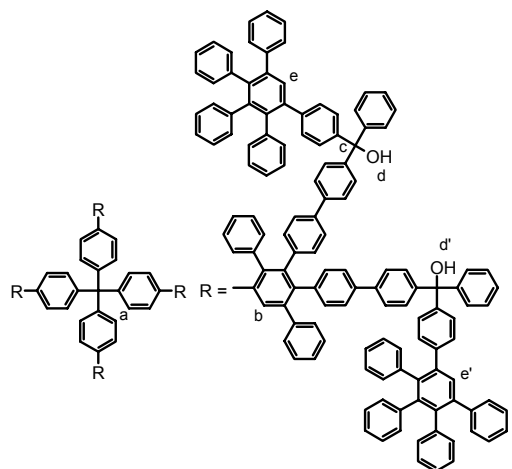
A mixture of **3-29** (34 mg, 9.8 μmol) and **1-44** (180 mg, 0.16 mmol) was dissolved in 6 mL of *o*-xylene and refluxed for 48 hrs at 170 $^{\circ}\text{C}$ under argon atmosphere. The solvent was removed under reduced pressure and the crude product purified by column chromatography (silica gel, PE/ CH_2Cl_2 1:1) to afford **3-31** as a white solid.

Yield: 110 mg (8.8 μmol), 90%. ^1H NMR Spectrum (500 MHz, d^8 -THF,
300 K) δ [ppm] = 7.67-7.53 (m, 44H, $\text{H}_{\text{arom.}}$), 7.45 (s, 8H), 7.40-7.30 (m, 20H, $\text{H}_{\text{arom.}}$), 7.24-6.67 (m, 540H, $\text{H}_{\text{arom.}}$), 6.61-6.47 (m, 32H, $\text{H}_{\text{arom.}}$).

^{13}C NMR Spectrum (175 MHz, d^8 -THF, 300 K) δ [ppm] = 194.8 (C_d), 154.6, 146.9, 145.5, 144.8, 142.8, 142.7, 142.7, 142.3, 142.1, 141.9, 141.8, 141.7, 141.5, 141.5, 141.4, 141.3, 141.3, 141.2, 141.1, 141.1, 141.0, 141.0, 140.9, 140.8, 140.3, 140.2, 140.2, 140.1, 140.0, 139.9, 139.6, 138.9, 137.7, 137.5, 137.3, 137.3, 136.5, 135.9, 135.2, 134.3, 134.2, 132.5, 132.4, 132.4, 131.9, 131.9, 131.8, 131.0, 130.8, 130.6, 130.4, 130.3, 130.2, 129.9, 129.8, 129.6, 129.3, 128.6, 128.4, 128.3, 128.0, 127.9, 127.6, 127.6, 127.3, 127.1, 126.9, 126.9, 126.4, 126.3, 126.2, 126.0, 126.0 (all Ar-C). MALDI TOF Mass Spectrum $m/z = 12515$ (20%, $(\text{M}+\text{Ag})^+$), 12451 (5%, $(\text{M}+\text{K})^+$), 6305 (50%, $(\text{M}+\text{Ag})^{2+}$), 3207 (100%, $(\text{M}+\text{Ag})^{4+}$),

calcd. for $C_{969}H_{644}O_8$ (12415).

3-32

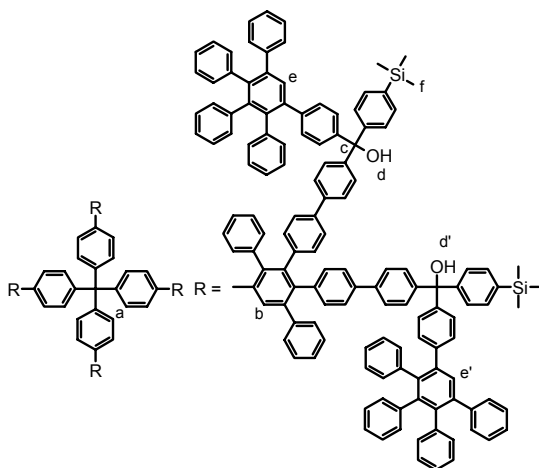


3-30 (600 mg, 94.8 μmol) was dissolved in 3 mL of dry THF under argon atmosphere. A solution of phenyllithium (5 mL, 10 mmol, 1.8-2.1M) in cyclohexane/ether (70:30) was added through a septum and the mixture heated for 16 h at 70 $^{\circ}\text{C}$. Afterwards 5 mL of H_2O were added, the mixture extracted with $\text{CH}_2\text{Cl}_2/\text{H}_2\text{O}$ and the organic solvent removed under reduced pressure. The crude product was purified by precipitating twice from MeOH.

Yield: 637 mg (91.6 μmol), 97 %. Mp: > 290 $^{\circ}\text{C}$ (decomposition). ^1H NMR Spectrum (500 MHz, CD_2Cl_2 , 300 K) δ [ppm] = 7.65 (s, 4H, H_b), 7.57&7.56 (2s, 8H, $\text{H}_{e+e'}$), 7.43-7.39 (m, 16H,

$\text{H}_{\text{arom.}}$), 7.27-6.90 (m, 328H, $\text{H}_{\text{arom.}}$), 6.76-6.74 (d, $^3\text{J}(\text{H,H}) = 7.9$ Hz, 8H, H_a), 2.85&2.84 (2s, 8H, $\text{H}_{d+d'}$). ^{13}C NMR Spectrum (175 MHz, CD_2Cl_2 , 300 K) δ [ppm] = 147.3, 146.3, 146.2, 145.1, 142.2, 142.1, 141.6, 141.3, 141.2, 140.9, 140.9, 140.5, 140.5, 140.2, 140.1, 139.9, 139.8, 139.6, 139.3, 137.8, 137.5, 132.5, 132.0, 131.9, 131.8, 131.4, 130.3, 129.8, 129.1, 127.6, 127.4, 127.2, 127.0, 126.7, 126.4, 126.4, 126.0, 125.7, 125.5, 81.9 (C_c). MALDI TOF Mass Spectrum $m/z = 6943$ (100%, $(\text{M})^+$), 6925 (60%, $(\text{M}-18 \equiv \text{OH})^+$), 6909 (40%, $(\text{M}-34 \equiv 2\cdot\text{OH})^+$) (calcd. 6943). Elemental Analysis for $C_{537}H_{372}O_8$ Calcd.: C, 92.77; H, 5.39. Found: C, 92.16; H, 5.66.

3-33



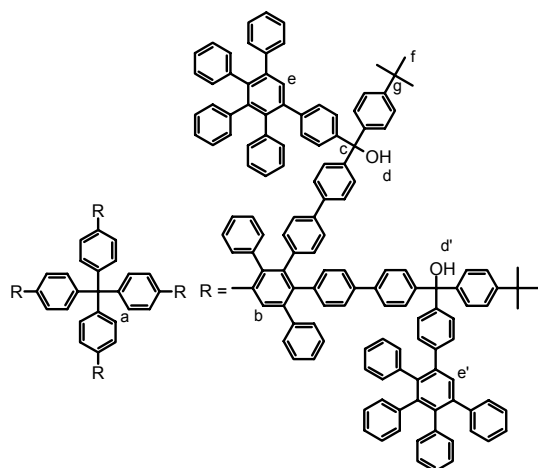
3-30 (250 mg, 39.5 μmol) was dissolved in 5 mL of dry THF under argon atmosphere (flask 1). In a second flask (4-bromo-phenyl)-trimethyl-silane (726 mg, 3.17 mmol) was dissolved in 5 mL of dry THF and cooled to -78 $^{\circ}\text{C}$. A solution of *t*-butyllithium in pentane (1.75 mL, 3.17 mmol, 1.7M) was added dropwise through a septum and the solution stirred for 1 h. The solution was allowed to reach -10 $^{\circ}\text{C}$ and transferred via canula in flask 1 and the resulting reaction mixture was stirred for 16 h at 70 $^{\circ}\text{C}$. Afterwards 5 mL of H_2O were added, the mixture extracted with $\text{CH}_2\text{Cl}_2/\text{H}_2\text{O}$ and the organic solvent

removed under reduced pressure. The crude white product was purified by precipitating twice from MeOH.

Yield: 285 mg (37.8 μmol), 96 %. Mp: > 300 $^{\circ}\text{C}$. ^1H NMR Spectrum (500 MHz, CD_2Cl_2 , 300 K) δ [ppm] = 7.61 (s, 4H, H_b), 7.53 (s, 8H, $\text{H}_{e+e'}$), 7.45-7.38 (m, 32H, $\text{H}_{\text{arom.}}$), 7.26-6.84 (m, 304H, $\text{H}_{\text{arom.}}$), 6.72-6.70 (d, $^3\text{J}(\text{H,H}) = 7.8$ Hz, 8H, H_a), 2.79&2.78 (2s, 8H, $\text{H}_{d+d'}$), 0.25 (s, 72H, H_f). ^{13}C NMR Spectrum (175 MHz, CD_2Cl_2 , 300 K) δ [ppm] = 147.7, 146.3, 146.2, 145.0, 144.9, 142.2, 142.1, 141.6, 141.2, 141.1, 140.9: 140.5, 140.5, 140.1, 139.8, 139.8, 139.6, 139.3, 137.8, 137.6, 133.3, 132.5, 132.4, 132.0, 131.9, 131.8, 131.4, 130.7, 130.3,

129.8, 129.1, 128.56, 128.5, 128.1, 127.9, 127.4, 127.4, 127.2, 126.9, 126.6, 126.4, 126.4, 126.0, 125.7, 125.4, 81.8 (C_c), -1.07 (C_f). MALDI TOF Mass Spectrum $m/z = 7519$ (100%, (M)⁺), 5656 (20%, (3/4M)⁺) (calcd. 7520). Elemental Analysis for C₅₆₁H₄₃₆O₈Si₈ Calcd.: C, 89.48; H, 5.84. Found: C, 89.52; H, 6.10.

3-34

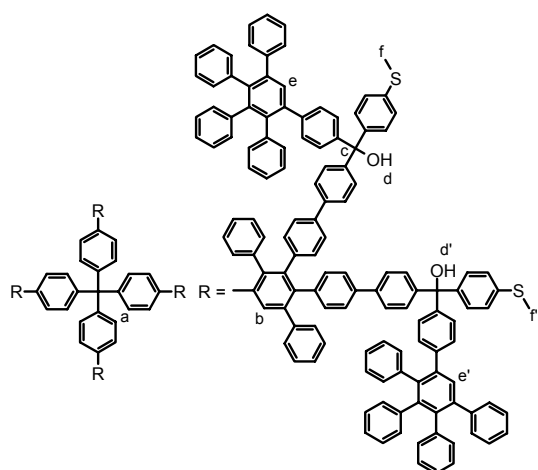


3-30 (100 mg, 15.8 μmol) was dissolved in 5 mL of dry THF under argon atmosphere (flask 1). In a second flask 1-bromo-4-*t*-butyl-benzene (539 mg, 2.53 mmol) was dissolved in 5 mL of dry THF and cooled to $-78\text{ }^\circ\text{C}$. A solution of *t*-butyllithium in pentane (1.34 mL, 2.28 mmol, 1.7M) was added dropwise through a septum and the solution stirred for 1 h. The solution was allowed to reach $-10\text{ }^\circ\text{C}$ and transferred via canula in flask 1 and the resulting reaction mixture was stirred for 24 h at $70\text{ }^\circ\text{C}$. 5 mL of H₂O were added through a septum and the reaction mixture extracted with CH₂Cl₂/H₂O. The

organic layer was concentrated under reduced pressure and the crude white product purified by precipitating twice from MeOH.

Yield: 91 mg (12.3 μmol), 78%. ¹H NMR Spectrum (700 MHz, CD₂Cl₂, 300 K) δ [ppm] = 7.60 (s, 4H, H_b), 7.53&7.52 (2s, 8H, H_{e+e'}), 7.41-7.37 (m, 16H, H_{arom.}), 7.30-7.28 (m, 16H, H_{arom.}), 7.25-7.03 (m, 155H, H_{arom.}), 7.00-6.83 (m, 165H, H_{arom.}), 6.71-6.70 (d, ³J(H,H) = 8.3 Hz, 8H, H_a), 2.76&2.75 (2s, 8H, H_{d+d'}), 1.30-1.29 (s, 72H, H_f). ¹³C NMR Spectrum (175 MHz, CD₂Cl₂, 300 K) δ [ppm] = 150.6, 146.5, 146.4, 145.3, 144.9, 144.3, 142.2, 142.1, 141.6, 141.3, 141.1, 140.9, 140.9, 140.6, 140.5, 140.2, 140.1, 139.9, 139.9, 139.8, 139.5, 139.4, 139.3, 137.9, 137.6, 132.5, 132.4, 132.1, 132.0, 131.9, 131.8, 131.4, 130.7, 130.4, 130.3, 129.8, 129.1, 128.5, 128.1, 127.9, 127.8, 127.4, 127.2, 126.9, 126.7, 126.6, 126.4, 126.3, 126.1, 126.0, 125.7, 125.4, 125.2, 81.7 (C_c), 34.7 (C_f), 31.5 (C_g). MALDI TOF Mass Spectrum $m/z = 7440$ (20%, (M+K)⁺), 7385 (100%, (M-17 \equiv OH)⁺), 7367 (40%, (M-35 \equiv 2·OH)⁺), calcd. for C₅₆₉H₄₃₆O₈ (7402).

3-35

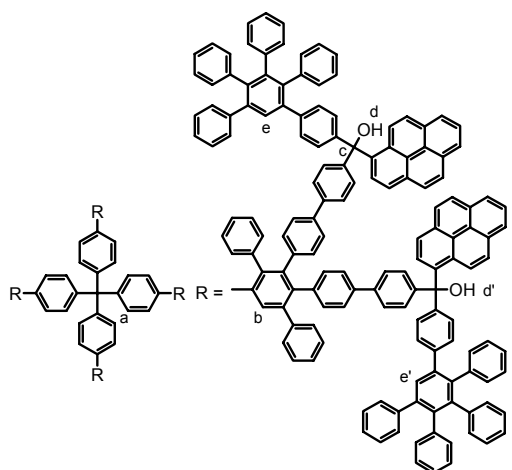


3-30 (75 mg, 11.9 μmol) was dissolved in 5 mL of dry THF under argon atmosphere (flask 1). In a second flask 4-bromo-thioanisole (241 mg, 1.19 mmol) was dissolved in 5 mL of dry THF and cooled to $-78\text{ }^\circ\text{C}$. A solution of *t*-butyllithium in pentane (0.6 mL, 1.02 mmol, 1.7M) was added dropwise through a septum and the solution stirred for 1 h. The solution was allowed to reach $-10\text{ }^\circ\text{C}$ and transferred via canula in flask 1 and the resulting reaction mixture was stirred for 24 h at $70\text{ }^\circ\text{C}$. 5 mL of H₂O were added through a septum and the reaction mixture extracted with CH₂Cl₂/H₂O. The organic layer was concentrated

under reduced pressure and the crude white product purified by precipitating twice from MeOH.

Yield: 65 mg (8.9 μmol), 75%. **^1H NMR Spectrum (500 MHz, CD_2Cl_2 , 300 K)** δ [ppm] = 7.61 (s, 4H, H_b), 7.52&7.52 (2s, 8H, $\text{H}_{e+e'}$), 7.40-7.37 (m, 16H, $\text{H}_{\text{arom.}}$), 7.25-6.83 (m, 320H, $\text{H}_{\text{arom.}}$), 6.71-6.70 (d, $^3\text{J}(\text{H},\text{H}) = 8.1$ Hz, 8H, H_a), 2.78&2.77 (2s, 8H, $\text{H}_{d+d'}$), 2.45&2.43 (s, 24H, $\text{H}_{f+f'}$). **^{13}C NMR Spectrum (125 MHz, CD_2Cl_2 , 300 K)** δ [ppm] = 146.1, 146.1, 144.9, 144.0, 142.1, 142.0, 141.5, 141.2, 141.1, 140.8, 140.5, 140.4, 140.1, 140.0, 139.8, 139.7, 139.6, 139.2, 138.0, 137.7, 137.4, 132.4, 132.4, 131.9, 131.8, 131.8, 132.0, 131.3, 130.6, 130.2, 130.3, 129.8, 129.1, 128.6, 128.4, 128.0, 127.9, 127.3, 127.1, 127.1, 126.9, 126.6, 126.4, 126.3, 125.9, 125.9, 125.7, 125.4, 81.5 (C_c), 15.7, (C_f). **MALDI TOF Mass Spectrum** $m/z = 7305$ (100%, ($\text{M}-16 \equiv \text{OH}$) $^+$), 7288 (40%, ($\text{M}-33 \equiv 2\cdot\text{OH}$) $^+$), 7273 (10%, ($\text{M}-58 \equiv 3\cdot\text{OH}$) $^+$), calcd. for $\text{C}_{545}\text{H}_{388}\text{O}_8\text{S}_8$ (7321). **Elemental Analysis for $\text{C}_{142}\text{H}_{90}\text{O}$** Calcd.: C, 89.41; H, 5.34. Found: C, 89.15; H, 5.30.

3-36

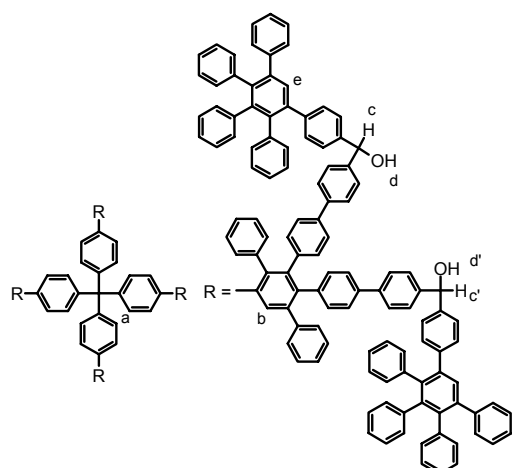


3-30 (100 mg, 15.8 μmol) was dissolved in 5 mL of dry THF under argon atmosphere (flask 1). In a second flask 1-bromopyrene (356 mg, 1.27 mmol) was dissolved in 5 mL of dry THF and cooled to -78 $^{\circ}\text{C}$. A solution of *t*-butyllithium in pentane (0.67 mL, 1.14 mmol, 1.7M) was added dropwise through a septum and the solution stirred for 1 h. The solution was allowed to reach -10 $^{\circ}\text{C}$ and transferred via canula in flask 1 and the resulting reaction mixture stirred at 70 $^{\circ}\text{C}$. After 3 days the same amount of freshly lithiated 1-bromopyrene was added and the reaction mixture was stirred for 3 more days at 70 $^{\circ}\text{C}$. 5 mL of H_2O was added

through a septum and the reaction mixture extracted with $\text{CH}_2\text{Cl}_2/\text{H}_2\text{O}$. The organic layer was concentrated under reduced pressure and the crude product was precipitated from hexane. Subsequent column chromatography (silica gel, hexane/ethyl acetate 1:1) gave **3-36** as a brown solid.

Yield: 95 mg (11.9 μmol), 76%. **^1H NMR Spectrum (700 MHz, $\text{d}^8\text{-THF}$, 300 K)** δ [ppm] = 8.37-8.34 (m, 8H, H_{pyrene}), 8.20-7.94 (m, 56H, H_{pyrene}), 7.86-7.82 (m, 8H, H_{pyrene}), 7.60 (s, 4H, H_b), 7.56&7.55 (2s, 8H, $\text{H}_{e+e'}$), 7.46-7.42 (m, 16H, $\text{H}_{\text{arom.}}$), 7.30-6.82 (m, 453H, $\text{H}_{\text{arom.}}$), 6.71-6.70 (d, $^3\text{J}(\text{H},\text{H}) = 7.7$ Hz, 8H, H_a), 3.45&3.45 (2s, 8H, $\text{H}_{d+d'}$). **^{13}C NMR Spectrum (175 MHz, $\text{d}^8\text{-THF}$, 300 K)** δ [ppm] = 146.8, 146.8, 145.8, 145.0, 142.4, 142.2, 142.0, 141.6, 141.3, 141.1, 141.1, 140.9, 140.7, 140.6, 140.4, 140.2, 140.2, 140.2, 140.0, 139.9, 139.8, 139.5, 139.3, 137.8, 137.5, 132.6, 132.5, 132.0, 131.9, 131.9, 131.8, 131.7, 131.4, 131.3, 130.8, 130.7, 130.4, 130.3, 130.0, 129.9, 129.7, 129.2, 128.6, 128.2, 128.1, 128.0, 127.9, 127.7, 127.5, 127.4, 127.2, 127.0, 126.8, 126.6, 126.6, 126.5, 126.3, 126.0, 125.7, 125.7, 125.5, 125.0, 123.9, 83.6 (C_d). **MALDI TOF Mass Spectrum** $m/z = 8062$ (20%, ($\text{M}+\text{Ag}$) $^+$), 7985 (100%, ($\text{M}+\text{K}$) $^+$), 7968 (10%, ($\text{M}+\text{Na}$) $^+$), 7929 (70%, ($\text{M}-17 \equiv \text{OH}$) $^+$), 7911 (40%, ($\text{M}-35 \equiv 2\cdot\text{OH}$) $^+$) (calcd. 7946). **Elemental Analysis for $\text{C}_{617}\text{H}_{404}\text{O}_8$** Calcd.: C, 93.26; H, 5.12. Found: C, 93.58; H, 6.21. **UV/Vis (CHCl_3)** λ [nm] = 269 (40800), 280 (44000), 331 (19700), 348 nm (27400 $\text{m}^2\text{mol}^{-1}$).

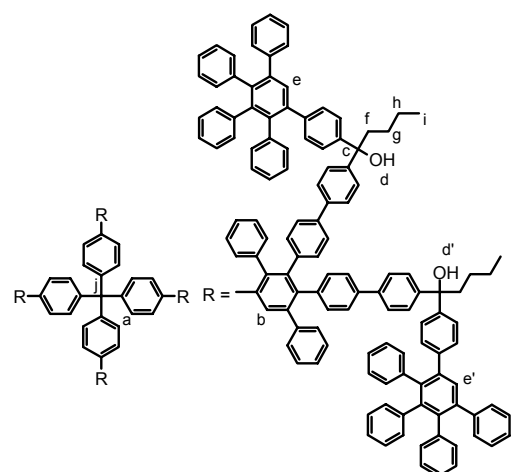
3-37



3-30 (75 mg, 11.9 μmol) was placed in a dry flask under argon atmosphere. A solution of LiAlH_4 in THF (2 mL, 2 mmol, 1M) was added slowly through a septum and the reaction mixture stirred for 48 h at 70 $^\circ\text{C}$. Ice was added slowly until no more hydrogen formation was observed. The resulting suspension was filtered, the residue washed with CH_2Cl_2 and the filtrate afterwards extracted with $\text{CH}_2\text{Cl}_2/\text{H}_2\text{O}$. The organic solvent was removed under reduced pressure and the crude product precipitated from MeOH to give **3-37** as a white solid.

Yield: 60 mg (9.46 μmol), 80%. ^1H NMR Spectrum (700 MHz, CD_2Cl_2 , 300 K) δ [ppm] = 7.61 (s, 4H, H_b), 7.49 (s, 8H, H_e), 7.43-7.39 (m, 16H, $\text{H}_{\text{arom.}}$), 7.28-7.13 (m, 130H, $\text{H}_{\text{arom.}}$), 6.99-6.82 (m, 190H, $\text{H}_{\text{arom.}}$), 6.72-6.71 (d, $^3\text{J}(\text{H},\text{H}) = 7.0$ Hz, 8H, H_a), 5.74&5.73 (2s, 8H, $\text{H}_{d+d'}$), 2.24&2.23 (2s, 8H, $\text{H}_{c+c'}$). ^{13}C NMR Spectrum (175 MHz, CD_2Cl_2 , 300 K) δ [ppm] = 144.9, 143.4, 143.3, 142.4, 142.2, 142.2, 141.6, 141.4, 141.3, 141.2, 140.9, 140.8, 140.5, 140.5, 140.1, 140.0, 139.9, 139.7, 139.7, 139.3, 138.0, 137.7, 132.4, 132.4, 132.1, 131.9, 131.8, 131.6, 131.4, 130.7, 130.4, 130.3, 129.1, 129.0, 128.1, 127.9, 127.2, 127.2, 127.1, 127.0, 127.0, 126.9, 126.7, 126.6, 126.1, 126.0, 126.0, 125.7, 125.5. 75.83 (C_c). MALDI TOF Mass Spectrum $m/z = 6933$ (100%, $(\text{M}+\text{Ag})^+$) (calcd. 6825). Elemental Analysis for $\text{C}_{537}\text{H}_{372}$ Calcd.: C, 92.58; H, 5.40. Found: C, 92.97; H, 5.05.

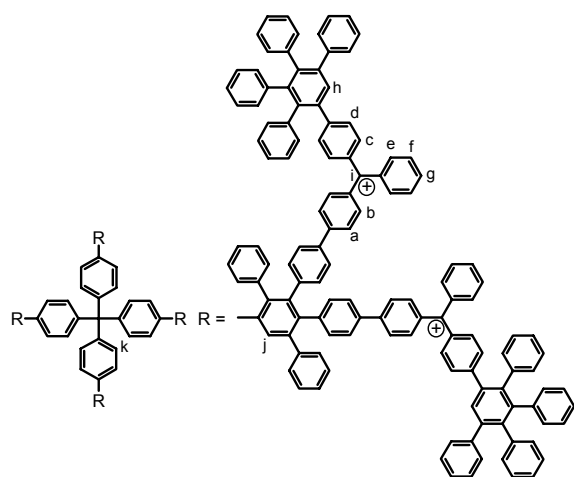
3-38



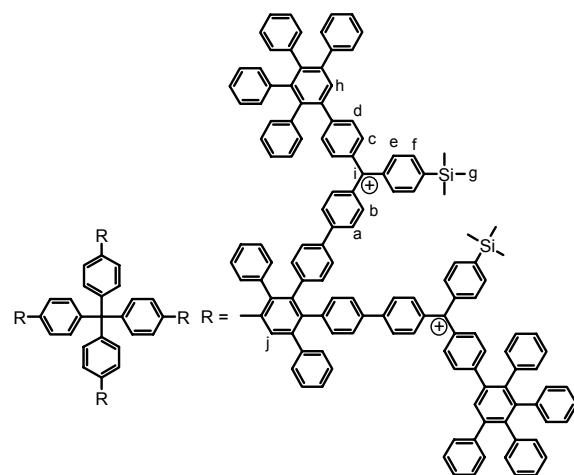
3-30 (50 mg, 7.9 μmol) was dissolved in 3 mL of dry THF under argon atmosphere. A solution of *n*-butyllithium (2 mL, 3.2 mmol, 1.6M in hexane) was added through a septum and the mixture heated for 16 h at 70 $^\circ\text{C}$. Afterwards 5 mL of H_2O were added, the mixture extracted with $\text{CH}_2\text{Cl}_2/\text{H}_2\text{O}$ and the organic solvent removed under reduced pressure. The crude product was purified by precipitating twice from MeOH.

Yield: 46 mg (6.8 μmol), 85 %. ^1H NMR Spectrum (500 MHz, CD_2Cl_2 , 300 K) δ [ppm] = 7.63 (s, 4H, H_b), 7.53 (s, 8H, $\text{H}_{e+e'}$), 7.43-6.86 (m, 304H, $\text{H}_{\text{arom.}}$), 6.74-6.73 (d, $^3\text{J}(\text{H},\text{H}) = 8.0$ Hz, 8H, H_a), 2.20 (t, $^3\text{J}(\text{H},\text{H}) = 3.5$ Hz, 16H, H_f), 2.11&2.12 (2s, 8H, $\text{H}_{d+d'}$), 1.30-1.33 (m, 16H, H_g), 1.18 (sb, 16H, H_h), 0.87 (t, 24H, H_i). ^{13}C NMR Spectrum (175 MHz, CD_2Cl_2 , 300 K) δ [ppm] = 146.7, 146.6, 145.7, 144.9, 142.4, 142.2, 142.1, 141.6, 141.3, 141.1, 140.9, 140.6, 140.5, 140.1, 140.0, 139.9, 139.8, 139.7, 139.3, 139.0, 137.9, 137.7, 132.4, 132.4, 132.0, 131.9, 131.8, 131.5, 130.7, 130.3, 130.3, 130.0, 129.1, 128.0, 127.9, 127.2, 127.2, 126.9, 126.7, 126.6, 126.6, 126.5, 126.1, 125.9, 125.7, 125.6, 125.4, 78.1 (C_c), 63.8 (C_j), 41.9 (C_f), 26.2 (C_g), 23.4 (C_h), 14.2 (C_i). MALDI TOF Mass Spectrum $m/z = 6841$ (50%, $(\text{M}+\text{K})^+$), 6785 (100%, $(\text{M})^+$), 6928 (90%, $(\text{M}-\text{butyl})^+$), 6671 (50%, $(\text{M}-2\cdot\text{butyl})^+$) (calcd. 6793). Elemental Analysis for $\text{C}_{521}\text{H}_{404}\text{O}_8$ Calcd.: C, 92.12; H, 5.99.

Preparation of the poly(trityl) cations **15a-15d**. For example: **14a** (50 mg, 7.2 μmol) was dissolved in a NMR tube in 0.5 mL of CD_2Cl_2 and 0.2 mL of deuterated trifluoroacetic acid was added whereupon the solution immediately turned deep blue due to the quantitative formation of **15a**. Solid poly(trityl) cations could be obtained after reaction of the alcoholic precursors with $\text{BF}_3 \cdot \text{OEt}_2$. Representative: **3-39** (75 mg, 10.8 μmol) was dissolved in 10 mL of dry CH_2Cl_2 . $\text{BF}_3 \cdot \text{OEt}_2$ (0.2 mL, 1.58 mmol) was added through a septum whereupon the color of the solution immediately turned deep blue. The solution was stirred for 30 min and the solvent afterwards removed under reduced pressure at ambient temperature. Further drying in high vacuum gave the poly(trityl) cations in quantitative yield.

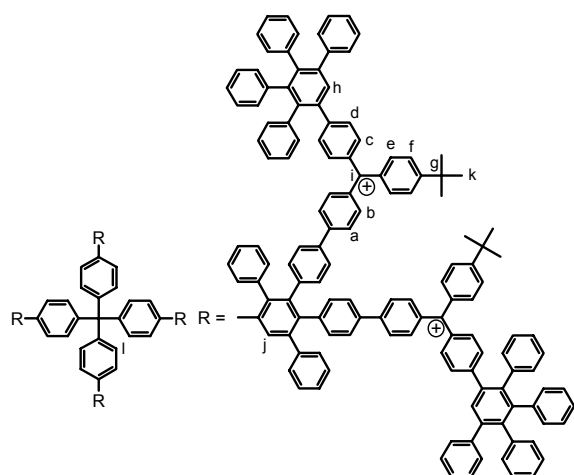
3-39

^1H NMR Spectrum (500 MHz, $\text{CD}_2\text{Cl}_2/\text{TFA}$, 300 K) δ [ppm] = 8.18&8.17 (2t, 8H, H_g), 8.08&8.06 (2d, 16H, H_a), 7.84-7.83 (m, 16H, H_f), 7.81-7.80 (m, 12H, H_{j+h}), 7.73-7.62 (m, 70H, $\text{H}_{\text{arom.}}$), 7.59&7.57 (2d, 16H, H_e), 7.52&7.50 (2d, 16H, H_c), 7.33-7.28 (m, 86H, $\text{H}_{\text{arom.}}$), 7.14-6.96 (m, 181H, $\text{H}_{\text{arom.}}$), 6.90-6.88 (d, $^3\text{J}(\text{H},\text{H}) = 8.1$ Hz, 8H, H_k). ^{13}C NMR Spectrum (125 MHz, $\text{CD}_2\text{Cl}_2/\text{d-TFA}$, 300 K) δ [ppm] = 203.6 (C_i), 159.2, 159.1, 155.9, 145.9, 145.7, 145.5, 143.7, 143.6, 143.5, 142.9, 142.7, 142.2, 142.1, 141.9, 141.7, 141.1, 140.8, 140.7, 140.4, 140.2, 139.3, 138.6, 135.2, 135.0, 134.1, 134.0, 133.0, 132.8, 132.6, 132.2, 132.0, 131.6, 131.3, 130.8, 130.6, 129.6, 129.0, 128.7, 128.6, 128.3, 127.9, 127.7, 127.6, 127.4, 126.9, 126.8, 126.7 (all Ar-C).

3-40

^1H NMR Spectrum (500 MHz, $\text{CD}_2\text{Cl}_2/\text{TFA}$, 300 K) δ [ppm] = 8.01&7.99 (2d, 16H, H_a), 7.95&7.94 (2d, 16H, H_f), 7.74 (s, 8H, H_h), 7.73 (s, 4H, H_j), 7.66-7.56 (m, 50H, $\text{H}_{\text{arom.}}$), 7.47 (2d, 16H, H_e), 7.43 (2d, 16H, H_c), 7.25-7.21 (m, 72H, $\text{H}_{\text{arom.}}$), 7.07-6.81 (m, 157H, $\text{H}_{\text{arom.}}$), 0.40 (s, 72H, H_g). ^{13}C NMR Spectrum (125 MHz, $\text{CD}_2\text{Cl}_2/\text{d-TFA}$, 300 K) δ [ppm] = 203.6 (C_i), 159.0, 158.9, 155.7, 145.9, 145.8, 145.5, 143.9, 143.9, 143.7, 143.7, 143.4, 143.0, 142.8, 142.3, 142.2, 142.1, 141.8, 140.9, 140.8, 140.6, 140.5, 140.4, 140.4, 140.3, 140.3, 139.9: 139.5, 139.4, 138.8, 138.8, 138.7, 135.7, 135.4, 135.2, 134.2, 134.2, 133.0, 132.9, 132.7, 132.3, 132.2, 131.8, 131.5, 131.0, 130.7, 129.8, 129.1, 128.8, 128.7, 128.4, 128.0, 127.9, 127.8, 127.7, 127.7, 127.7, 127.5, 127.1, 126.9, 126.8 (all Ar-C), -1.67 (C_g).

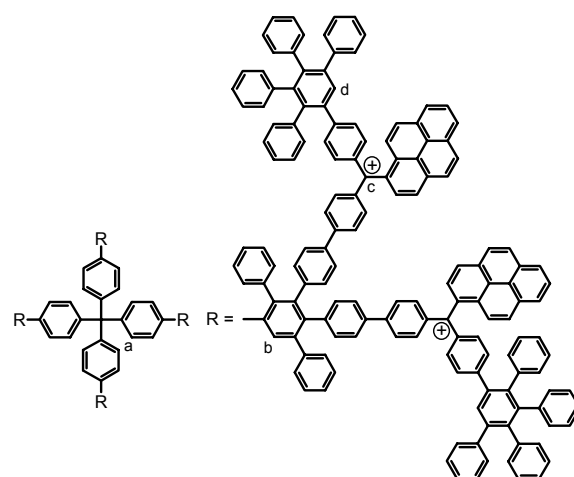
3-41



^1H NMR Spectrum (500 MHz, $\text{CD}_2\text{Cl}_2/\text{TFA}$, 300 K) δ [ppm] = 8.00&7.98 (2d, 16H, H_a), 7.85&7.84 (2d, 16H, H_f), 7.75-7.73 (m, 12H, H_{j+h}), 7.65-7.50 (m, 68H, H_{arom}), 7.51 (2d, 16H, H_e), 7.42 (2d, 16H, H_c), 7.27-7.22 (m, 84H, H_{arom}), 7.10-6.95 (m, 154H, H_{arom}), 6.90-6.89 (m, 16H, H_{arom}), 6.84-6.82 (d, $^3\text{J}(\text{H},\text{H}) = 8.1$ Hz, 8H, H_i), 1.47&1.46 (2s, 72H, H_k). ^{13}C NMR Spectrum (125 MHz, $\text{CD}_2\text{Cl}_2/\text{d-TFA}$, 300 K) δ [ppm] = 201.8 (C_i), 169.7, 161.5, 161.1, 160.8, 160.4, 157.7, 157.6, 154.7, 145.4, 145.2, 144.8, 143.4, 143.4, 143.1, 143.0, 142.6, 142.5, 142.3, 141.9, 141.7, 140.9, 140.9, 140.6,

140.3, 140.2, 140.0, 139.8, 138.9, 138.9, 138.5, 138.4, 138.2, 137.9, 135.1, 134.9, 133.7, 133.7, 132.4, 132.3, 131.9, 131.8, 131.3, 131.0, 130.5, 130.4, 129.4, 128.6, 128.5, 128.4, 128.3, 128.0, 127.6, 127.4, 127.4, 127.3, 127.2, 127.2, 127.1, 126.7, 126.5, 126.4, 118.4, 116.1, 113.8, 111.6 (all Ar-C), 37.3, 37.2 (all C_k), 30.8, 30.7 (all C_g).

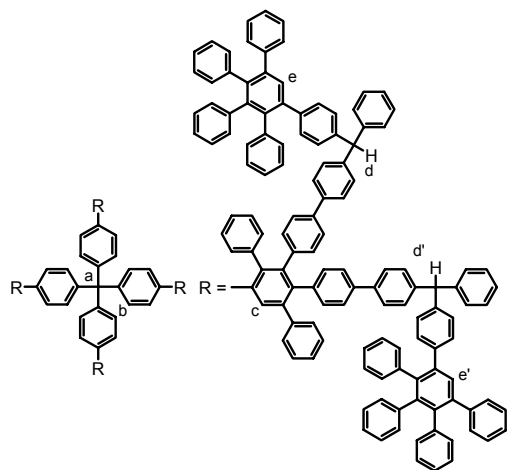
3-42



^1H NMR Spectrum (500 MHz, $\text{CD}_2\text{Cl}_2/\text{TFA}$, 300 K) δ [ppm] = 8.64&7.60 (4d, 16H, H_{pyrene}), 8.48 (2d, 8H, H_{pyrene}), 8.30-8.24 (m, 24H), 8.18 (2d, 8H, H_{pyrene}), 7.95 (m, 16H, H_{arom}), 7.84-7.77 (m, 16H, H_{arom}), 7.74 (s, 8H, H_d), 7.73 (s, 4H, H_b), 7.60-7.50 (m, 40H, H_{arom}), 7.42 (m, 16H, H_{arom}), 7.28-7.20 (m, 76H, H_{arom}), 7.01-6.89 (156H, H_{arom}), 6.85-6.83 (d, $^3\text{J}(\text{H},\text{H}) = 8.2$ Hz, 8H, H_a). ^{13}C NMR Spectrum (175 MHz, $\text{CD}_2\text{Cl}_2/\text{d-TFA}$, 300 K) δ = [ppm] 196.1 (C_c), 153.4, 143.7, 143.2, 143.1, 142.8, 142.3, 142.2, 142.1, 141.8, 141.4, 140.8, 140.6, 140.5, 140.4, 140.3,

140.0, 139.0, 138.7, 137.2, 135.8, 134.2, 134.0, 134.0, 133.0, 132.6, 132.2, 132.1, 131.6, 131.4, 130.9, 130.7, 129.7, 129.4, 129.0, 129.0, 128.7, 128.6, 128.2, 127.9, 127.7, 127.6, 127.6, 127.5, 127.4, 127.3, 127.0, 126.9, 126.7, 126.7, 126.5, 124.1.

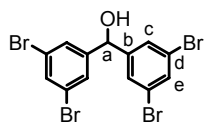
3-43



3-39 (50 mg, 7.3 μmol) was dissolved in 10 mL of dry CH_2Cl_2 under argon atmosphere at 0°C . Triethylsilane (0.11 mL, 0.68 mmol) was added through a septum whereupon the solution quickly decolorized. After 10 min of stirring, the organic layer was extracted with saturated NaHCO_3 , H_2O and afterwards evaporated to dryness to give the crude product. Further purification was achieved by precipitation from MeOH to give **3-43** as white solid.

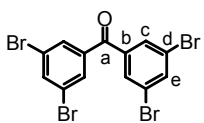
Yield: 45 mg (6.6 μmol), 90%. ^1H NMR Spectrum (700 MHz, CD_2Cl_2 , 300 K) $\delta = 7.62$ (s, 4H, H_c), 7.55&7.54 (2s, 8H, $\text{H}_{e+e'}$), 7.41-7.37 (m, 16H,

$\text{H}_{\text{arom.}}$), 7.26-6.84 (m, 328H, $\text{H}_{\text{arom.}}$), 6.74-6.71 (d, $^3\text{J}(\text{H,H}) = 8.3$ Hz, 8H, H_b), 5.47&5.46 (2s, 8H, $\text{H}_{d+d'}$). ^{13}C NMR Spectrum (175 MHz, CD_2Cl_2 , 300 K) $\delta = 144.9$, 144.3, 143.4, 143.4, 142.2, 142.2, 142.1, 141.7, 141.3, 141.1, 141.1, 140.9, 140.6, 140.6, 140.5, 140.4, 140.1, 134.0, 139.9, 139.7, 139.6, 139.4, 138.8, 138.0, 137.8, 132.5, 132.4, 132.1, 132.0, 131.9, 131.9, 131.4, 130.7, 130.4, 130.3, 130.3, 130.0, 129.7, 129.2, 128.9, 128.6, 128.1, 127.9, 127.2, 127.2, 127.0, 126.9, 126.8, 126.7, 126.6, 126.0, 125.7, 125.6, 125.4 (all Ar-C), 63.9 (C_a), 56.4 (C_d). MALDI TOF Mass Spectrum $m/z = 6933$ (100%, $(\text{M}+\text{Ag})^+$) (calcd. for $\text{C}_{537}\text{H}_{372}$, 6825).

Bis-(3,5-dibromo-phenyl)-methanol (3-49)

1,3,5-Tribromobenzene (**1-27**) (2.6 g, 8.3 mmol) was placed in 150 mL of dry diethyl ether at -78°C under argon atmosphere. Within 60 min *n*-butyllithium (5.07 mL, 8.3 mmol, 1.6 M in hexane) were added dropwise and the solution stirred for 2 h at this temperature. 3,5-dibromobenzaldehyde (**3-48**) (2.4 g, 9.1 mmol) were dissolved in 30 mL of diethyl ether and added to the solution within 5 min. The reaction mixture was stirred for another 2 h at -78°C and then allowed to reach room temperature. 100 mL of MeOH were added and the solution stirred for 30 min. The organic layer was concentrated under reduced pressure and the crude product purified by column chromatography (silica gel, PE/ CH_2Cl_2 1:2) to afford **3-49** as a white solid.

Yield: 3.3 g (6.6 mmol) 80 %. ^1H NMR Spectrum (700 Mhz, $\text{C}_2\text{D}_2\text{Cl}_4$, 353 K) δ [ppm] = 7.88 (s, 2H, H_e), 7.69 (s, 4H, H_c). ^{13}C NMR Spectrum (175 MHz, $\text{C}_2\text{D}_2\text{Cl}_4$, 353 K) δ [ppm] = 146.5 (C_b), 134.1 (C_e), 128.6 (C_c), 123.7 (C_d), 74.2 (C_a). FD Mass Spectrum (8kV) $m/z = 499.8$ (100%, $(\text{M})^+$) (calcd. 499.8). Elemental Analysis for $\text{C}_{13}\text{H}_8\text{Br}_4\text{O}$ Calcd.: C, 31.24; H, 1.61. Found: C, 31.33; H, 1.62.

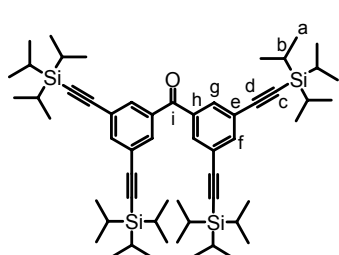
2,2',4,4'-Tetrabromo-benzophenone (3-50)

25 mL of dry CH_2Cl_2 were placed in a flask under argon atmosphere and cooled to -78°C under argon atmosphere. Oxalyl chloride (1.1 mL, 2.15 mmol) was added through a septum and the solution was stirred for 15 min. Afterwards DMSO (0.31 mL, 4.41 mmol), dissolved in 2 mL of CH_2Cl_2 , was added and after 15 min of stirring **3-49** (1 g, 2.0 mmol), dissolved in 2 mL of CH_2Cl_2 , was added and the solution stirred for another 15 min. Thereafter TEA (1.41 mL, 10.0 mmol) was added and the solution allowed to reach room temperature. Subsequent

extraction with brine, 1% H₂SO₄, H₂O and 5% NaHCO₃ gave the crude product which could be purified by recrystallisation from EtOH to give **3-50** as a white solid.

Yield: 846 mg (1.7 mmol), 85 %. ¹H NMR Spectrum (700 MHz, C₂D₂Cl₄, 353 K) δ [ppm] = 7.89 (s, 4H, H_c), 7.74 (s, 8H, H_e). ¹³C NMR Spectrum (175MHz, C₂D₂Cl₄, 353 K) δ [ppm] = 190.8 (C_a), 139.7 (C_b), 138.6 (C_e), 131.4 (C_c), 123.8 (C_d). FD Mass Spectrum (8kV) m/z = 497.9 (100%, (M)⁺) (calcd. 497.8). Elemental Analysis for C₁₃H₆Br₄O Calcd.: C, 31.37; H, 1.21. Found: C, 31.38; H, 1.26.

2,2',4,4'-Tetra-[ethynyl(triisopropylsilyl)]-benzophenone (**3-51**)

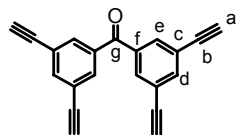


3-50 (3.6 g, 7.23 mmol) was suspended in 60 mL of TEA and 20 mL of toluene. Bis(triphenylphosphine)palladium(II) dichloride (1.02 g, 1.45 mmol), copper(I) iodide (550 mg, 2.89 mmol), and triphenylphosphine (1.02 g, 1.45 mmol) were added and the flask evacuated and flushed with argon for several times. Under stirring the reaction mixture was heated to 60 °C and tri-*isopropylsilyl*ethyne (9.65 mL, 43.4 mmol) was injected

through a septum. After 15 min stirring at this temperature the reaction was heated to 80 °C and stirred over night under argon atmosphere. After cooling the reaction mixture was diluted with CH₂Cl₂ and extracted with H₂O. The organic phase was dried over MgSO₄, and the solvent was removed under reduced pressure. The crude product was purified by column chromatography (silica gel, PE/CH₂Cl₂ 100:4) to afford **3-51** as a white solid.

Yield: 3.87 g (4.3 mmol), 60%. ¹H NMR Spectrum (500 MHz, CD₂Cl₂, 300K) δ [ppm] = 7.78-7.79 (m, 6H, H_{arom.}), 1.14 (s, 84H, H_{a+b}). ¹³C NMR Spectrum (175 MHz, CD₂Cl₂, 300 K) δ [ppm] = 193.9 (C_i), 139.1 (C_f), 137.8 (C_h), 133.0 (C_g), 124.8 (C_e), 105.2 (C_d), 93.6 (C_c), 18.9 (C_b), 11.8 (C_a). FD Mass Spectrum (8kV) m/z = 902.8 (100%, (M)⁺) (calcd. 903.7). Elemental Analysis for C₅₇H₉₀OSi₄ Calcd.: C, 75.76; H, 10.04. Found: C, 76.07; H, 10.08.

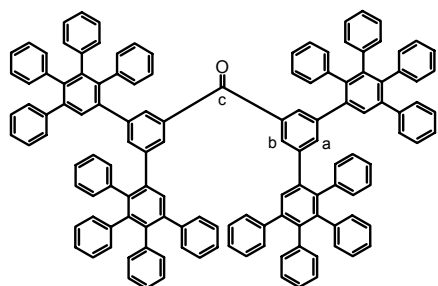
2,2',4,4'-Tetra-ethynyl-benzophenone (**3-52**)



3-51 (500 mg, 0.55 mmol) was dissolved in 10 mL of dry THF and reacted with TBAF (175 mg, 0.5 mmol) following the general desilylation procedure. Purification was performed by column chromatography (silica gel, PE/CH₂Cl₂ 3:2) to afford **3-52** as a white solid.

Yield: 103 mg (0.37 mmol), 67%. ¹H NMR Spectrum (250 Mhz, CD₂Cl₂, 300K) δ [ppm] = 7.82 (s, 6H, H_{d+e}); 3.77 (s, 4H, H_a). ¹³C NMR Spectrum (175 MHz, CD₂Cl₂, 300 K) δ [ppm] = 192.9 (C_g), 139.3 (C_d), 138.6 (C_f), 133.5 (C_e), 124.3 (C_c), 82.1 (C_b), 81.0 (C_a). FD Mass Spectrum (8kV) m/z = 278.4 (100%, (M)⁺) (calcd. 278.3). Elemental Analysis for C₂₁H₁₀O C, 90.63; H, 3.62. Found: C, 90.70; H, 3.89.

3-53

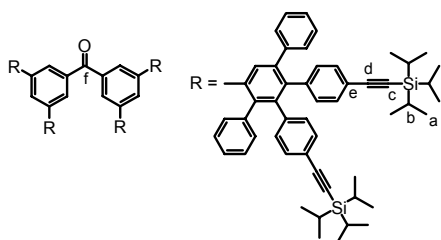


A mixture of **3-52** (75 mg, 0.27 mmol) and **1-32** (620 mg, 1.61 mmol) was dissolved in 6 mL of *o*-xylene and refluxed for 16 h at 150 °C under argon atmosphere. The solvent was removed under reduced pressure and the crude product purified by column chromatography (silica gel, PE/CH₂Cl₂ 3:2) to afford **3-53** as a white solid.

Yield: 0.35 g (0.2 mmol), 77%. ¹H NMR Spectrum (500 MHz, CD₂Cl₂, 300 K) δ [ppm] = 7.25 (s, 2H, H_a), 7.20-

7.17 (m, 22H, H_{arom.}), 7.04 (s, 4H, H_b), 6.95-6.70 (m, 62H, H_{arom.}). ¹³C NMR Spectrum (175 MHz, CD₂Cl₂, 300 K) δ [ppm] = 196.5 (C_c) 142.2, 142.0, 141.6, 141.3, 140.7, 140.4, 140.1, 134.0, 139.6, 137.4, 135.6, 131.8, 131.8, 131.6, 130.3, 129.0, 127.4, 127.2, 127.0, 126.7, 126.2, 126.0, 125.8. FD Mass Spectrum (8kV) m/z = 1704 (100%, (M)⁺) (calcd. 1704). Elemental Analysis for C₁₃₃H₉₀O Calcd.: C, 93.74; H, 5.32. Found: C, 93.84; H, 5.34.

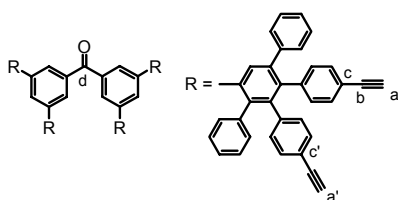
3-54



A mixture of **3-52** (75 mg, 0.27 mmol) and **1-35** (1.2 g, 1.61 mmol) was dissolved in 6 mL of *o*-xylene and refluxed for 18 hrs at 160 °C under argon atmosphere. The solvent was removed under reduced pressure and the crude product purified by column chromatography (silica gel, PE/CH₂Cl₂ 6:1 → 3:1). Precipitation from MeOH afforded **3-54** as a white solid.

Yield: 0.4 g (0.13 mmol), 47%. ¹H NMR Spectrum (500 MHz, CD₂Cl₂, 300 K) δ [ppm] = 7.24-6.97 (m, 46 H, H_{arom.}), 6.83-6.72 (m, 36H, H_{arom.}), 1.09 (s, 168 H, H_{a+b}). ¹³C NMR Spectrum (175 MHz, CD₂Cl₂, 300 K) δ [ppm] = 196.4 (C_f) 141.6, 141.5, 141.3, 141.2, 140.8, 140.5, 140.2, 139.6, 139.6, 139.2, 137.4, 135.6, 131.9, 131.7, 131.7, 131.1, 130.8, 130.2, 128.9, 128.1, 127.6, 127.0, 126.5, 121.3 (C_e), 121.1, 107.3 (C_d), 91.1 (C_c), 91.0, 18.8 (C_b), 11.7 (C_a). FD Mass Spectrum (8kV) m/z = 3148 (100%, (M)⁺), 1574 (10%, (M)²⁺) (calcd. 3147). Elemental Analysis for C₂₂₁H₂₅₀OSi₈ Calcd.: C, 84.35; H, 8.01. Found: C, 84.57; H, 7.82.

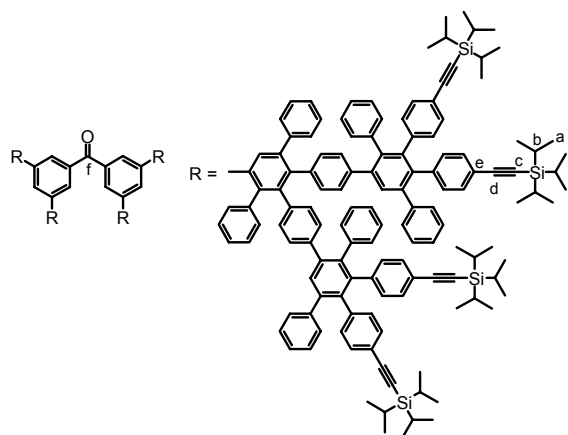
3-55



3-54 (200 mg, 63.5 μmol) was dissolved in 10-mL of dry THF and reacted with TBAF (160 mg, 0.51 mmol) following the general desilylation procedure. Purification was performed by precipitation from MeOH/H₂O (3:1) to afford **3-55** as a white solid.

Yield: 115 mg (60 μmol), 95%. ¹H NMR Spectrum (500 Mhz, CD₂Cl₂, 300K) δ [ppm] = 7.21-7.17 (m, 18H, H_{arom.}), 7.11-6.99 (m, 12H, H_{arom.}), 6.91-6.82 (m, 38H, H_{arom.}), 3.04, 3.02 (2s, 8H, H_a). ¹³C NMR Spectrum (175 MHz, CD₂Cl₂, 300 K) δ [ppm] = 196.3 (C_d) 141.4, 141.3, 141.2, 141.0, 140.3, 139.5, 139.1, 137.4, 135.6, 131.9, 131.8, 131.7, 131.2, 131.0, 130.2, 128.9, 128.1, 127.6, 127.1, 126.5, 119.9 & 119.6 (C_{c+c'}), 83.8 (C_b), 77.5 & 77.4 (C_{a+a'}). MALDI TOF Mass Spectrum m/z = 1898 (100%, (M+Ag)⁺) (calcd. 1896). Elemental Analysis for C₁₄₂H₉₀O Calcd.: C, 94.73; H, 4.78. Found: C, 94.46; H, 5.33.

3-56

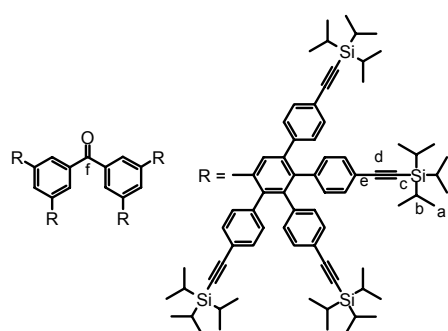


A mixture of **3-55** (60 mg, 32 μmol) and **1-35** (380 mg, 0.34 mmol) was dissolved in 6 mL of *o*-xylene and refluxed for 2 days at 170 $^{\circ}\text{C}$ under argon atmosphere. The solvent was removed under reduced pressure and the crude product purified by column chromatography (silica gel, PE/ CH_2Cl_2 3:1 \rightarrow THF). Precipitation from MeOH afforded **3-56** as a white solid.

Yield: 0.21 g (28 μmol), 90%. ^1H NMR Spectrum (700 MHz, CD_2Cl_2 , 300 K) δ [ppm] = 7.41 (s, 4H), 7.35 (s, 4H), 7.19-7.02 (m, 102H),

6.93-6.91 (m, 30H), 6.84-6.81 (m, 16H), 6.75-6.58 (m, 62H), 6.53 (d, $^3\text{J}(\text{H,H}) = 7.7\text{Hz}$, 8H), 6.44 (d, $^3\text{J}(\text{H,H}) = 7.7\text{Hz}$, 8H), 1.10 (s, 336H, $\text{H}_{\text{a+b}}$). ^{13}C NMR Spectrum (175 MHz, CD_2Cl_2 , 300 K) δ [ppm] = 196.5 (C_f), 146.5, 146.4, 146.4, 145.7, 145.6, 145.2, 144.5, 144.5, 144.4, 144.1, 144.0, 143.5, 143.2, 143.1, 143.0, 142.8, 136.3, 135.8, 135.7, 135.5, 135.2, 134.8, 134.7, 133.4, 133.2, 132.6, 132.4, 131.9, 131.3, 131.2, 130.7, 125.7&125.4 (C_e), 111.8 (C_d), 95.4&95.3 (C_c), 23.2&23.2 (C_b), 16.2 (C_a). MALDI TOF Mass Spectrum $m/z = 7637$ (100%, (M) $^+$), 7663 (30%, ($\text{M}+\text{Na}$) $^+$), 7744 (15%, ($\text{M}+\text{Ag}$) $^+$) (calcd. for $\text{C}_{549}\text{H}_{570}\text{OSi}_{16}$, 7634).

3-57

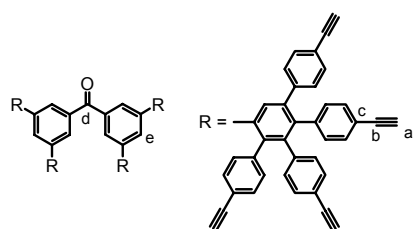


A mixture of **3-52** (50 mg, 0.18 mmol) and **1-36** (1.2 g, 1.09 mmol) was dissolved in 6 mL of *o*-xylene and refluxed for 20 h at 160 $^{\circ}\text{C}$ under argon atmosphere. The solvent was removed under reduced pressure and the crude product purified by column chromatography (silica gel, PE/ CH_2Cl_2 9:1 \rightarrow 1:1). Precipitation from MeOH afforded **3-57** as a white solid.

Yield: 625 mg (136 μmol), 76%. ^1H NMR Spectrum (500 MHz, CD_2Cl_2 , 300 K) δ [ppm] = 7.33-7.06 (m, 50

H, $\text{H}_{\text{arom.}}$), 6.80-6.64 (m, 24H, $\text{H}_{\text{arom.}}$), 1.14-1.09 (m, 336H, $\text{H}_{\text{a+b}}$). ^{13}C NMR Spectrum (175 MHz, CD_2Cl_2 , 300 K) δ [ppm] = 194.5 (C_f), 141.6, 141.5, 141.4, 140.8, 140.5, 140.3, 140.2, 140.0, 139.4, 139.3, 137.1, 133.8, 131.9, 131.8, 131.6, 131.4, 131.1, 130.2, 129.4 (all Ar-C), 122.3, 121.8, 121.7, 121.5 (all C_e), 107.3, 107.2 (all C_d), 91.3, 91.2 (all C_c), 19.0, 18.9, 18.9 (all C_a), 11.2 (C_b). MALDI TOF Mass Spectrum $m/z = 4552$ (50%, ($\text{M}-43 \equiv \text{isopropyl}$) $^+$), 4595 (100%, (M) $^+$), 4618 (20%, ($\text{M}+\text{Na}$) $^+$), 4633 (40%, ($\text{M}+\text{K}$) $^+$) (calcd. 4590). Elemental Analysis for $\text{C}_{309}\text{H}_{410}\text{OSi}_{16}$ Calcd.: C, 80.86; H, 9.00. Found: C, 80.94; H, 7.11.

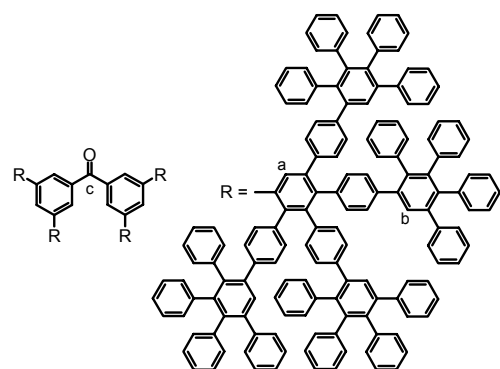
3-58



3-57 (350 mg, 76.2 μmol) was dissolved in 10 mL of dry THF and reacted with TBAF (385 mg, 1.22 mmol) following the general desilylation procedure. Purification was performed by precipitation from MeOH/H₂O (3:1) to afford **3-58** as a white solid.

Yield: 125 mg (60 μmol), 78%. ¹H NMR Spectrum (500 MHz, CD₂Cl₂, 300K) δ [ppm] = 7.33-7.31 (m, 12H, H_{arom.}), 7.17 (s, 2H, H_e), 7.11-7.03 (m, 28H, H_{arom.}), 6.98-6.96 (d, ³J(H,H) = 8.2Hz, 8H, H_{arom.}), 6.79-6.77 (d, ³J(H,H) = 8.2 Hz, 8H, H_{arom.}), 6.71-6.70 (d, ³J(H,H) = 8.2Hz, 8H, H_{arom.}), 6.67-6.65 (d, ³J(H,H) = 8.2Hz, 8H, H_{arom.}), 3.13&3.05&3.04&2.99 (4s, 16H, H_a). ¹³C NMR Spectrum (175 MHz, CD₂Cl₂, 300 K) δ [ppm] = 195.3 (C_d), 141.9, 141.3, 141.3, 140.8, 140.6, 140.4, 140.4, 140.3, 139.3, 139.2, 137.3, 135.3, 132.0, 131.7, 131.6, 131.5, 131.4, 131.3, 131.2, 130.2, 129.2 (all Ar-C), 120.9 120.3, 120.1 (all C_c), 83.5, 83.6, (all C_b) 78.1, 78.0, 77.7, 77.7 (all C_a). MALDI TOF Mass Spectrum m/z = 2090 (100%, (M)⁺), 4182 (10%, (2M)⁺) (calcd. 2089). Elemental Analysis for C₁₆₅H₉₀O Calcd.: C, 94.89; H, 4.34. Found: C, 93.68; H, 5.11.

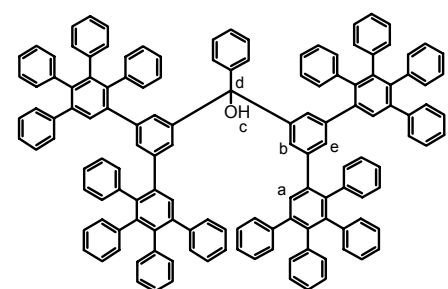
3-59



A mixture of **3-58** (60 mg, 28.7 μmol) and **1-32** (530 mg, 1.38 mmol) was dissolved in 4 mL of *o*-xylene and refluxed for 3 days at 170 °C under argon atmosphere. The solvent was removed under reduced pressure and the crude product purified by column chromatography (silica gel, PE/CH₂Cl₂ 2:1→CH₂Cl₂). Precipitation from MeOH afforded **3-59** as a white solid.

Yield: 190 mg (24.4 μmol), 85%. ¹H NMR Spectrum (500 MHz, CD₂Cl₂, 300 K) δ [ppm] = 7.43-7.39 (m, 20H, H_{a+b}), 7.26 (s, 4H, H_{arom.}), 7.13 (m, 370H, H_{arom.}), 6.54-6.34 (s, 16H, H_{arom.}). ¹³C NMR Spectrum (175 MHz, CD₂Cl₂, 300 K) δ [ppm] = 196.4 (C_c), 142.2, 142.2, 142.1, 142.1, 142.0, 142.0, 141.2, 141.1, 141.0, 141.0, 140.8, 140.6, 140.6, 140.5, 140.4, 139.7, 139.6, 139.6, 139.4, 139.3, 131.9, 131.5, 131.5, 131.4, 130.3, 130.3, 130.2, 130.2, 129.7, 129.6, 127.9, 127.8, 127.8, 127.2, 127.1, 127.1, 126.9, 126.9, 126.5, 126.5, 126.0, 125.9, 125.6, 125.5. MALDI TOF Mass Spectrum m/z = 7792 (100%, (M)⁺), 7819 (40%, (M+Na)⁺), 7898 (45%, (M+Ag)⁺) (calcd. 7792). Elemental Analysis for C₆₁₃H₄₁₀O Calcd.: C, 94.49; H, 5.30. Found: C, 94.46; H, 5.33.

3-60

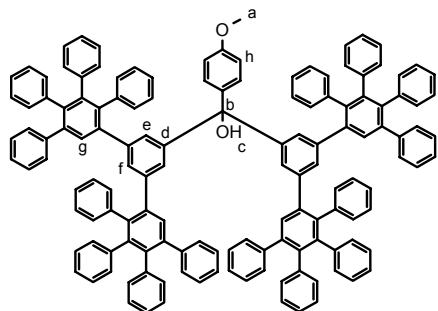


precipitation from MeOH to afford **3-53** as a white solid.

3-53 (110 mg, 64.5 μmol) was dissolved in 5 mL of dry THF under argon atmosphere. A solution of phenyllithium (2 mL, 3.8 mmol, 1.8-2.1M) in cyclohexane/ether (70:30) was added through a septum and the mixture heated for 16 h at 70 °C. Afterwards 5 mL of H₂O were added, the mixture extracted with CH₂Cl₂/H₂O and the organic solvent removed under reduced pressure. The crude product was purified by

Yield: 80 mg (45 μmol), 70 %. **^1H NMR Spectrum (500 MHz, CD_2Cl_2 , 300 K)** δ [ppm] = 7.21 (s, 4H, H_a), 7.16-7.11 (m, 20H, $\text{H}_{\text{arom.}}$), 6.99-6.62 (m, 65H, $\text{H}_{\text{arom.}}$), 6.53 (s, 4H, H_b), 6.47-6.46 (d, $^3J = 8.5\text{Hz}$, 2H, H_c), 1.89 (s, 1H, H_c). **^{13}C NMR Spectrum (125 MHz, CD_2Cl_2 , 300 K)** δ [ppm] = 146.6, 145.6, 142.1, 141.1, 141.0, 140.8, 140.5, 140.3, 139.8, 139.6, 131.9, 131.8, 131.8, 131.3, 130.6, 130.3, 128.2, 128.1, 128.0, 127.9, 127.3, 127.2, 126.9, 126.7, 125.9, 125.7, 81.6 (C_d). **FD Mass Spectrum (8kV)** $m/z = 1783.7$ (100%, (M) $^+$); 892.3 (85%, (M) $^{2+}$) (calcd 1782.3). **Elemental Analysis for $\text{C}_{139}\text{H}_{96}\text{O}$** Calcd.: C, 93.67; H, 5.43. Found: C, 93.67; H, 5.48.

3-61

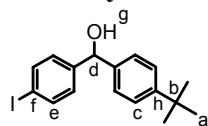


3-53 (100 mg, 58.7 μmol) was placed in a schlenk tube under argon atmosphere. 4-Methoxyphenylmagnesiumbromide (3 mL, 1.5 mmol, 0.5 M in THF) was added and the reaction mixture refluxed for 24 h at 70 $^\circ\text{C}$. After cooling, 5 ml of H_2O were added and the solution stirred for another 30 min. Extraction with $\text{CH}_2\text{Cl}_2/\text{H}_2\text{O}$ and concentration of the organic layer under reduced pressure gave the crude product which was further purified by column chromatography (silica gel,

PE/ CH_2Cl_2 3:2) and precipitation from MeOH to afford **3-61** as a white solid.

Yield: 70 mg (39 μmol), 66%. **^1H NMR Spectrum (700 MHz, CD_2Cl_2 , 300 K)** δ [ppm] = 7.21 (s, 4H, H_g), 7.18-7.11 (m, 20H, $\text{H}_{\text{arom.}}$), 6.99 (s, 2H, H_f), 6.93-6.92 (m, 12H, $\text{H}_{\text{arom.}}$), 6.86-6.83 (m, 22H, $\text{H}_{\text{arom.}}$), 6.78-6.75 (m, 16H, $\text{H}_{\text{arom.}}$), 6.68-6.67 (m, 4H, $\text{H}_{\text{arom.}}$), 6.63-6.61 (m, 8H, $\text{H}_{\text{arom.}}$), 6.53&6.52 (2s, 4H, H_e), 6.35-6.34 (d, $^3J = 8.8\text{ Hz}$, 2H, H_h), 3.80 (s, 3H, H_a), 1.87 (s, 1H, H_c). **^{13}C NMR Spectrum (175 MHz, CD_2Cl_2 , 300 K)** δ [ppm] = 158.6 (C_e), 146.8, 142.1, 142.0, 141.2, 141.1, 141.0, 140.8, 140.5, 140.4, 139.7, 139.6, 138.1, 132.0, 131.9, 131.8, 131.4, 130.6, 130.3, 129.8, 128.2, 127.9, 127.8, 127.2, 126.9, 126.7, 126.0, 125.9, 125.7, 113.3 (C_b), 81.3 (C_c), 55.6 (C_a). **FD Mass Spectrum (8kV)** $m/z = 1815.2$ (100%, (M) $^+$), 1797.8 (30%, ($\text{M}-17 \equiv \text{OH}$) $^+$) (calcd. 1812.3). **Elemental Analysis for $\text{C}_{140}\text{H}_{98}\text{O}_2$** Calcd.: C, 92.78; H, 5.45. Found: C, 92.43; H, 5.38.

4-*t*-Butyl-4'-iodo-diphenylmethanol (3-65)



1,4-Diiodo-benzene (**3-12**) (15 g, 45.4 mmol) was placed in 300 mL of dry diethyl ether at -78 $^\circ\text{C}$ under argon atmosphere. Within 30 min *n*-butyllithium (28.4 mL, 45.4 mmol, 1.6 M in hexane) were added drop wise and the solution stirred for 2 h at this temperature. 4-*t*-butylbenzaldehyde (**3-64**) (8.36 mL, 50.0 mmol) were dissolved in 30 mL of diethyl ether and added to the solution within 15 min. The reaction mixture was stirred for another 2 h at -78 $^\circ\text{C}$ and then allowed to reach room temperature. 50 mL of H_2O were added, the solution stirred for 30 min and then extracted with diethyl ether. The organic layer was concentrated under reduced pressure and the crude product purified by column chromatography (silica gel, PE/ CH_2Cl_2 2:3) to afford **3-65** as a white solid.

Yield: 13.3 g (36.2 mmol), 80 %. **^1H -NMR Spectrum-Spektrum (250 MHz, CD_2Cl_2 , 300 K)** δ [ppm] = 7.68-7.65 (d, $^3J(\text{H,H}) = 8.5\text{ Hz}$, 2H, H_e), 7.37-7.35 (d, $^3J(\text{H,H}) = 8.5\text{Hz}$, 2H, H_c), 7.28-7.25 (d, $^3J(\text{H,H}) = 8.3\text{Hz}$, 2H), 7.17-7.15 (d, $^3J(\text{H,H}) = 8.1\text{Hz}$, 2H), 5.76-5.75 (d, $^3J(\text{H,H}) = 3.4\text{Hz}$, 1H, H_g), 2.35-2.33 (d, $^3J(\text{H,H}) = 3.6\text{Hz}$, 1H, H_d), 1.29 (s, 9H, H_a). **^{13}C -NMR Spectrum-Spektrum (75 MHz, CD_2Cl_2 , 300 K)** δ [ppm] = 151.2 (C_h), 144.4, 141.2, 137.8, 128.7, 126.5,

125.8, 92.9 (C_f), 75.7 (C_d), 34.8 (C_b), 31.4 (C_a). FD Mass Spectrum (8kV) m/z = 366.6 (100%, (M)⁺) (calcd. 366.2). Elemental Analysis for C₁₇H₁₉IO Calcd.: C, 55.75; H, 5.23. Found: C, 55.17; H, 3.05.

4-*t*-Butyl-4'-iodo-benzophenone (3-66)

200 mL of dry CH₂Cl₂ were placed in a flask under argon atmosphere and cooled to -78 °C under argon. Oxalyl chloride (3.2 mL, 16.9 mmol) was added through a septum and the solution was stirred for 15 min. Afterwards DMSO (5.3 mL, 61.7 mmol), dissolved in 30 mL of CH₂Cl₂, was added and after 15 min of stirring **3-65** (12.3 g, 33.6 mmol), dissolved in CH₂Cl₂ was added and the solution stirred for another 15 min. Thereafter, TEA (23.4 mL, 0.32 mol) was added and the solution allowed to warm to room temperature. Subsequent extraction with brine, 1% H₂SO₄, H₂O and 5% NaHCO₃ gave the crude product which could be purified by column chromatography (silica gel, PE/CH₂Cl₂ 1:1) yielding **3-66** as a white solid.

Yield: 12.0 g (32.8 mmol), 98 %. ¹H NMR Spectrum (300MHz, CD₂Cl₂, 300 K) δ [ppm] = 7.88-7.85 (d, ³J(H,H) = 8.7Hz, 2H, H_f), 7.73-7.70 (d, ³J(H,H) = 8.6Hz, 2H, H_d), 7.54-7.50 (m, 4H), 1.37 (s, 9H, H_a). ¹³C NMR Spectrum (75 MHz, CD₂Cl₂, 300 K) δ [ppm] = 195.6 (C_e), 156.9 (C_c), 137.9, 137.7, 134.7, 131.7, 130.2, 125.8, 99.9 (C_g), 35.4 (C_b), 31.2 (C_a). FD Mass Spectrum (8kV) m/z = 365.0 (100%, (M)⁺) (calcd. for C₁₇H₁₇IO, 364.2).

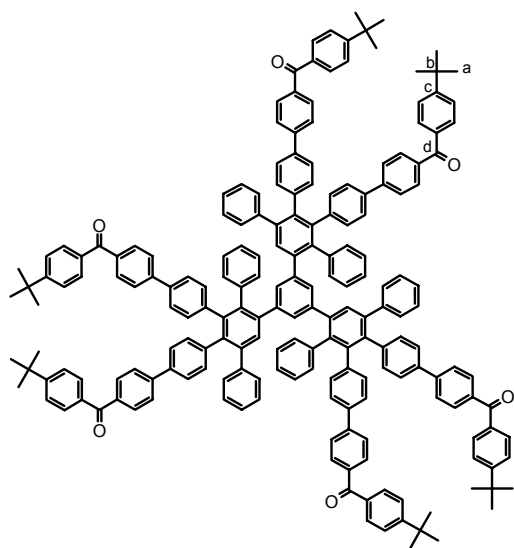
3,4-Bis-[4'-(4-*t*-butyl-benzoyl)-biphenyl-4-yl]-2,5-diphenyl-cyclopenta-2,4-dienone (3-69)



3-20 (2.0 g, 3.15 mmol) and **3-66** (3.44 g, 9.43 mmol) were dissolved in 26 mL of toluene. 13 mL of EtOH and 6.5 mL of a solution of 2.6 g K₂CO₃ in H₂O (2.3M) were added and the reaction mixture was flushed with argon. Pd(PPh₃)₄ catalyst (750 mg, 0.65 mmol) was added and the reaction mixture was stirred at 80 °C for 16 h. The resulting solution was washed three times with CH₂Cl₂/H₂O. The organic layer was separated and dried over MgSO₄. The crude product was purified by column chromatography (silica gel, PE/CH₂Cl₂ 1:5) to give **3-69** as a brown solid.

Yield: 1.2 g (1.4 mmol), 45 %. ¹H-NMR Spektrum (300 MHz, CD₂Cl₂, 300 K) δ [ppm] = 7.87-7.84 (d, ³J(H,H) = 8.5Hz, 4H), 7.76-7.71 (m, 8H), 7.57-7.51 (m, 8H), 7.30 (s, 10H), 7.14-7.11 (d, ³J(H,H) = 8.5Hz, 4H), 1.37 (s, 18H, H_a). ¹³C-NMR Spectrum (75 MHz, CD₂Cl₂, 300 K) δ [ppm] = 200.3 (C_f), 195.9 (C_d), 156.6 (C_c), 154.3 (C_e), 144.1, 140.3, 135.2, 133.4, 131.3, 130.9, 130.6, 130.5, 130.3, 128.5, 128.0, 127.1, 127.0, 126.3, 125.7, 35.4 (C_b), 31.22 (C_a). FD Mass Spectrum (8kV) m/z = 857.4 (100%, (M)⁺) (calcd. 857.1). Elemental Analysis for C₆₃H₅₂O₃ Calcd.: C, 88.28; H, 6.12. Found: C, 88.65; H, 5.92.

3-70

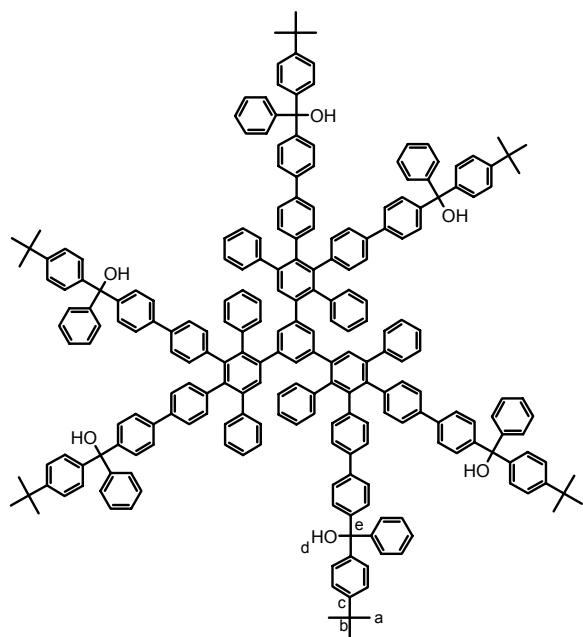


1-46 (11 mg, 73 μmol) and **3-69** (250 mg, 290 μmol) were dissolved in 5 mL of *o*-xylene and reacted for 16 h at 160 $^{\circ}\text{C}$ under argon atmosphere. Purification was performed by column chromatography (silica gel, toluene/MeOH 100:1) to afford **3-70** as a slightly yellow solid.

Yield: 90 mg (34 μmol), 47%. ^1H NMR Spectrum (500 MHz, d^8 -THF, 300 K) δ [ppm] = 7.72-6.92 (m, 105H), 6.75 (sb, 3H), 1.36 (s, 54H, H_a). ^{13}C NMR Spectrum (125 MHz, d^8 -THF, 300 K) δ [ppm] = 194.9 (C_d), 156.3 (C_c), 144.8, 144.7, 144.3, 144.2, 142.6, 141.9, 141.8, 141.7, 141.4, 141.1, 141.0, 140.2, 139.5, 137.8, 137.7, 137.5, 136.2, 136.2, 133.2, 133.1, 132.7, 131.8, 131.4, 131.0, 130.5, 130.1, 129.5, 129.0, 128.8, 128.3,

128.1, 127.9, 127.1, 126.9, 126.7, 126.7, 126.4, 126.1, 125.9, 35.6 (C_a), 31.4 (C_b). FD Mass Spectrum (8kV) m/z = 2638 (100%, (M) $^+$), 1319 (90%, (M) $^{2+}$), 873 (M) $^{3+}$) (calcd. 2637.5). Elemental Analysis for $C_{198}H_{162}O_6$ Calcd.: C, 90.17; H, 6.19. Found: C, 89.07; H, 6.04.

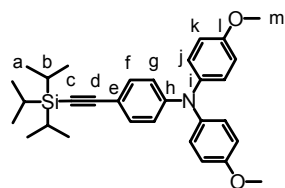
3-71



3-70 (55 mg, 21 μmol) was dissolved in 5 mL of dry THF under argon atmosphere. A solution of phenyllithium (1 mL, 2 mmol, 1.8-2.1M) in cyclohexane/ether (70:30) was added through a septum and the mixture heated for 16 h at 70 $^{\circ}\text{C}$. Afterwards 5 mL of H_2O were added, the mixture extracted with $\text{CH}_2\text{Cl}_2/\text{H}_2\text{O}$ and the organic solvent removed under reduced pressure. The crude product was purified by precipitation from *n*-pentane.

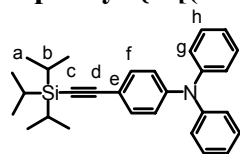
Yield: 50 mg (16 μmol), 76%. ^1H NMR Spectrum (500 MHz, CD_2Cl_2 , 300 K) δ [ppm] = 7.34-7.06 (m, 114H), 6.86-6.67 (m, 24H), 2.60 (s, 6H, H_d), 1.27 (s, 54H, H_a). ^{13}C NMR Spectrum (175 MHz, CD_2Cl_2 , 300 K) δ [ppm] = 149.9&149.2 (C_c), 148.0, 146.0, 142.7, 142.0, 141.8, 141.6, 141.1, 140.3, 140.1,

139.3, 138.4, 138.2, 132.9, 132.6, 132.5, 130.8, 130.5, 128.9, 128.7, 128.0, 129.1, 127.2, 126.9, 126.5, 126.2, 125.8, 125.6, 125.0, 81.4 (C_e), 34.9 (C_b), 31.7 (C_a). MALDI TOF Mass Spectrum m/z = 3154 (5%, ($M+K$) $^+$), 3128 (5%, ($M+Na$) $^+$), 3104 (5%, (M) $^+$), 3088 (100%, ($M-18 \equiv \text{OH}$) $^+$), 3071 (30%, ($M-35 \equiv 2\cdot\text{OH}$) $^+$), 3054 (10%, ($M-52 \equiv 3\cdot\text{OH}$) $^+$) (calcd. 3106). Elemental Analysis for $C_{234}H_{198}O_6$ Calcd.: C, 90.48; H, 6.43. Found: C, 89.11; H, 5.62.

Bis-(4-methoxy-phenyl)-{4-[(triisopropylsilyl)-ethynyl]-phenyl}-amine (4-9)

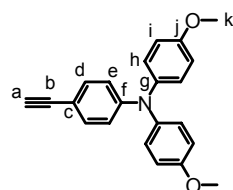
Sodium *t*-butanolat (1.23 g, 8.05 mmol), Pd₂dba₃ (17 mg, 18.2 μmol) and tri-*t*-butylphosphine (12 mg, 73 μmol) were placed in a sealed schlenk flask under argon atmosphere. 4-(triisopropylsilyl-ethynyl)-aniline (**4-6**) (1 g, 3.66 mmol) and 4-bromo-anisol (**4-7**) (2.05 g, 10.97 mmol), dissolved in 20 mL of dry toluene, were added and the reaction mixture stirred at 80 °C for 3 days. The solvent was removed under reduced pressure and the crude product purified by column chromatography (silica gel, PE/CH₂Cl₂ 4:1) to give **4-9** as a slightly brown oil.

Yield: 1.3 g (2.67 mmol), 73 %. **¹H NMR Spectrum (250 MHz, CD₂Cl₂, 300 K)** δ [ppm] = 7.26-7.23 (d, ³J(H,H) = 8.8 Hz, 2H, H_f), 7.07-7.03 (d, ³J(H,H) = 9.1 Hz, 4H, H_k), 6.87-6.83 (d, ³J(H,H) = 9.1 Hz, 4H, H_j), 6.79-6.76 (d, ³J(H,H) = 8.8 Hz, 2H, H_g), 3.78 (s, 6H, H_m), 1.12 (s, 21H, H_{a+b}). **¹³C NMR Spectrum (62.9 MHz, CD₂Cl₂, 300 K)** δ [ppm] = 156.8 (C_i), 149.3 (C_h), 140.4 (C_i), 133.0 (C_f), 127.4 (C_j), 119.2 (C_g), 115.1 (C_k), 114.4 (C_e), 108.1 (C_d), 88.7 (C_c), 55.8 (C_m), 18.8 (C_a), 11.7 (C_b). **FD Mass Spectrum (8kV)** m/z = 486 (100%, (M)⁺) (calcd. for C₃₁H₃₉NO₂Si, 486).

Diphenyl-{4-[(triisopropylsilyl)-ethynyl]-phenyl}-amine (4-10)

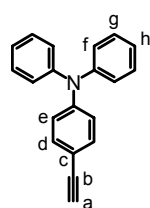
Sodium *t*-butanolat (903 mg, 8.03 mmol), Pd₂dba₃ (17 mg, 18.2 μmol) and tri-*t*-butylphosphine (12 mg, 73 μmol) were placed in a sealed Schlenk flask under argon atmosphere. 4-(triisopropylsilyl-ethynyl)-aniline (**4-6**) (1 g, 3.66 mmol) and bromobenzene (**4-8**) (1.26 g, 8.03 mmol), dissolved in 18 mL of dry toluene, were added and the reaction mixture stirred at 80 °C for 2 days. The solvent was removed under reduced pressure and the crude product purified by column chromatography (silica gel, PE/CH₂Cl₂ 8:1) to give **4-10** as a slightly yellow oil.

Yield: 1.54 g (3.62 mmol), 99 %. **¹H NMR Spectrum (250 MHz, CD₂Cl₂, 300 K)** δ [ppm] = 7.33-7.22 (m, 6H, Ar-H), 7.08-6.93 (m, 8H, Ar-H), 1.15 (s, 21H, H_{a+b}). **¹³C NMR Spectrum (62.9 MHz, CD₂Cl₂, 300 K)** δ [ppm] = 149.1, 148.1, 133.6 (C_f), 130.1 (C_h), 125.5 (C_g), 124.2, 123.1, 117.3 (C_e), 108.6 (C_d), 89.1 (C_c), 19.0 (C_a), 12.2 (C_b). **FD Mass Spectrum (8kV)** m/z = 425 (100%, (M)⁺) (calcd. for C₂₉H₃₅NSi, 425.7).

(4-Ethynyl-phenyl)-bis-(4-methoxy-phenyl)-amine (4-11)

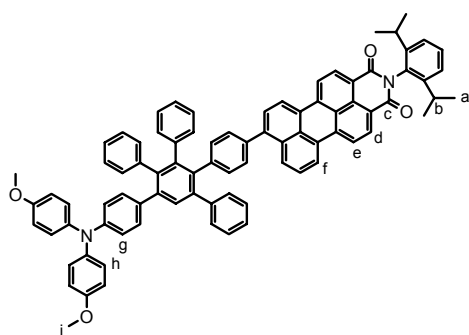
4-9 (6 g, 12.35 mmol) was dissolved in 50 mL of dry THF and reacted with TBAF (430 mg, 1.37 mmol) following the general desilylation procedure. After 4 h the reaction was quenched with H₂O and the reaction mixture extracted with CH₂Cl₂/H₂O. The organic layer was concentrated under reduced pressure and the crude product purified by column chromatography (silica gel, PE/CH₂Cl₂ 3:1) to give **4-11** as a slightly yellow solid.

Yield: 3.85 g (11.7 mmol), 95 %. **¹H NMR Spectrum (250 MHz, CD₂Cl₂, 300 K)** δ [ppm] = 7.17-7.14 (d, ³J(H,H) = 8.8 Hz, 2H, H_d); 7.00-6.96 (d, ³J(H,H) = 9.1 Hz, 4H, H_i); 6.78-6.75 (d, ³J(H,H) = 8.8 Hz, 4H, H_h); 6.69-6.66 (d, ³J(H,H) = 8.8 Hz, 2H, H_e); 3.69 (s, 6H, H_k); 2.94 (s, 1H, H_a). **¹³C NMR Spectrum (125 MHz, CD₂Cl₂, 300 K)** δ [ppm] = 157.0 (C_j), 149.7 (C_f), 140.3 (C_g), 133.1 (C_d), 127.6 (C_h), 118.8 (C_e), 115.1 (C_i), 112.6 (C_c), 84.5 (C_b), 75.7 (C_a), 55.7 (C_k). **FD Mass Spectrum (8kV)** m/z = 329 (100%, (M)⁺) (calcd. for C₂₂H₁₉NO₂, 329).

(4-Ethynyl-phenyl)-diphenyl-amine (4-12)

4-10 (1.2 g, 2.82 mmol) was dissolved in 15 mL of dry THF and reacted with TBAF (79 mg, 0.22 mmol) following the general desilylation procedure. After 20 min, the reaction was quenched with H₂O and the reaction mixture extracted with CH₂Cl₂/H₂O. The organic layer was concentrated under reduced pressure and the crude product purified by column chromatography (silica gel, PE/CH₂Cl₂ 8:1) to give **4-12** as a slightly yellow solid.

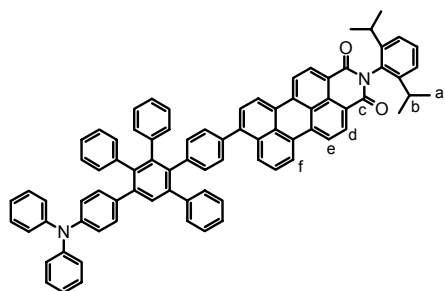
Yield: 665 mg (2.47 mmol), 88 %. ¹H NMR Spectrum (250 MHz, CD₂Cl₂, 300 K) δ [ppm] = 7.35-7.27 (m, 6H, H_{g+h}), 7.13-7.09 (m, 6H, H_{e+f}), 6.98-6.95 (d, ³J(H,H) = 7.4 Hz, 2H, H_d), 3.08 (s, 1H, H_a). ¹³C NMR Spectrum (62.9 MHz, CD₂Cl₂, 300 K) δ [ppm] = 148.8, 147.5, 133.4 (C_d), 129.8 (C_g), 125.5 (C_f), 124.1, 122.2, 115.0 (C_c), 84.1 (C_b), 76.5 (C_a). FD Mass Spectrum (8kV) m/z = 269.3 (100%, (M)⁺) (calcd. for C₂₀H₁₅N, 269.4).

4-14

A mixture of **4-11** (229 mg, 0.69 mmol) and **4-13** (0.9 g, 1.04 mmol) was dissolved in 20 mL of *o*-xylene and refluxed for 24 h at 150 °C under argon atmosphere. The solvent was removed under reduced pressure and the crude product purified by column chromatography (silica gel, 1st column CH₂Cl₂, 2nd column PE/CH₂Cl₂ 1:1) to afford **4-14** as a red solid. For single molecule spectroscopy, **4-14** was further purified by preparative thin layer chromatography

(silica gel, PE/CH₂Cl₂ 1:4).

Yield: 730 mg (0.63 mmol), 90%. ¹H NMR Spectrum (250 MHz, CD₂Cl₂, 300 K) δ [ppm] = 8.63-8.60 (d, ³J(H,H) = 8.2 Hz, 2H, H_d), 8.51-8.45 (m, 4H, H_{e+f}), 7.61-7.44 (m, 4H, H_{arom.}), 7.37-7.21 (m, 7H, H_{arom.}), 7.09-6.96 (m, 27H, H_{arom.}), 6.83-6.80 (d, ³J(H,H) = 8.8 Hz, 4H, H_h), 6.72-6.68 (d, ³J(H,H) = 8.8 Hz, 2H, H_g), 2.81-2.70 (sept., ³J(H,H) = 6.9 Hz, 2H, H_b), 1.16-1.13 (d, ³J(H,H) = 7.0 Hz, 12H, H_a). ¹³C NMR Spectrum (75 MHz, CD₂Cl₂, 300 K) δ [ppm] = 164.5 (C_c), 146.7, 144.0, 143.9, 142.4, 141.3, 141.2, 140.8, 138.3, 138.1, 137.5, 133.3, 132.2, 132.1, 131.1, 130.6, 130.4, 129.7, 129.6, 128.9, 128.7, 128.6, 128.3, 128.2, 128.1, 128.0, 127.5, 127.4, 127.4, 127.3, 127.3, 127.1, 126.8, 126.1, 126.1, 125.8, 124.4, 124.0, 124.0, 124.0, 121.4, 121.3, 120.8, 120.5, 55.9 (C_i), 29.5 (C_b), 24.1 (C_a). FD Mass Spectrum (8kV) m/z = 1165 (100%, (M)⁺) (calcd. 1165). Elemental Analysis for C₈₄H₆₄N₂O₄ Calcd.: C, 86.57; H, 5.54; N, 2.40. Found: C, 84.84; H, 6.01; N, 2.39. UV/Vis (CHCl₃) λ [nm] = 268 (2475), 338 (1000), 504 (1760), 524 nm (1720 m²mol⁻¹).

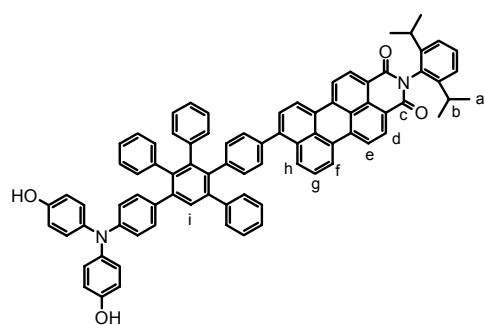
4-15

A mixture of **4-10** (80 mg, 0.30 mmol) and **4-13** (334 mg, 0.39 mmol) was dissolved in 8 mL of *o*-xylene and refluxed for 2 days at 160 °C under argon atmosphere. The solvent was removed under reduced pressure and the crude product purified by column chromatography (silica gel, PE/CH₂Cl₂ 2:3). Precipitation from THF in MeOH afforded **4-15** as a red solid.

Yield: 160 mg, (145 μmol), 49%. ¹H NMR Spectrum (500 MHz, CD₂Cl₂, 300 K) δ [ppm] = 8.64-8.62 (d, ³J(H,H) = 7.9 Hz, 2H, H_d), 8.52-8.50 (m,

4H, H_{e+f}), 7.64-7.47 (m, 5H, H_{arom.}), 7.36-6.87 (m, 35H, H_{arom.}), 2.79-2.73 (sept., ³J(H,H) = 7.0 Hz, 2H, H_b), 1.15-1.14 (d, ³J(H,H) = 6.7 Hz, 12H, H_a). ¹³C NMR Spectrum (175 MHz, CD₂Cl₂, 300 K) δ [ppm] = 164.4 (C_c), 146.5, 143.8, 142.2, 141.8, 141.2, 141.1, 141.0, 140.7, 140.6, 139.8, 139.1, 138.1, 137.9, 137.4, 133.1, 132.2, 132.1, 132.0, 131.2, 130.9, 130.5, 130.3, 129.8, 129.8, 129.6, 129.5, 128.9, 128.6, 128.2, 128.1, 128.0, 127.4, 127.3, 127.1, 126.8, 126.7, 126.1, 125.8, 124.5, 124.3, 123.9, 123.3, 123.2, 121.2, 121.1, 120.6, 120.4, 29.4 (C_b), 24.1 (C_a). **FD Mass Spectrum (8kV)** m/z = 1105 (100%, (M)⁺) (calcd. 1105). **Elemental Analysis for C₈₂H₆₀N₂O₂** Calcd.: C, 89.10; H, 5.47; N, 2.53. Found: C, 89.16; H, 5.36; N, 2.55. **UV/Vis (CHCl₃)** λ [nm] = 265 (3210), 331 (1450), 504 (2300), 525 nm (2250 m²mol⁻¹).

4-16

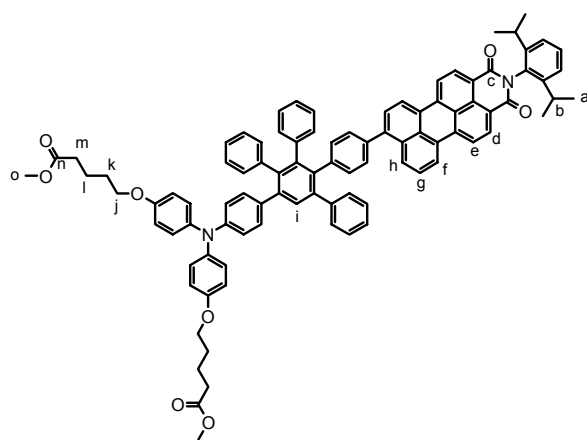


4-14 (500 mg, 0.43 mmol) was dissolved in 20 mL of dry CH₂Cl₂ under argon atmosphere at -78 °C. A solution of BBr₃ (1.72 mL, 0.86 mmol) in CH₂Cl₂ was added dropwise. After complete addition the solution was allowed to reach room temperature and was further stirred for 1.5 days. The reaction was quenched with HCl/H₂O 5% and afterwards extracted with CH₂Cl₂/H₂O. The solvent was removed under reduced pressure and the crude product purified by column

chromatography (silica gel, hexane/ethyl acetate 3:2) to afford **4-16** as a red solid.

Yield: 320 mg (0.28 mmol), 66%. **¹H NMR Spectrum (250 MHz, CD₂Cl₂, 300 K)** δ [ppm] = 8.64-8.61 (d, ³J(H,H) = 8.2 Hz, 2H, H_d), 8.50-8.43 (m, 4H, H_{e+f}), 7.61-7.47 (m, 4H, H_{g-i}), 7.36-6.95 (m, 36H, H_{arom.}), 2.84-2.61 (sept., ³J(H,H) = 6.9 Hz, 2H, H_b), 1.15-1.13 (d, ³J(H,H) = 6.9 Hz, 12H, H_a). **¹³C NMR Spectrum (75 MHz, CD₂Cl₂, 300 K)** δ [ppm] = 164.5 (C_c), 146.4, 143.8, 142.2, 138.2, 138.1, 138.0, 133.0, 132.7, 132.2, 132.2, 132.0, 131.9, 130.9, 130.4, 130.4, 130.2, 129.6, 129.2, 128.8, 128.5, 128.4, 128.4, 128.1, 128.0, 127.9, 127.3, 127.3, 127.2, 127.1, 124.3, 121.0, 120.9, 120.6, 120.3, 29.4 (C_b), 24.0 (C_a). **FD Mass Spectrum (8kV)** m/z = 1137 (100%, (M)⁺) (calcd. 1137). **Elemental Analysis for C₈₂H₆₀N₂O₄** Calcd.: C, 86.59; H, 5.32; N, 2.64. Found: C, 84.78; H, 5.81; N, 2.52.

4-18



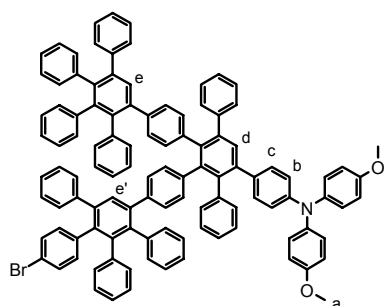
4-16 (175 mg, 154 μmol) and K₂CO₃ (47 mg, 340 μmol) were placed in a Schlenk tube with 8 mL of dry acetone. Argon was bubbled through the solution for ½ h and the reaction mixture further stirred for 1 h. 0.44 mL (340 μmol) of a solution of 5-bromo-valerianacid-methylester (**4-17**) (300 mg in 2 ml of acetone) was added dropwise to the reaction mixture which was afterwards stirred for another 1 h at room temperature and then refluxed overnight. A catalytic amount of potassium iodide and another 0.44 mL

(340 μmol) of the solution of **4-17** was added and the reaction mixture further refluxed for 4 days. The reaction mixture was diluted with CH₂Cl₂ and extracted with CH₂Cl₂/H₂O. The solvent was removed under reduced pressure and the crude product purified by column

chromatography (silica gel, hexane/ethyl acetate 3:2) to afford **4-18** as a red solid.

Yield: 179 mg (131 μmol), 85%. **^1H NMR Spectrum (250 MHz, CD_2Cl_2 , 300 K)** δ [ppm] = 8.62-8.59 (d, $^3\text{J}(\text{H},\text{H}) = 8.2$ Hz, 2H, H_d), 8.48-8.41 (m, 4H, H_{e+f}), 7.61-7.48 (m, 4H, H_{g-i}), 7.37-6.80 (m, 34H, $\text{H}_{\text{arom.}}$), 3.93 (m, 4H, H_j), 3.65 (s, 6H, H_o), 2.84-2.58 (sept., $^3\text{J}(\text{H},\text{H}) = 7.0$ Hz, 2H, H_b), 2.39-2.38 (m, 4H, H_m), 1.79-1.78 (m, 8H, H_{l+k}), 1.16-1.13 (d, $^3\text{J}(\text{H},\text{H}) = 7.0$ Hz, 12H, H_a). **^{13}C NMR Spectrum (175 MHz, CD_2Cl_2 , 300 K)** δ [ppm] = 173.9 (C_c), 164.3, 155.7, 147.5, 146.4, 143.8, 143.7, 142.2, 142.0, 141.7, 141.2, 141.1, 141.0, 140.6, 138.7, 138.0, 138.0, 137.8, 133.7, 132.7, 132.7, 132.1, 132.0, 132.0, 130.8, 130.4, 130.3, 130.2, 129.6, 129.2, 128.3, 128.0, 127.9, 127.3, 127.2, 127.1, 126.8, 126.1, 124.3, 123.8, 121.1, 120.9, 120.5, 120.2, 119.7, 115.5, 68.0 (C_j), 51.6 (C_o), 33.9, 32.3, 30.0, 29.7, 29.4, 29.0, 24.1, 23.0, 21.9 (C_l). **FD Mass Spectrum (8kV)** $m/z = 1365$ (100%, M^+) (calcd. 1366). **Elemental Analysis for $\text{C}_{94}\text{H}_{80}\text{N}_2\text{O}_8$** Calcd.: C, 82.67; H, 5.90; N, 2.05. Found: C, 82.30; H, 6.39; N, 2.15.

4-19

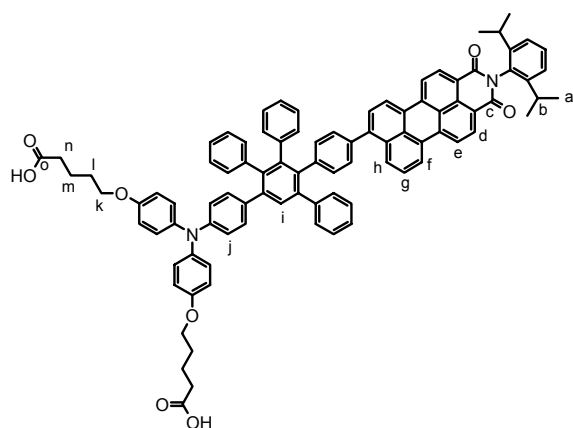


4-18 (100 mg, 73.2 μmol) and a 2M NaOH solution (0.24 mL, 440 μmol) were placed in a flask together with 2 mL of MeOH and 4 mL of THF. The reaction mixture was stirred for 4 days. After that the solvent was removed under reduced pressure and the crude product purified by column chromatography (silica gel, ethyl acetate/acidic acid 100:0.5) to afford **4-19** as a red solid. To remove the acidic acid the product was subsequently precipitated from THF in hexane. For single molecule spectroscopy 20 mg of **4-19** were further

purified by preparative thin layer chromatography (silica gel, ethyl acetate/acidic acid 100:0.25).

Yield: 86 mg (64 μmol), 88%. **^1H NMR Spectrum (250 MHz, CD_2Cl_2 , 300 K)** δ [ppm] = 8.62-8.59 (d, $^3\text{J}(\text{H},\text{H}) = 7.9$ Hz, 2H, H_d), 8.50-8.39 (m, 4H, H_{e+f}), 7.60-7.47 (m, 4H, H_{g-i}), 7.36-6.76 (m, 32H, $\text{H}_{\text{arom.}}$), 6.72-6.65 (m, 2H, H_j), 3.95 (s, 4H, H_k), 2.81-2.70 (sept., $^3\text{J}(\text{H},\text{H}) = 7.0$ Hz, 2H, H_b), 2.42 (s, 4H, H_n), 1.79 (s, 8H, H_{l+m}), 1.15-1.13 (d, $^3\text{J}(\text{H},\text{H}) = 7.0$ Hz, 12H, H_a). **^{13}C NMR Spectrum (175 MHz, CD_2Cl_2 , 300 K)** δ [ppm] = 178.0 (C_o), 178.0 (C_o), 164.4 (C_c), 155.6, 155.6, 146.5, 143.8, 142.2, 141.2, 141.0, 140.6, 139.0, 138.7, 138.2, 138.2, 138.0, 133.4, 133.2, 133.0, 132.8, 132.8, 132.2, 132.2, 132.1, 132.1, 132.0, 131.6, 131.5, 130.9, 130.4, 130.3, 130.3, 129.9, 129.9, 129.8, 129.6, 129.5, 129.4, 129.3, 128.8, 128.5, 128.4, 128.1, 128.0, 127.9, 128.1, 127.5, 127.4, 127.4, 127.3, 127.2, 127.2, 127.0, 126.9, 126.9, 126.7, 126.6, 126.1, 126.0, 125.9, 125.8, 125.7, 124.3, 123.9, 120.6, 120.4, 121.0, 121.1, 119.6, 115.6, 68.0 (C_k), 33.6 (C_n), 29.4, 28.8, 24.0 (C_a), 21.7 (C_m). **MALDI TOF Mass Spectrum** $m/z = 1338$ (100%, (M) $^+$) (calcd. 1338). **Elemental Analysis for $\text{C}_{92}\text{H}_{76}\text{N}_2\text{O}_8$** Calcd.: C, 82.61; H, 5.73; N, 2.09. Found: C, 78.87; H, 5.85; N, 2.26. **UV/Vis (CHCl_3)** λ [nm] = 267 (2975), 339 (1330), 503 (1985), 523 nm (1940 $\text{m}^2\text{mol}^{-1}$).

4-21

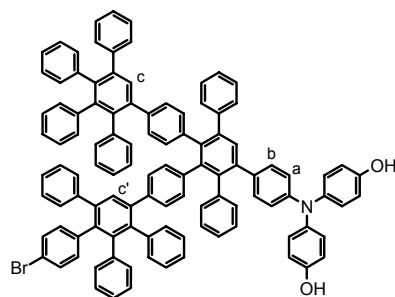


A mixture of **4-11** (50 mg, 0.15 mmol) and **4-20** (280 mg, 0.23 mmol) was dissolved in 5 mL of *o*-xylene and refluxed for 2 d at 160 °C under argon atmosphere. The solvent was removed under reduced pressure and the crude product purified by column chromatography (silica gel, PE/CH₂Cl₂ 3:2) to afford **4-21** as a white solid.

Yield: 225 mg (0.147 mmol), 97%. ¹H NMR Spectrum (250 MHz, CD₂Cl₂, 300 K) δ [ppm] = 7.50 (s, 1H, H_d), 7.44&7.40 (2s, 2H, H_{e+e'}), 7.16-6.66 (m, 65H, H_{arom.}), 6.58-6.55 (d, ³J(H,H) = 7.6 Hz, 2H, H_b), 6.52-6.49 (d,

³J(H,H) = 7.6 Hz, 2H, H_c), 3.77 (s, 6H, H_a). ¹³C NMR Spectrum (175 MHz, CD₂Cl₂, 300 K) δ [ppm] = 142.2, 142.0, 141.9, 141.9, 141.5, 141.2, 141.1, 141.0, 140.9, 140.9, 140.8, 140.7, 140.7, 140.7, 140.6, 140.5, 140.4, 140.4, 140.2, 140.2, 140.2, 140.1, 140.1, 140.0, 139.7, 139.6, 139.5, 139.5, 139.4, 139.4, 139.3, 139.1, 138.9, 138.9, 138.8, 138.7, 138.7, 138.6, 138.4, 138.3, 138.2, 138.1, 133.6, 133.5, 132.0, 131.8, 131.8, 131.4, 131.3, 130.2, 129.9, 128.9, 128.9, 128.6, 128.6, 128.5, 128.0, 127.9, 127.8, 127.3, 127.3, 127.2, 127.1, 127.1, 127.0, 126.8, 126.5, 126.1, 125.8, 125.6, 120.0, 119.7, 55.7 (C_a). FD Mass Spectrum (8kV) m/z = 1527 (100%, (M)⁺) (calcd. 1526). Elemental Analysis for C₁₁₀H₇₈BrNO₂ Calcd.: C, 86.59; H, 5.15; N, 0.92. Found: C, 86.49; H, 5.71; N, 1.05.

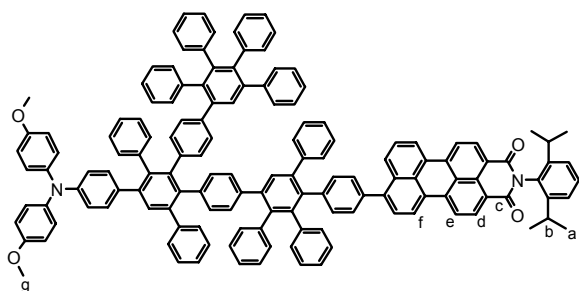
4-22



4-21 (1.59 g, 0.98 mmol) was dissolved in 50 mL of dry CH₂Cl₂ under argon atmosphere at -78 °C. A solution of BBr₃ (3.98 mL, 1.96 mmol) in CH₂Cl₂ was added dropwise. After the addition, the solution was allowed to reach room temperature and stirred for further 1.5 d. The reaction was quenched with HCl/H₂O (5%) and afterwards extracted with CH₂Cl₂/H₂O. The solvent was removed under reduced pressure and the crude product purified by column chromatography (silica gel, hexane/ethyl acetate 2:1) to afford **4-22** as a slightly grey solid.

Yield: 1.2 g (0.80 mmol), 82%. ¹H NMR Spectrum (250 MHz, CD₂Cl₂, 300 K) δ [ppm] = 7.42&7.38 (2s, 2H, H_{c+c'}), 7.15-6.65 (m, 68H, H_{arom.}), 6.56-6.53 (d, ³J(H,H) = 8.2 Hz, 2H, H_a), 6.50-6.47 (d, ³J(H,H) = 8.2 Hz, 2H, H_b). ¹³C NMR Spectrum (175 MHz, CD₂Cl₂, 300 K) δ [ppm] = 142.3, 142.3, 142.1, 142.0, 141.9, 141.6, 141.6, 141.2, 141.1, 141.1, 141.0, 140.8, 140.8, 140.8, 140.7, 140.7, 140.6, 140.4, 140.4, 140.3, 140.2, 140.2, 140.1, 140.1, 139.8, 139.7, 139.6, 139.6, 139.6, 139.5, 139.4, 139.3, 139.1, 139.0, 139.0, 138.9, 138.8, 138.8, 138.7, 138.6, 138.6, 138.5, 138.4, 138.2, 138.2, 133.6, 133.6, 132.1, 131.9, 131.9, 131.8, 131.6, 131.5, 131.4, 131.4, 131.3, 131.3, 130.3, 130.3, 130.0, 128.9, 128.9, 128.7, 128.6, 128.1, 127.9, 127.9, 127.9, 127.4, 127.3, 127.2, 127.2, 127.1, 127.0, 126.8, 126.8, 126.6, 126.5, 126.1, 125.9, 125.6, 120.0, 119.7. FD Mass Spectrum (8kV) m/z = 1499 (100%, (M)⁺) (calcd. 1498). Elemental Analysis for C₁₀₈H₇₄BrNO₂ Calcd.: C, 86.61; H, 4.98; N, 0.94. Found: C, 85.73; H, 5.43; N, 1.00.

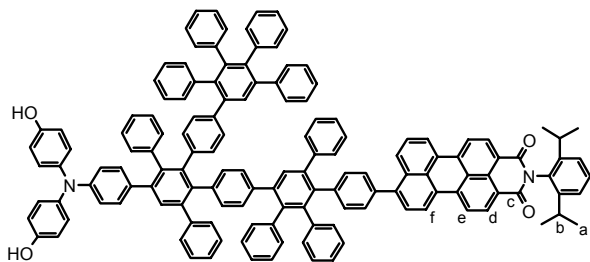
4-24



4-21 (150 mg, 98 μmol) and 4-23 (120 mg, 200 μmol) were dissolved in 7 mL of toluene. 0.5 mL of EtOH and 2.3 mL of a solution of 0.72 g K_2CO_3 in H_2O were added and the reaction mixture was flushed with argon. $\text{Pd}(\text{PPh}_3)_4$ catalyst (20 mg, 17 μmol) was added and the reaction mixture was stirred at 80 $^\circ\text{C}$ for 16 h. The resulting solution was extracted three times with $\text{CH}_2\text{Cl}_2/\text{H}_2\text{O}$. The organic layer was separated and dried over MgSO_4 . The crude product was purified by column chromatography (silica gel, CH_2Cl_2) to give 4-24 as a red solid. For single molecule spectroscopy 20 mg of 4-24 were further purified by preparative thin layer chromatography (silica gel, CH_2Cl_2).

Yield: 83 mg (43 μmol), 44 %. ^1H NMR Spectrum (500 MHz, CD_2Cl_2 , 300 K) δ [ppm] = 8.64-8.62 (m, 2H, H_d), 8.52-8.48 (m, 4H, H_{e+f}), 7.60-6.52 (m, 78H, $\text{H}_{\text{arom.}}$), 3.77 (s, 6H, H_g), 2.78-2.73 (sept, $^3\text{J}(\text{H,H}) = 6.5$ Hz, 2H, H_b), 1.15-1.13 (d, $^3\text{J}(\text{H,H}) = 6.5$ Hz, 12H, H_a). ^{13}C NMR Spectrum (125 MHz, CD_2Cl_2 , 300 K) δ [ppm] = 163.8 (C_c), 145.9, 143.2, 143.2, 141.7, 141.6, 141.6, 141.5, 140.6, 140.6, 140.5, 140.4, 140.3, 140.2, 140.2, 140.1, 140.0, 140.0, 139.8, 139.0, 139.0, 138.9, 138.9, 138.6, 138.6, 138.2, 138.1, 138.1, 137.6, 137.4, 136.7, 132.6, 132.5, 131.6, 131.6, 131.4, 131.3, 130.9, 130.8, 130.7, 130.4, 130.2, 129.8, 129.7, 129.7, 128.4, 128.2, 128.1, 128.0, 127.9, 127.6, 127.5, 127.4, 127.3, 127.3, 126.7, 126.6, 126.6, 126.5, 126.4, 126.2, 126.0, 125.4, 125.3, 125.1, 125.0, 123.7, 123.4, 120.7, 120.6, 120.1, 119.9, 119.3, 114.3, 55.2 (C_g), 28.8 (C_b), 23.4 (C_a). FD Mass Spectrum (8kV) m/z = 1925.6 (100%, $(\text{M})^+$) (calcd. 1926 $\text{C}_{144}\text{H}_{104}\text{N}_2\text{O}_4$).

4-25

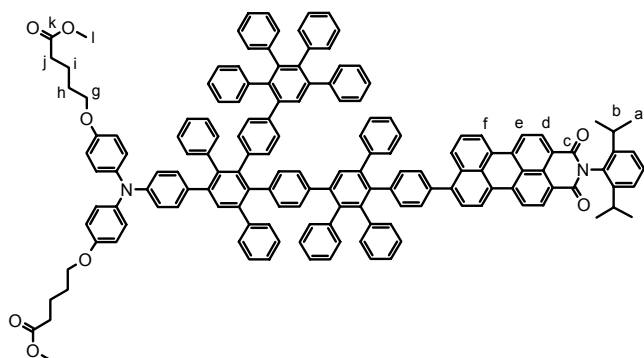


4-22 (0.9 g, 0.60 mmol) and 4-23 (0.73 g, 1.2 mmol) were dissolved in 18 mL of toluene. 1.2 mL of EtOH and 6.0 mL of a solution of 1.9 g K_2CO_3 in H_2O (2.3M) were added and the reaction mixture was flushed with argon. $\text{Pd}(\text{PPh}_3)_4$ catalyst (100 mg, 87 μmol) was added and the reaction mixture was stirred at 80 $^\circ\text{C}$ for 16 h. The resulting solution was extracted three times with $\text{CH}_2\text{Cl}_2/\text{H}_2\text{O}$. The organic layer was separated and dried over MgSO_4 . The crude product was purified by column chromatography (silica gel, 1st column hexane/ethyl acetate 1:1, 2nd column hexane/ethyl acetate 4:1) to give 4-25 as a red solid.

Yield: 506 mg (0.27 mmol), 44 %. ^1H NMR Spectrum (250 MHz, CD_2Cl_2 , 300 K) δ [ppm] = 8.64-8.61 (d, $^3\text{J}(\text{H,H}) = 7.9$ Hz, 2H, H_d), 8.51-8.46 (m, 4H, H_{e+f}), 7.59-6.50 (m, 80H, $\text{H}_{\text{arom.}}$), 2.81-2.71 (sept, $^3\text{J}(\text{H,H}) = 6.9$ Hz, 2H, H_b), 1.16-1.13 (d, $^3\text{J}(\text{H,H}) = 6.7$ Hz, 12H, H_a). ^{13}C NMR Spectrum (62.9 MHz, CD_2Cl_2 , 300 K) δ [ppm] = 164.4 (C_c), 146.4, 142.2, 142.2, 142.1, 142.0, 141.7, 141.6, 141.1, 141.0, 140.9, 140.6, 140.5, 140.3, 139.5, 139.5, 138.7, 138.6, 138.1, 138.0, 137.2, 133.0, 132.2, 132.0, 131.9, 131.8, 131.4, 131.4, 131.3, 130.9, 130.7, 130.4, 130.3, 130.2, 129.8, 129.4, 129.6, 128.9, 128.8, 128.5, 128.0, 127.9, 127.8, 127.3, 127.1, 127.2, 127.1, 127.0, 126.8, 126.5, 126.0, 125.9, 125.6, 124.3, 121.1, 121.0, 120.6, 120.4, 116.3, 24.9 (C_b), 24.0 (C_a). FD Mass Spectrum (8kV) m/z = 1898 (100%, $(\text{M})^+$) (calcd.

1898). Elemental Analysis for $C_{142}H_{100}N_2O_4$ Calcd.: C, 89.84; H, 5.31; N, 1.48. Found: C, 89.90; H, 5.29; N, 1.51.

4-26

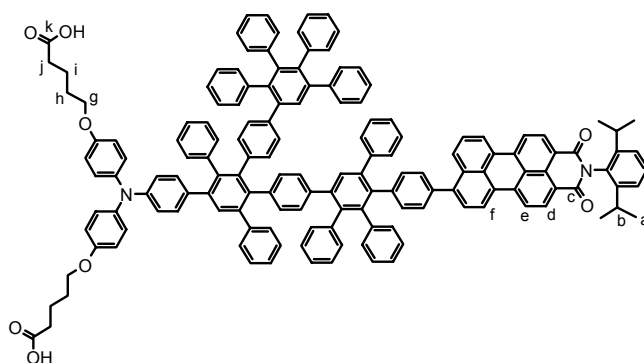


4-25 (120 mg, 58 μmol) and K_2CO_3 (20 mg, 150 μmol) were placed in a Schlenk tube with 2 mL of dry acetone and 5 mL of dry DMF. Argon was bubbled through the solution for 30 min and the reaction mixture further stirred for 1 h. 0.6 mL (150 μmol) of a solution of 5-bromo-valerianic acid-methylester (**4-17**) (100 mg in 2 mL of acetone) was added dropwise to the reaction mixture

which was afterwards stirred for another 1 h at room temperature and the refluxed overnight. A catalytic amount of potassium iodide and another 0.6 mL (150 μmol) of the solution of **4-17** was added and the reaction mixture further refluxed for 4 days. The reaction mixture was diluted with CH_2Cl_2 and extracted with $\text{CH}_2\text{Cl}_2/\text{H}_2\text{O}$. The solvent was removed under reduced pressure and the crude product purified by column chromatography (silica gel, hexane/ethyl acetate 3:2) to afford **4-26** as a red solid.

Yield: 108 mg (51 μmol), 80%. ^1H NMR Spectrum (250 MHz, CD_2Cl_2 , 300 K) δ [ppm] = 8.64-8.61 (d, $^3\text{J}(\text{H,H}) = 7.9$ Hz, 2H, H_d), 8.52-8.46 (m, 4H, H_{e+f}), 7.59-6.51 (m, 78H, $\text{H}_{\text{arom.}}$), 3.94-3.91 (m, 4H, H_g), 3.65 (s, 6H, H_i), 2.82-2.71 (sept, $^3\text{J}(\text{H,H}) = 6.6$ Hz, 2H, H_a), 2.38 (m, 4H, H_j), 1.79 (m, 8H, H_{h+i}), 1.13-1.16 (d, $^3\text{J}(\text{H,H}) = 7.0$ Hz, 12H, H_b). ^{13}C NMR Spectrum (175 MHz, CD_2Cl_2 , 300 K) δ [ppm] = 174.0 (C_k), 164.4 (C_c), 155.6, 147.4, 146.4, 143.7, 142.2, 142.1, 142.1, 142.0, 141.7, 141.5, 141.1, 141.0, 140.8, 140.6, 140.5, 139.5, 139.4, 139.4, 138.7, 138.6, 138.4, 138.3, 138.1, 138.0, 137.3, 134.0, 133.0, 132.2, 132.1, 132.0, 131.8, 131.4, 131.3, 130.9, 130.7, 130.4, 130.3, 130.2, 129.5, 129.4, 128.9, 128.8, 128.6, 128.5, 128.5, 128.0, 127.9, 127.8, 127.2, 127.1, 127.1, 127.0, 126.7, 126.5, 125.8, 125.5, 124.3, 121.2, 121.0, 120.7, 120.4, 119.8, 115.4, 68.0 (C_g), 51.8 & 51.6 (C_l), 33.9 (C_j), 30.0, 29.4 & 29.0 (C_b), 24.0 (C_a), 21.9 (C_i). FD Mass Spectrum (8kV) $m/z = 2127$ (100%, $(\text{M})^+$) (calcd. 2127). Elemental Analysis for $C_{154}H_{120}N_2O_8$ Calcd.: C, 86.98; H, 5.96. Found: C, 85.76; H, 6.10.

4-27



4-26 (80 mg, 38 μmol) and a 2M NaOH (0.12 mL, 220 μmol) were placed in a flask together with 2 mL of MeOH and 4 mL of THF. The reaction mixture was stirred for 4 days. After that, the solvent was removed under reduced pressure and the crude product purified by column chromatography (silica gel, ethyl acetate/acidic acid 500:1) to afford **4-27** as a red solid. To remove the acidic acid

the product was further precipitated from THF in hexane. For single molecule spectroscopy 20 mg of **4-27** were further purified by preparative thin layer chromatography (silica gel,

ethyl acetate/acidic acid 1000:1).

Yield: 60 mg (29 μ mol), 76%. **^1H NMR Spectrum (250 MHz, CD_2Cl_2 , 300 K)** δ [ppm] = 8.62-8.59 (d, $^3\text{J}(\text{H,H}) = 7.9$ Hz, 2H, H_d), 8.51-8.41 (m, 4H, H_{e+f}), 7.62-6.50 (m, 80H, $\text{H}_{\text{arom.}}$), 3.95 (s, 4H, H_g), 2.85-2.68 (sept, $^3\text{J}(\text{H,H}) = 6.6$ Hz, 2H, H_b), 2.44 (s, 4H, H_j), 1.81 (s, 8H, H_{h+i}), 1.16-1.13 (d, $^3\text{J}(\text{H,H}) = 7.0$ Hz, 12H, H_a). **^{13}C NMR Spectrum (175 MHz, CD_2Cl_2 , 300 K)** δ [ppm] = 179.2 (C_k), 164.4 (C_c), 155.6, 147.4, 146.5, 143.7, 143.7, 142.2, 142.1, 141.8, 141.6, 141.6, 141.2, 141.0, 140.9, 140.7, 140.6, 140.6, 140.4, 140.4, 139.6, 139.4, 139.2, 138.8, 138.7, 138.7, 138.4, 138.0, 137.8, 137.3, 134.1, 132.9, 132.1, 131.9, 131.4, 130.8, 130.4, 130.3, 130.3, 129.6, 129.3, 129.0, 128.8, 128.7, 128.4, 128.4, 128.0, 127.9, 127.9, 127.3, 127.2, 127.2, 127.1, 127.0, 126.8, 126.5, 125.9, 125.6, 124.3, 124.3, 123.9, 121.1, 121.0, 120.5, 120.3, 119.9, 115.6, 68.1 (C_g), 34.1 (C_j), 29.5 (C_b), 29.0 (C_h), 24.1 (C_a), 21.9 (C_i). **MALDI TOF Mass Spectrum** $m/z = 2099$ (100%, $(\text{M})^+$) (calcd. 2099). **Elemental Analysis for $\text{C}_{152}\text{H}_{116}\text{N}_2\text{O}_8$** Calcd.: C, 86.99; H, 5.57; N, 1.33. Found: C, 86.57; H, 5.96; N, 1.52. **UV/Vis (CHCl_3)** λ [nm] = 259 (7114), 337 (1750), 505 (2371), 524 nm (2334 $\text{m}^2\text{mol}^{-1}$).

6.2.3 Crystal Structure Data of 2-31

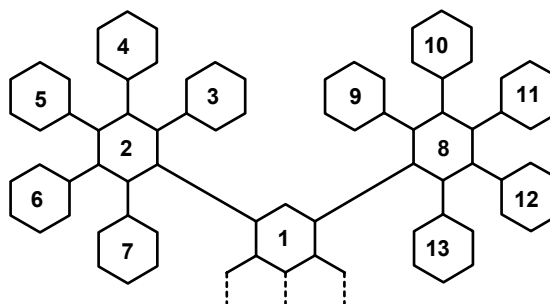
Crystal Structure. The crystal structure determinations were carried out in glass capillaries on a Nonius KCCD diffractometer with graphite monochromated $\text{MoK}\alpha$ radiation at 120 K. The structures were solved by direct methods (Shelxs97). Refinement was done with anisotropic temperatures factors for C, the hydrogen atoms were refined with fixed isotropic temperature factors in the riding mode.

Unit cell parameters of 2-31.

a (Å)	42.2264 (9)	μ (mm^{-1})	0.377
b (Å)	12.3538 (4)	D_x (g cm^{-3})	1.32
c (Å)	32.0039 (8)	no. of reflcns (meas.)	93092
α (deg)	90	no. of reflcns (unique)	16820
β (deg)	125.139 (1)	no. of reflcns (obsd)	6998
γ (deg)	90	R (%)	0.0804
Z	8	R_w (%)	0.0511
V (Å ³)	13652.5 (12)		

Interplanar angles (deg) between the phenyl rings in dendrimer 2-31.

	planes		
planes	1	2	8
2	110.1		
3		117.1	
4		115.3	
5		119.1	
6		112.1	
7		104.5	
8	107.2		
9			107.4
10			101.9
11			105.7
12			111.2
13			112.4



Assignment of the planes for the dihedral angles.

Atom	x/a	y/b	z/c	U(iso)	Occ
C1(1)	0.22753(4)	0.50481(12)	0.24935(6)	0.0507	
C1(2)	0.24381(5)	0.30012(14)	0.22035(6)	0.0629	
C1(3)	0.34196(4)	0.18692(13)	0.23586(6)	0.0508	
C1(4)	0.32163(4)	0.14460(15)	0.13361(6)	0.0616	
C1(5)	-0.03619(5)	0.73576(15)	-0.00473(6)	0.0649	
C1(6)	0.01796(6)	0.87590(15)	-0.00447(8)	0.0756	
C1(7)	0.15738(5)	0.39445(15)	0.27907(7)	0.0694	
C1(8)	0.21473(5)	0.23636(15)	0.34557(7)	0.0646	
C(1)	0.00448(11)	0.6952(3)	0.27553(14)	0.0138	
C(2)	-0.02553(11)	0.6981(3)	0.28257(14)	0.0147	
C(3)	-0.01634(11)	0.7015(3)	0.33239(15)	0.0167	
C(5)	0.05231(11)	0.6846(3)	0.36782(14)	0.0149	
C(6)	0.04385(11)	0.6910(3)	0.31807(15)	0.0153	
C(9)	-0.04698(11)	0.7192(4)	0.34171(14)	0.0175	
C(10)	-0.06615(11)	0.8193(3)	0.33047(15)	0.0182	
C(11)	-0.09364(12)	0.8381(3)	0.34105(15)	0.0202	
C(12)	-0.10227(12)	0.7544(4)	0.36286(15)	0.0204	
C(13)	-0.08362(12)	0.6537(4)	0.37374(15)	0.0204	
C(14)	-0.05659(11)	0.6358(3)	0.36223(15)	0.0177	
C(15)	-0.05938(13)	0.9062(4)	0.30321(18)	0.0242	
C(21)	-0.11313(12)	0.9457(4)	0.32991(16)	0.0209	
C(27)	-0.13214(11)	0.7693(4)	0.37425(15)	0.0210	
C(33)	-0.09194(11)	0.5671(4)	0.39966(15)	0.0198	
C(39)	-0.04129(12)	0.5226(4)	0.36838(16)	0.0215	
C(45)	0.09350(11)	0.6644(3)	0.41295(15)	0.0173	
C(46)	0.11571(11)	0.7472(4)	0.44815(15)	0.0198	
C(47)	0.15370(12)	0.7246(4)	0.49043(15)	0.0200	
C(48)	0.16955(11)	0.6214(4)	0.49664(15)	0.0201	

Experimental Part

C(49)	0.14812 (11)	0.5402 (4)	0.46042 (15)	0.0177
C(50)	0.11015 (12)	0.5618 (4)	0.41857 (15)	0.0188
C(51)	0.09992 (12)	0.8601 (4)	0.43986 (16)	0.0214
C(57)	0.17731 (11)	0.8126 (4)	0.52792 (15)	0.0220
C(63)	0.20982 (12)	0.5977 (4)	0.54231 (15)	0.0229
C(69)	0.16521 (12)	0.4310 (4)	0.46429 (16)	0.0234
C(75)	0.08805 (12)	0.4765 (3)	0.37780 (16)	0.0214
C(4)	0.02240 (12)	0.6920 (3)	0.37375 (15)	0.0186
C(7)	0.07341 (11)	0.6932 (3)	0.30941 (15)	0.0173
C(8)	-0.06483 (11)	0.6961 (3)	0.23812 (14)	0.0161
C(16)	-0.09093 (14)	0.9361 (4)	0.25382 (18)	0.0293
C(17)	-0.0870 (2)	1.0131 (5)	0.2263 (2)	0.0517
C(18)	-0.0511 (2)	1.0598 (5)	0.2469 (3)	0.0680
C(19)	-0.0203 (2)	1.0325 (5)	0.2952 (3)	0.0656
C(20)	-0.02383 (15)	0.9539 (4)	0.3238 (2)	0.0367
C(22)	-0.15272 (12)	0.9577 (4)	0.29391 (17)	0.0248
C(23)	-0.17034 (14)	1.0570 (4)	0.28303 (19)	0.0344
C(24)	-0.14854 (15)	1.1485 (4)	0.3092 (2)	0.0363
C(25)	-0.10884 (15)	1.1380 (4)	0.3460 (2)	0.0358
C(26)	-0.09155 (14)	1.0379 (4)	0.35595 (19)	0.0318
C(28)	-0.12686 (13)	0.8437 (4)	0.40990 (17)	0.0257
C(29)	-0.15256 (13)	0.8470 (4)	0.42386 (17)	0.0309
C(30)	-0.18300 (13)	0.7756 (4)	0.40279 (18)	0.0324
C(31)	-0.18917 (12)	0.7038 (4)	0.36590 (17)	0.0271
C(32)	-0.16391 (11)	0.7013 (4)	0.35130 (16)	0.0236
C(34)	-0.08081 (12)	0.5871 (4)	0.44932 (16)	0.0236
C(35)	-0.08975 (13)	0.5141 (4)	0.47378 (18)	0.0316
C(36)	-0.10957 (14)	0.4207 (4)	0.44916 (19)	0.0348
C(37)	-0.12092 (14)	0.4007 (4)	0.4000 (2)	0.0349
C(38)	-0.11183 (13)	0.4727 (4)	0.37542 (18)	0.0283
C(40)	-0.01518 (12)	0.4770 (4)	0.41691 (17)	0.0277
C(41)	-0.00554 (14)	0.3678 (4)	0.42097 (19)	0.0337
C(42)	-0.02234 (14)	0.3026 (4)	0.37821 (19)	0.0349
C(43)	-0.04788 (14)	0.3478 (4)	0.33015 (19)	0.0309
C(44)	-0.05676 (13)	0.4581 (4)	0.32528 (17)	0.0241
C(52)	0.09626 (14)	0.9247 (4)	0.40205 (19)	0.0331
C(53)	0.08378 (15)	1.0311 (4)	0.3962 (2)	0.0442
C(54)	0.07379 (16)	1.0731 (5)	0.4261 (2)	0.0481
C(55)	0.07679 (16)	1.0092 (5)	0.4636 (2)	0.0492
C(56)	0.08988 (14)	0.9022 (4)	0.47113 (19)	0.0330
C(58)	0.18335 (13)	0.8148 (4)	0.57602 (16)	0.0285
C(59)	0.20494 (14)	0.8976 (4)	0.61023 (18)	0.0356
C(60)	0.22142 (13)	0.9758 (4)	0.59854 (19)	0.0343
C(61)	0.21657 (14)	0.9741 (4)	0.5522 (2)	0.0352
C(62)	0.19456 (13)	0.8928 (4)	0.51723 (19)	0.0324
C(64)	0.21483 (13)	0.5499 (4)	0.58535 (17)	0.0294
C(65)	0.25234 (14)	0.5292 (4)	0.62856 (18)	0.0385
C(66)	0.28415 (16)	0.5541 (5)	0.6290 (2)	0.0456
C(67)	0.27952 (14)	0.6002 (5)	0.5867 (2)	0.0484
C(68)	0.24211 (13)	0.6230 (4)	0.54368 (18)	0.0359
C(70)	0.19359 (12)	0.4194 (4)	0.45560 (17)	0.0271
C(71)	0.20670 (13)	0.3176 (4)	0.45357 (18)	0.0323
C(72)	0.19130 (14)	0.2264 (4)	0.46084 (17)	0.0334
C(73)	0.16398 (13)	0.2365 (4)	0.47064 (18)	0.0309
C(74)	0.15086 (13)	0.3390 (4)	0.47281 (16)	0.0265
C(76)	0.10117 (12)	0.4484 (4)	0.34840 (16)	0.0262
C(77)	0.08079 (15)	0.3712 (5)	0.3093 (2)	0.0456
C(78)	0.04809 (16)	0.3250 (6)	0.3013 (3)	0.0640
C(79)	0.03514 (17)	0.3528 (5)	0.3298 (3)	0.0634
C(80)	0.05482 (14)	0.4293 (4)	0.3689 (2)	0.0374
H(41)	0.02855 (12)	0.6902 (3)	0.40735 (15)	0.0165
H(71)	0.09976 (11)	0.6923 (3)	0.33797 (15)	0.0156
H(81)	-0.08524 (11)	0.6968 (3)	0.24253 (14)	0.0140

H(161)	-0.11547 (14)	0.9035 (4)	0.23988 (18)	0.0303		
H(171)	-0.1086 (2)	1.0332 (5)	0.1932 (2)	0.0541		
H(181)	-0.0478 (2)	1.1098 (5)	0.2272 (3)	0.0722		
H(191)	0.0037 (2)	1.0690 (5)	0.3099 (3)	0.0704		
H(201)	-0.00222 (15)	0.9334 (4)	0.3568 (2)	0.0391		
H(221)	-0.16787 (12)	0.8954 (4)	0.27641 (17)	0.0236		
H(231)	-0.19742 (14)	1.0633 (4)	0.25782 (19)	0.0342		
H(241)	-0.16077 (15)	1.2172 (4)	0.3018 (2)	0.0392		
H(251)	-0.09365 (15)	1.2000 (4)	0.3639 (2)	0.0417		
H(261)	-0.06449 (14)	1.0309 (4)	0.38113 (19)	0.0339		
H(281)	-0.10582 (13)	0.8931 (4)	0.42465 (17)	0.0258		
H(291)	-0.14890 (13)	0.8985 (4)	0.44834 (17)	0.0328		
H(301)	-0.19962 (13)	0.7753 (4)	0.41383 (18)	0.0322		
H(311)	-0.21083 (12)	0.6564 (4)	0.35023 (17)	0.0271		
H(321)	-0.16852 (11)	0.6524 (4)	0.32543 (16)	0.0243		
H(341)	-0.06690 (12)	0.6511 (4)	0.46662 (16)	0.0212		
H(351)	-0.08223 (13)	0.5283 (4)	0.50751 (18)	0.0296		
H(361)	-0.11542 (14)	0.3701 (4)	0.46616 (19)	0.0375		
H(371)	-0.13487 (14)	0.3366 (4)	0.3829 (2)	0.0357		
H(381)	-0.11919 (13)	0.4581 (4)	0.34178 (18)	0.0298		
H(401)	-0.00405 (12)	0.5204 (4)	0.44671 (17)	0.0253		
H(411)	0.01259 (14)	0.3370 (4)	0.45365 (19)	0.0337		
H(421)	-0.01660 (14)	0.2275 (4)	0.38141 (19)	0.0395		
H(431)	-0.05903 (14)	0.3038 (4)	0.30052 (19)	0.0348		
H(441)	-0.07360 (13)	0.4893 (4)	0.29234 (17)	0.0255		
H(521)	0.10236 (14)	0.8951 (4)	0.38008 (19)	0.0341		
H(531)	0.08246 (15)	1.0756 (4)	0.3710 (2)	0.0461		
H(541)	0.06457 (16)	1.1453 (5)	0.4212 (2)	0.0477		
H(551)	0.07002 (16)	1.0391 (5)	0.4848 (2)	0.0514		
H(561)	0.09172 (14)	0.8579 (4)	0.49672 (19)	0.0380		
H(581)	0.17302 (13)	0.7585 (4)	0.58504 (16)	0.0261		
H(591)	0.20770 (14)	0.9004 (4)	0.64184 (18)	0.0349		
H(601)	0.23635 (13)	1.0312 (4)	0.62268 (19)	0.0364		
H(611)	0.22814 (14)	1.0292 (4)	0.5445 (2)	0.0339		
H(621)	0.19173 (13)	0.8911 (4)	0.48556 (19)	0.0355		
H(641)	0.19294 (13)	0.5333 (4)	0.58554 (17)	0.0316		
H(651)	0.25565 (14)	0.4959 (4)	0.65759 (18)	0.0416		
H(661)	0.30941 (16)	0.5392 (5)	0.6584 (2)	0.0439		
H(671)	0.30151 (14)	0.6174 (5)	0.5868 (2)	0.0516		
H(681)	0.23887 (13)	0.6561 (4)	0.51465 (18)	0.0354		
H(701)	0.20426 (12)	0.4822 (4)	0.45105 (17)	0.0307		
H(711)	0.22580 (13)	0.3104 (4)	0.44688 (18)	0.0330		
H(721)	0.20014 (14)	0.1568 (4)	0.45918 (17)	0.0346		
H(731)	0.15356 (13)	0.1735 (4)	0.47553 (18)	0.0320		
H(741)	0.13247 (13)	0.3462 (4)	0.48073 (16)	0.0267		
H(761)	0.12410 (12)	0.4806 (4)	0.35515 (16)	0.0242		
H(771)	0.08933 (15)	0.3532 (5)	0.2885 (2)	0.0449		
H(781)	0.03436 (16)	0.2731 (6)	0.2747 (3)	0.0618		
H(791)	0.01261 (17)	0.3182 (5)	0.3233 (3)	0.0642		
H(801)	0.04565 (14)	0.4487 (4)	0.3888 (2)	0.0379		
C(91)	0.25047 (16)	0.3784 (4)	0.27015 (19)	0.0400		
H(911)	0.27745 (16)	0.3896 (4)	0.29452 (19)	0.0429		
H(912)	0.24030 (16)	0.3400 (4)	0.28569 (19)	0.0429		
C(92)	0.30423 (15)	0.1628 (5)	0.1717 (2)	0.0492		
H(921)	0.28726 (15)	0.2233 (5)	0.1591 (2)	0.0510		
H(922)	0.29047 (15)	0.0998 (5)	0.1696 (2)	0.0510		
C(93)	-0.00090 (19)	0.8353 (6)	0.0294 (3)	0.0656		
H(931)	-0.01166 (19)	0.8958 (6)	0.0354 (3)	0.0603		
H(932)	0.01955 (19)	0.8056 (6)	0.0611 (3)	0.0603		
C(94)	0.16599 (16)	0.2730 (5)	0.3129 (3)	0.0530		
H(941)	0.15997 (16)	0.2837 (5)	0.3370 (3)	0.0506		
H(942)	0.15009 (16)	0.2172 (5)	0.2898 (3)	0.0506		
Atom	u(11)	u(22)	u(33)	u(23)	u(13)	u(12)

Experimental Part

C1(1)	0.0458(8)	0.0449(8)	0.0481(8)	0.0081(7)	0.0192(7)	0.0170(7)
C1(2)	0.0657(10)	0.0587(10)	0.0635(10)	-0.0184(9)	0.0367(9)	-0.0027(9)
C1(3)	0.0361(7)	0.0621(10)	0.0565(9)	-0.0273(8)	0.0279(7)	-0.0166(7)
C1(4)	0.0396(8)	0.0843(12)	0.0535(9)	-0.0250(9)	0.0225(7)	0.0062(8)
C1(5)	0.0653(10)	0.0795(12)	0.0511(9)	-0.0048(9)	0.0342(8)	-0.0024(9)
C1(6)	0.0810(13)	0.0628(12)	0.0942(14)	-0.0001(10)	0.0569(12)	-0.0046(10)
C1(7)	0.0644(11)	0.0617(11)	0.0681(11)	0.0199(9)	0.0300(9)	0.0172(9)
C1(8)	0.0503(9)	0.0772(12)	0.0678(10)	0.0159(9)	0.0348(8)	0.0295(9)
C(1)	0.0155(18)	0.0097(18)	0.0153(19)	-0.0007(16)	0.0083(16)	0.0016(16)
C(2)	0.0157(19)	0.014(2)	0.0130(18)	-0.0046(17)	0.0075(16)	-0.0031(17)
C(3)	0.019(2)	0.012(2)	0.024(2)	-0.0037(18)	0.0153(18)	-0.0044(17)
C(5)	0.0144(19)	0.013(2)	0.0145(19)	-0.0033(17)	0.0068(16)	-0.0025(17)
C(6)	0.0142(19)	0.0101(19)	0.020(2)	-0.0002(17)	0.0092(17)	0.0007(16)
C(9)	0.0108(19)	0.027(2)	0.0101(18)	-0.0031(17)	0.0032(16)	-0.0038(17)
C(10)	0.016(2)	0.022(2)	0.018(2)	-0.0068(18)	0.0110(17)	-0.0070(18)
C(11)	0.017(2)	0.022(2)	0.018(2)	-0.0064(18)	0.0087(18)	-0.0054(18)
C(12)	0.017(2)	0.029(3)	0.016(2)	-0.0061(18)	0.0106(18)	-0.0024(19)
C(13)	0.020(2)	0.026(2)	0.0140(19)	-0.0053(18)	0.0086(17)	-0.0092(18)
C(14)	0.015(2)	0.026(2)	0.0151(19)	-0.0074(18)	0.0101(17)	-0.0060(18)
C(15)	0.033(3)	0.018(2)	0.034(3)	-0.003(2)	0.026(2)	0.002(2)
C(21)	0.027(2)	0.019(2)	0.025(2)	-0.0051(19)	0.020(2)	-0.0004(19)
C(27)	0.016(2)	0.030(3)	0.016(2)	0.0002(19)	0.0093(18)	-0.0002(19)
C(33)	0.015(2)	0.032(3)	0.017(2)	0.0003(19)	0.0113(18)	0.0029(18)
C(39)	0.015(2)	0.032(3)	0.023(2)	0.001(2)	0.0139(18)	-0.0027(19)
C(45)	0.016(2)	0.026(2)	0.0142(19)	0.0011(18)	0.0108(17)	-0.0016(18)
C(46)	0.016(2)	0.028(2)	0.018(2)	-0.0014(18)	0.0105(17)	-0.0031(18)
C(47)	0.019(2)	0.025(2)	0.016(2)	-0.0021(18)	0.0103(18)	-0.0073(18)
C(48)	0.015(2)	0.028(3)	0.015(2)	0.0035(19)	0.0081(18)	-0.0055(18)
C(49)	0.017(2)	0.022(2)	0.018(2)	0.0003(18)	0.0119(18)	-0.0045(18)
C(50)	0.020(2)	0.023(2)	0.017(2)	-0.0005(18)	0.0121(18)	-0.0034(18)
C(51)	0.014(2)	0.025(2)	0.023(2)	-0.0079(19)	0.0095(18)	-0.0101(18)
C(57)	0.016(2)	0.024(2)	0.019(2)	-0.0016(19)	0.0058(17)	-0.0043(18)
C(63)	0.021(2)	0.025(2)	0.014(2)	-0.0053(18)	0.0057(18)	-0.0033(19)
C(69)	0.018(2)	0.029(3)	0.016(2)	0.0023(19)	0.0054(18)	0.0008(19)
C(75)	0.019(2)	0.018(2)	0.019(2)	0.0016(18)	0.0064(18)	0.0021(18)
C(4)	0.023(2)	0.020(2)	0.0135(19)	-0.0042(18)	0.0115(18)	-0.0054(19)
C(7)	0.0120(19)	0.018(2)	0.020(2)	-0.0019(18)	0.0085(17)	0.0009(17)
C(8)	0.0140(19)	0.019(2)	0.020(2)	-0.0006(18)	0.0125(17)	0.0020(17)
C(16)	0.041(3)	0.025(3)	0.035(3)	0.002(2)	0.030(3)	0.004(2)
C(17)	0.073(4)	0.039(3)	0.058(4)	0.017(3)	0.046(4)	0.013(3)
C(18)	0.090(5)	0.043(4)	0.098(6)	0.019(4)	0.070(5)	-0.008(4)
C(19)	0.069(5)	0.040(4)	0.102(6)	0.007(4)	0.058(5)	-0.016(3)
C(20)	0.038(3)	0.028(3)	0.053(3)	0.002(3)	0.032(3)	-0.004(2)
C(22)	0.024(2)	0.027(3)	0.025(2)	-0.005(2)	0.014(2)	-0.002(2)
C(23)	0.028(3)	0.036(3)	0.037(3)	0.002(2)	0.018(2)	0.005(2)
C(24)	0.043(3)	0.024(3)	0.052(3)	0.000(2)	0.034(3)	0.008(2)
C(25)	0.033(3)	0.026(3)	0.055(3)	-0.016(2)	0.029(3)	-0.008(2)
C(26)	0.025(2)	0.036(3)	0.037(3)	-0.010(2)	0.019(2)	-0.004(2)
C(28)	0.023(2)	0.030(3)	0.025(2)	-0.004(2)	0.014(2)	-0.001(2)
C(29)	0.025(2)	0.047(3)	0.025(2)	0.001(2)	0.017(2)	0.007(2)
C(30)	0.024(2)	0.049(3)	0.037(3)	0.008(2)	0.025(2)	0.011(2)
C(31)	0.018(2)	0.035(3)	0.030(2)	0.006(2)	0.015(2)	0.003(2)
C(32)	0.015(2)	0.032(3)	0.024(2)	-0.001(2)	0.0109(18)	-0.0015(19)
C(34)	0.018(2)	0.033(3)	0.021(2)	-0.002(2)	0.0117(19)	-0.0044(19)
C(35)	0.027(2)	0.051(3)	0.023(2)	0.007(2)	0.018(2)	0.002(2)
C(36)	0.036(3)	0.041(3)	0.041(3)	0.008(3)	0.030(3)	-0.003(2)
C(37)	0.035(3)	0.034(3)	0.045(3)	-0.005(2)	0.029(3)	-0.009(2)
C(38)	0.033(3)	0.032(3)	0.029(3)	-0.005(2)	0.023(2)	-0.007(2)
C(40)	0.019(2)	0.037(3)	0.024(2)	-0.002(2)	0.010(2)	-0.003(2)
C(41)	0.022(2)	0.041(3)	0.028(3)	0.008(2)	0.009(2)	0.003(2)
C(42)	0.038(3)	0.025(3)	0.043(3)	0.001(2)	0.023(3)	-0.002(2)
C(43)	0.033(3)	0.028(3)	0.032(3)	-0.003(2)	0.019(2)	-0.003(2)

C(44)	0.024 (2)	0.029 (3)	0.020 (2)	-0.004 (2)	0.0128 (19)	-0.003 (2)
C(52)	0.035 (3)	0.027 (3)	0.036 (3)	0.002 (2)	0.020 (2)	-0.004 (2)
C(53)	0.045 (3)	0.023 (3)	0.055 (4)	0.003 (3)	0.023 (3)	-0.001 (2)
C(54)	0.046 (3)	0.021 (3)	0.057 (4)	-0.010 (3)	0.018 (3)	0.002 (2)
C(55)	0.042 (3)	0.055 (4)	0.044 (3)	-0.029 (3)	0.020 (3)	0.003 (3)
C(56)	0.033 (3)	0.033 (3)	0.030 (3)	-0.009 (2)	0.016 (2)	-0.004 (2)
C(58)	0.029 (2)	0.032 (3)	0.019 (2)	0.000 (2)	0.011 (2)	-0.008 (2)
C(59)	0.028 (3)	0.043 (3)	0.020 (2)	-0.006 (2)	0.005 (2)	-0.004 (2)
C(60)	0.021 (2)	0.025 (3)	0.032 (3)	-0.007 (2)	0.001 (2)	0.001 (2)
C(61)	0.026 (3)	0.023 (3)	0.045 (3)	0.004 (2)	0.014 (2)	-0.005 (2)
C(62)	0.029 (3)	0.034 (3)	0.036 (3)	0.002 (2)	0.020 (2)	-0.005 (2)
C(64)	0.018 (2)	0.039 (3)	0.024 (2)	0.005 (2)	0.007 (2)	-0.001 (2)
C(65)	0.032 (3)	0.040 (3)	0.023 (2)	0.009 (2)	0.005 (2)	0.005 (2)
C(66)	0.030 (3)	0.050 (4)	0.030 (3)	0.002 (3)	0.002 (2)	0.003 (3)
C(67)	0.016 (2)	0.081 (5)	0.037 (3)	-0.006 (3)	0.009 (2)	-0.006 (3)
C(68)	0.024 (2)	0.055 (4)	0.023 (2)	-0.003 (2)	0.011 (2)	-0.009 (2)
C(70)	0.020 (2)	0.031 (3)	0.025 (2)	0.004 (2)	0.009 (2)	-0.001 (2)
C(71)	0.027 (2)	0.041 (3)	0.030 (2)	0.004 (2)	0.016 (2)	0.010 (2)
C(72)	0.031 (3)	0.031 (3)	0.026 (2)	0.006 (2)	0.010 (2)	0.011 (2)
C(73)	0.031 (3)	0.025 (3)	0.032 (3)	0.003 (2)	0.015 (2)	-0.003 (2)
C(74)	0.026 (2)	0.030 (3)	0.023 (2)	0.001 (2)	0.014 (2)	-0.002 (2)
C(76)	0.018 (2)	0.028 (3)	0.022 (2)	-0.005 (2)	0.0048 (19)	0.0035 (19)
C(77)	0.036 (3)	0.053 (4)	0.033 (3)	-0.014 (3)	0.011 (2)	0.018 (3)
C(78)	0.024 (3)	0.062 (4)	0.079 (5)	-0.045 (4)	0.014 (3)	-0.005 (3)
C(79)	0.033 (3)	0.054 (4)	0.104 (5)	-0.044 (4)	0.040 (4)	-0.023 (3)
C(80)	0.029 (3)	0.031 (3)	0.054 (3)	-0.014 (3)	0.025 (3)	-0.007 (2)
C(91)	0.042 (3)	0.043 (3)	0.031 (3)	0.011 (2)	0.019 (2)	0.009 (3)
C(92)	0.030 (3)	0.057 (4)	0.059 (4)	-0.019 (3)	0.025 (3)	-0.009 (3)
C(93)	0.061 (4)	0.062 (5)	0.079 (5)	0.033 (4)	0.044 (4)	0.012 (3)
C(94)	0.037 (3)	0.050 (4)	0.074 (4)	0.008 (3)	0.034 (3)	0.002 (3)

C1(1) - C(91)	1.755 (5)
C1(2) - C(91)	1.743 (5)
C1(3) - C(92)	1.754 (6)
C1(4) - C(92)	1.762 (6)
C1(5) - C(93)	1.747 (7)
C1(6) - C(93)	1.747 (7)
C1(7) - C(94)	1.761 (6)
C1(8) - C(94)	1.748 (6)
C(1) - C(1)	1.450 (7)
C(1) - C(2)	1.409 (5)
C(1) - C(6)	1.419 (5)
C(2) - C(3)	1.408 (5)
C(2) - C(8)	1.436 (5)
C(3) - C(9)	1.502 (5)
C(3) - C(4)	1.396 (6)
C(5) - C(6)	1.419 (5)
C(5) - C(45)	1.510 (5)
C(5) - C(4)	1.384 (5)
C(6) - C(7)	1.426 (5)
C(9) - C(10)	1.407 (6)
C(9) - C(14)	1.401 (6)
C(10) - C(11)	1.403 (6)
C(10) - C(15)	1.511 (6)
C(11) - C(12)	1.408 (6)
C(11) - C(21)	1.494 (6)
C(12) - C(13)	1.405 (6)
C(12) - C(27)	1.512 (6)
C(13) - C(14)	1.404 (6)
C(13) - C(33)	1.513 (6)
C(14) - C(39)	1.505 (6)
C(15) - C(16)	1.409 (6)
C(15) - C(20)	1.377 (6)

Experimental Part

C(21) - C(22)	1.388 (6)
C(21) - C(26)	1.396 (6)
C(27) - C(28)	1.379 (6)
C(27) - C(32)	1.383 (6)
C(33) - C(34)	1.396 (6)
C(33) - C(38)	1.386 (6)
C(39) - C(40)	1.405 (6)
C(39) - C(44)	1.389 (6)
C(45) - C(46)	1.406 (6)
C(45) - C(50)	1.410 (6)
C(46) - C(47)	1.408 (6)
C(46) - C(51)	1.503 (6)
C(47) - C(48)	1.400 (6)
C(47) - C(57)	1.496 (6)
C(48) - C(49)	1.401 (6)
C(48) - C(63)	1.501 (6)
C(49) - C(50)	1.401 (6)
C(49) - C(69)	1.500 (6)
C(50) - C(75)	1.511 (6)
C(51) - C(52)	1.382 (6)
C(51) - C(56)	1.393 (6)
C(57) - C(58)	1.408 (6)
C(57) - C(62)	1.384 (6)
C(63) - C(64)	1.399 (6)
C(63) - C(68)	1.375 (6)
C(69) - C(70)	1.385 (6)
C(69) - C(74)	1.388 (6)
C(75) - C(76)	1.383 (6)
C(75) - C(80)	1.388 (6)
C(7) - C(8)	1.346 (5)
C(16) - C(17)	1.371 (7)
C(17) - C(18)	1.384 (9)
C(18) - C(19)	1.371 (9)
C(19) - C(20)	1.400 (8)
C(22) - C(23)	1.372 (7)
C(23) - C(24)	1.392 (7)
C(24) - C(25)	1.394 (7)
C(25) - C(26)	1.377 (7)
C(28) - C(29)	1.392 (6)
C(29) - C(30)	1.374 (7)
C(30) - C(31)	1.377 (7)
C(31) - C(32)	1.389 (6)
C(34) - C(35)	1.382 (6)
C(35) - C(36)	1.376 (7)
C(36) - C(37)	1.378 (7)
C(37) - C(38)	1.379 (7)
C(40) - C(41)	1.393 (7)
C(41) - C(42)	1.381 (7)
C(42) - C(43)	1.390 (7)
C(43) - C(44)	1.398 (7)
C(52) - C(53)	1.389 (7)
C(53) - C(54)	1.354 (8)
C(54) - C(55)	1.379 (8)
C(55) - C(56)	1.400 (8)
C(58) - C(59)	1.388 (7)
C(59) - C(60)	1.362 (7)
C(60) - C(61)	1.374 (7)
C(61) - C(62)	1.389 (7)
C(64) - C(65)	1.402 (6)
C(65) - C(66)	1.371 (8)
C(66) - C(67)	1.375 (8)
C(67) - C(68)	1.402 (7)
C(70) - C(71)	1.391 (7)

C (71) - C (72)	1.386 (7)
C (72) - C (73)	1.364 (7)
C (73) - C (74)	1.399 (7)
C (76) - C (77)	1.405 (7)
C (77) - C (78)	1.375 (9)
C (78) - C (79)	1.350 (9)
C (79) - C (80)	1.398 (8)

C (1) - C (1) - C (2)	120.3 (4)
C (1) - C (1) - C (6)	118.9 (4)
C (2) - C (1) - C (6)	120.8 (3)
C (1) - C (2) - C (3)	119.7 (3)
C (1) - C (2) - C (8)	118.3 (3)
C (3) - C (2) - C (8)	122.0 (3)
C (2) - C (3) - C (9)	121.5 (3)
C (2) - C (3) - C (4)	118.7 (4)
C (9) - C (3) - C (4)	119.8 (4)
C (6) - C (5) - C (45)	119.3 (3)
C (6) - C (5) - C (4)	119.3 (3)
C (45) - C (5) - C (4)	121.3 (3)
C (1) - C (6) - C (5)	118.5 (3)
C (1) - C (6) - C (7)	119.1 (4)
C (5) - C (6) - C (7)	122.4 (3)
C (3) - C (9) - C (10)	120.8 (4)
C (3) - C (9) - C (14)	120.1 (4)
C (10) - C (9) - C (14)	119.2 (4)
C (9) - C (10) - C (11)	121.2 (4)
C (9) - C (10) - C (15)	120.0 (4)
C (11) - C (10) - C (15)	118.7 (4)
C (10) - C (11) - C (12)	119.0 (4)
C (10) - C (11) - C (21)	120.5 (4)
C (12) - C (11) - C (21)	120.5 (4)
C (11) - C (12) - C (13)	120.3 (4)
C (11) - C (12) - C (27)	121.3 (4)
C (13) - C (12) - C (27)	118.3 (4)
C (12) - C (13) - C (14)	119.9 (4)
C (12) - C (13) - C (33)	119.2 (4)
C (14) - C (13) - C (33)	120.8 (4)
C (9) - C (14) - C (13)	120.4 (4)
C (9) - C (14) - C (39)	121.7 (4)
C (13) - C (14) - C (39)	117.7 (4)
C (10) - C (15) - C (16)	117.6 (4)
C (10) - C (15) - C (20)	123.0 (4)
C (16) - C (15) - C (20)	119.4 (4)
C (11) - C (21) - C (22)	121.8 (4)
C (11) - C (21) - C (26)	120.2 (4)
C (22) - C (21) - C (26)	118.0 (4)
C (12) - C (27) - C (28)	121.4 (4)
C (12) - C (27) - C (32)	119.1 (4)
C (28) - C (27) - C (32)	119.3 (4)
C (13) - C (33) - C (34)	117.9 (4)
C (13) - C (33) - C (38)	123.1 (4)
C (34) - C (33) - C (38)	119.0 (4)
C (14) - C (39) - C (40)	121.5 (4)
C (14) - C (39) - C (44)	118.8 (4)
C (40) - C (39) - C (44)	119.2 (4)
C (5) - C (45) - C (46)	121.1 (4)
C (5) - C (45) - C (50)	119.0 (4)
C (46) - C (45) - C (50)	119.8 (4)
C (45) - C (46) - C (47)	119.5 (4)
C (45) - C (46) - C (51)	120.7 (4)
C (47) - C (46) - C (51)	119.8 (4)
C (46) - C (47) - C (48)	120.2 (4)

Experimental Part

C (46) - C (47) - C (57)	119.4 (4)
C (48) - C (47) - C (57)	120.3 (4)
C (47) - C (48) - C (49)	120.4 (4)
C (47) - C (48) - C (63)	119.8 (4)
C (49) - C (48) - C (63)	119.8 (4)
C (48) - C (49) - C (50)	119.5 (4)
C (48) - C (49) - C (69)	121.6 (4)
C (50) - C (49) - C (69)	118.8 (4)
C (45) - C (50) - C (49)	120.4 (4)
C (45) - C (50) - C (75)	120.2 (4)
C (49) - C (50) - C (75)	119.4 (4)
C (46) - C (51) - C (52)	120.3 (4)
C (46) - C (51) - C (56)	120.5 (4)
C (52) - C (51) - C (56)	119.2 (5)
C (47) - C (57) - C (58)	120.5 (4)
C (47) - C (57) - C (62)	121.6 (4)
C (58) - C (57) - C (62)	117.8 (4)
C (48) - C (63) - C (64)	119.1 (4)
C (48) - C (63) - C (68)	122.3 (4)
C (64) - C (63) - C (68)	118.7 (4)
C (49) - C (69) - C (70)	120.5 (4)
C (49) - C (69) - C (74)	120.6 (4)
C (70) - C (69) - C (74)	118.7 (4)
C (50) - C (75) - C (76)	118.2 (4)
C (50) - C (75) - C (80)	121.3 (4)
C (76) - C (75) - C (80)	120.5 (4)
C (3) - C (4) - C (5)	122.6 (4)
C (6) - C (7) - C (8)	121.6 (4)
C (2) - C (8) - C (7)	121.7 (4)
C (15) - C (16) - C (17)	121.2 (5)
C (16) - C (17) - C (18)	119.1 (6)
C (17) - C (18) - C (19)	120.3 (6)
C (18) - C (19) - C (20)	121.2 (6)
C (15) - C (20) - C (19)	118.8 (5)
C (21) - C (22) - C (23)	121.6 (4)
C (22) - C (23) - C (24)	119.9 (4)
C (23) - C (24) - C (25)	119.4 (5)
C (24) - C (25) - C (26)	119.9 (5)
C (21) - C (26) - C (25)	121.2 (4)
C (27) - C (28) - C (29)	120.1 (4)
C (28) - C (29) - C (30)	120.4 (4)
C (29) - C (30) - C (31)	119.8 (4)
C (30) - C (31) - C (32)	120.0 (4)
C (27) - C (32) - C (31)	120.4 (4)
C (33) - C (34) - C (35)	120.5 (4)
C (34) - C (35) - C (36)	119.8 (4)
C (35) - C (36) - C (37)	120.1 (5)
C (36) - C (37) - C (38)	120.5 (5)
C (33) - C (38) - C (37)	120.1 (4)
C (39) - C (40) - C (41)	119.5 (4)
C (40) - C (41) - C (42)	121.1 (5)
C (41) - C (42) - C (43)	119.5 (5)
C (42) - C (43) - C (44)	120.2 (5)
C (39) - C (44) - C (43)	120.4 (4)
C (51) - C (52) - C (53)	120.5 (5)
C (52) - C (53) - C (54)	121.0 (6)
C (53) - C (54) - C (55)	119.2 (5)
C (54) - C (55) - C (56)	121.3 (5)
C (51) - C (56) - C (55)	118.9 (5)
C (57) - C (58) - C (59)	120.0 (4)
C (58) - C (59) - C (60)	120.9 (5)
C (59) - C (60) - C (61)	120.2 (4)

C (60) - C (61) - C (62)	119.7 (5)
C (57) - C (62) - C (61)	121.4 (5)
C (63) - C (64) - C (65)	119.6 (4)
C (64) - C (65) - C (66)	120.9 (5)
C (65) - C (66) - C (67)	120.0 (5)
C (66) - C (67) - C (68)	119.4 (5)
C (63) - C (68) - C (67)	121.5 (5)
C (69) - C (70) - C (71)	121.1 (5)
C (70) - C (71) - C (72)	119.3 (4)
C (71) - C (72) - C (73)	120.3 (5)
C (72) - C (73) - C (74)	120.4 (5)
C (69) - C (74) - C (73)	120.1 (4)
C (75) - C (76) - C (77)	119.7 (4)
C (76) - C (77) - C (78)	118.9 (5)
C (77) - C (78) - C (79)	121.5 (5)
C (78) - C (79) - C (80)	120.9 (5)
C (75) - C (80) - C (79)	118.6 (5)
C1 (1) - C (91) - C1 (2)	112.6 (3)
C1 (3) - C (92) - C1 (4)	111.9 (3)
C1 (5) - C (93) - C1 (6)	110.1 (4)
C1 (7) - C (94) - C1 (8)	110.1 (3)

Lebenslauf

Stefan Bernhardt
xxx
63069 Offenbach
Tel.: xxx (privat)
06181/593305 (geschäftlich)
E-mail.: stefan.bernhardt@degussa.com



Persönliche Angaben

Name: Stefan Bernhardt
Geburtsdatum: 30. April 1976
Geburtsort: Hofheim am Taunus
Staatsangehörigkeit: deutsch
Familienstand: verheiratet, zwei Kinder

Berufstätigkeit

Okt. 2000-Okt. 2001 Merck KGaA, Darmstadt im Bereich „Cosmetics Health Nutrition“. Verfahrenstechnische Betreuung bei der Einführung neuer Synthesen.
Seit Nov. 2005 Degussa AG, Hanau in der Abteilung Process Technology & Engineering, Fluid Processing.

Ausbildungsweg und Schule

Okt. 2001-Okt. 2005 Promotion am Max-Planck-Institut für Polymerforschung, Mainz unter der Betreuung von Prof. Dr. K. Müllen.
Dissertation: “Polyphenylene Dendrimers – Design and Synthesis of Monodisperse Functional Nanoparticles”
Abschluss: Dr. rer. nat.
Okt. 2001-Okt. 2003 promotionsbegleitendes Aufbaustudium an der Universität Mainz zur Zulassung zur Promotion.
Sept. 1996-Juli 2000 Studium zum Diplom-Chemieingenieur an der Europa Fachhochschule Fresenius, Idstein.
Diplomarbeit: “Untersuchungen zur Homo- und Copolymerisation von Cyclodextrin-komplexierten Acrylaten in wässriger Phase“
Abschluss: Diplom
Juli 1995-Juli 1996 Zivildienst in der Notrufzentrale des ASB Niederhausen.
Juli 1986-Juli 1995 Leibniz- und Friedrich-Dessauer Gymnasium, Frankfurt am Main Höchst.
Abschluss: Abitur

Kenntnisse/ Fähigkeiten/ Hobbys

EDV-Kenntnisse:	Gute bis sehr gute Kenntnisse in der Software: Windows XP, Microsoft Office XP, Corel Draw
Fremdsprachen:	Englisch fließend, Französisch Grundkenntnisse
Besondere Stärken:	Problemlösungsorientiert, engagiert, hilfsbereit, selbständig
Ehrenamt:	Medizinisches Transportmanagement ASB Niederhausen
Hobbys:	Volleyball, Modellbau, Radfahren
Sonstiges:	Führerschein Klasse 3

Offenbach, den 5. Juli 2006

Publikationsliste

S. Bernhardt, P. Glöckner, H. Ritter *Polym. Bull.* **2001**, *46*, 153-157. "Cyclodextrins in Polymer Synthesis: Influence of Methylated beta-Cyclodextrin as Host on the Free Radical Copolymerization Reactivity Ratios of Hydrophobic Acrylates as Guest Monomers in Aqueous Medium"

S. Bernhardt, P. Glöckner, A. Theis, H. Ritter *Macromolecules* **2001**, *34*, 1647-1649.
"Cyclodextrins in Polymer Synthesis: Influence of Acrylate Side Groups on the Initial Rate of Radical Polymerization of Various Acrylate/methylated beta-Cyclodextrin Complexes in Water"

T. D. M. Bell, A. Stefan, S. Masuo, P. Vosch, M. Lor, M. Cotlet, J. Hofkens, S. Bernhardt, K. Müllen, M. Van der Auweraer, J. W. Verhoeven, F. C. DeSchryver *Chem. Phys. Chem.* **2005**, *6*, 942-948.
"Electron Transfer at the Singel Molecule Level in a Triphenyl Amine (Donor) – Perylene (Acceptor) Molecule"

S. Bernhardt, M. Baumgarten, M. Wagner, K. Müllen *J. Am. Chem. Soc.* **2005**, *127*, 12392-12399.
"Multiple Functionalization of Benzophenones inside Polyphenylene Dendrimers – Towards Entrapped Ions and Radicals"

S. Bernhardt, M. Kastler, V. Enkelmann, M. Baumgarten, K. Müllen *Chem. Eur. J.* **2006**, *12*(23), 6117-6128.
"Pyrene as Chromophore and Electrophore – Encapsulation in a Rigid Polyphenylene Shell"

S. Bernhardt, M. Baumgarten, K. Müllen *Eur. J. Org. Chem.* **2006**, *11*, 2523-2529.
"Dendritic Encapsulation – "Postsynthetic" Functionalizations of a Single Benzophenone Shielded by Shape-Persistent Polyphenylene Dendrons"